

INSTITUTE OF THEORETICAL PHYSICS AND ASTRONOMY,  
VILNIUS UNIVERSITY

Vygandas Laugalys

**YOUNG STARS AND INTERSTELLAR EXTINCTION  
IN THE NORTH AMERICA AND PELICAN NEBULAE**

Doctoral dissertation

Physical sciences, physics (02 P),  
astronomy, space research, cosmic chemistry (P 520)

Vilnius, 2009

Disertacija rengta 1995 - 2009 metais Vilniaus universiteto Teorinės fizikos ir astronomijos institute

Disertacija ginama eksternu

Mokslinis konsultantas

prof.habil.dr. V. Straižys (Vilniaus universiteto Teorinės fizikos ir astronomijos institutas, fiziniai mokslai, fizika – 02 P)

VILNIAUS UNIVERSITETO TEORINĖS FIZIKOS  
IR ASTRONOMIJOS INSTITUTAS

Vygandas Laugalys

**JAUNOS ŽVAIGŽDĖS IR TARPŽVAIGŽDINĖ EKSTINKCIJA  
ŠIAURĖS AMERIKOS IR PELIKANO DEBESYSE**

Daktaro disertacija

Fiziniai mokslai, fizika (02 P),  
astronomija, erdvės tyrimai, kosminė chemija (P 520)

Vilnius, 2009



# Contents

PUBLICATION ON THE SUBJECT OF THE DISSERTATION . . . . .	5
<b>1. INTRODUCTION</b>	<b>9</b>
1.1. Galactic structure in the investigated direction . . . . .	9
1.2. The North America and Pelican Nebulae . . . . .	10
1.3. Young Stars . . . . .	10
1.4. The Ionizing Source(s) . . . . .	10
1.5. Open Clusters . . . . .	11
<b>2. OBSERVATIONAL DATA AND REDUCTIONS</b>	<b>12</b>
2.1. Wide Field CCD Observations with the Maksutov telescope . . . . .	12
2.1.1. Observed Targets . . . . .	12
2.1.2. Reductions . . . . .	13
2.1.3. The Catalog and Classification of Stars . . . . .	13
2.2. CCD Observations with the Flagstaff telescope . . . . .	14
2.2.1. Introduction . . . . .	14
2.2.2. Advanced M 67 Flatfield Corrections . . . . .	14
2.2.3. Comparison With Other Photometric Data . . . . .	16
2.2.4. Conclusions . . . . .	24
2.2.5. Observed Targets and Data Reductions: NGC 6997 . . . . .	30
2.2.6. Observed Targets and Data Reductions: The Dark Cloud L 935 . . . . .	30
2.2.7. Observed Targets and Data Reductions: Collinder 428 . . . . .	31
2.2.8. Classification of Stars and Their Color Excesses, Extinctions and Distances . . . . .	31
2.3. Zero-Age Main Sequence in the <i>Vilnius</i> System . . . . .	33
2.3.1. Introduction . . . . .	33
2.3.2. Photometry of the Hyades, Pleiades, Praesepe and Orion OB1 in the <i>Vilnius</i> System . . . . .	33
2.3.3. Absolute Magnitude vs. Color Diagram . . . . .	34
<b>3. DUST AND MOLECULAR CLOUDS</b>	<b>36</b>
3.1. Interstellar Extinction Law . . . . .	36
3.1.1. Introduction . . . . .	36
3.1.2. Near-UV and Optical . . . . .	37
3.1.3. NGC 6997 Area . . . . .	39
3.1.4. 2MASS Data in the North America and Pelican Area and Cyg OB2 Association . . . . .	42
3.2. Interstellar Extinction . . . . .	50
3.2.1. Introduction . . . . .	50
3.2.2. Relatively Transparent NAP Areas . . . . .	50
3.2.3. The Region of NGC 6997 . . . . .	53
3.2.4. L 935 Dark Cloud Area . . . . .	55
3.2.5. The Region of Collinder 428 . . . . .	58
3.2.6. Extinction from 2MASS star counts . . . . .	59

<b>4. YOUNG STARS AND IONIZING SOURCES</b>	<b>60</b>
4.1. Suspected Emission-Line and T Tauri Type Stars . . . . .	60
4.2. Ionizing Sources . . . . .	62
4.2.1. Introduction . . . . .	62
4.2.2. The Comerón & Pasquali Star . . . . .	63
4.2.3. More O-Like Stars Behind The L 935 Cloud . . . . .	63
4.2.4. The I-J vs. J-H Diagram . . . . .	65
4.2.5. Spectral Energy Distributions . . . . .	69
4.2.6. Comments on Individual Stars . . . . .	69
4.2.7. Conclusions . . . . .	71
<b>5. OBSERVED OPEN CLUSTERS</b>	<b>72</b>
5.1. NGC 6997 . . . . .	72
5.2. Collinder 428 . . . . .	74
<b>6. THE MAIN RESULTS AND CONCLUSIONS</b>	<b>76</b>
6.1. SUMMARY OF THE MAIN RESULTS . . . . .	76
6.2. CONCLUSIONS . . . . .	77
<b>REFERENCES</b>	<b>78</b>
<b>ACKNOWLEDGMENTS</b>	<b>83</b>
<b>APPENDIX</b>	<b>84</b>
Table 2.2.4 . . . . .	84
Table 2.2.5 . . . . .	90
Table 2.2.6 . . . . .	91
Table 2.2.7 . . . . .	92
Table 2.2.8 . . . . .	94
Table 2.2.9 . . . . .	95
Table 2.3.1 . . . . .	103
Table 2.3.2 . . . . .	105
Table 2.3.3 . . . . .	105
Table 3.1.5 . . . . .	106
Table 3.2.1 . . . . .	109
Table 3.2.2 . . . . .	110
Table 3.2.3 . . . . .	112
Table 3.2.4 . . . . .	113

## PUBLICATION ON THE SUBJECT OF THE DISSERTATION

1. Straizys V., Corbally C. J., Laugalys V. 1999, "Interstellar Extinction Law in the Vicinity of the North America and Pelican Nebulae", Baltic Astronomy, 8, 355
2. Laugalys V., Straizys V. 2002, "CCD Photometry and Classification of Stars in the North America and Pelican Nebulae Region. I. Molėtai Photometry", Baltic Astronomy, 11, 205
3. Laugalys V., Kazlauskas A., Boyle R. P., Vrba F.J., Philip A. G. D. Straizys V. 2004, "CCD Photometry of the M67 Cluster in the Vilnius System. II. New Photometry of High Accuracy", Baltic Astronomy, 13, 1
4. Laugalys V., Straizys V., Vrba F.J., Boyle R. P., Philip A. G. D. Kazlauskas A. 2006, "CCD Photometry and Classification of Stars in the North America and Pelican Nebulae Region. II. The Region of NGC 6997", Baltic Astronomy, 15, 327
5. Laugalys V., Straizys V., Vrba F.J., Boyle R. P., Philip A. G. D. Kazlauskas A. 2006, "CCD Photometry and Classification of Stars in the North America and Pelican Nebulae Region. III. The Dark Cloud L 935", Baltic Astronomy, 15, 483
6. Kazlauskas A., Straizys V., Bartasiūtė S., Laugalys V., Černis K., Boyle R. P., Philip A. G. D. 2006, "Zero-age Main Sequence in the HR Diagram of the Vilnius Photometric System", Baltic Astronomy, 15, 511
7. Laugalys V., Straizys V., Vrba F.J., Černis K., Kazlauskas A., Boyle R. P., Philip A. G. D. 2007, "CCD Photometry and Classification of Stars in the North America and Pelican Nebulae Region. IV. The Region of a Supposed Cluster Collinder 428", Baltic Astronomy, 16, 349
8. Straizys V., Corbally C. J., Laugalys V. 2008, "2MASS Two-color Interstellar Reddening Line in the Direction of the North America and Pelican Nebulae and the Cyg OB2 Association", Baltic Astronomy, 17, 125
9. Straizys V., Laugalys V. 2008, "O-like Stars in the Direction of the North America and Pelican Nebulae", Baltic Astronomy, 17, 143
10. Straizys V., Laugalys V. 2008, "2MASS Two-color Interstellar Reddening Lines in the Inner Galaxy", Baltic Astronomy, 17, 253

## CONTRIBUTION RELATED TO THE DISSERTATION AT THE INTERNATIONAL CONFERENCES

1. Laugalys V. "Vilnius, 2MASS and IRAS data together", in Strömvil workshop, Poland, Krakow 2008 September 11
2. Laugalys V. "An Experience with Aperture and PSF Reductions of CCD Exposures from Flagstaff", in Strömvil workshop, Lithuania, Molėtai 2006. August 28 - September 09
3. Boyle R. P., Janusz R., Philip A. G. D., Laugalys V., Kazlauskas A. "CCD Flatfielding for Strömvil Photometry in M67", in American Astronomical Society Meeting 207, # 29.06; Bulletin of the American Astronomical Society, Vol. 37, p.1212, 2005
4. Boyle R. P., Janusz R., Philip A. G. D., Laugalys V. "Automation and Iteration Methods for Processing CCD Stellar Photometry in the Strömvil System", in American Astronomical Society Meeting 205, # 153.02; Bulletin of the American Astronomical Society, Vol. 36, p.1602, 2004
5. Straizys V., Zdanavičius J., Zdanavičius K., Laugalys V., Kazlauskas A., Černis K., Boyle R. P., Philip A. G. D. 2004, "Interstellar extinction in the MBM 12 molecular cloud area in Aries", American Astronomical Society Meeting 205, # 59.04; Bulletin of the American Astronomical Society, Vol. 36, p.1439, 2004
6. Laugalys V., Boyle R.P., Kazlauskas A., Vrba F. J., Philip A. G. D., Straizys V. , "Accuracy of CCD photometry: open cluster M67" in Dynamical and Chemical Evolution of Galactic Star Clusters, Taiwan, Chung-Li, National Central University, 2003 November 24-28
7. Laugalys V., Boyle R. P., Kazlauskas A., Vrba F.J., Philip A. G. D. Straizys V. "Large-Scale Errors in CCD Photometry of M67" in Stellar Photometry: Past, Present and Future, Lithuania, Vilnius 2003 September 17-20

8. Boyle R. P., Janusz R., Philip A. G. D. , Kazlauskas A., Laugalys V. *"Flatfielding Errors in Stromvil CCD Photometry"* in Stellar Photometry: Past, Present and Future, Lithuania, Vilnius 2003 September 17-20
9. Boyle R. P., Janusz R., Laugalys V., Philip A. G. D. *"CCD Flatfield Correction by Differential Stellar Photometry: Automated Methods"*, in American Astronomical Society Meeting 203, # 04.02; Bulletin of the American Astronomical Society, Vol. 35, p.1207, 2003
10. Boyle R. P., Laugalys V., Philip A. G. D. *"Flatfield Correction by Differential CCD Photometry in M67"*, in American Astronomical Society, 201, # 91.09; Bulletin of the American Astronomical Society, Vol. 34, p.1257, 2002
11. Corbally C., Straižys V., Laugalys V. *"Interstellar Extinction Law in the Vicinity of the North America and Pelican Nebulae"*, in American Astronomical Society, 195, # 74.01; Bulletin of the American Astronomical Society, Vol. 31, p.1478, 1999

## The main aim of the dissertation

The main aim of this work was a comprehensive photometric investigation of the Milky Way region at Galactic longitudes around  $l=83^{\circ}\text{--}87^{\circ}$  in the direction of the North America and Pelican nebulae in order to get distances, absorbing properties of the dust clouds and to evaluate the relationship between two open clusters and the surrounding star-forming region.

## The main tasks

1. Wide-field CCD photometry of stars down to  $V = 13$  mag in the area of  $2^{\circ}\times 2^{\circ}$  including the North America and Pelican (hereafter NAP) nebulae, one of the known star-forming regions (hereafter SFR).
2. CCD photometry of fainter stars ( $V$  down to 16–17 mag) in smaller regions of the dark cloud Lynds 935.
3. CCD photometry in two areas centered on two open clusters , NGC 6997 and Collinder 428.
4. CCD photometry of the open cluster M 67 with the aim to create a standard field of high accuracy in the *Vilnius* system.
5. The determination of interstellar extinction law in the investigated area.
6. Photometric classification of the observed stars, determination of their distances and interstellar reddening, investigation of changes of the interstellar extinction run with distance in different parts of the NAP nebulae.
7. Determination of ages, distances, interstellar extinctions and membership of two open clusters, and the investigation of their relation to the NAP star-forming region.
8. The search for new candidates to young stellar objects in the area and possible candidates to ionizing sources of the NAP gas clouds.

## Scientific novelty

1. For 2600 stars in the NAP areas multicolor photometry and two-dimensional spectral classification have been done for the first time.
2. The distribution of interstellar dust in different parts of the dark cloud is given.
3. Reliable interstellar reddenings, distances and ages for the stars of open clusters NGC 6997 and Collinder 428 are determined. Membership of stars to the clusters is estimated using their distance, reddening and concentration criteria. It is shown that the cluster NGC 6997 is not related to the NAP star-forming region. The cluster Collinder 428 is found to be just a window in the surrounding dust clouds, not a real cluster.
4. About 30 young stellar objects and 13 possible O-type stars, candidates to the ionizing sources of the nebulae are identified.
5. The interstellar extinction law in the near-UV, optical and near-infrared spectral regions is determined in the area and shown to be slightly different from the mean extinction law in the Galaxy. The ratio of color excesses  $E_{J-H}/E_{H-K_s}$  is found to be 2.0, a larger value than it was in use until now.

## Practical importance of the dissertation

1. The determined interstellar extinction run with distance is important for the future investigations of the objects both inside the NAP SFR and more distant areas along the Local spiral arm.
2. The identified possible O-type stars may help to solve the long-standing problem of ionizing sources of the nebulae and to construct evolution models of this star-forming region.
3. The determined extinction law and the ratios of color excesses in the area will be useful for estimating physical properties and modeling the interstellar dust in this direction.
4. The created standard region for CCD photometry in the *Vilnius* system in the M 67 cluster will serve for future investigations both as a source for the determination of color-equations between the instrumental and standard systems and for the flatfielding corrections in future CCD photometric investigations.

## **Statements presented for defence**

1. A method, which significantly reduces systematic errors in the CCD data, is developed. This allowed us to produce high accuracy M 67 HR diagrams in the *Vilnius* photometric system. They are important to study stellar evolution and the number of binary stars in open clusters.
2. Interstellar extinction law in North America and Pelican area is very similar to the law for a much wider area in Cygnus. It differs from the normal law by exhibiting somewhat stronger extinction in the violet and the near ultraviolet spectral region.
3. The L 935 dark cloud, which separates North America and Pelican nebulae, begins at a distance of  $520 \pm 50$  pc.
4. Open cluster NGC 6997 has no genetic relation to the star-forming region in the North America and Pelican nebulae. The group of stars known as Collinder 428 is not a real star cluster.

## **Author's contribution**

The author chose the optimum boundaries of the investigated area, took part in all CCD observations at the Molétai Observatory and the data reductions, and was the main observer during CCD observations. The author also took part in CCD observations at the Flagstaff USNO station and photoelectric observations of standard stars at Mt. Lemmon, Arizona. The IRAF package has been studied and used in the CCD data reductions. Methodology and programs for large-scale CCD flatfielding corrections was also developed by author. The author took part in the photometric classification of stars and the interstellar extinction analysis, the literature analysis and preparation of all published articles.

## **Overview of the dissertation**

The work consists of six sections, Bibliography and Appendix. The first section is Introduction.

In the second section the methods of CCD observations, data reductions and photometric classification are described.

In the third section the investigation of the interstellar extinction law and the interstellar extinction run with distance in the dust clouds are described.

In the fourth section we describe the search of young stellar objects and possible sources ionizing the nebulae.

In the fifth section two open clusters, their properties and relation to North America and Pelican Nebulae are described.

The main results and conclusions are given in the sixth section.

Bibliography of the dissertation includes 210 references.

In the Appendix the photometric data for the investigated stars and their parameters are given.

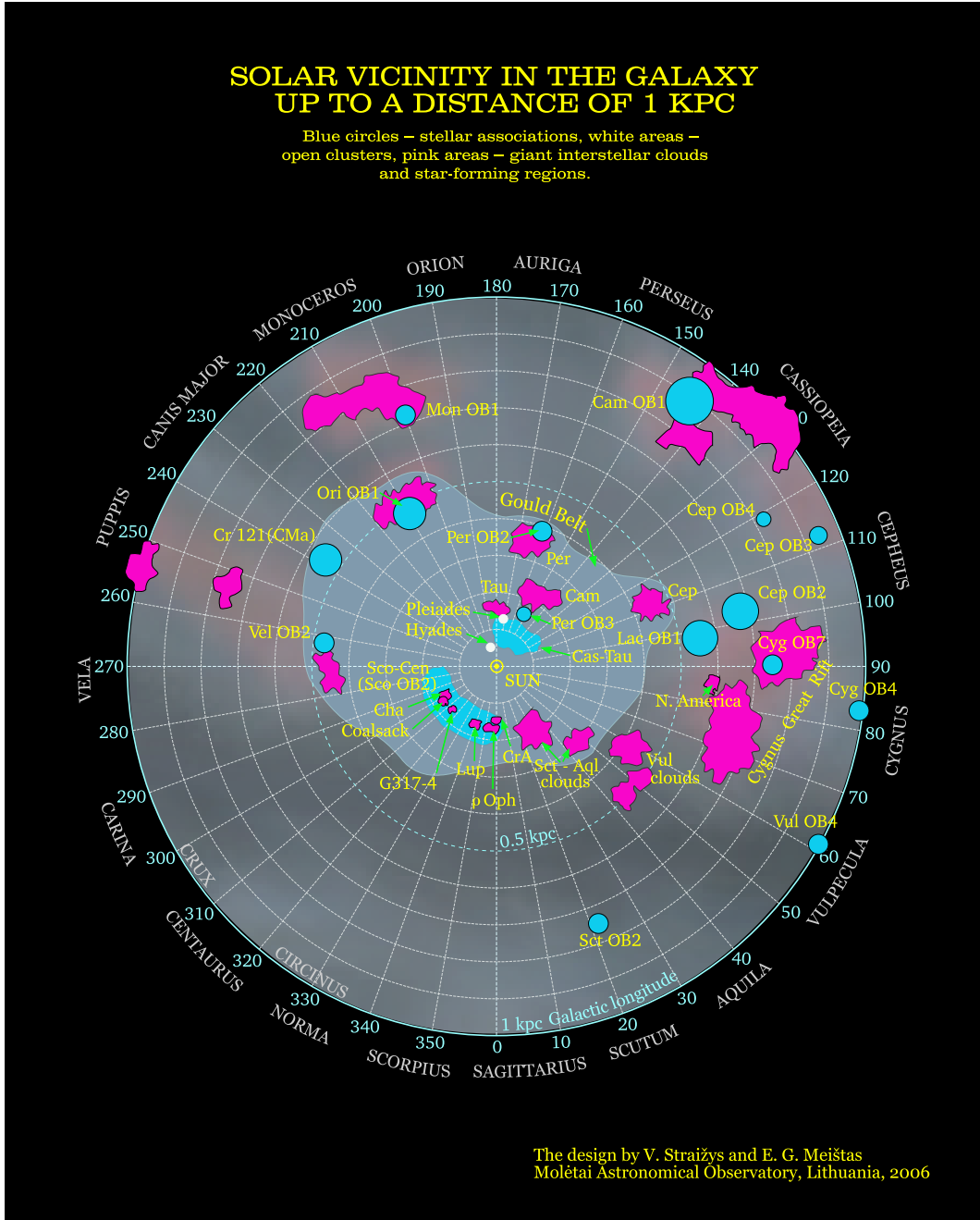


**Fig. 1.1.1.** Schematic picture of the solar vicinity in the Galaxy according to Straizys (2005).

## 1. INTRODUCTION

### 1.1. Galactic structure in the investigated direction

In the Cygnus direction our line of sight runs along the Local (or Orion) spiral arm. Here the Milky Way is split into two branches by a concentration of large dust clouds near the Galactic plane, known as the Great Cygnus Rift. However, separate dark clouds are also scattered over the whole constellation. The wealth of interstellar clouds create favorable conditions for star-forming processes, where the density of interstellar matter reaches the critical value. Therefore most of the dark clouds are places of active formation of stars of different masses – massive stars in OB associations and low-mass stars in T associations. The IRAS, MSX, 2MASS and other recent infrared surveys disclosed thousands of infrared sources in the Cygnus clouds, many of them having color indices typical of young stellar objects (YSOs).

The distribution of interstellar clouds and young stars in the Cygnus direction of the Local arm can be understood having reliable distances of dust and molecular clouds and star-forming regions. However, the problem of determining distances to interstellar clouds in the Cygnus direction is quite problematic, since in this direction our line of sight is almost perpendicular to the direction of the Galaxy rotation (see the direction to  $l=85^\circ$  in Figure 1.1.1).

In this case the kinematical method of distance determination for gas clouds is ineffective because of the near-zero radial velocity gradient, which is smaller than the typical velocity dispersion of interstellar gas clouds. Therefore, for the reliable distance determinations in this direction one must use individual stars for which it is possible to estimate absolute magnitudes, interstellar extinctions and distances using spectroscopic and photometric methods.

### *1.2. The North America and Pelican Nebulae*

We have concentrated our efforts on the direction to the dust clouds covering the large area between the emission nebulae known as North America and Pelican. This region is well known to astronomers since the early days of astronomical photography. The North America Nebula was named by Max Wolf (Wolf 1925), it is also known as NGC 7000. The nearby emission Pelican Nebula (IC 5070) in the west is separated from North America by a lane of dark cloud. Radio continuum observations show that the both nebulae form a single large H II region with a diameter of about  $3^\circ$  known as W80 (Westerhout 1958) or DR 27 (Downes & Rinehart 1966).

The North America and Pelican nebulae (hereafter NAP) are separated by a dense dust and molecular cloud L935 (Wendkler 1968). The overall extent and low density of the North America and Pelican Nebulae complex indicate that W80 is an evolved H II region (Matthews & Goss 1980), and CO observations show that it is ringed by a complex and expanding network of molecular clouds (Bally & Scoville 1980). Also North America and Pelican Nebulae each contain associations of T Tauri stars, providing evidence that star formation has been in action in the recent past (Herbig & Bell 1988).

The distance of the NAP complex of nebulae and dark clouds for a long time was known with a very low accuracy. By different methods the distance values from 500 pc to 1 kpc were obtained (Herbig 1958; Wendker 1968; Giesecking 1973; Goudis 1976a; Goudis & Johnson 1978; Wendker et al. 1983; Heske & Wendker 1985), although values as extreme as 200 pc and 2 kpc can also be found in the literature.

### *1.3. Young Stars*

The classical study of young stars in the North America and Pelican Nebulae is the survey for H $\alpha$  emission stars by Herbig (1958), who presents a list of 68 emission-line stars. He points out that in a region like Cygnus, where we are looking along a spiral arm, the H $\alpha$  emission stars can belong to two categories: (1) Be stars, which are not related to star-forming regions, they can be seen along the spiral arm to large distances, and (2) T Tauri stars, which are likely to be local to the North America and Pelican cloud complex. The work of Herbig was followed by another survey by Welin (1973), who lists 141 H $\alpha$  emission stars in the region. However, in a subsequent study by Giesecking & Schumann (1976) only a fraction of these stars was confirmed to be true H $\alpha$  emitters. More H $\alpha$  emission stars were found by Tsvetkov (1975), Marcy (1980) and some other researchers. Deep interference filter images of selected regions in the North America and Pelican Nebulae have revealed a number of Herbig-Haro flows, testifying to the presence of newborn stars in the associated clouds (Bally & Reipurth 2003). The presence of H $\alpha$  emission stars demonstrates that the L935 cloud is an active region of recent low-mass star formation. However, for a long time the open question was about the presence in the complex of young high-mass stars, such as are seen in OB associations.

### *1.4. The Ionizing Source(s)*

The identification of the source or sources of ionization for the North America and Pelican Nebulae has been attempted for 50 years, and seems only recently to have been resolved in a satisfactory manner (see for discussion in section 4.2). Osterbrock (1957) and Herbig (1958)

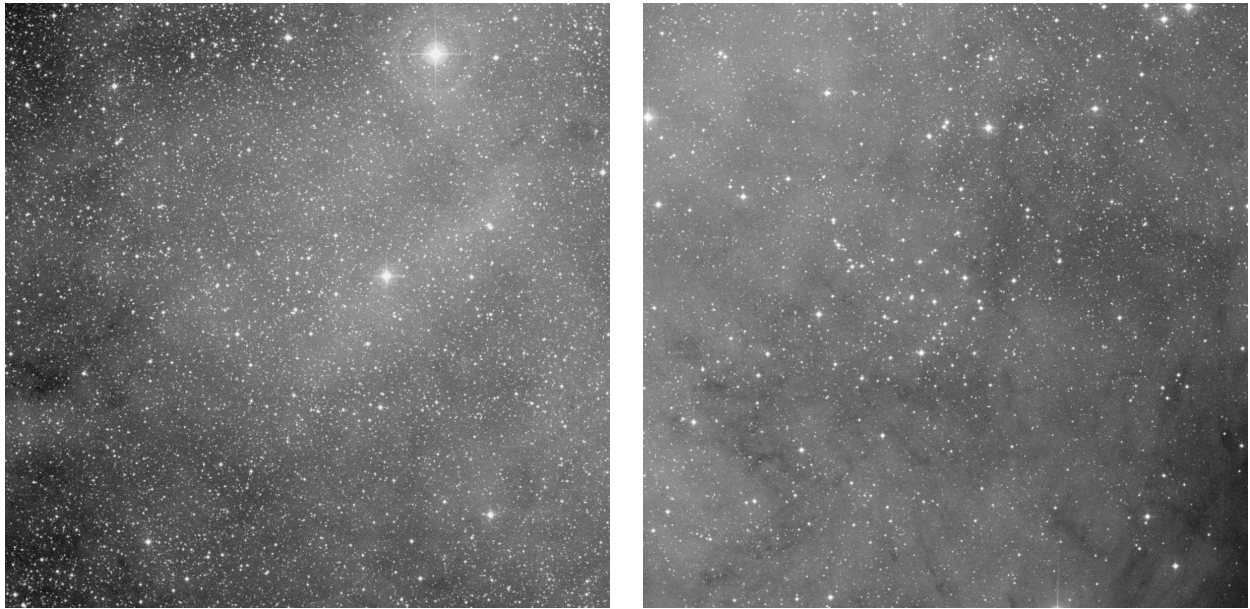


**Fig. 1.5.1.** Collinder 428 (left) and NGC 6997 (right) open clusters from DSS2 plates located at 21h03m +44d35' and 20h56m30s +44d38', field of view  $0.5^\circ \times 0.5^\circ$ .

presented early discussions of potential ionizing sources, and concluded that they would most likely be found as highly obscured stars behind the L 935 cloud in the “Gulf of Mexico” region. This was further supported by radio continuum observations of Matthews & Goss (1980), who found a number of ionized cloud rims, whose orientation pointed towards a location at the geometric center of W80 behind L 935. Using deep I-band images, Neckel et al. (1980) found a very red object, which was extremely bright in the near-infrared (2nd magnitude in the  $L$  passband), and suggested this as the illuminating source of the whole W80 complex. However, further observations by Eiroa et al. (1983) showed it to be an evolved background star not related to W80. Bally & Scoville (1980) listed 11 infrared sources, among which the ionizing source(s) might be found. Wendker et al. (1983) analyzed a 2695 MHz radio continuum map of the whole W80 cloud, and inferred the rather precise locations of eight early type (O8 to B0) stars scattered throughout the ionized region. However, these stars were not identified. Most recently, Comerón & Pasquali (2005) used the 2MASS catalog with color selection criteria to identify 19 candidates behind the L 935 cloud. Further near-infrared spectroscopy could exclude 18 of these objects. The remaining object, 2MASS J205551.25+435224.6, is a bright near-infrared object ( $K \sim 5.0$ ), and is also detectable in the optical region ( $B \sim 15.5$ ,  $R \sim 11.7$ ). Optical spectroscopy reveals an O5 V spectral type. Combined with optical/infrared photometry this indicates a star with about 9.6 magnitudes of visual extinction at a distance of 610 pc (see discussion in section 4.2).

### 1.5. Open Clusters

In the North America and Pelican area three open clusters were known: NGC 6997, Collinder 428 and Barkhatova 1. Figure 1.5.1 shows two investigated clusters seen in DSS2 blue plates.

## 2. OBSERVATIONAL DATA AND REDUCTIONS

### 2.1. Wide Field CCD Observations with the Maksutov telescope

#### 2.1.1. Observed Targets

CCD frames were obtained in 2000 and 2002 with the 35/51 cm Maksutov telescope at the Molėtai Observatory in Lithuania. The camera, loaned from the Trømsø University Observatory (Norway), was fixed in the Newtonian focus, having the scale of  $2.87'/\text{mm}$  or  $4.25''/\text{pixel}$ . The field size was  $25 \times 25 \text{ mm}^2$  or  $1.2 \times 1.2 \text{ sq. degrees}$ . The camera has a thinned back-illuminated Tektronix  $1012 \times 1012$  pixel chip with  $25 \mu\text{m}$  pixels and with a thermoelectric cooling down to  $-40^\circ\text{C}$ .

The focal sizes of images are very small: even at a seeing of  $3''$  they are  $17 \mu\text{m}$  only, i.e., smaller than the CCD pixel size. Therefore, the exposures were made with a small defocussing. Usually a star image contained from 4 to 9 pixels. A set of round (60 mm diameter) filters of the *Vilnius* system was used. The ultraviolet filters *U* and *P* are glass filters and *X*, *Y*, *Z*, *V* and *S* are interference filters. The exposure times in different filters were from 0.5 to 4 min. Each night in each filter several twilight flats were obtained. The centers of the exposed areas were shifted aiming to cover the  $2 \times 2 \text{ sq. degree}$  field bounded by the coordinates (2000.0): RA =  $20^{\text{h}}51.5^{\text{m}}$  –  $21^{\text{h}}00^{\text{m}}$ , DEC =  $+43^\circ30' - +45^\circ30'$ . A schematic map of the investigated area is given in Figure 2.1.1 with the contours of the dark cloud corresponding to  $A_V = 5$  mag according to Cambrésy et al. (2002).

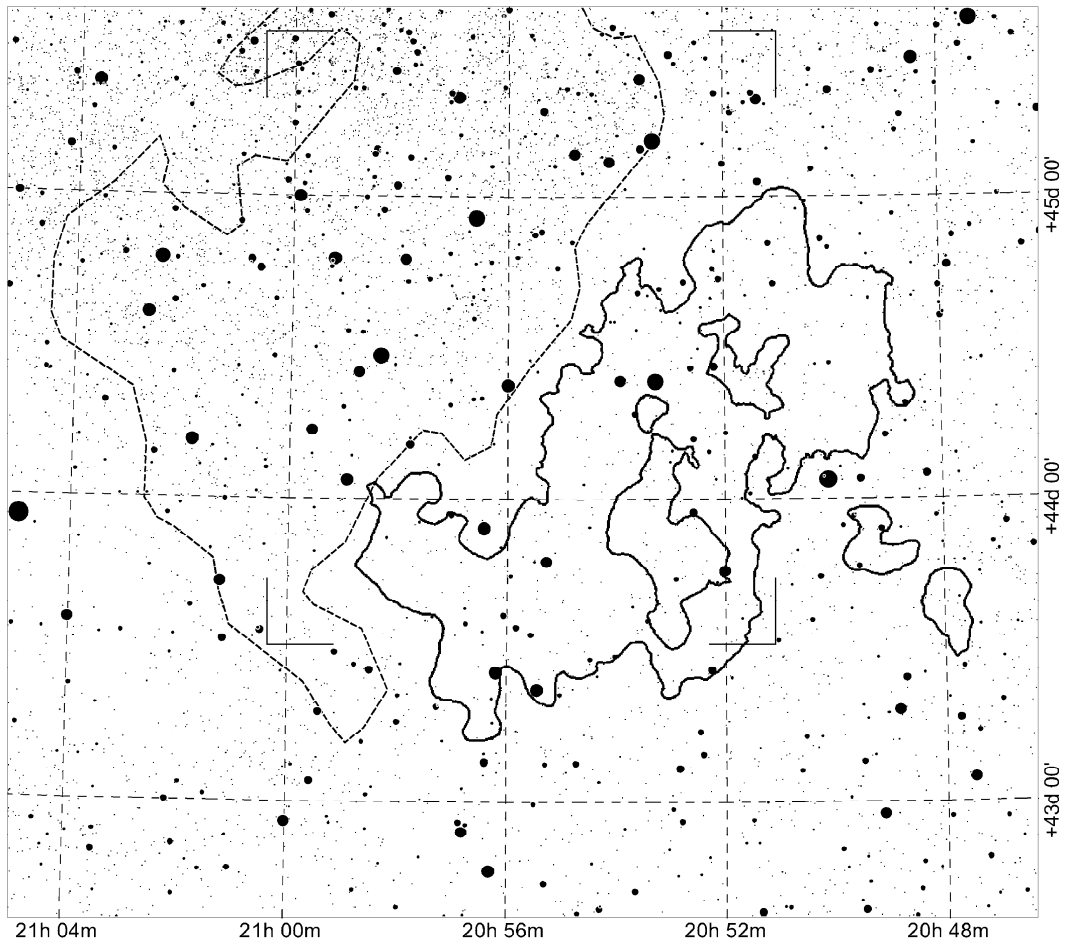


**Fig. 2.1.1.** Schematic map of the investigated area and its surroundings. The angles mark the corners of the investigated area. The broken line shows the contours of the North America Nebula. The solid line shows the contours of the dark cloud corresponding to  $A_V = 5$  mag according to Cambrésy et al. (2002).

Additionally, we have measured magnitudes and color indices of 150 stars in the *Vilnius* system photoelectrically. The observations were done with the 165 cm telescope of the Molėtai Observatory in 1999.

### 2.1.2. Reductions

For obtaining the instrumental magnitudes of stars the multi-aperture method of the IRAF program package was used. The size of the aperture used was 15–20''. Instrumental  $V$  magnitudes and color indices were transformed to the standard *Vilnius* system by color equations obtained by comparing about 60–100 standard stars in the same field observed photoelectrically and taken mostly from Straizys et al. (1993).

Transformation equations obtained from observations were verified by synthetic photometry, calculating the magnitude differences between the standard and the CCD systems by the equation:

$$m_{\text{st}} - m_{\text{CCD}} = -2.5 \log \frac{\int F(\lambda) R_{\text{st}}(\lambda) \tau^x(\lambda) d\lambda}{\int F(\lambda) R_{\text{CCD}}(\lambda) \tau^x(\lambda) d\lambda} + \text{const}, \quad (2.1.1)$$

where  $m_{\text{st}}$  and  $m_{\text{CCD}}$  are magnitudes defined by the response functions  $R_{\text{st}}(\lambda)$  and  $R_{\text{CCD}}(\lambda)$ ,  $F(\lambda)$  is the energy flux distribution function in the spectrum of a star,  $\tau^x(\lambda)$  is the transmittance function of interstellar dust of  $x$  unit masses (interstellar extinction law).

The energy distribution curves for 25 stars of various spectral classes and luminosity classes V–IV–III were taken from Straizys & Sviderskienė (1972) with the corrected ultraviolet, as described by Straizys et al. (1996). The response curves of the standard *Vilnius* system were taken from the Straizys (1992) monograph, Table 59. The response curves of the CCD system were obtained by multiplying the sensitivity function  $s(\lambda)$  of the CCD chip, the transmittance functions of the filters  $f(\lambda)$  and the meniscus lens of the telescope  $m(\lambda)$ , and the reflection functions of two aluminized mirrors  $a^2(\lambda)$ . For the ultraviolet filter the mean atmospheric transmittance function  $p(\lambda)$  at zenith was taken into account. The functions are taken from the following sources:  $s(\lambda)$  – from the manufacturer's description of the Tektronix 1024×1024 CCD camera,  $f(\lambda)$  – from the measurements with a photoelectric spectrometer,  $m(\lambda)$ ,  $a(\lambda)$  and  $p(\lambda)$  – from Straizys (1983).

The coefficients of synthetic color-equations for indices  $P-V$ ,  $Y-V$ ,  $Z-V$  and  $V-S$  are close to those of the equations determined from observations. For color indices  $U-V$  and  $X-V$  some nonlinearity of the synthetic equations was found. The response curve of the instrumental magnitude  $U$  is shifted toward long wavelengths by the meniscus lens. This lens is made from ultraviolet transmitting glass; however it is  $\sim 30$  mm thick and this makes its transmittance in the ultraviolet wavelengths  $< 330$  nm rather low. This causes the mentioned nonlinearity in the transformation equation of  $U-V$ . In case of  $X-V$ , the nonlinearity originates from the shift of the transmittance curve of the filter onto the H $\delta$  line.

### 2.1.3. The Catalog and Classification of Stars

The stars which had double or multiple images in the CCD frames were omitted from photometry. However, the binary stars (both physical and optical) with a separation of  $< 5''$  are unresolvable in our CCD images and seem as single stars. Trying to find more binaries, all stars down to the limiting magnitude (13.2 mag in  $V$ ) were verified for duplicity on the Internet's virtual telescope SkyView of NASA based on the DSS (Digital Sky Survey) scans of the Palomar atlas red and blue plates (<http://skyview.gsfc.nasa.gov>). About 80 stars showing double or multiple images or close stars were also rejected from further analysis.

Classification of stars, their color excesses  $E_{Y-V}$ , extinctions  $A_V$  and distances  $d$  were calculated as described in section 2.2.8. The final catalog contains 690 stars down to  $V = 13.2$  mag observed by CCD and 150 stars down to  $V = 12.0$  mag observed photoelectrically, 130 stars are common. For 27% of stars all color indices are available, 53% of stars are without  $U-V$  and 20% – without both  $U-V$  and  $P-V$ . The catalog has been published in Laugalys & Straizys (2002).

## 2.2. CCD Observations with the Flagstaff telescope

### 2.2.1. Introduction

The old open cluster M 67 in Cancer is one of the best studied objects in a number of photometric systems. In the *Vilnius* seven-color photometric system it was first investigated by Boyle et al. (1998, hereafter Paper I) by determining magnitudes and color indices of 279 stars down to  $V = 15$  mag. The investigation was based on a set of CCD exposures obtained in 1993/94 with the 1 meter Ritchey telescope of the US Naval Observatory, Flagstaff Station. The observations were reduced using the standard IRAF software package. For flat-fielding twilight exposures were used. For reduction to the standard *Vilnius* system a set of 13 standard stars with magnitudes and color indices observed photoelectrically were used.

However, we were not satisfied with the accuracy of photometry reached in Paper I which for the faintest stars at  $V = 15$  mag was worse than 0.02 mag. It was also evident that some systematic effects depending on the star's position in the CCD frame were present. Since the cluster area is accepted to be one of the standard areas of the *Vilnius* system, we decided to increase the accuracy of photometry by obtaining more CCD exposures, by increasing the number of photoelectric standards and by improving the method of the flat-fielding.

In Paper I we used only three M 67 exposures for each filter obtained in our first two observing runs in 1993 February 18/19 and 1994 December 3/4. In the present investigation we used 9–14 exposures in each filter (Table 2.2.1) and the *Cousins I* passband has been added. The exposures of the first run of 1993 were not taken into account.

**Table 2.2.1.** Logbook of the CCD observations in 1994–2001.

Run	Time	<i>U</i>	<i>P</i>	<i>X</i>	<i>Y</i>	<i>Z</i>	<i>V</i>	<i>S</i>	<i>I</i>
2	1994 Dec 3, 4	2	3	2	2	2	1	2	1
3	1999 Oct 11	1	1	1	1	1	1	1	1
4	2000 Apr 7	3	3	3	3	3	3	3	3
5	2000 Apr 22, 25	2	2	2	2	2	2	2	–
6	2000 Nov 13	3	3	3	3	2	2	2	2
7	2001 Dec 3, 6	2	2	1	1	2	1	2	2
Total:		13	14	12	12	12	10	12	9

Exposure times were 20 min for *U* and *P*, 6 min for *X* and *V*, 3 min for *Y*, *Z* and *S* and 1 min for *I*. The filters were combined from two sets: a glass filter set of  $80 \times 80$  mm<sup>2</sup> size (the *Vilnius* filters *U*, *P*, *Y*, *V* and *Cousins I*) and an interference filter set of 60 mm diameter (the *Vilnius* filters *X*, *Z* and *S*). The glass filters covered the whole CCD area without vignetting ( $23' \times 23'$ ) and the interference filters gave an unvignetted field of 20' diameter.

The standard routines of the IRAF software package were used in the reductions. We made an average bias image consisting of about one hundred separate images taken in all runs. A small nonlinearity of the CCD response was corrected as described in Paper I. For flat-fielding we used averaged evening or morning twilight flats for each observing run.

### 2.2.2. Advanced M 67 Flatfield Corrections

After a careful inspection of our photometry in Paper I, we found some large-scale systematic effects depending on a star's position on CCD frame. This can be clearly seen by comparing photometry from three shifted exposures (see the left panels of Figure 2.2.1).

These large-scale systematic differences between shifted exposures indicate that our flat field images were contaminated by non-uniformly distributed scattered light within the telescope and/or CCD camera. We used our own program to calculate necessary corrections from shifted field photometry data. The main idea was that the shifted field photometry should be free of any large-scale systematic differences after we apply photometrically derived flat-field corrections. This measure should effectively remove any large-scale non-uniformly distributed scattered light from flat fields.

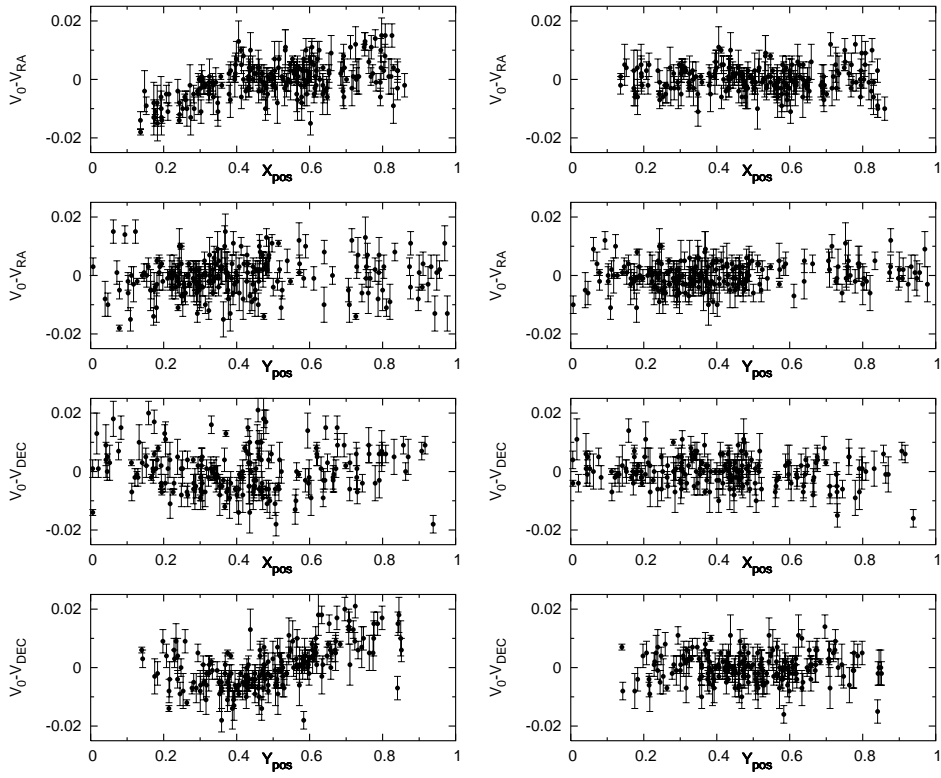


**Fig. 2.2.1.** Large-scale systematic errors detected by comparing three shifted field  $V$  filter exposures of M67 obtained in the 4th observing run on 2000 April 7 (left panels). Right panels show how large-scale differences between shifted exposures get considerably smaller after applying photometric flat-field correction (see the text).

The photometric flat-field corrections were derived (see Figure 2.2.2) by minimizing  $\chi^2$  sum in following equation:

$$\chi^2 = \sum_{i=1}^{N_i} (m_i^0 - m_i^{\text{RA}}) + \sum_{j=1}^{N_j} (m_j^0 - m_j^{\text{DEC}}), \quad (2.2.1)$$

where  $m^0$  is the magnitude for the central exposure,  $m^{\text{RA}}$  – for the exposure shifted in right ascension and  $m^{\text{DEC}}$  – for the exposure shifted in declination. The shift was set to 1/4 of CCD field of view.

In the case of proper flat-fielding, this  $\chi^2$  sum should contain only random errors, and the measured magnitudes of stars should not depend on their position in CCD frame. However, the presence of large-scale systematic errors in the data will always lead to increase of  $\chi^2$ .

We have used iterative procedures in our program to minimize  $\chi^2$  and to find the best fit (with a given function) to the large-scale systematic error in our data. Functions for a surface fit were chosen to be either two-dimensional Legendre cross-polynomials of the 2nd or 4th orders or two-dimensional low-order bi-cubic splines. For each filter we have used the best combination of those functions. We have tested our program on simulated star fields with non-uniformly distributed scattered light in flat fields. These tests have proved that the program can detect large-scale systematic errors from shifted field photometry data if we carefully choose the function to fit and if the effective large-scale offensive features in the flat field are larger than or equal to the shift size we have made in our exposures (Figure 2.2.1, right panels). Unfortunately, it was not technically possible to obtain an additional exposure (rotated by 180 degrees) with the Flagstaff telescope. This limited our capability to detect large-scale systematic errors in our data to only non-linear ones. Linear large-scale systematic errors in our data should have been determined by comparing the results of photometry with the external data.

We have established a good and uniform set of about 50 photoelectric standards in M67 in the *Vilnius* and *Strömvil* photometric systems. These photoelectric observations were obtained during three runs in 2000–2003 with the 1.5 m telescope of the Steward Observatory

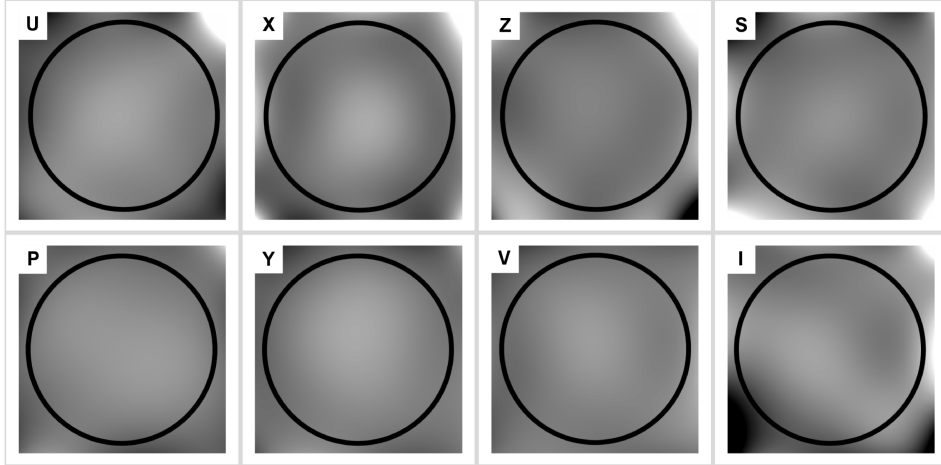


**Fig. 2.2.2.** Photometric corrections for flat fields. Only the circled unvignetted field of 20' diameter was used.

on Mt. Lemmon. The list of photoelectric standards for the *Vilnius* photometric system is given in Laugalys et. al 2004.

We have used these standards to calculate the coefficients for reduction of magnitudes in the instrumental CCD system to the standard *Vilnius* system by the following equation:

$$m_{\text{st}} = a + b \times X_{\text{pos}} + c \times Y_{\text{pos}} + d \times (Y - V) + e \times m_{\text{instr}} + f \times X_{\text{air}}, \quad (2.2.2)$$

where  $m_{\text{st}}$  is the magnitude (or color index) in the standard system,  $X_{\text{pos}}$  and  $Y_{\text{pos}}$  are the relative positions of the star in CCD frame being normalized within 0 and 1,  $m_{\text{instr}}$  is the magnitude (or color index) in the instrumental system and  $X_{\text{air}}$  is the weighted mean of the relative air-mass corresponding to the given exposure (important only for the  $U$  magnitude and  $U-V$  color index). For  $V-I$ , the coefficients  $b$  and  $c$  were determined by a linear fit of our instrumental colors to  $V-I$  of Sandquist (2004) and Stassun et al. (2002), and the coefficients  $a$  and  $d$  were calculated using 14 photoelectric standards of Joner & Taylor (1990). The coefficient values of Equation (2.2.2) are given in Table 2.2.2.

**Table 2.2.2.** Transformation coefficients of CCD magnitudes and color indices to the standard *Vilnius* system.

	$a$	$b$	$c$	$d$	$e$	$f$	$\sigma$	$N$
$V$	-1.0482	-0.0051	0.0153	-0.0406	1.0037	0	0.0078	47
$Y-V$	0.3995		0	1.0734	0	0	0.0067	50
$U-V$	1.7249		0	0.0061	1.0122	0.052	0.0082	47
$P-V$	1.7627		0	-0.2135	1.0334	0	0.0090	48
$X-V$	0.8959		0	-0.0105	-0.2295	1.0797	0	0.0061
$Z-V$	0.1848	0.0109	0.0168		0	1.1574	0	0.0044
$V-S$	1.2261	-0.0744	-0.0397		0	0.9155	0	0.0091
$V-I$	1.0337		0	0.0450	-0.0293	0	0	14

The final catalog contains 412 stars with magnitudes and color indices down to  $V = 16$  mag. The stars brighter than  $V \sim 10$  mag, saturated in CCD exposures, are not included. The catalog also does not contain known physical and optical binary stars, but variable stars are included. Instrumental errors of magnitude  $V$  and color indices as a function of  $V$  are shown in Figure 2.2.3. Identification charts and catalog are given in Laugalys et. al 2004.

### 2.2.3. Comparison With Other Photometric Data

In this section we compare our  $V$  magnitudes (and color indices, in some cases) of M 67 with similar magnitudes in other photometric systems, with special emphasis on detecting possible large-scale systematic errors in different data-sets.

Since photoelectric photometry does not suffer from flat-fielding effects, it is most suitable for testing the CCD results. We have about 50 stars measured photoelectrically in the *Vilnius*

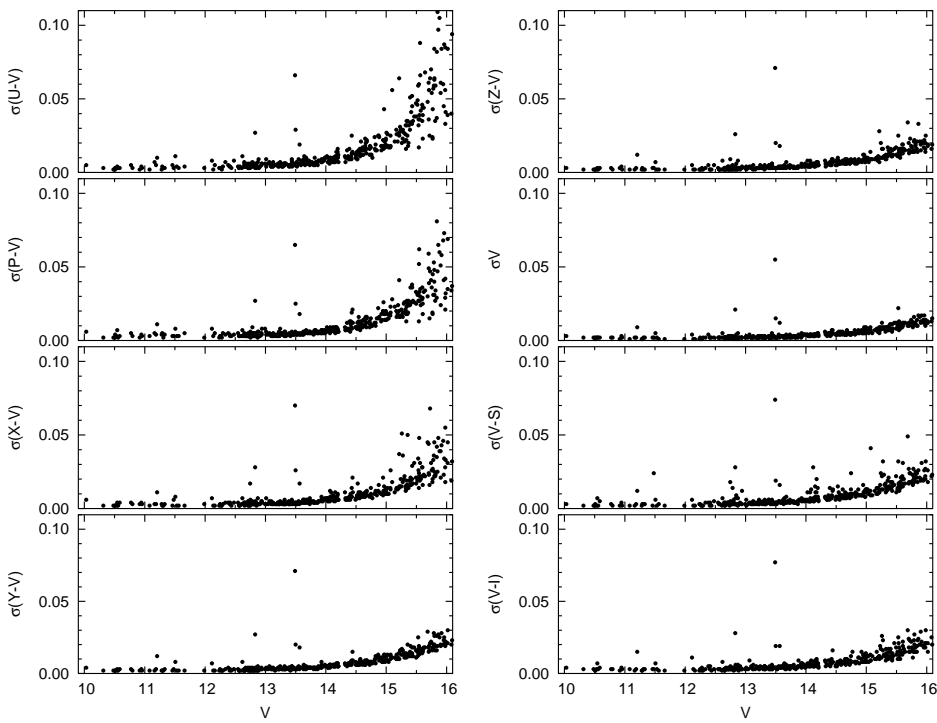


**Fig. 2.2.3.** Standard deviations of  $V$  magnitudes and color indices of the new M 67 catalog.

system scattered across the Flagstaff CCD field, and they may be used to detect possible large-scale flat-fielding errors. Figure 2.2.6 shows a comparison of the CCD and photoelectric data for  $V$  magnitudes and  $U-V$  color indices. It is obvious that the agreement of both data-sets is very good, with no large-scale systematic errors exceeding  $\pm 1\%$ . Because of this excellent agreement, we can use our CCD photometry as a benchmark to investigate potential systematic errors in previous CCD investigations of M 67.

For the next comparison we use the multicolor CCD data of M 67 published by the Beijing-Arizona-Taipei-Connecticut (hereafter *BATC*) group (Fan et al. 1996). Since their photometric system does not contain a filter close to  $V$ , we have calculated  $V_{\text{BATC}}$  magnitudes from  $m_{5795}$  using their Eq. (4). The magnitudes  $V_{\text{BATC}}$  and  $V_{\text{VIL}}$  are compared in Figure 2.2.7. Left panels show that there are some systematic differences between  $V_{\text{BATC}}$  and  $V_{\text{VIL}}$  depending on  $Y-V$ , with the scatter increasing for fainter stars. In the right panels, however, which exclude faint stars and are limited within a narrow color range, no large-scale position-dependent differences, exceeding  $\pm 1\%$ , are seen.

Another wide-field  $BV$  CCD photometry of M 67 was obtained by Momany et al. (2001, hereafter ESO) with the 2.2 meter telescope at ESO. We find very large systematic differences between  $V_{\text{ESO}}$  and  $V_{\text{VIL}}$  data-sets as it is shown in Figure 2.2.8 (left panels). The comparison of  $V_{\text{ESO}}$  and  $V_{\text{BATC}}$  (Figure 2.2.8, right panels) reveals even larger errors (up to 10%) which likely are related with systematic flat-field errors of the ESO observations.

Figure 2.2.9 shows the comparison of  $V$  magnitudes from the Montgomery, Marshall & Janes (1993) data-set (hereafter MMJ) with our magnitudes (left panels) and the reduced *BATC* magnitudes (right panel). Along the RA axis there are several inclined strips of about 5–6% amplitude. Thus, MMJ photometry is also affected by considerable systematic errors which likely originate in incorrect flat-fielding.

Similar large-scale errors are also present in the  $I$  magnitudes. However, since the systematic errors for  $V$  and  $I$  are of similar size, they cancel each other in the  $V-I$  color index (Figure 2.2.10). Also, there is a zero point difference of about 0.02–0.03 mag between our and MMJ  $V-I$  data.

Gilliland et al. (1991) have published a search for M 67 stellar variability with an accuracy of their differential photometry better than 1 mmag for the brightest stars. They also gave the absolute calibration for their photometry. The comparison of their  $V$  magnitudes with our  $V$  and with  $V_{\text{BATC}}$  is shown in Figure 2.2.11. Even though their field of view is small, we find radial systematic errors of the order of 2–3%.

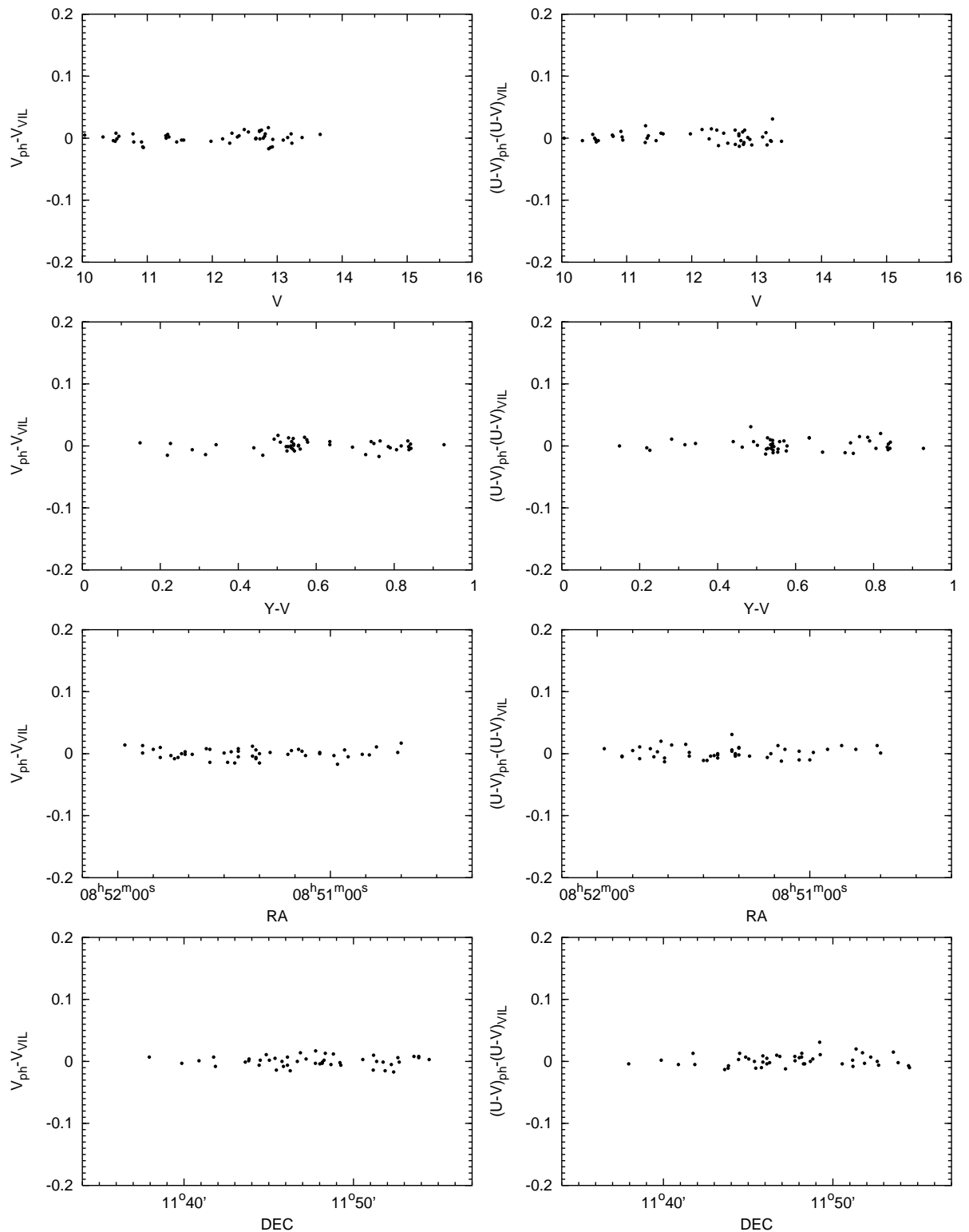


**Fig. 2.2.6.** Differences between the photoelectric and CCD data for  $V$  magnitude and  $U - V$  color index as the functions of  $V$ ,  $Y - V$ , RA and DEC.

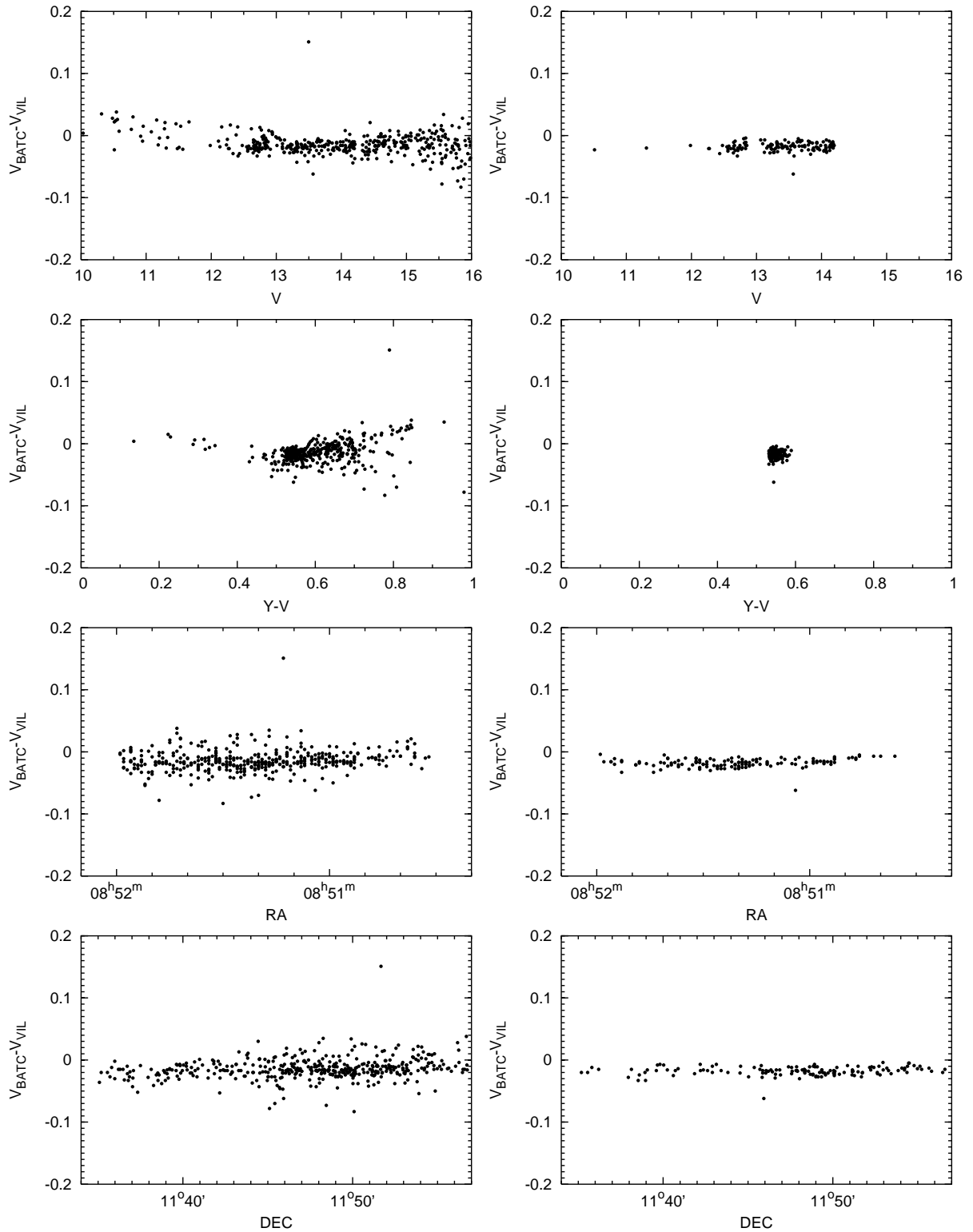


**Fig. 2.2.7.** Differences between the  $V_{BATC}$  and  $V_{VIL}$  magnitudes. Left panels show all 412 stars in common, and right panels are only for the stars brighter than 14.2 mag in  $V$  and within the narrow color interval:  $0.53 < Y - V < 0.59$ .

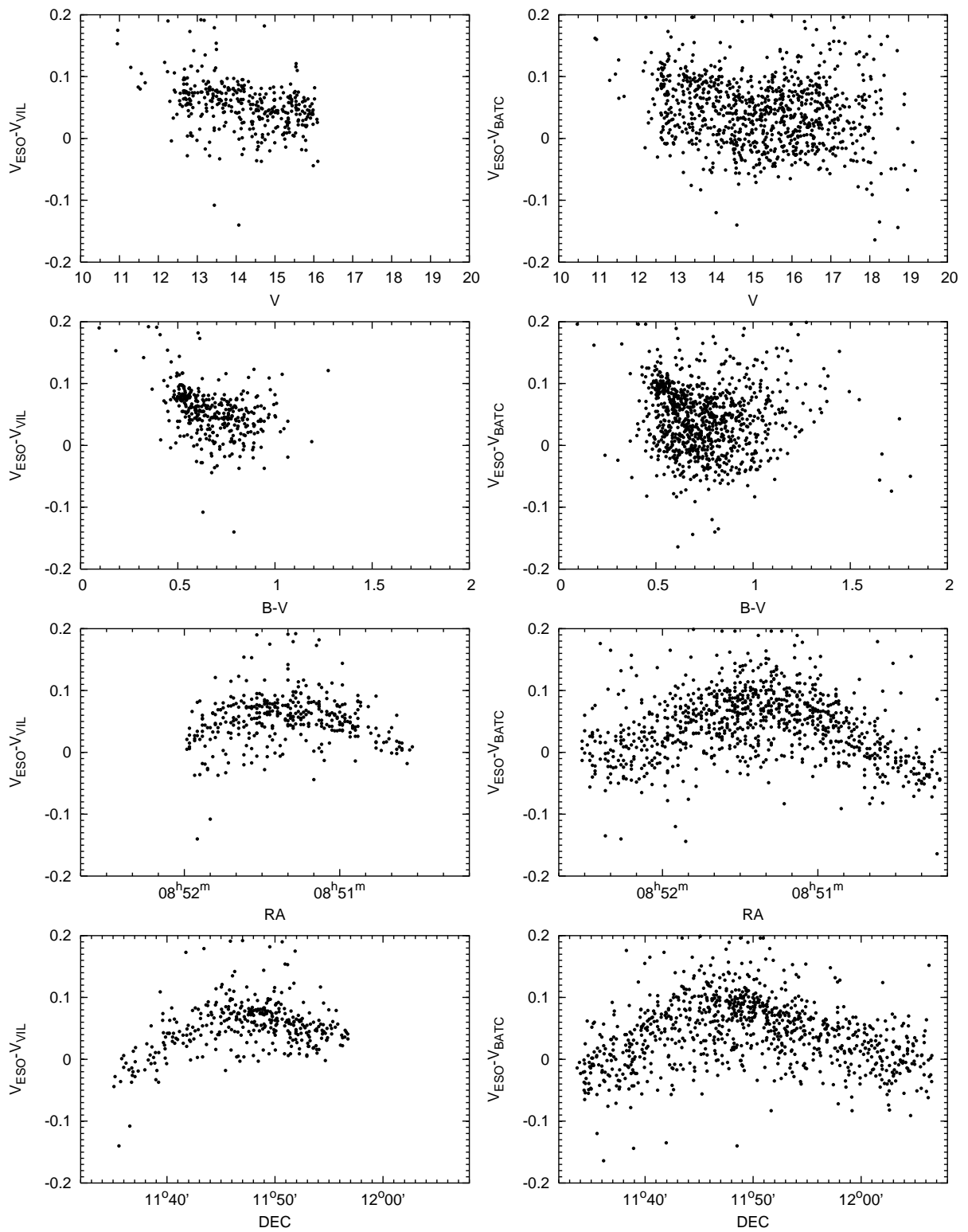


**Fig. 2.2.8.** Differences between  $V_{\text{ESO}}$  and  $V_{\text{VIL}}$  (left panels), and between  $V_{\text{ESO}}$  and  $V_{\text{BATC}}$  (right panels). Large-scale systematic errors up to 10% are seen in the ESO data.

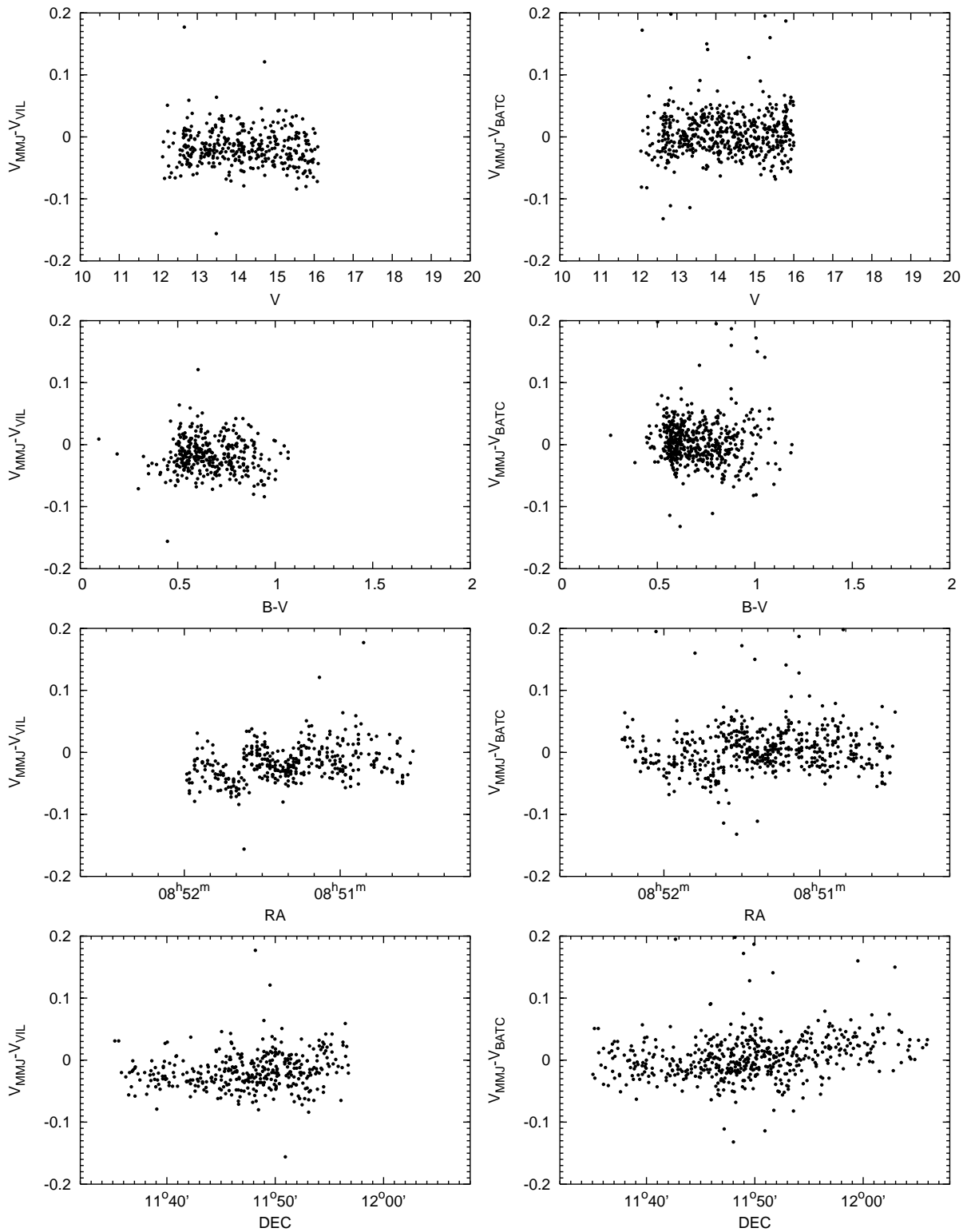


**Fig. 2.2.9.** Differences between  $V_{\text{MMJ}}$  and  $V_{\text{VIL}}$  magnitudes (left panels), and  $V_{\text{MMJ}}$  and  $V_{\text{BATC}}$  magnitudes (right panels). This comparison reveals 5–6% large-scale systematic errors along RA in the MMJ photometry.

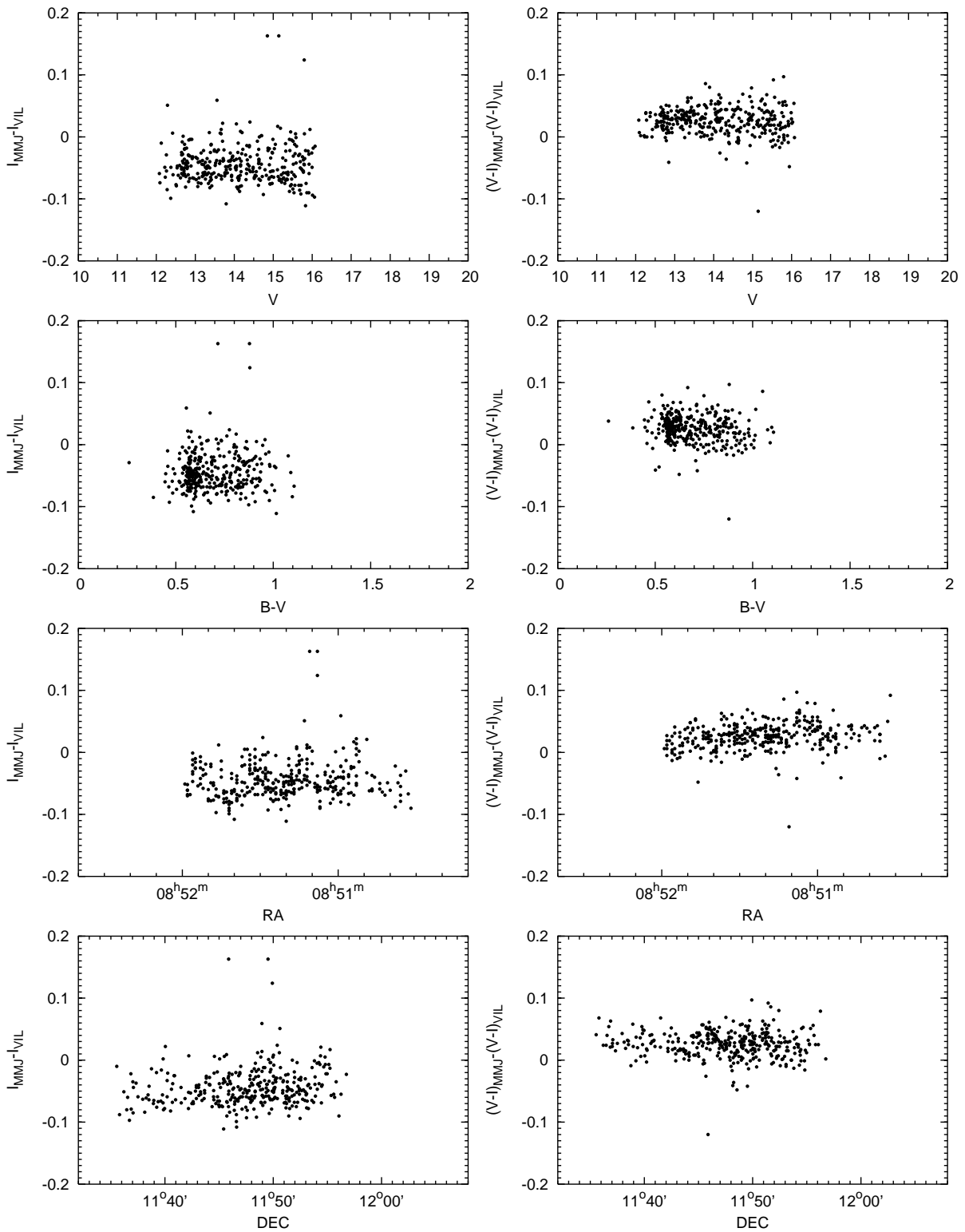


**Fig. 2.2.10.** Differences between  $I_{\text{MMJ}}$  and our  $I_{\text{VIL}}$  (left panels), and between  $(V-I)_{\text{MMJ}}$  and our  $(V-I)_{\text{VIL}}$  (right panels). This comparison also shows large-scale systematic errors of 5–6% along RA in the MMJ photometry.

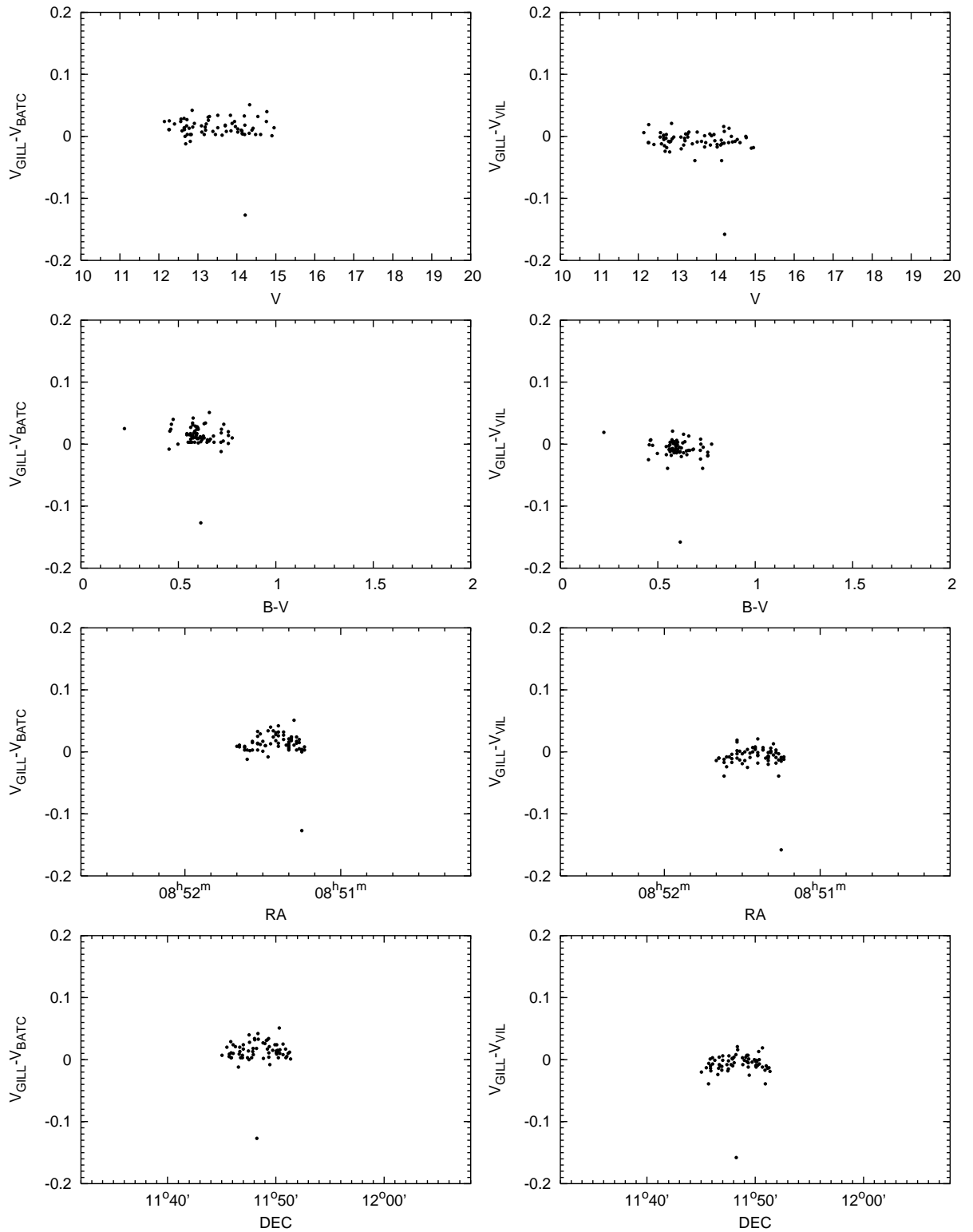


**Fig. 2.2.11.** Differences between  $V_{\text{GILL}}$  from Gilliland et al. (1991) and  $V_{\text{BATC}}$  (left panels), and between  $V_{\text{GILL}}$  and  $V_{\text{VIL}}$  (right panels). This comparison reveals the radial large-scale systematic errors of the Gilliland et al. data up to 2–3%.

A color-magnitude diagram of M 67 with high relative precision was published by Sandquist (2004). He has used his own CCD photometry and *BATC* photometry from Fan et al. (1996) to determine precisely the single-star sequence of M 67. In Figure 2.2.12 we compare Sandquist's  $V$  magnitudes with the corresponding magnitudes in our and *BATC* photometries. Large-scale systematic errors of up to 5–6% are detected. We conclude that the Sandquist magnitudes are less accurate than the magnitudes from our and *BATC* catalogs.

However, Sandquist's and our color indices  $V-I$  are in good agreement within  $\pm 1\%$ , as can be seen in Figure 2.2.13. This can be explained by similarity of large-scale systematic errors in his  $V$  and  $I$  filters. These errors disappear in taking the magnitude difference (like  $V-I$  of MMJ, as was shown earlier).

Another photometric variability study of M 67 stars was published by Stassun et al. (2002). Comparison of their  $V$  magnitude with  $V_{VIL}$ ,  $V_{BATC}$  and  $V_{MMJ}$  shows systematic errors up to 4–6% over 5 magnitude interval (see Figure 2.2.14) caused probably by a response nonlinearity of the CCD chip. Correcting their  $V$  magnitudes for nonlinearity (by a simple linear fit) and then comparing with  $V_{VIL}$ ,  $V_{BATC}$  and  $V_{MMJ}$  allows us to test their data for large-scale errors (Figure 2.2.15). While the corrected  $V_{STAS}^*$  data agree with our data within 1–2%, they differ from  $V_{BATC}$  up to 4%: this happens due to the fact that *BATC* photometry covers the whole field of Stassun et al. while our field is smaller. Comparison of  $V_{STAS}^*$  with  $V$  of MMJ shows the complicated large-scale differences since systematic errors of both data-sets are convolved.

The  $V-I$  color indices of Stassun et al. (2002) show a smaller scatter when compared with the same indices in our and MMJ photometry (Figure 2.2.16). However, a zero-point offset of the order of 0.1 mag is seen. Note also that  $(V-I)_{STAS}$  shows smaller scatter when compared with our  $(V-I)_{VIL}$  data (left panels) than with  $(V-I)_{MMJ}$  (right panels). Although large-scale errors for  $V_{MMJ}$  and  $I_{MMJ}$  are similar (see Figure 2.2.12), they do not eliminate each other completely in  $(V-I)_{MMJ}$ , increasing the  $(V-I)_{MMJ}$  random errors.

The accuracy of photometry can also be estimated by looking at the scatter of stars in the CMD diagram of M 67 (Figure 2.2.17). It is evident that the *Vilnius* and the *BATC* magnitudes and color indices are of comparable accuracy, while the ESO and MMJ photometry are less accurate. This confirms that our method of flat-fielding, which uses the shifted exposures of the standard stars, gives good results.

## 2.2.4. Conclusions

We have obtained high accuracy photometry for 412 stars of the M 67 cluster down to  $V=16$  mag in the *Vilnius* photometric system, supplemented by a broad-band  $I$  passband. For all stars photometric spectral types were estimated and used in determining the interstellar reddening and extinction of the cluster.

Comparison of  $V$  magnitudes and  $V-I$  color indices of different CCD photometric investigations of M 67 (Table 2.2.3) leads to the conclusion that some data-sets contain large systematic errors due to insufficient accuracy of flat-fielding. The best agreement is found between  $V$  in *Vilnius* and *BATC* photometries. The internal accuracy at  $V=16$  in both investigations is comparable:  $\sim 0.015$  mag in *Vilnius* and  $\sim 0.020$  in *BATC*, and the large-scale errors across the field of about  $20'$  diameter do not exceed 1–2%. The internal accuracy of  $V$  magnitudes is also high in ESO photometry but it exhibits large-scale systematic errors up to 10% across the field. MMJ photometry has a reasonable internal accuracy ( $\sim 0.02$  mag at  $V=16$ ), but large-scale systematic errors are as large as 5–6%. Gilliland's and Sandquist's photometries both have high internal accuracy and radial errors of the order of 2–3% and 5%, respectively. Stassun's photometry has high internal accuracy but systematic errors due to nonlinearity of CCD response (up to 5%) and large-scale errors up to 2–5%. For achieving an overall accuracy of 0.01 mag, the data reduction methods in most of the investigations should be improved.

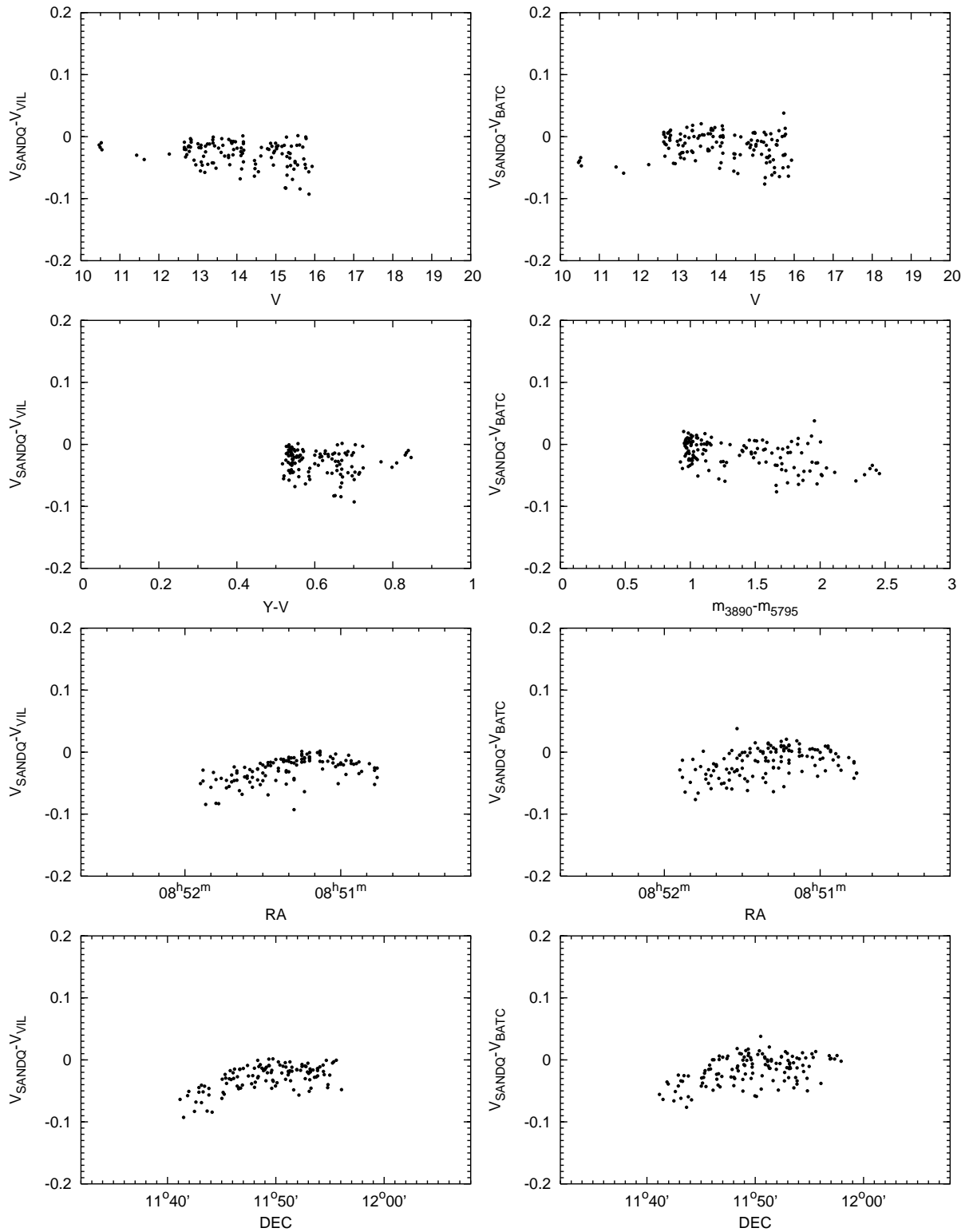


**Fig. 2.2.12.** Differences between  $V_{\text{SANDQ}}$  from Sandquist (2004) and  $V_{\text{VIL}}$  (left panels), and between  $V_{\text{SANDQ}}$  and  $V_{\text{BATC}}$  (right panels). This comparison reveals 5–6% large-scale systematic errors in the Sandquist photometry.

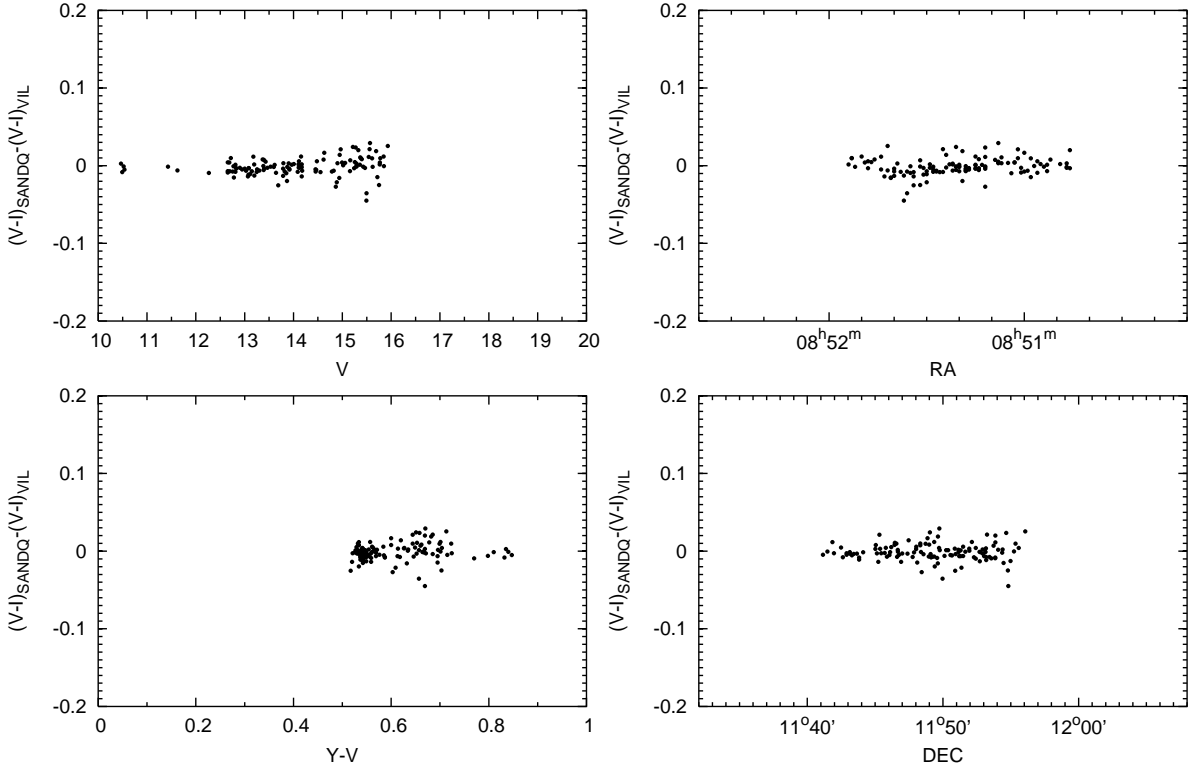


**Fig. 2.2.13.** Differences between  $(V-I)_{\text{SANDQ}}$  from Sandquist (2004) and  $(V-I)_{\text{VIL}}$ . Both photometries agree within  $\pm 1\%$  because large-scale systematic errors of  $V$  and of  $I$  in the Sandquist (2004) data are similar and nullify each other in forming the  $V-I$  color index.

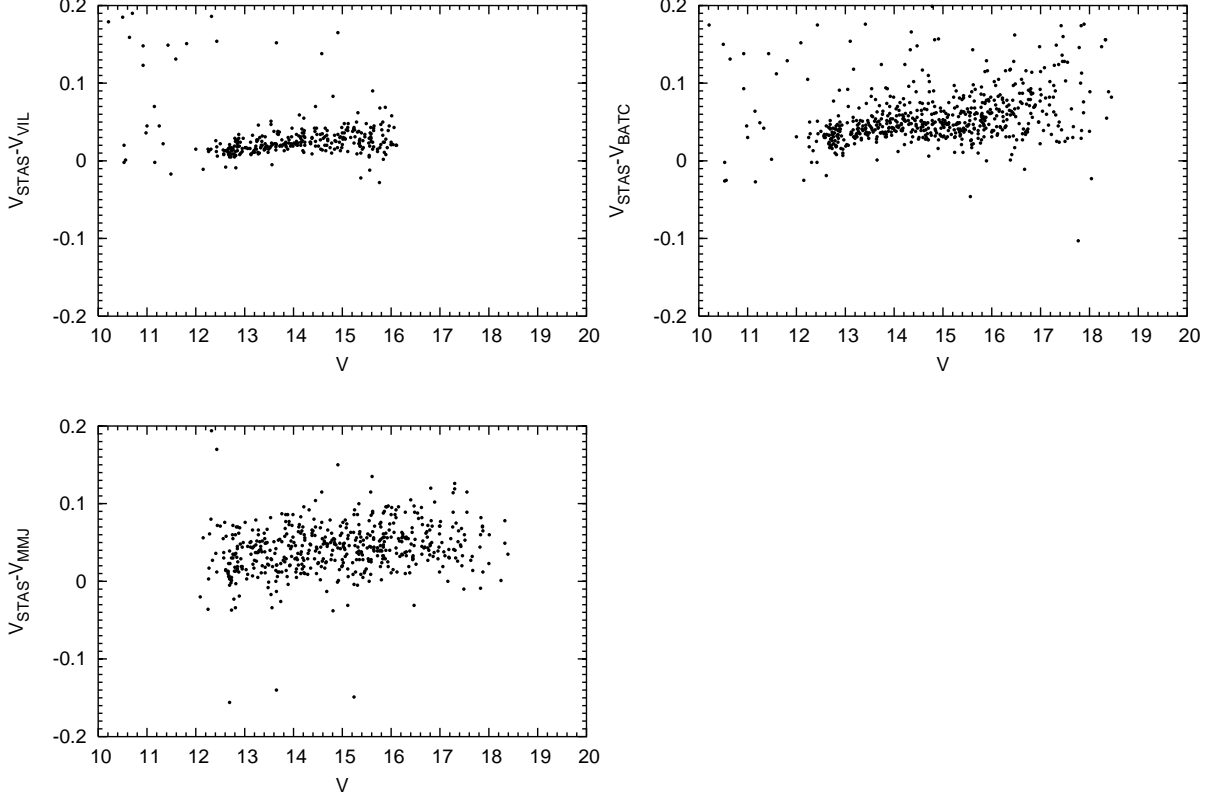


**Fig. 2.2.14.** Differences between  $V_{\text{STAS}}$  from Stassun et al. (2002) and  $V_{\text{VIL}}$ ,  $V_{\text{BATC}}$  and  $V_{\text{MMJ}}$ . Nonlinearity errors up to 4–6% over 5 magnitudes are seen in the Stassun et al. photometry.

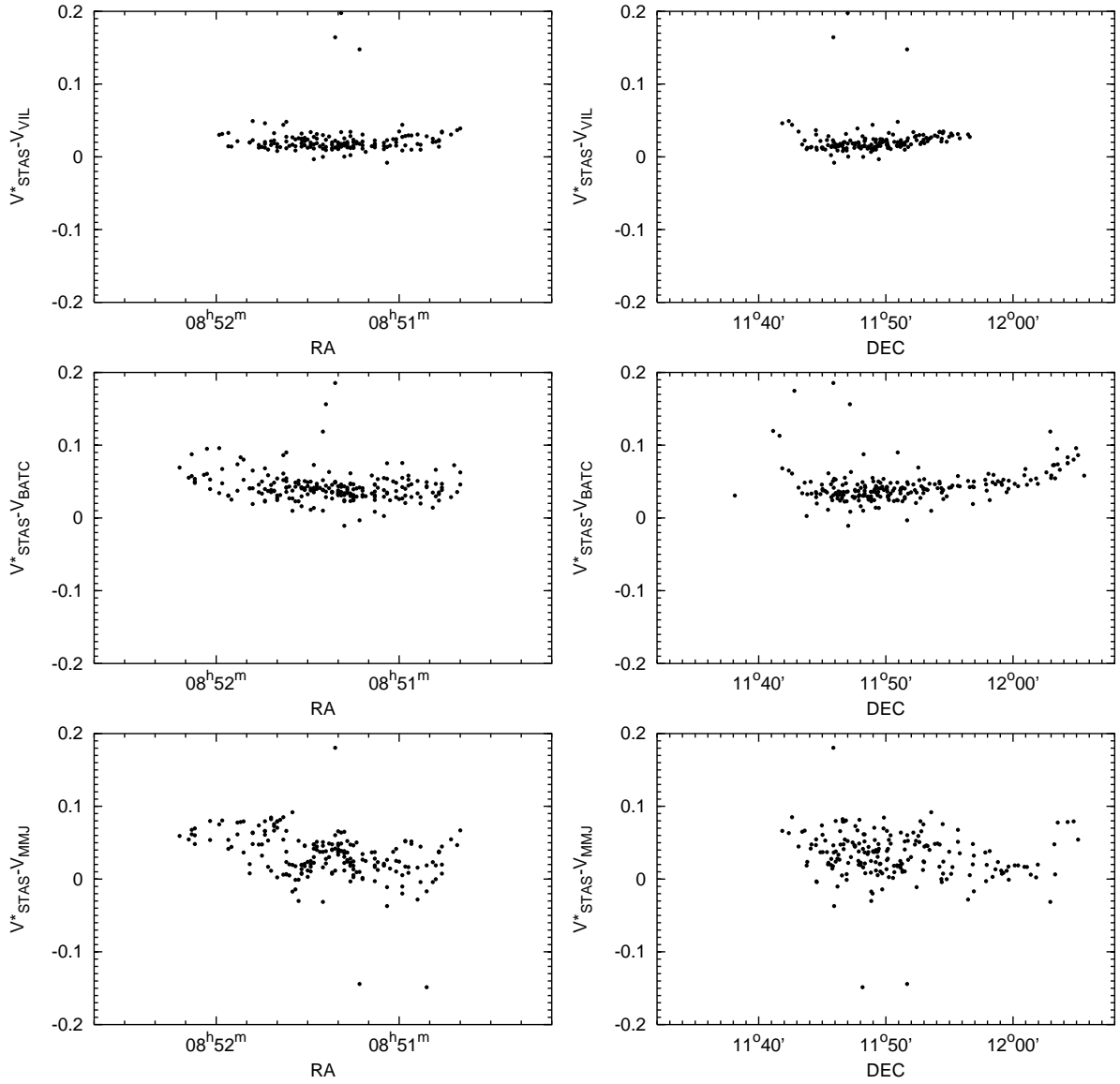


**Fig. 2.2.15.** Differences between the Stassun et al. (2002) magnitudes  $V_{\text{STAS}}^*$ , corrected for nonlinearity and  $V_{\text{VIL}}$ ,  $V_{\text{BATC}}$  and  $V_{\text{MMJ}}$ . This comparison reveals large-scale systematic errors of 2–4% in Stassun et al. (2002)  $V$  photometry (see the text for details).

**Table 2.2.3.** The comparison of CCD  $V$  magnitudes of M 67 stars.

Photometry	System	Field of view	Number of stars	Errors at $V=16$	Large-scale errors
Vilnius	<i>Vilnius + I</i>	$\sim 20'$	412	~0.015	1–2%
BATC	<i>BATC</i>	$> 1^\circ$	6558	~0.020	1–2%
ESO	<i>BV</i>	$\sim 33'$	4290	~0.005	10%
MMJ	<i>UBVI</i>	$30'$	1468	~0.020	5–6%
Gilliland	<i>UBVRI</i>	$6'$	257	~0.010	2–3%
Sandquist	<i>BVI</i>	$\sim 17'$	168	~0.003	5%
Stassun	<i>BVI</i>	$23'$	977	~0.010	2–5%

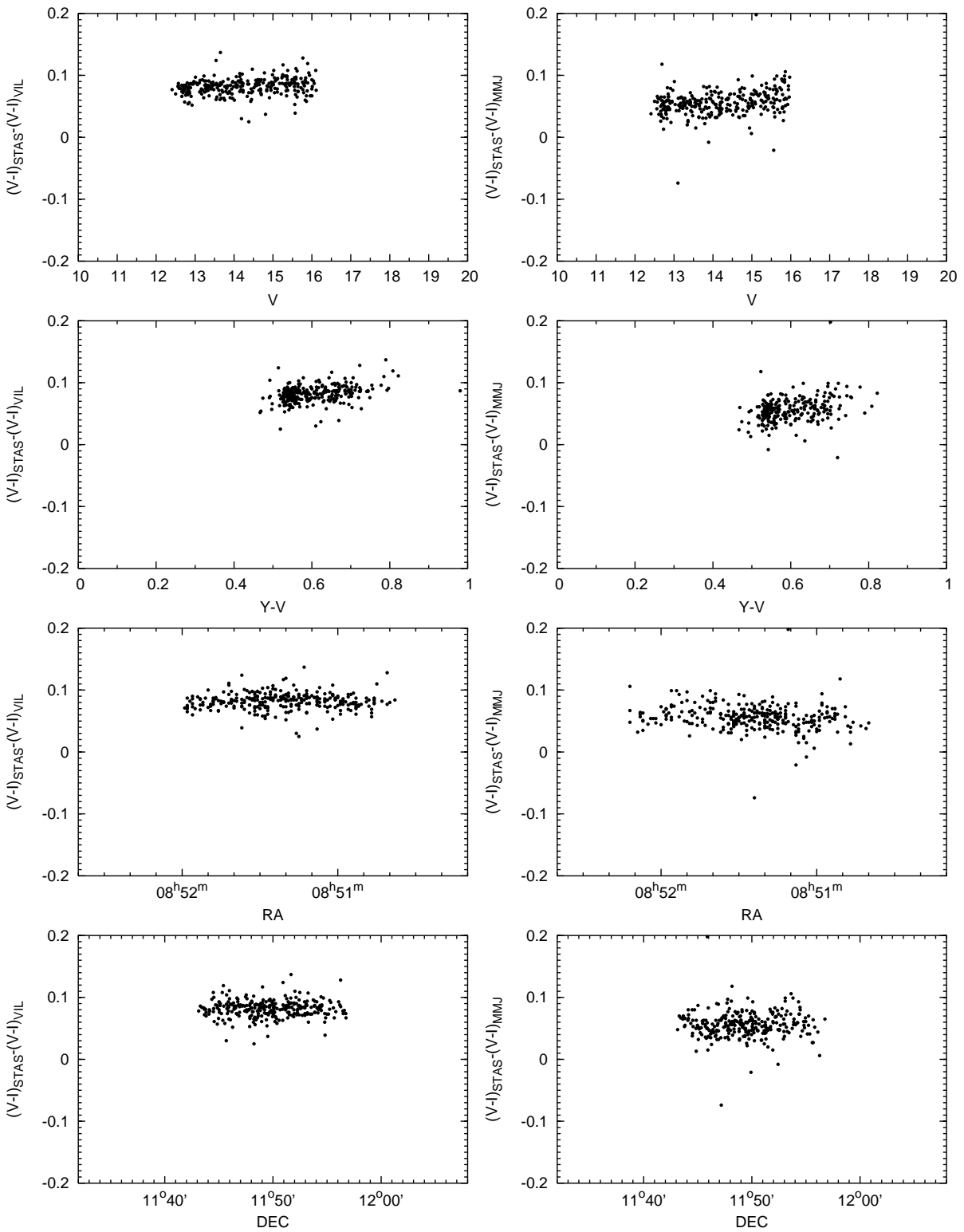


**Fig. 2.2.16.** The differences of the Stassun et al. (2002)  $(V-I)_{\text{STAS}}$  color indices and  $(V-I)_{\text{VIL}}$  and  $(V-I)_{\text{MMJ}}$ . While large-scale errors in  $(V-I)_{\text{STAS}}$  in comparison with our data are within  $\pm 1\%$ , a 0.1 mag offset is present (see the text for more details).

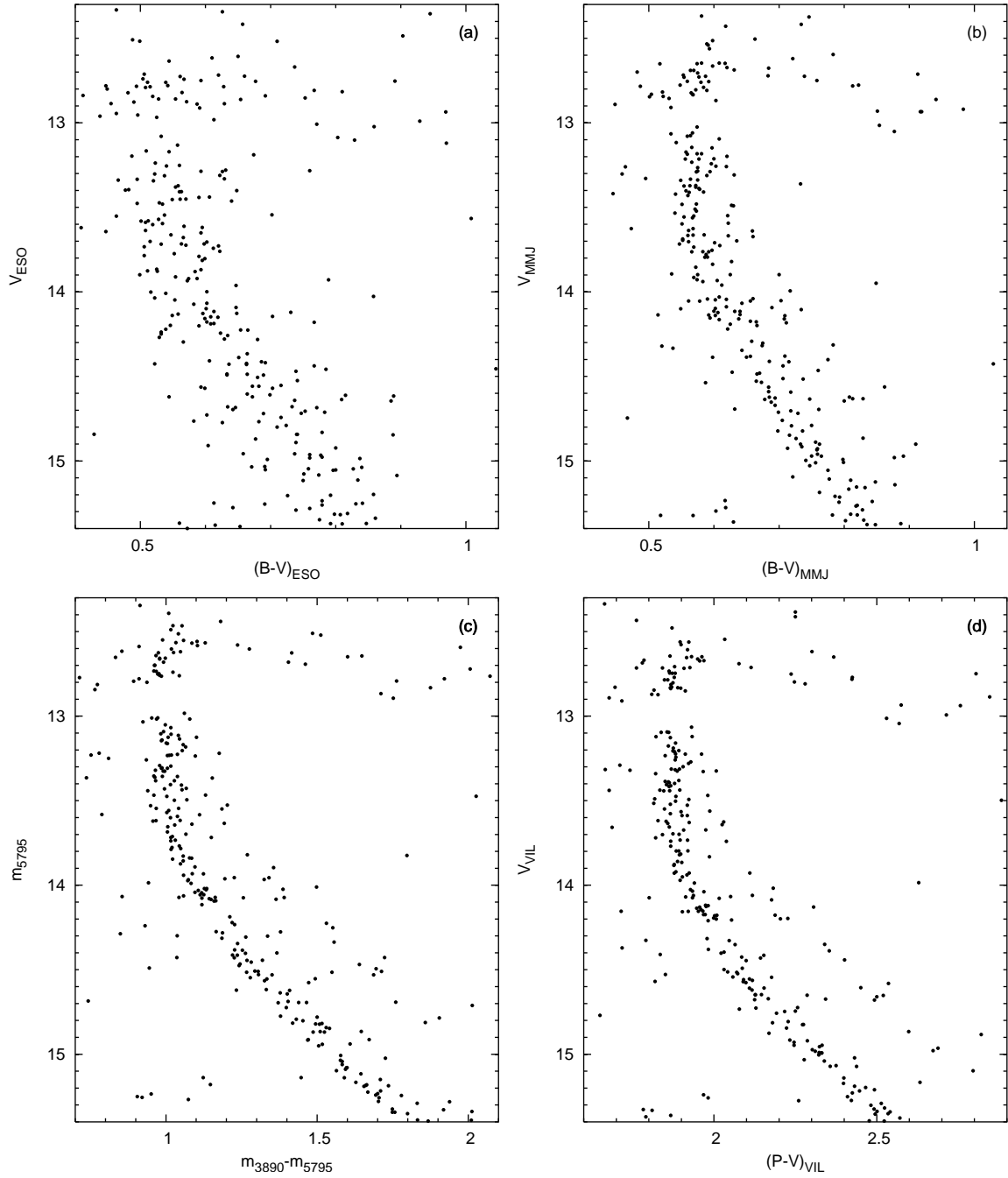


**Fig. 2.2.17.** CMD diagrams of M67 near the main-sequence turnoff plotted using the magnitudes and color indices from the following CCD data-sets: (a) ESO, (b) MMJ, (c) BATC and (d) Vilnius. In all panels the same stars are plotted. The sharpness of gaps in the main sequence at  $V \approx 13.0$  and  $V \approx 14.2$ , the subgiant and binary sequences can be used as the indicators of photometric accuracy.

## 2.2.5. Observed Targets and Data Reductions: NGC 6997

The area centered on RA (2000) =  $20^{\text{h}}56.5^{\text{m}}$ , DEC (2000) =  $+44^{\circ}35'$  ( $\ell = 85.4^{\circ}$ ,  $b = -0.5^{\circ}$ ) contains the NGC 6997 cluster which is registered  $4'$  north of the field center to avoid some CCD defects. The field of view was  $20'$  in diameter. CCD frames in the seven filters of the *Vilnius* photometric system and the  $I$  filter of the *Cousins* system were obtained in November 2000 on the 1 meter Ritchey telescope of the USNO Flagstaff Station with a nitrogen-cooled Tektronix CCD camera ( $2048 \times 2048$  pixels). The exposure durations were 30 min for  $U$ ,  $P$  and  $X$ , 6 min for  $Y$ ,  $Z$ ,  $V$  and  $S$ , 3 min for  $I$  filters.

For reductions the IRAF 2.11 software package was used. Instrumental CCD magnitudes were determined by PSF photometry. Flat-fielding corrections were obtained from twilight exposures with macro corrections determined from multiple exposures of the standard field – open cluster M 67 (for details see Laugalys et al. 2003 or Section 2.2.2).

The measured stars are identified in Laugalys et al. 2006a (Figures 1 and 2) and Figure 3 shows the rms errors  $\sigma$  for the magnitude  $V$  and seven color indices. For the stars brighter than  $\sim 15$  mag the values of  $\sigma$  in all colors are  $< 0.015$  mag. For these stars a good classification accuracy is expected. For the majority of stars down to 15.5 mag  $\sigma$  does not exceed 0.02 mag: their classification should also be of reasonable accuracy. For fainter stars  $\sigma$  of  $U-V$ ,  $P-V$  and  $Y-V$  color indices is  $> 0.03$  mag, and this accuracy is too low to allow two-dimensional spectral classification of stars. However, stars of K and M spectral classes can be classified in two dimensions even without the ultraviolet magnitudes  $U$  and  $P$ . As a result, they can be identified to much fainter limiting magnitude than the hotter stars.

Instrumental  $V$  magnitudes and  $U-V$ ,  $P-V$ ,  $X-V$ ,  $Y-V$ ,  $Z-V$  and  $V-S$  color indices were transformed to the standard *Vilnius* system by color equations obtained for the cluster M 67 observed with the same equipment. Zero points of the transformation equations were fixed by *Vilnius* photometry of 22 stars of magnitudes 10–13 from Zdanavičius & Straizys 1990 (hereafter ZS90). The zero-point of  $V-I$  color indices in the *Cousins* system was defined by using 200 brightest NGC 6997 stars from Villanova et al. (2004). However, these color indices have not been used in classification.

$Q$ -parameters were calculated with the ratios taken for the Cygnus interstellar reddening law from Sūdžius (1974, Table 4b) which, according to the study of Straizys, Corbally & Laugalys (1999), is valid in the North America and Pelican nebulae area.

The results of photometry for 620 stars down to  $V = 17.5$  are given in Table 2.2.4 (see in Appendix) which lists the identification number, the coordinates for 2000.0,  $V$  magnitudes, six *Vilnius* color indices,  $V-I$ , photometric spectral types, interstellar extinctions, distances and the probable cluster membership determined as described in sections 2.2.8, and 5.1. The lower-case letters indicate that our spectral classes are determined photometrically. The last column also contains the numbers from ZS90.

## 2.2.6. Observed Targets and Data Reductions: The Dark Cloud L 935

CCD frames of four areas in the seven filters of the *Vilnius* photometric system and the  $I$  filter of the *Cousins* system were obtained in 1994–2001 on the 1 meter Ritchey telescope of the USNO Flagstaff Station. The exposure durations were the same as for NGC 6997. The centers of the three areas are at similar declinations DEC(2000) =  $+43^{\circ} 50'$  and at right ascensions RA(2000) =  $20^{\text{h}}55^{\text{m}}$ ,  $20^{\text{h}}57^{\text{m}}$  and  $20^{\text{h}}59^{\text{m}}$ . The center of the fourth area is at RA(2000) =  $20^{\text{h}}54^{\text{m}}40^{\text{s}}$ , DEC(2000) =  $+44^{\circ}30'$ .

The measured stars are identified in Laugalys et al. 2006b (Figures 2–5), Figures 6 and 7 show the rms errors  $\sigma$  for the magnitude  $V$  and six color indices. CCD data reductions and transformations to the standard system were identical to NGC 6997. Zero points of the transformation equations were fixed by photoelectric and CCD photometry of stars of magnitudes 10–13 observed earlier.

For the calculation of  $Q$ -parameters the ratios of color excesses were taken for the normal interstellar reddening law from Straizys (1992) which gives somewhat lower photometric classification errors than the Cygnus law used for NGC 6997.

The results of photometry for 430 stars in the four areas down to  $V = 17.5$ – $18.0$  are given in Tables 2.2.5, 2.2.6, 2.2.7 and 2.2.8 (see in Appendix) which list the identification number, the coordinates for 2000.0,  $V$  magnitudes, six *Vilnius* color indices, photometric spectral types, interstellar extinctions and distances, determined as described in Section 2.2.8. The lower-case letters indicate that our spectral classes are determined photometrically. We do

not publish the results of  $I$  photometry since they are not reduced to the standard system due to the absence of  $I$  standards in the investigated areas. Since Areas II and III partly overlap, there are nine stars common between Tables 2.2.6 and 2.2.7. They are listed in the Notes to Table 2.2.7.

### 2.2.7. Observed Targets and Data Reductions: Collinder 428

In 1991–1996 K. Černis measured 118 stars in and around the cluster in the *Vilnius* photometric system with a photoelectric photometer on the 1 m telescope located at the Maidanak Observatory. The results of the photometry are available from the author. However, the limiting magnitude of photometry (13 mag) was too low to determine stellar classifications and distances with sufficient accuracy. Also, some stars in the list later were found to be multiple stars which were unresolved in photoelectric photometry. Therefore we decided to extend photometry to fainter stars by CCD techniques using the stars measured by K. Černis as zero-point standards.

CCD frames in the seven filters of the *Vilnius* photometric system and the  $I$  filter of the *Cousins* system were obtained in November of 2000 on the same 1 meter Ritchey telescope.

The exposure durations were the same as for NGC 6997 and L 935. The area was centered on RA (2000) =  $21^{\text{h}}3.2^{\text{m}}$ , DEC (2000) =  $+44^{\circ}35'$  ( $\ell = 86.2^{\circ}$ ,  $b = -1.4^{\circ}$ ), the cluster center given by the Webda database. The field of view was  $20'$  in diameter.

CCD data reductions and transformations to the standard system were also identical to NGC 6997 and L 935. The measured stars are identified in Laugalys et al. 2007. Zero points of the transformation equations were fixed by *Vilnius* photometry of stars of magnitudes 10–13 selected from the Černis measurements. Since  $I$  magnitude standards in the investigated area were absent, the results were left in the instrumental system and remain unpublished.

The accuracy of photometry in this area is somewhat lower than in the areas of NGC 6997 and the dark cloud L 935. For the stars brighter than  $\sim 14$  mag the  $\sigma$  values in all colors are  $\leq 0.02$ . For these stars a good classification accuracy is expected. With decreasing brightness the number of outstanding points in color indices containing ultraviolet and violet passbands increases, and the accuracy of the classification falls. This is explained by the fact that the ultraviolet and violet parts of stellar spectra of late-type stars and stars affected by interstellar reddening are much fainter than in the  $V$  passband. A sufficiently good classification accuracy is expected for the stars down to 15 mag for stars of spectral classes K and M, since for their classification in two dimensions we do not need the ultraviolet magnitudes  $U$  and  $P$ .

The results of photometry for 860 stars down to  $V = 16.7$  are given in Table 2.2.9 (see in Appendix) which lists the identification number, the coordinates for 2000.0,  $V$  magnitudes, six *Vilnius* color indices, photometric spectral types, interstellar extinctions and distances in parsecs. The lower-case letters indicate that our spectral classes are determined photometrically. Color indices with  $\sigma \geq 0.05$  mag are marked by colons. If  $\sigma \geq 0.1$ , color indices are not given.

Spectral and luminosity classes were determined for 290 stars as described in section 2.2.8.  $Q$ -parameters were calculated with the ratios taken for the Cygnus interstellar reddening law but in case of the normal reddening law classification differences are very small.

Color excesses  $E_{Y-V}$ , extinctions  $A_V$  and distances  $d$  of the stars were calculated as described in section 2.2.8. For the stars brighter than  $V = 15$  the following values of  $3\sigma$  errors for the determined quantities are expected (including the cosmic dispersion):  $\pm 0.03$  mag for color excesses,  $\pm 0.1$  mag for extinctions,  $\pm 0.5$  mag for absolute magnitudes and  $(-20, +26)\%$  for distances.

### 2.2.8. Classification of Stars and Their Color Excesses, Extinctions and Distances

For photometric classification of stars the “stellar box” method has been used. When all six color indices available, spectral types were determined by using the method of matching of 14 different interstellar reddening-free  $Q$ -parameters of a program star to those of about 12000 standard stars of various spectral and luminosity classes, metallicities and peculiarity types from the General Photometric Catalog of Stars Observed in the *Vilnius* System (Straižys & Kazlauskas 1993). The  $Q$ -parameters are defined by the equation:

$$Q_{1234} = (m_1 - m_2) - (E_{12}/E_{34})(m_3 - m_4), \quad (2.2.3)$$

where  $m$  are the magnitudes in four (sometimes three) passbands,  $m_1 - m_2$  and  $m_3 - m_4$  are the two color indices and  $E_{12}$  and  $E_{34}$  are the corresponding color excesses. The

$E_{12}/E_{34}$  ratio slightly depends on spectral type, and this dependence is taken into account by iterations. The ratios are taken for the Cygnus interstellar reddening law which, according to the study of Straizys, Corbally & Laugalys (1999), is valid in the North America and Pelican nebulae.

The matching of  $Q$ -parameters leads to a selection of some standard stars with a set of  $Q$ s most similar to those of the program star. The match quality is characterized by

$$\sigma Q = \pm \sqrt{\frac{\sum_n \Delta Q_i^2}{n}}, \quad (2.2.4)$$

where  $\Delta Q$  are differences of corresponding  $Q$ -parameters of the program star and the standard,  $n$  is a number of the compared  $Q$ -parameters (in our case,  $n = 14$ ). For the stars observed with an accuracy of  $\pm 0.01$  mag, the  $\sigma Q$  value is of the order of  $\pm 0.01$ – $0.02$  mag. In such a case the match is considered to be sufficiently good, and the spectral type (spectral class + luminosity class) of the standard star may be prescribed to the program star. In our case, for the program star we have accepted the average spectral and luminosity classes of the three to five best matching stars. Since the errors of the observed color indices for a part of the stars is  $> 0.01$  mag, their classification accuracy is lower. If the matching accuracy was of the order of  $\pm 0.03$  mag or larger, the star was not classified at all.

In the case when one or two ultraviolet color indices of a star were missing, we have used the same method, but the number of the  $Q$ -parameters was smaller: in the absence of  $U-V$ ,  $n$  was 10, in the absence of  $U-V$  and  $P-V$ ,  $n$  was 7. The accuracy of classification in these cases for B–A–F–G stars was lower, especially in luminosity classes. For two-dimensional classification of K and M stars the ultraviolet color indices are not essential.

For the estimation of the classification accuracy in the range of spectral classes B0–K0, we have made the following test. The real program stars were replaced by the test stars having the mean intrinsic color indices instead of the observed ones. After that the matching classification method was applied, taking  $\sigma Q$  values  $\leq 0.02$  mag.

The conclusion is made that spectral classes of B–A–F stars are determinable with acceptable accuracy when all color indices are available or only color indices  $U-V$  are missing. In the case if  $U-V$  and  $P-V$  color indices are missing, the accuracy of spectral classes of these stars is very different in various spectral class ranges.

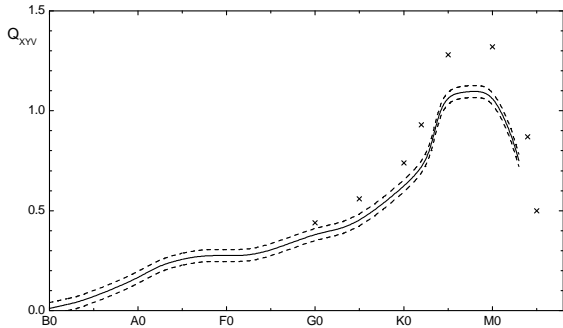


**Fig. 2.2.18.** The dependence of the interstellar reddening-free parameter  $Q_{XYV}$  on spectral class for luminosity V stars. Crosses are for luminosity III stars.

luminosity V, which statistically is not far from reality (F and early G giants of Population I fall into the Hertzsprung gap in the HR diagram). These stars were used in the investigation of interstellar extinction, paying attention to the lower accuracy of their luminosity classes.

In the absence of  $U-V$  and  $P-V$  color indices, the best criterion of spectral class is the  $Q_{XYV}$  parameter. Its dependence on spectral class is shown in Figure 2.2.18. The width of the area between the two broken lines corresponds to the observed “cosmic scatter” of the parameter. In the B8–A3, F6–G0 and especially in G5–K5 spectral ranges the  $Q_{XYV}$  parameter shows a gradient which is sufficient for the classification of stars with an accuracy of 1–2 spectral subclasses. However, in the range of A5–F5 classes the classification is of very low accuracy.

Color excesses  $E_{Y-V}$ , extinctions  $A_V$  and distances  $d$  were calculated only for the stars with reliable spectral and luminosity classes. The following equations were used:

$$E_{Y-V} = (Y - V)_{\text{obs}} - (Y - V)_0, \quad (2.2.5)$$

$$A_V = R_{YV} E_{Y-V}, \quad (2.2.6)$$

$$5 \log d = V - M_V + 5 - A_V, \quad (2.2.7)$$

where the intrinsic color indices  $(Y - V)_0$  for different spectral and luminosity classes were taken from Straižys (1992, Tables 66–69). The coefficient  $R_{YV} = 1.32 R_{BV}$ , for the normal interstellar extinction law it is 4.16 (corresponding to  $R_{BV} = 3.15$ ). The validity of this value of  $R_{YV}$  in the general North America and Pelican nebulae area was shown in Laugalys et al. 2006a. Absolute magnitudes  $M_V$  were taken from Straižys (1992, Appendix 1), according to spectral and luminosity classes of stars, with a correction of –0.1 mag, adjusting the old  $M_V$  scale to the new distance modulus of the Hyades ( $V - M_V = 3.3$ , Perryman et al. 1998).

### 2.3. Zero-Age Main Sequence in the *Vilnius* System

#### 2.3.1. Introduction

The zero-age main sequence (hereafter ZAMS) in two-color diagrams of the *Vilnius* system was first determined by one of the authors (Straižys 1970, 1977, 1992) on the grounds of photoelectric photometry of stars in the Hyades and Pleiades clusters and the Orion OB1 association around the Orion Belt. These groups of stars have been used because of little interstellar reddening and different ages. This permits us to determine ZAMS over a wide range of temperatures covering spectral classes from B to M. However, the investigation was not finished as some systematic errors were noticed in the photometric data of the Hyades observed in different seasons. A new attempt to find the ZAMS lines in the *Vilnius* system was undertaken by Černiauskas (2004) in his graduate thesis. For determining ZAMS in the  $M_V$  vs.  $(Y - V)_0$  and two-color diagrams he used a larger number of open clusters but the accuracy of the calibration was not sufficient.

Recent investigations of open clusters in the *Vilnius* photometric system (Straižys et al. 2003; Laugalys et al. 2004, 2006; Zdanavičius et al. 2004, 2005) have shown its effectiveness in identifying cluster members and in determining their individual interstellar reddenings. However, there is a difficulty in determining cluster distances and ages because of the absence of reliable ZAMS in various diagrams of the system, including the absolute magnitude vs. color diagram. Our aim was to fill this gap in the calibration of the *Vilnius* system. For this purpose we reobserved some of the key clusters so that we could eliminate possible systematic zero-point errors and thus improve the accuracy of photometry in these clusters.

#### 2.3.2. Photometry of the Hyades, Pleiades, Praesepe and Orion OB1 in the *Vilnius* System

The first *Vilnius* photometry of 95 stars in the Hyades cluster was obtained by Gürklyté et al. (1974). Their results were published in the General Photometric Catalog of Stars Observed in the *Vilnius* System (Straižys & Kazlauskas 1993). Later on, 98 stars in the Hyades were observed by Dzervitis & Paupers (1994). The results of photometry of 76 stars in the Pleiades were published by Straižys et al. (1970). The fainter 93 stars in the Merope dark cloud were measured later on by Černis (1987). Photometry of 59 stars in the Praesepe cluster was obtained by Straižys, Černis & Meištas (1992) and published in the General Catalog by Straižys & Kazlauskas (1993). Photometric observations of 81 Orion OB1 association stars around the Orion Belt were published by Černis et al. (1998).

New photometry of stars in the Hyades, the Pleiades and Praesepe was obtained in October to December of 2004 with a two-channel photometer on the 1.0 m and 1.5 m telescopes of the Steward Observatory on Mt. Lemmon, Arizona. The details of observations and reductions can be found in Kazlauskas et al. (2005). The results of photometry for 83 stars in the Hyades, 19 stars in the Pleiades and 87 stars in Praesepe are given in Tables 2.3.1–3 (see in Appendix), respectively. The successive columns give the star numbers in HD, HDE or BD catalogs, the coordinates,  $V$  magnitudes, six color indices and the number of observations on different nights,  $n$ . These stars were used to find the relations between the new and earlier (both published and unpublished) observations in these clusters. Color indices of earlier observations were transformed to the Arizona system of 2004. We used

these results to define the ZAMS line in the absolute magnitude vs. color diagram of the *Vilnius* system. For the Orion OB1 stars we used the results of photometry published by Černis et al. (1998).

### 2.3.3. Absolute Magnitude vs. Color Diagram

To define the ZAMS in the  $M_V$  vs.  $(Y - V)_0$  diagram we used main-sequence stars lying more than three magnitudes below the brightest stars of each cluster. In the case of the Hyades, these stars are of spectral class F3 and cooler. For Praesepe this limit is close to F0 and for the Pleiades – B8. We took only the stars whose cluster membership probability given in the WEBDA database was greater than 50 %. In Orion we used only the stars selected by Warren & Hesser (1977a,b, 1978) as members of the B1, B2 and B3 subgroups of the Orion association. All B- and early A-type association members may be considered as belonging to the ZAMS. Since the Arizona observations of 2004 (Tables 2.3.1 to 2.3.3) contain relatively bright stars, many of them are located on the evolved portion of the main sequence and could not be used in defining the ZAMS. Also, some stars with Arizona observations are not cluster members or their membership is unknown. We also rejected from the ZAMS sample known binary stars.

The absolute magnitudes of the cluster stars were calculated from their true magnitudes,  $V_0 = V - A_V$ , and the true distance moduli  $(V - M_V)_0$  of the clusters. The following values of the true distance moduli were accepted: 3.33 mag for the Hyades (Perryman et al. 1998), 6.16 mag for Praesepe (Pinsonneault et al. 1998), 5.63 mag for the Pleiades (Soderblom et al. 2005) and 8.1 for the Orion Belt stars (mean value of Warren & Hesser 1978; Anthony-Twarog 1982; Brown et al. 1994; scaled to a Hyades distance modulus of 3.33 mag). The interstellar extinction  $A_V$  for the Hyades and Praesepe was considered to be zero. For the Pleiades and the Orion stars it was taken into account individually for each star. The absolute magnitudes of stars in the clusters were corrected for metallicity, considering that the increase in [Fe/H] by 0.1 dex leads to the reduction of absolute magnitude  $M_V$  by 0.1 mag (Pinsonneault et al. 1998). The following values of metallicity [Fe/H] were accepted: for the Hyades +0.15 dex, for the Pleiades -0.03 dex and for Praesepe +0.04 dex. The metallicity of the Orion association stars was considered to be the same as of the Sun.

The absolute magnitudes and interstellar extinctions of the Pleiades and Orion association stars were determined individually in the following way. At first, the color excesses  $E_{Y-V}$  for each star were determined as differences of the observed  $Y-V$  values and the intrinsic  $(Y-V)_0$  values taken according to the MK spectral type:

$$E_{Y-V} = (Y - V)_{\text{obs}} - (Y - V)_0, \quad (2.3.1)$$

The mean spectral types were taken from Jaschek (1978) and the intrinsic color indices from the Straizys (1992) monograph. Then absolute magnitudes were obtained by the equation

$$M_V = V - 4.16 E_{Y-V} - (V - M_V)_0, \quad (2.3.2)$$

where  $V$  are observed magnitudes,  $4.16 E_{Y-V}$  is the interstellar extinction  $A_V$  and  $(V - M_V)_0$  is the true distance modulus of the Pleiades cluster or the Orion association.

Figure 2.3.1 shows the stars of the Hyades, the Pleiades, Praesepe and the Orion Belt plotted on the  $M_V$  vs.  $(Y - V)_0$  diagram. The entire main sequence from early B-type stars to M4 dwarfs is covered. All shown M-type dwarfs are taken from the Hyades area but their membership in the cluster is not certain. Thus, the faint end of the ZAMS for  $(Y - V)_0 > 0.8$  remains undetermined.

Deviations of stars upwards from the ZAMS in the HR diagram are caused mainly by their unresolved binarity, in some cases by fast axial rotation and evolutionary effects. Therefore, the location of the ZAMS should be close to the lower envelope of the main-sequence belt.

To make the delineation of the ZAMS line easier, we plotted on the  $M_V$  vs.  $Y-V$  diagram the theoretical isochrone for the solar chemical composition stars from the Victoria-Regina set (VandenBerg et al. 2006), corresponding to an age of 10 million years. For the luminosities of B-type stars and for the ages younger than 10 million years the isochrones are not available. Since the set of isochrones is given in the  $M_V$  vs.  $B-V$  plane, we have transformed the color indices  $B-V$  to  $Y-V$  by applying the observational relation between both

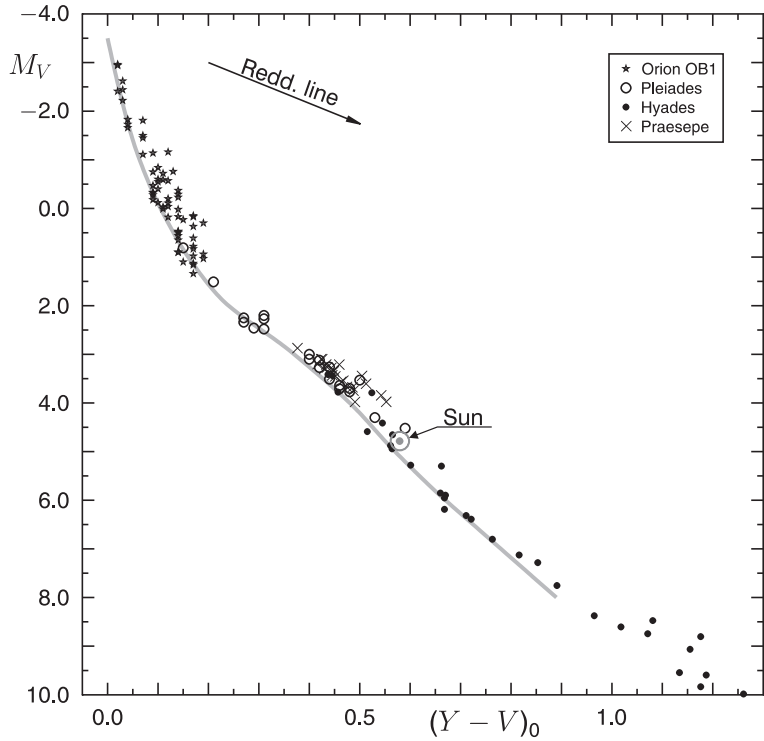


**Fig. 2.3.1.** The  $M_V$  vs.  $(Y - V)_0$  diagram for the unevolved and dereddened stars of the three nearby clusters and the Orion association. The length of the reddening line corresponds to  $E_{B-V} = 0.4$ . The ZAMS line is shown in grey, see the text.

color indices from Sviderskienė & Straizys (1970) and a semi-theoretical relation obtained by convolution of spectral energy distributions of stars from Straizys & Sviderskienė (1972) and the response functions of corresponding passbands.

The gray curve shown in Figure 2.3.1 for the absolute magnitudes  $M_V > 0.0$  mag is the described isochrone which perfectly envelopes the observational sequence from the low luminosity side. Consequently, it may be considered as a good approximation of the ZAMS for A-type and cooler stars. This theoretical ZAMS line was extended to  $M_V < 0.0$  (i.e., B-type stars) as an extrapolation, enveloping the Orion association stars from the lower side and ending at the point  $Y - V = 0.0$  and  $M_V = -4.0$ , the color and absolute magnitude of O-type stars, as is shown in Figure 2.3.1. Numerical data of the whole ZAMS line are given in Table 2.3.4. Together we give the corresponding values of  $B - V$  to facilitate reduction of other isochrones to the Vilnius system. This zero-age main sequence may be recommended for use in determining the distance moduli of open clusters by fitting to it the unevolved part of the dereddened main sequences in the  $V_0$  vs.  $(Y - V)_0$  diagram.

**Table 2.3.4.** Zero-age main sequence in the  $M_V$  vs.  $(Y - V)_0$  diagram of the Vilnius photometric system.

$M_V$	$Y - V$	$B - V$	$M_V$	$Y - V$	$B - V$	$M_V$	$Y - V$	$B - V$
-4.0	0.000	-0.32	+0.5	0.130	-0.11	+4.5	0.535	0.59
-3.0	0.010	-0.31	+1.0	0.160	-0.06	+5.0	0.570	0.65
-2.5	0.020	-0.30	+1.5	0.200	0.01	+5.5	0.615	0.73
-2.0	0.035	-0.27	+2.0	0.240	0.09	+6.0	0.670	0.84
-1.5	0.050	-0.25	+2.5	0.325	0.24	+6.5	0.720	0.98
-1.0	0.065	-0.23	+3.0	0.400	0.37	+7.0	0.770	1.09
-0.5	0.085	-0.20	+3.5	0.450	0.44	+7.5	0.830	1.20
0.0	0.110	-0.16	+4.0	0.490	0.50	+8.0	0.890	1.30

### 3. DUST AND MOLECULAR CLOUDS

#### 3.1. *Interstellar Extinction Law*

##### 3.1.1. Introduction

Soon after the implementation of the *UBV* photometric system it was shown that stars in the Great Cygnus Rift exhibit an anomalous interstellar reddening law: the reddening line in the  $U-B, B-V$  diagram for this area has a somewhat larger slope in comparison with other Milky Way areas for which the normal interstellar reddening law is valid (Johnson & Morgan 1955, Hiltner & Johnson 1956). Later on, Serkowski (1963) has analyzed *UBV* observations of B-type stars compiled from many publications and estimated that the difference in  $E_{U-B}/E_{B-V}$  is about 0.05 and that the Cygnus anomaly is present between the galactic longitudes 74 and 85 deg. Despite the critical papers by Divan (1956), Rozis-Saulgeot (1956) and Schalen (1959), the Cygnus Rift anomaly was confirmed by more careful analysis of *UBV* and *RI* observations done by Wampler (1961, 1962, 1964), Borgman & Johnson (1962), Johnson & Borgman (1963), Bogdanovich & Straizys (1966) and Ažusienis, Straizys & Sūdžius (1966) as well as by a new medium-band photometry by Borgman (1961), Köhler (1967), Goy (1972), Sūdžius (1974) and Lucke (1980).

A lower blue “knee” of the interstellar extinction law in Cygnus was confirmed by spectrophotometric observations by Nandy (1964), Whiteoak (1966) and Schild (1977). Ažusienis & Straizys (1966) confirmed the  $E_{U-B}/E_{B-V}$  anomaly in Cygnus by synthetic photometry using the Nandy and Whiteoak interstellar extinction laws. The increased extinction in the near ultraviolet has been detected by Meyer & Savage (1981) from photometric measurements by the Astronomical Netherlands Satellite (ANS).

According to Johnson & Borgman (1963) and Johnson (1965, 1968, 1977), the Cygnus stars show no anomaly in the infrared wavelengths. The ratio  $R = A_V/E_{B-V}$  also seems to be normal (Johnson & Borgman 1963, Fernie & Marlborough 1963, Gammelgaard 1968, Grubissich 1968, Serkowski 1968, Voelcker & Elsasser 1973, Rieke 1974, Serkowski et al. 1975, Herbst 1975, Turner 1976, Whittet 1977, 1979, McMillan & Tapia 1977, Tapia 1981, Torres et al. 1991).

It is highly improbable, that the Cygnus Rift anomaly is related to intrinsic properties of the individual stars. This question has been raised in many of the cited papers and answered negatively. Most probably, the anomaly is related with the composition of interstellar dust grains or their alignment. Greenberg & Meltzer (1960) and Wilson (1960) have interpreted the anomaly as the result of different orientation of elongated dielectric dust grains, aligned by the magnetic field: in Cygnus our view runs more or less along the galactic magnetic field lines, and we see dust particles along their short axes. According to theoretical calculations, this orientation leads to the enhanced extinction in the ultraviolet. However, Voshchinnikov et al. (1986) have estimated that its size is too small to be detected from observations, since it can be “washed out” by variations of the dust particle size and by variations of the radial component of the galactic magnetic field along the line of sight. The new theoretical calculations of Greenberg & Chlewicki (1987) for the case of  $P_{\max}/A_V = 0.03$  also exhibit the orientation effect to be of much smaller size in comparison with the case of perfect alignment.

The boundaries of the anomaly are very uncertain due to the uneven distribution of the observed stars. Therefore, it would be important to determine a more exact location of the anomaly to help its interpretation. Close to the northern boundary of the anomaly given by Serkowski, a number of heavily reddened stars have been found by Straizys et al. (1989a,b, 1993) in the course of an investigation of interstellar extinction in the vicinity of the North America and Pelican nebulae using the *Vilnius* photometric system. These stars are located between  $\ell = 84$  deg and 87 deg. Most of them are of spectral class B. For some of them the interstellar extinction  $A_V$  is as large as 4–5 mag. These stars are well suited to the determination of the interstellar extinction law, provided their MK spectral types are known.

### 3.1.2. Near-UV and Optical

For this investigation we selected from Straizys et al. (1989a and 1993) 33 stars with  $A_V = (1-5)$  mag, listed in Table 3.1.1. Their  $V$  magnitudes are between 8.4 and 12.8, and their photometric classes are distributed as follows: 23 are B-stars, 7 are A-stars and the remaining 3 are F- and G-stars. All these stars were classified by *Vilnius* photometry applying some methods based on the interstellar reddening-free  $Q$ -parameters, calculated for the normal interstellar reddening law. Almost all these stars have also one-dimensional spectral classes determined from low-dispersion objective prism spectra. Only for three stars MK spectral types are available.

Grating spectra with 2.8 Å resolution and a signal-to-noise ratio of 100 or more were obtained by Chris Corbally with the Boller and Chivens spectrograph on the 2.3 m (90") telescope of Steward Observatory at Kitt Peak. The CCD spectra were processed and extracted using standard IRAF routines, but they were not flux calibrated, just normalized.

**Table 3.1.1.** Heavily reddened stars in the area of the North America and Pelican nebulae. The strength of the interstellar 4430 band is indicated in last column. Notes for the stars denoted by an asterisk are given below table. Star numbers 112–249 are from Straizys et al. (1989a), star numbers 1044–1209 are from Straizys et al. (1993, Table 2). Identification charts are given in these catalogs.

No.	BD	RA (1950)	DEC (1950)	$V$	$A_V$	Sp (Viln.)	Sp (other)	Sp (Corbally)	4430 Å
112.	42.3880	20 48 06	+42 39.0	9.79	1.04	A2 V	A2	A6 III	—
131.		20 49 53	+43 48.2	10.78	2.07	B6: Vp?	B8	B2 V	mod.
140.		20 50 21	+43 52.4	10.52	2.74	B5 V	B5	B3 V	mod.
141.	43.3747	20 50 24	+44 14.7	8.66	2.70	Be	B1 Ve	B1 Ve *	mod.
148.	43.3751	20 50 46	+44 00.3	9.66	2.16	B3 V	B8	B2 Vp *	mod.
1044.		20 51 00	+43 44.4	11.02	2.47	B6: V	A0	B7 V	mod.
153.	42.3894	20 51 04	+42 25.1	8.39	2.74	B1.5 IV	B3 & B1 IV		mod.
1052.		20 51 18	+43 25.9	11.18	3.82	B2 V	G0	B2 Vn	mod.
1057.		20 51 28	+43 36.6	12.49	4.95	B2 V		B1 V	v.str.
163.		20 51 47	+43 57.7	11.45	3.96	B5 V	B5	B3 V	mod.
176.	44.3627	20 53 01	+44 39.2	9.85	3.02	B3 III	B8	B2 III	str.
177.	44.3629	20 53 18	+44 34.0	10.06	1.53	B8 III	B8	B8 V	wk.
1130.		20 54 12	+42 30.3	11.61	1.04	F0 V	F5	F3 V *	v.wk.
190.		20 54 18	+45 10.0	11.27	1.98	B3 V	B5	B5 IV *	wk.
195.	42.3914	20 54 35	+42 56.2	8.43	4.05	B2 IV	B0 III	B0.5 IV	mod.
197.		20 54 37	+44 27.8	11.13	1.80	B6 V	A2	B5 V	wk.
1174.		20 56 07	+43 15.3	10.92	3.22	A8 II	A0	A3 III	wk.
1178.		20 56 09	+43 02.6	12.28	2.29	A0 V		A0.5 III-IV	wk.
218.	44.3655	20 56 39	+44 57.3	9.19	1.62	B3 III	B1 IV	B1 IV	mod.
1190.		20 56 46	+43 36.5	12.81	1.15	A6 V		F0 V	—
1191.		20 56 48	+43 00.0	10.04	1.08	B9 IV	A0	A0 IV	v.wk.
1196.		20 57 00	+42 51.8	11.31	1.22	A2 V	A2	A2 V	v.wk.
1198.		20 57 12	+42 44.0	11.34	2.79	B9 III	A0	B9.5 IV-V *	mod.
1205.		20 57 24	+43 33.5	11.90	1.08	A7 V		F0 V	—
226.		20 57 27	+44 35.2	10.33	2.07	B7 Vp?	A2	B4 III(n)	mod.
1207.		20 57 34	+43 40.8	12.42	1.76	F5 III?		G4 V	—
230.		20 57 44	+45 05.6	11.08	1.84	B6 V	B5	B4 III	wk.
1209.		20 57 46	+43 02.4	12.02	1.13	A5 V	A0	A5 Vm *	—
236.	44.3664	20 58 10	+45 08.4	10.19	2.43	B2.5 V	B9	B1 Vn	mod.
238.	42.3935	20 58 16	+42 24.2	9.83	3.06	G9 II?	cG0:	G1 Ib	mod.
239.	44.3666	20 58 19	+44 51.0	10.18	2.25	B2 V	B5	B1 Ve *	mod.
245.	42.3937	20 59 10	+42 34.8	9.34	1.76	B8 III	A0	B8 III-IV	mod.
249.		20 59 36	+43 58.2	11.18	2.56	B6.5 V	B8	B5 III	mod.
242.	42.3936	20 58 40	+43 21.9	8.36	0.40	B9 V	A0, A2	B9 V	—
246.	42.3939	20 59 21	+43 20.2	8.57	0.14	F0 V	F0	F0 V	—

Notes to MK classifications:

- 140. Fill-in by emission of Balmer-line cores and the Fe II (42) nebular lines;
- 148. Helium (=B3 strength) is slightly too weak;
- 1130. Fe I 4046 slightly weak;
- 190. Luminosity is a compromise: He I 4121 = V; H-wings = III-IV;
- 1198. Mild shell star;
- 1209. A2 according to K-line, A5 according to H lines and A7 according to metallic lines;
- 239. Emission fill-in in same lines as 140, but a little stronger.

MK spectral classification has been done by the same author using a grid of standard star spectra established for this spectrograph. The results are given in Table 3.1.1 together with other estimates of spectral types collected from the literature. A comparison of the present results with the three MK types from the literature suggests the usual accuracy of better than a luminosity class and a temperature subclass.

For the extinction law determination 15 early B-type stars were selected. We have limited ourselves to B0–B5 stars since these stars give the highest accuracy of the extinction law. For cooler stars the ultraviolet color indices vary with the temperature so rapidly that any error of spectral class determination leads to large errors of color excesses and their ratios. We have also rejected two stars of early B subclasses: the star 131 shows contradiction between its spectroscopic and photometric spectral classes, and its  $Q$ -parameters seem to be peculiar. A similar situation holds with the star 190 which photometrically is B3 V and spectroscopically is about B5 IV. Two Be stars (141 and 239) have  $H\beta$  in emission, and so presumably  $H\alpha$  should be also in emission; for them the ratio  $E_{V-S}/E_{Y-V}$  was not calculated.

For deriving the interstellar reddening law we used the following sequence of calculations:

- Intrinsic color indices  $(U - V)_0$ ,  $(P - V)_0$ ,  $(X - V)_0$ ,  $(Y - V)_0$ ,  $(Z - V)_0$  and  $(V - S)_0$  for each star were taken from the Straizys (1992) monograph according to their MK spectral types;

- Color excesses  $E_{U-V}$ ,  $E_{P-V}$ ,  $E_{X-V}$ ,  $E_{Y-V}$ ,  $E_{Z-V}$  and  $E_{V-S}$  were calculated as differences of the observed and the intrinsic color indices:

$$E_{U-V} = (U - V)_{\text{obs}} - (U - V)_0,$$

$$E_{P-V} = (P - V)_{\text{obs}} - (P - V)_0,$$

$$E_{X-V} = (X - V)_{\text{obs}} - (X - V)_0,$$

$$E_{Y-V} = (Y - V)_{\text{obs}} - (Y - V)_0,$$

$$E_{Z-V} = (Z - V)_{\text{obs}} - (Z - V)_0,$$

$$E_{V-S} = (V - S)_{\text{obs}} - (V - S)_0.$$

Observed color indices were taken from Straizys et al. (1989a, 1993).

- Ratios of color excesses with respect to  $E_{Y-V}$ , i.e.  $E_{m-V}/E_{Y-V}$ , were calculated.

These ratios are given in Table 3.1.2 and their arithmetic mean values (circles) are plotted in Fig. 3.1.1 as a function of the reciprocal effective wavelengths of the passbands taken from Kuriliene (1983). The y-axis gets normalized to 1.0 at  $\lambda_e^{-1}$  of the  $Y$  passband, and to 0.0 at  $\lambda_e^{-1}$  of the  $V$  passband. The crosses for each passband represent the normal interstellar extinction law from Straizys (1992). A systematic displacement of the circles upwards for the  $X$ ,  $P$  and  $U$  passbands is evident. The scatter of the ratios for individual stars can be explained either by real differences of the extinction law or by the limitation in the accuracy of inferring intrinsic colors from spectral classification. This limitation comes both from the “cosmic scatter” within a spectral subclass and from any errors in the spectral classification itself. For an estimate of such errors we took the intrinsic colors of stars differing from our MK spectral class by  $\pm 1$  subclass. In this case, for the B0–B5 stars the  $E_{m-V}/E_{Y-V}$  errors are listed in Table 3.1.3.

**Table 3.1.2.** Color-excess ratios  $E_{m-V}/E_{Y-V}$  for 15 B0–B5 stars used to derive the mean interstellar reddening law for the North America and Pelican nebulae area. The  $m$  passbands are  $U, P, X, Y, Z, V$  and  $S$ .

$m$	$\lambda^{-1}$	140	141	148	153	1052	1057	163	176	195	197	218	226	230	236	239	Mean
$U$	2.925	2.91	2.76	2.84	2.76	2.54	2.74	2.74	2.83	2.94	2.68	3.05	3.00	3.00	3.00	2.88	2.83
$P$	2.683	2.36	2.23	2.33	2.18	2.14	2.18	2.26	2.23	2.30	2.22	2.32	2.35	2.35	2.35	2.35	2.27
$X$	2.479	1.83	1.83	1.88	1.84	1.81	1.80	1.74	1.80	1.86	1.80	1.83	1.86	1.79	1.82	1.88	1.82
$Y$	2.152	1.00	1.00	1.00	1.00	1.00	1.00	1.00	1.00	1.00	1.00	1.00	1.00	1.00	1.00	1.00	1.00
$Z$	1.943	0.33	0.35	0.35	0.34	0.35	0.33	0.32	0.38	0.33	0.32	0.36	0.37	0.28	0.33	0.36	0.34
$V$	1.843	0.00	0.00	0.00	0.00	0.00	0.00	0.00	0.00	0.00	0.00	0.00	0.00	0.00	0.00	0.00	0.00
$S$	1.541	0.91	—	0.92	0.82	0.92	0.89	0.87	0.94	0.87	0.95	0.93	0.96	0.88	0.95	—	0.91

**Table 3.1.3.** Errors of color-excess ratios for B0–B5 stars, including  $U$ ,  $P$ ,  $X$  and  $S$  passbands. For  $\Delta(E_{V-S}/E_{Y-V})$  errors are negligible.

	$\Delta \frac{E_{U-V}}{E_{Y-V}}$	$\Delta \frac{E_{P-V}}{E_{Y-V}}$	$\Delta \frac{E_{X-V}}{E_{Y-V}}$	$\Delta \frac{E_{V-S}}{E_{Y-V}}$
Absolute error	$\pm 0.23$	$\pm 0.13$	$\pm 0.02$	$\pm 0.01$

**Table 3.1.4.** The North America and Pelican interstellar extinction law compared to the Cygnus law and the normal law.

	$\frac{E_{U-V}}{E_{Y-V}}$	$\frac{E_{P-V}}{E_{Y-V}}$	$\frac{E_{X-V}}{E_{Y-V}}$	$\frac{E_{Z-V}}{E_{Y-V}}$	$\frac{E_{V-S}}{E_{Y-V}}$
North America and Pelican	$2.83 \pm 0.20$	$2.27 \pm 0.10$	$1.82 \pm 0.02$	$0.34 \pm 0.01$	$0.91 \pm 0.01$
Südžius (1974) law for O-stars	2.75	2.24	1.81	0.36	0.91
Südžius (1974) synthetic	2.76	2.25	1.81	0.36	0.90
Südžius (1974) normal law	2.62	2.14	1.76	0.36	0.84

The errors show that the observed scatter of color-excess ratios can be explained exclusively by spectral class errors and the impossibility of giving spectral classes to tenths of a subclass.

To obtain the average extinction law for the North America and Pelican area we took the arithmetic mean of points of all 15 stars. The results are given in Table 3.1.4. The other lines in Table 3.1.4 give color-excess ratios from Südžius (1974): the 2nd line gives the values for Cygnus from observations of O-type stars at  $\ell = 72\text{--}81$  deg, the 3rd line gives the synthetic color-excess ratios calculated for the Cygnus extinction law and the 4th line gives the values obtained from observations of O-stars elsewhere except Cygnus. It is seen that the values of  $E_{m-V}/E_{Y-V}$  for the North America and Pelican nebulae are very close to the values obtained for O-type stars in Cygnus at smaller galactic longitudes. This means that the Cygnus Rift anomaly also includes the area of the North America and Pelican nebulae, extending the galactic longitude range up to 87 deg.

The overall majority of the stars used for the extinction law determination (14 from 15) are situated at distances 450–900 pc (Straižys et al. 1989a, 1993), i.e., most of them should belong to the North America and Pelican nebulae complex. Consequently, they should be reddened predominantly by the dark cloud at the distance of the nebulae, at  $580 \pm 100$  pc (Straižys et al. 1993).

### 3.1.3. NGC 6997 Area

The interstellar extinction law in the 345–656 nm wavelength range in the North America and Pelican nebulae was investigated in one of our earlier papers (Straižys, Corbally & Laugalys 1999 or see Section 3.1.2) using *Vilnius* seven-color photometry and MK spectral types of 15 heavily reddened stars. The mean law in this area was found to be similar to the law for a much larger area in Cygnus derived earlier by other authors. It differs from the normal law by exhibiting a little smaller change of the slope at 435 nm, i.e., it is closer to the  $\lambda^{-1}$  law without a break. We could not investigate the law at longer wavelengths due to absence of published infrared photometric data at that time.

Since then, the  $J$ ,  $H$  and  $K$  photometry of the 2MASS survey has been released for free use (Cutri et al. 2003a). This allows us to investigate the interstellar extinction law in the infrared and to determine the ratio  $R_{BV} = A_V/E_{B-V}$  in the area. Before using the 2MASS values,  $K$  magnitudes and  $J-H$ ,  $J-K$  and  $H-K$  color indices were transformed to the Bessell & Brett (1988) system which is close to the original Arizona  $J,H,K$  system for which the intrinsic colors  $V-J$ ,  $V-H$  and  $V-K$  are available for all MK spectral types. The transformation equations are taken from Cutri et al. (2003b).

In the area with a  $3^\circ$  radius centered on 57 Cyg we found 33 O–B–A stars with available MK spectral types and  $BV$  photometry collected from the literature (mostly from Reed 2003, 2005). We took only early-type stars, trying to avoid the dependence of color excesses on spectral type due to the bandwidth effect. For these stars color indices  $V-J$ ,  $V-H$  and  $V-K$  were formed, taking infrared magnitudes from the 2MASS survey, transformed to the standard Arizona system. After that color excesses  $E_{B-V}$ ,  $E_{V-J}$ ,  $E_{V-H}$  and  $E_{V-K}$  were calculated, taking the intrinsic color indices from Straižys (1992, Tables 22–24). For early-type stars these values are close to the Koornneef (1983) data.

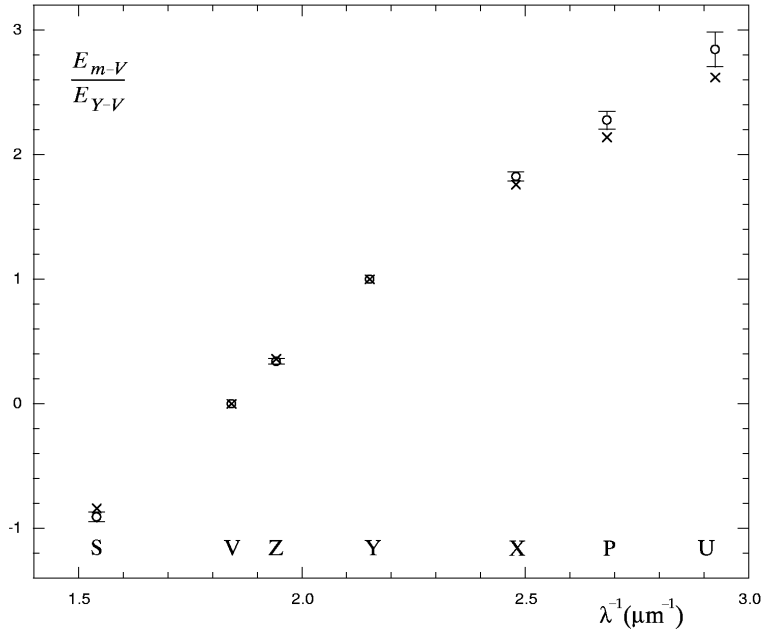


**Fig. 3.1.1.** Interstellar reddening law in the North America and Pelican nebulae area. The circles with the error bars are for the North America and Pelican area and the crosses are for the normal extinction law.

These 33 stars are plotted as dots in Figure 3.1.2 (left panels), which show the dependence of  $E_{V-J}$ ,  $E_{V-H}$  and  $E_{V-K}$  on  $E_{B-V}$ . The least-square solutions give the following equations (with the fixed zero-point of all color excesses at 0.0):

$$E_{V-J} = 2.222 \pm 0.027 \times E_{B-V}, \quad (3.1.1)$$

$$E_{V-H} = 2.589 \pm 0.032 \times E_{B-V}, \quad (3.1.2)$$

$$E_{V-K} = 2.677 \pm 0.040 \times E_{B-V}. \quad (3.1.3)$$

From these ratios of color excesses the following ratios  $R_{BV} = A_V/E_{B-V}$  were calculated by equations (A3), (A4) and (A5) from Fitzpatrick (1999): 3.07, 3.12 and 3.02. The average value 3.07 is very close to the average value of  $R_{BV}$  for diffuse interstellar dust (3.15, Straizys 1992).

However, this is not the end of the story. Since NGC 6997 probably is located in the same complex as the North America and Pelican nebulae and the dust clouds separating them, we may expect that the same ratio  $R$  is valid for the cluster. However, Villanova et al. (2004) have found a much larger value of  $R_{BV}$  in the cluster area.

From Villanova et al. (2004) we took their  $B-V$  values and MK spectral types for 15 B and A stars in the cluster area and found their color excesses with  $(B-V)_0$  from Straizys (1992). Color excesses  $E_{V-J}$ ,  $E_{V-H}$  and  $E_{V-K}$  for the same stars were calculated from 2MASS. In Figure 3.1.2 these stars, shown as crosses, despite much larger scatter exhibit steeper dependence of color excesses than the stars in the  $3^\circ$  radius field (dots). The least-square solutions with the fixed zero-point for 14 stars give the following equations (without the star No. 220 which shows too large deviation):

$$E_{V-J} = 2.737 \pm 0.075 \times E_{B-V}, \quad (3.1.4)$$

$$E_{V-H} = 3.237 \pm 0.086 \times E_{B-V}, \quad (3.1.5)$$

$$E_{V-K} = 3.298 \pm 0.094 \times E_{B-V}. \quad (3.1.6)$$

which lead to the following values of  $R_{BV}$ : 3.78, 3.89 and 3.71, with an average value of 3.79. This value of  $R_{BV}$  exceeds considerably the value found in the large surrounding area (where  $R_{BV}$  was found to be 3.07).

Now we are in a position to construct similar dependencies of  $E_{V-J}$ ,  $E_{V-H}$  and  $E_{V-K}$  versus  $E_{Y-V}$  of the *Vilnius* system. Figure 3.1.2 (right panels) show such plots for 83 B and

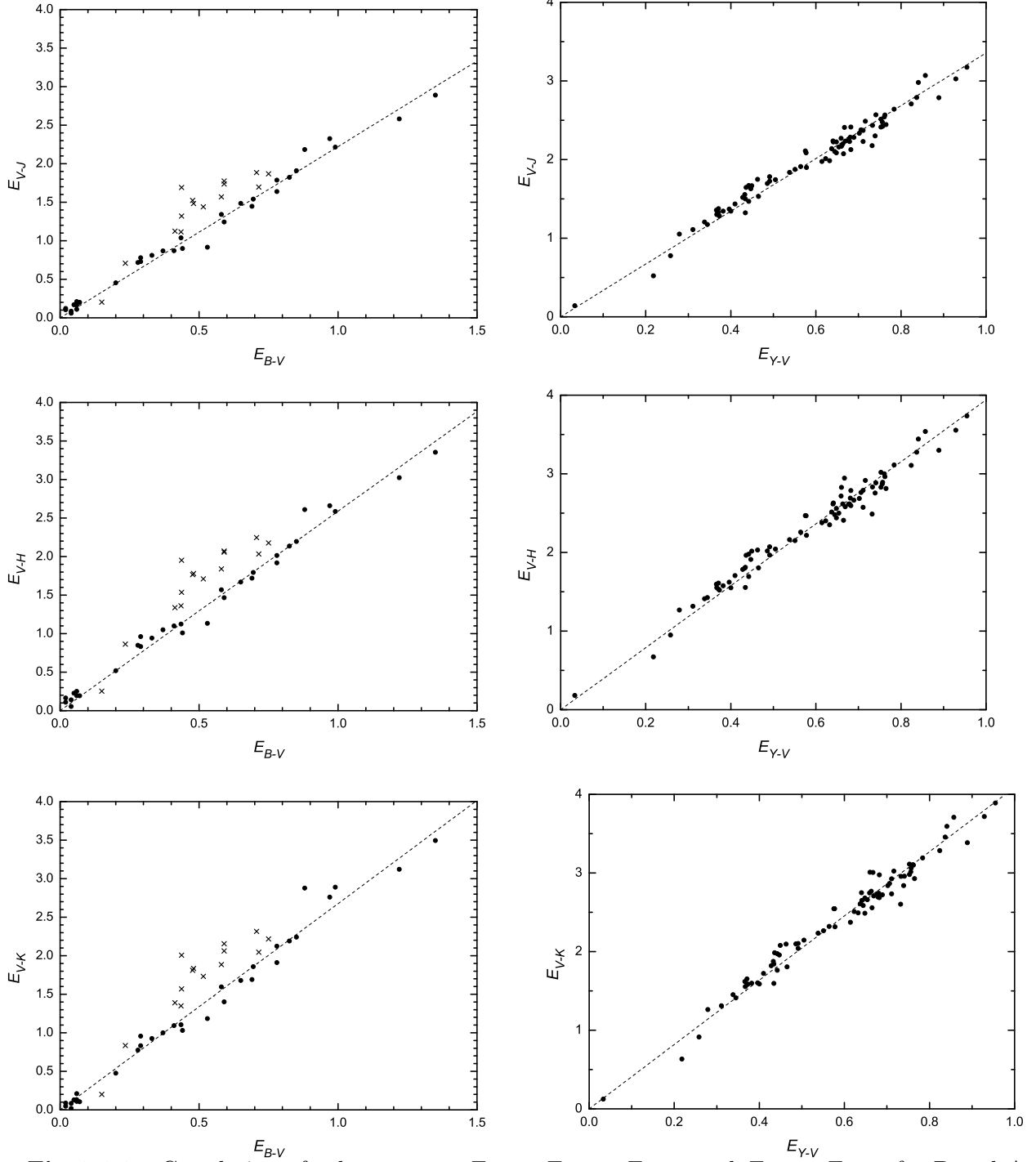


**Fig. 3.1.2.** Correlation of color excesses  $E_{V-J}$ ,  $E_{V-H}$ ,  $E_{V-K}$  and  $E_{B-V}$ ,  $E_{Y-V}$  for B and A stars in the North America and Pelican nebulae region;  $\times$  symbols are the NGC 6997 area stars.

A stars classified photometrically. The least-square solutions with the fixed zero-point give the following equations:

$$E_{V-J} = 3.357 \pm 0.019 \times E_{B-V}, \quad (3.1.7)$$

$$E_{V-H} = 3.941 \pm 0.023 \times E_{B-V}, \quad (3.1.8)$$

$$E_{V-K} = 4.089 \pm 0.023 \times E_{B-V}. \quad (3.1.9)$$

which lead to the following values of  $R_{BV}$ : 3.48, 3.56 and 3.46, with an average value of  $\sim 3.5$ . In this calculation we have accepted that for B and A stars  $E_{Y-V} = 0.75E_{B-V}$  (Straižys 1992). The obtained mean value of  $R_{BV}$  is larger than the normal one (3.15), but not as large as the ratio determined from a comparison of the infrared color indices with  $E_{B-V}$ .

### 3.1.4. 2MASS Data in the North America and Pelican Area and Cyg OB2 Association

The 2MASS survey presents all-sky photometry in the near-infrared  $J$ ,  $H$  and  $K_s$  passbands which is useful for a variety of investigations of the Galaxy. The system has been successfully used for study of star-forming regions and search for young stellar objects (YSOs), for investigation of the interstellar extinction in dust/molecular clouds, large-scale distribution of interstellar dust, the interstellar reddening law in the infrared, spectral energy distributions, etc.

Recently, the interstellar reddening law in the infrared wavelengths was studied by Fitzpatrick & Massa (2005, 2007), Indebetouw et al. (2005) and Flaherty et al. (2007) applying the 2MASS data alone or joining them with the *Spitzer* results at longer wavelengths. In some papers regional values of the color excess ratio  $E_{J-H}/E_{H-K_s}$  were investigated (Indebetouw et al. 2005; Nishiyama et al. 2006; Lombardi et al. 2006; Djupvik et al. 2006; Naoi et al. 2006; Román-Zúñiga et al. 2007). In most cases this ratio was evaluated from the statistical distribution of red giants with various reddenings in the  $J-H$  vs.  $H-K_s$  diagram. The red clump giants of early K spectral subclasses are the most abundant population in 2MASS near the Galactic plane, since they are very bright in the near infrared and, despite the interstellar extinction, have been observed at large distances – up to the Galactic central bulge and the disk edges in the direction of the 2nd and 3rd quadrants.

In the listed papers some regional variations of the  $E_{J-H}/E_{H-K_s}$  ratio or the interstellar reddening law in the infrared wavelengths have been noted. Consequently, before applying the  $J-H$  vs.  $H-K_s$  diagram for star classification or other tasks, it is important to investigate the color-excess ratio in each specific area.

To our knowledge, the ratio  $E_{J-H}/E_{H-K_s}$  in the area of the North America and Pelican nebulae, including the L935 dust cloud, separating the nebulae, has not been determined till now. Cambrésy et al. (2002), Comerón et al. (2002) and Comerón & Pasquali (2005) in their studies, based on the 2MASS data in Cygnus, have applied a value of 1.70 which follows from the Rieke & Lebofsky (1985) interstellar extinction law. However, this ratio corresponds to the Arizona  $J,H,K$  system, which is slightly different from the 2MASS system. On the other hand, this extinction law was obtained by using heavily reddened stars located in various directions (five stars in the Galactic center direction,  $\alpha$  Sco and Cyg OB2 No. 12). Among them, Cyg OB2 No. 12 is an emission-line B supergiant with a number of peculiarities.

We decided to investigate the ratio  $E_{J-H}/E_{H-K_s}$  in the NAP direction applying the classical method which determines slopes of reddening lines plotted for stars in narrow intervals of spectral classes. For this aim the most suitable are early-type stars of spectral classes O and B since these types of stars are sufficiently luminous and apparently bright to be accessible for spectral classification and sufficiently distant to be considerably reddened. A similar method has been successfully used by He et al. (1995) for reddened O–B stars in the southern Milky Way.

### THE LIST OF O–B STARS:

The starting step in composing the list of early-type stars in NAP, classified in the MK system, was the search of the Simbad database for the ALS stars (Reed 1998, 2005) in the area  $3^\circ \times 3^\circ$  with the center at J2000:  $20^{\text{h}} 56^{\text{m}}$ ,  $+44^\circ$ . The next step was the check of the catalogs of stars measured and classified in two dimensions using the *Vilnius* seven-color photometric system (Straižys et al. 1989a, 1993; Laugalys & Straižys 2002; Laugalys et al. 2006a,b, 2007). To verify the quality of photometric classifications, 37 B-stars from the *Vilnius* lists were classified by Chris Corbally using blue grating spectra of  $2.8 \text{ \AA}$  resolution obtained with the Boller and Chivens spectrograph on the 2.3 m telescope of Steward Observatory at Kitt Peak. Part of these classifications were published in Straižys et al. (1999), the spectral types of the remaining 14 are given in Table 3.1.5 (see in Appendix).

Since the coincidence between spectroscopic and photometric spectral types was quite good, we have added to the list 29 B-type stars in the cluster NGC 6997 and Collinder 428 areas with reliable two-dimensional classifications obtained using the *Vilnius* seven-color photometric system (Laugalys et al. 2006a, 2007); in Table 3.1.5 their spectral classes are marked by lower-case letters.

However, for the selected B-stars in the region of the North America and Pelican nebulae the largest values of  $E_{H-K_s}$  are about 0.25 which correspond to  $A_V \approx 4$  mag. To have a longer reddening line, we added O–B stars from the Cyg OB2 association located behind

the Great Cygnus Rift,  $4^\circ$  from the NAP nebulae. Investigations of the extinction law in Cygnus discussed in our earlier work (Straižys et al. 1999 or see Section 3.1.2) do not show any significant differences in extinction properties between various directions in Cygnus. Table 3.1.5 (see in Appendix) lists 95 OB-type stars from the NAP region and 98 O–B1 stars from the Cyg OB2 association. We list only those Cyg OB2 stars which were used for plotting the reddening line. They include 15 brightest stars from Johnson & Morgan (1954) and Morgan et al. (1954), 45 stars from Massey & Thompson (1991) and 42 stars from Comerón et al. (2002). The last list contains stars having ‘featureless’ infrared spectra and considered as the candidate O-type stars. Hanson (2003) and Negueruela et al. (2008) have classified 27 of them in MK and confirmed that they indeed are O–B0 type stars. The stars with blended images have been excluded. We also excluded two stars from the Massey & Thompson list (575 and 793) which show a considerable deviation from the reddening line of other O–B1 stars. The reddest star in the NAP region is the CP054 star with spectral type O5 determined by Comerón & Pasquali (2005). The  $J-H$  and  $H-K_s$  color indices given in the table were calculated from the 2MASS  $J$ ,  $H$  and  $K_s$  data.

### INTRINSIC COLOR INDICES:

Despite a wide use of the 2MASS photometric system, intrinsic color indices  $(J-H)_0$  and  $(H-K_s)_0$  of stars of different spectral and luminosity classes are unknown. Usually they are being obtained by transformation from the Koornneef (1983) or Bessell & Brett (1988) tabulations with the Carpenter (2001) equations. Since these transformation equations for O and B stars are rather uncertain, we decided to determine their intrinsic color indices directly in the 2MASS system by dereddening relatively bright stars with small interstellar reddening.

For determining the intrinsic color indices for O- and B-type stars we took some little reddened stars listed in Table 3.1.6. The three O-stars are the least reddened field stars. The B5–B6 and B8–B9 stars were selected in the vicinity of the NAP nebulae from our Table 3.1.5 and from the Fehrenbach et al. (1961) catalog of stars in the Kapteyn Selected Area 40. For each star color excesses  $E_{B-V}$  were transformed to  $E_{J-H}$  and  $E_{H-K}$  by the equations given by Bessell & Brett (1988). Since the reddenings are small,  $E_{H-K} \approx E_{H-K_s}$ . After that color indices were dereddened for all stars individually taking differences of the observed color indices and the corresponding color excesses:

$$(J-H)_0 = (J-H) - E_{J-H}, \quad (3.1.10)$$

$$(H-K_s)_0 = (H-K_s) - E_{H-K_s}. \quad (3.1.11)$$

Then dereddened color indices were averaged to obtain the intrinsic color indices  $(J-H)_0$  and  $(H-K_s)_0$  for O8, B5.5 and B8.5 stars listed in Table 3.1.7.

### EQUATIONS OF THE REDDENING LINES:

Table 3.1.5 stars were divided into three spectral groups: O–B1, B2–B6 and B7–B9.5, neglecting their luminosity classes. However, we excluded all emission-line B-stars which exhibit excesses of  $H-K_s$  at constant  $J-H$ . For each spectral group we have plotted the  $J-H$  vs.  $H-K_s$  diagram shown in Figures 3.1.8–10. Figure 3.1.8 shows that O–B1 type stars in the NAP region and in the Cyg OB2 association exhibit the same slope of the reddening line. The CP054 star at  $H-K_s = 0.47$  (the uppermost dot) lies also together with the association stars. Two Cyg OB2 stars, No. 5 (O7e) and No. 12 (B5 Iab), deviate downwards from the reddening line considerably, imitating the presence of circumstellar thermal emission in the dust or electron free-free transitions. Peculiarities of star No. 12 were widely discussed by Massey & Thompson (1991); they find H $\beta$  line in emission. In the direction of these two stars condensations of CO have been discovered (Scappini et al. 2002; Casu et al. 2005). These two stars were rejected from the reddening line solutions. After the listed rejections, we have 118 O–B1 stars, 29 B2–B6 stars and 46 B7–B9.5 stars.

The least-square solutions for Figures 3.1.8–10 have been made with the fixed intrinsic positions of O–B1, B2–B6 and B7–B9.5, respectively. The following equations were obtained:

$$J - H = 2.004(\pm 0.016)(H - K_s) - 0.050, \quad (3.1.12)$$

$$J - H = 1.876(\pm 0.105)(H - K_s) - 0.014, \quad (3.1.13)$$

$$J - H = 2.106(\pm 0.094)(H - K_s) - 0.039. \quad (3.1.14)$$

**Table 3.1.6.** Color excesses of little reddened O–B stars used in the determination of intrinsic color indices.

Name	Spectral type	$E_{B-V}$	$E_{J-H}$	$E_{H-K_s}$
O-type stars				
S Mon	O7 Ve	0.09	0.033	0.017
68 Cyg	O8e	0.26	0.096	0.050
10 Lac	O9 V	0.11	0.041	0.021
B5–B6 stars				
BD+45 3242	B5 V	0.19	0.073	0.036
BD+45 3279	B6 V	0.25	0.092	0.048
HD 198915	B5 V	0.10	0.037	0.019
BD+44 3579	B5 V	0.30	0.111	0.057
BD+46 3141	B5 V	0.06	0.022	0.011
B8–B9 stars				
HD 197374	B9 V	0.00	0.000	0.000
HD 197391	B8 V	0.15	0.055	0.028
HD 199121	B8 V	0.00	0.000	0.000
HD 199417	B9 V	0.10	0.037	0.019
BD+45 3247	B9 V	0.12	0.044	0.023
BD+43 3701	B9 V	0.08	0.030	0.015
BD+45 3256	B8 V	0.09	0.033	0.017
BD+45 3264	B8 III	0.14	0.052	0.027

**Table 3.1.7.** Intrinsic color indices of stars in the 2MASS system.

Color index	O8	B5.5	B8.5
$(J-H)_0$	-0.164	-0.081	-0.062
$(H-K_s)_0$	-0.058	-0.035	-0.009

**Table 3.1.8.** Red clump giants in the M 67 cluster.

Star	$V$	$B-V$	$J-H$	$H-K_s$
MMJ 6485	10.48	1.11	0.485	0.133
MMJ 6492	10.59	1.12	0.528	0.146
MMJ 6494	10.48	1.10	0.506	0.153
MMJ 6503	10.55	1.12	0.494	0.114
MMJ 6506	10.58	1.10	0.504	0.118
MMJ 6512	10.55	1.10	0.513	0.125
MMJ 6516	10.47	1.12	0.485	0.164
Average				
		0.502	0.136	

These equations show the slope of the reddening line,  $E_{J-H}/E_{H-K_s}$ , for O–B stars is between 1.9 and 2.1. Probably, the average value 2.0 can be accepted for future analysis of the distribution of reddened stars in the 2MASS two-color diagram. Zero-points of the equations mean the points on the  $J-H$  axis at which the reddening lines cross the line  $H-K_s = 0.0$ . They are the same as the values of the interstellar reddening-free  $Q_{JHK_s}$  parameters:

$$Q_{JHK_s} = (J - H) - E_{J-H} / E_{H-K_s}(H - K_s). \quad (3.1.15)$$

Equations (3.1.12), (3.1.13) and (3.1.14) show that the  $Q_{JHK_s}$  values for the three spectral classes are  $-0.050$ ,  $-0.014$  and  $-0.039$ . The maximum absolute deviations of individual values from the mean are 0.015, and this means that all O–B stars lie practically on one line which

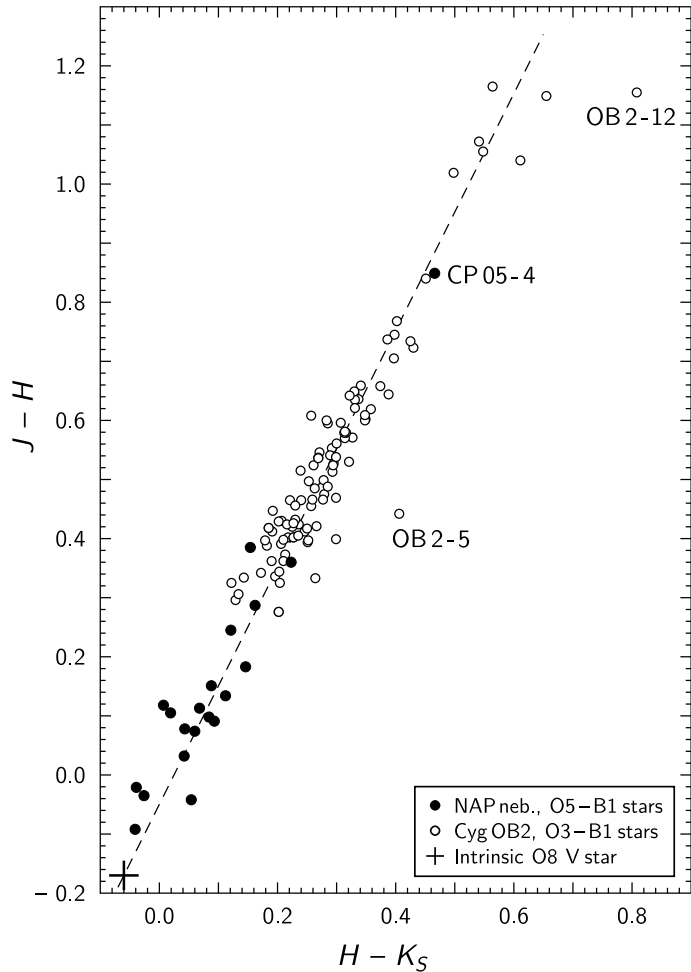


**Fig. 3.1.8.** Interstellar reddening line for O–B1 stars in the NAP nebulae region and the Cyg OB2 association. The broken line is the least-square solution for all 118 stars with the fixed intrinsic colors  $J - H = -0.17$ ,  $H - K_s = -0.06$ . The Cyg OB2 stars Nos. 5 and 12 are rejected.

coincides with the reddening line (Figure 3.1.11). Thus, we may solve the least square equation using all 193 stars together (with the intrinsic position of an O8-type star):

$$J - H = 2.024(\pm 0.018)(H - K_s) - 0.048 . \quad (3.1.16)$$

#### THE REDDENING LINE OF RED GIANTS:

We have one more possibility to find the reddening line slope in the  $J - H$  vs.  $H - K_s$  diagram. In Figure 3.1.12 we show the plot of this diagram for 99 000 stars in the  $3^\circ \times 3^\circ$  area with the center at J2000:  $20^{\text{h}} 56^{\text{m}}$ ,  $+44^\circ$ . These stars were selected from the 2MASS database with an error limit of  $< 0.05$  mag for the three magnitudes. The stars form a comet-like crowding in which we show approximate intrinsic positions of the main sequence and K-M giants. The interstellar reddening vector is shown, its slope is 2.0 and its length corresponds to the extinction  $A_V = 10$  mag. The tail of the ‘comet’ is composed of normal reddened stars, mostly of red clump giants of early K subclasses (the discussion see in López-Corredoira et al. 2002). This means that the stars at the upper end of the tail are reddened K-type red clump giants with  $A_V \approx 30$  mag. The comparison of their colors with the intrinsic colors of red giants may be used to estimate the slope of the reddening line. However, we need to know the intrinsic position of red clump giants in the  $J - H$  vs.  $H - K_s$  diagram.

For determining the intrinsic position of red clump giants we used the old open cluster M 67 which is very suitable, as the cluster is practically unreddened and its stars have solar chemical composition. Seven clump stars with  $V$  at 10.5 and  $B - V$  at 1.1 were selected from the Montgomery et al. (1993) catalog and are listed in Table 3.1.8.

The straight line connecting the center of red clump stars with the end of the ‘comet’ tail at  $J - H = 3.1$  and  $H - K_s = 1.4$  has the slope 2.06. This value in good agreement with the values obtained for O- and B-stars.

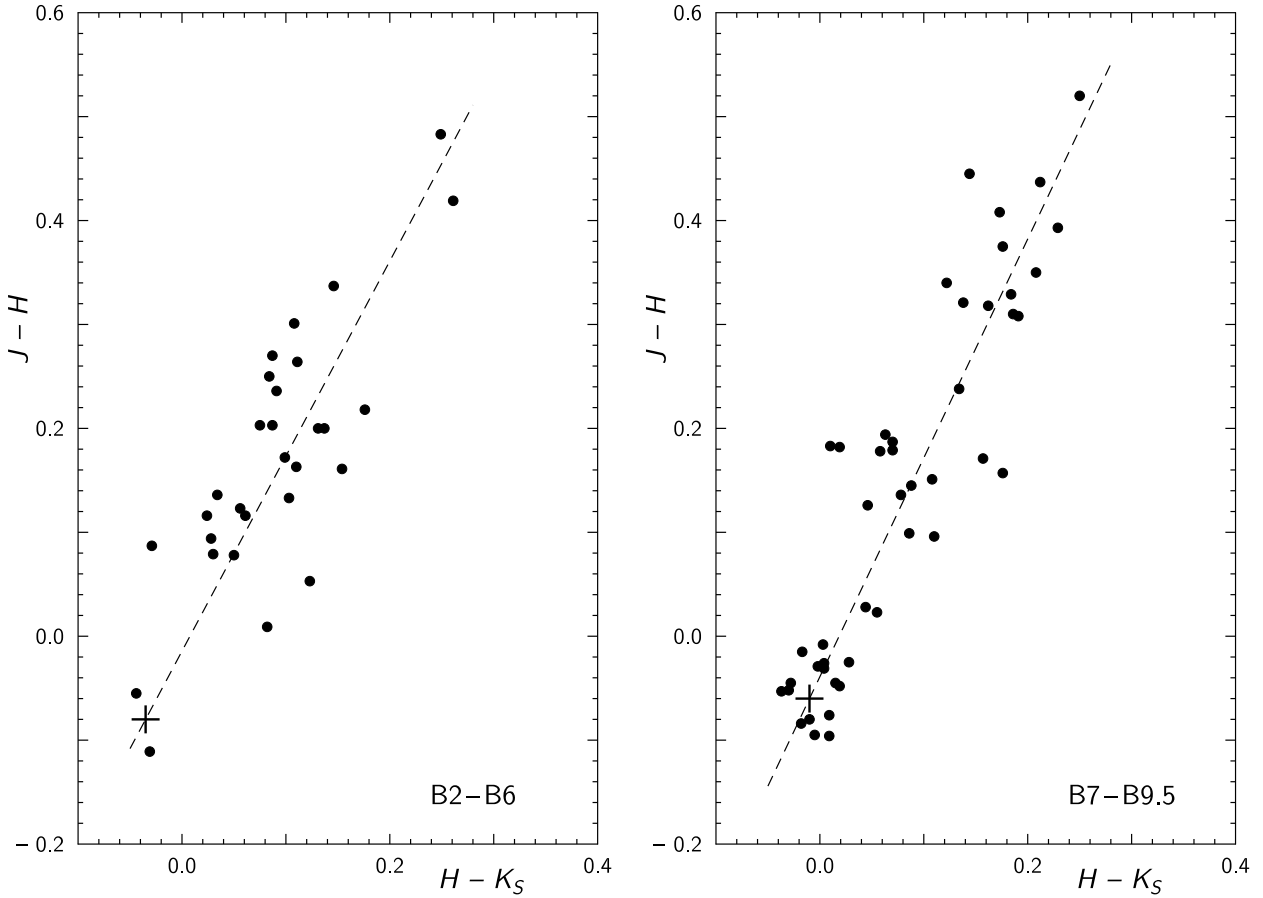


**Fig. 3.1.9.** (left) Interstellar reddening line for B2–B6 stars in the NAP nebulae region. The broken line is the least-square solution for 29 stars with the fixed intrinsic colors  $J-H = -0.08$ ,  $H-K_s = -0.035$ .

**Fig. 3.1.10.** (right) Interstellar reddening line for B7–B9.5 stars in the NAP nebulae region. The broken line is the least-square solution for 46 stars with the fixed intrinsic colors  $J-H = -0.06$ ,  $H-K_s = -0.01$ .

In Figure 3.1.13 we show a similar diagram for 66 000 stars selected in the association Cyg OB2 area. The area is of  $3^\circ \times 3^\circ$  size and its center is at  $20^{\text{h}} 33^{\text{m}}$ ,  $+41^\circ 20'$  (J2000). The straight red line joins the intrinsic position of the red clump giants and the upper end of the ‘comet’ tail at  $J-H = 3.65$  and  $H-K_s = 1.56$ . The slope of the reddening line, drawn by eye, is  $E_{J-H} / E_{H-K_s}$  is 2.02, in perfect agreement with the NAP area.

### Summary and Discussion:

To our knowledge, the Cygnus Rift anomaly is the largest region of the Milky Way to show a well confirmed, uniform peculiarity of the interstellar extinction law. If the anomaly extends from  $\ell = 74$  deg to  $\ell = 87$  deg, i.e. by 13 deg, at a distance of 580 pc it should be about 134 pc wide. If it has a similar depth, the size of the anomaly would be comparable to large stellar associations, such as the Orion OB1 association. However, the size of the anomaly probably is considerably larger, which follows from the following considerations.

It is considered that the dark clouds of the Great Cygnus Rift extend from 500 pc to 2000 pc (Bochkarev & Sitnik 1985). This oblong structure should be about 290 pc across in the middle (at 1250 pc distance), i.e., the ratio of axes of the structure is 1:5. The dust cloud separating the North America and Pelican nebulae probably belongs to the same Rift system, being in the front side of it, at a distance of 580 pc from the Sun. A similar distance for another dark cloud at the galactic longitude 90 deg has been found (Straizys, Kalaitis & Sudzius 1979). In the volume of the Great Cygnus Rift Cash et al. (1980) have identified a giant superbubble of gas, dust and luminous stars, emitting soft X-rays.

Our investigation shows that the same type of anomaly of the extinction law is valid for the stars both near the front edge of the structure (in the North America and Pelican area)

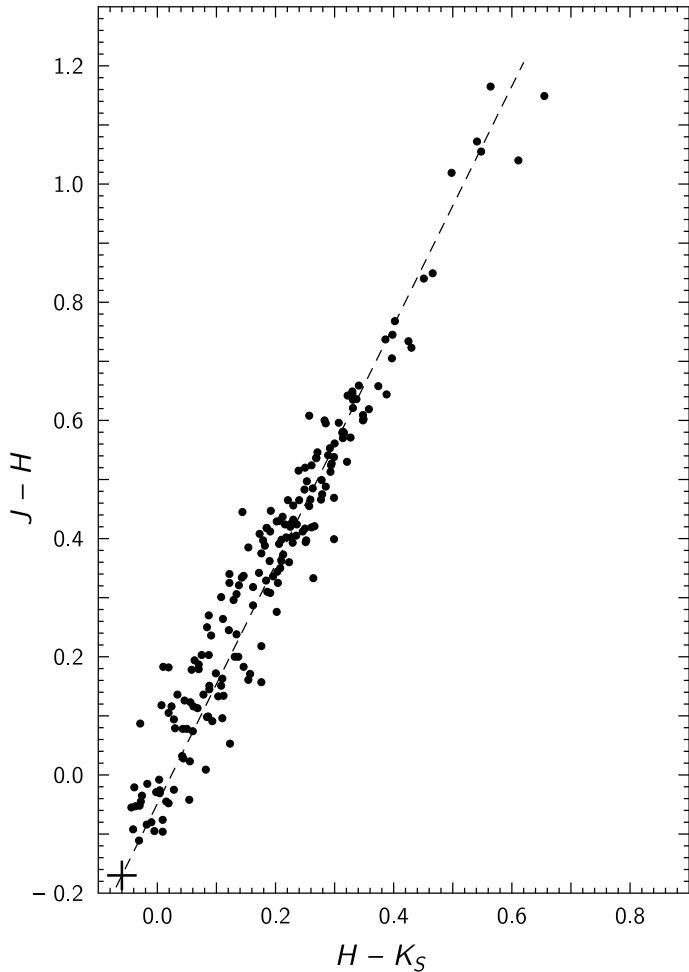


**Fig. 3.1.11.** Interstellar reddening line in the NAP nebulae region and the Cyg OB2 association for O–B9.5 stars together. The broken line is the least-square solution for all 193 stars with the fixed intrinsic colors  $J-H = -0.17$ ,  $H-K_s = -0.06$ .

and in all its volume, including the far edge at 2 kpc (O-type stars investigated by Sūdžius 1974). Somewhere in the middle of this structure the associations Cyg OB1, Cyg OB2 and Cyg OB9 are situated, their distances being 1.8, 1.8 and 1.2 kpc, respectively (Bochkarev & Sitnik 1985).

It is highly improbable that dust particles in the whole of the structure are modified by the radiation of hot luminous stars. Most of them are too far from the front edge of the structure. Probably, the region of the North America and Pelican nebulae is not even seen from these OB-associations, being covered by dark clouds of the Rift.

On the other hand, hot luminous stars usually modify the interstellar extinction law in the opposite direction: they remove small dust particles from their vicinity, making the extinction law similar to that observed in the Orion OB1 association. This law has a larger break of slope near the blue “knee” and shows lower extinction in the ultraviolet, opposite to what is observed in Cygnus.

Therefore, it is more acceptable that the anomaly of the extinction law in Cygnus is the intrinsic property of dust particles within all this huge volume of space due to their alignment by the galactic magnetic field. Another global agent, which could affect the dust chemistry, is the X-ray radiation within the Cygnus superbubble, described by Cash et al. (1980).

The anomalous interstellar extinction law in Cygnus should be taken into account when classifying reddened stars by their multicolor photometric  $Q$ -parameters. The methods of stellar classification in the presence of anomalous interstellar reddening are described by (Straižys 1992, 1999).

A comparison of color excesses  $E_{B-V}$  and the infrared color excesses from the 2MASS survey shows that in the area of the North America and Pelican nebulae the ratio  $R_{BV} = A_V/E_{B-V}$  is normal (about 3.15). A similar comparison of color excesses in the NGC 6997

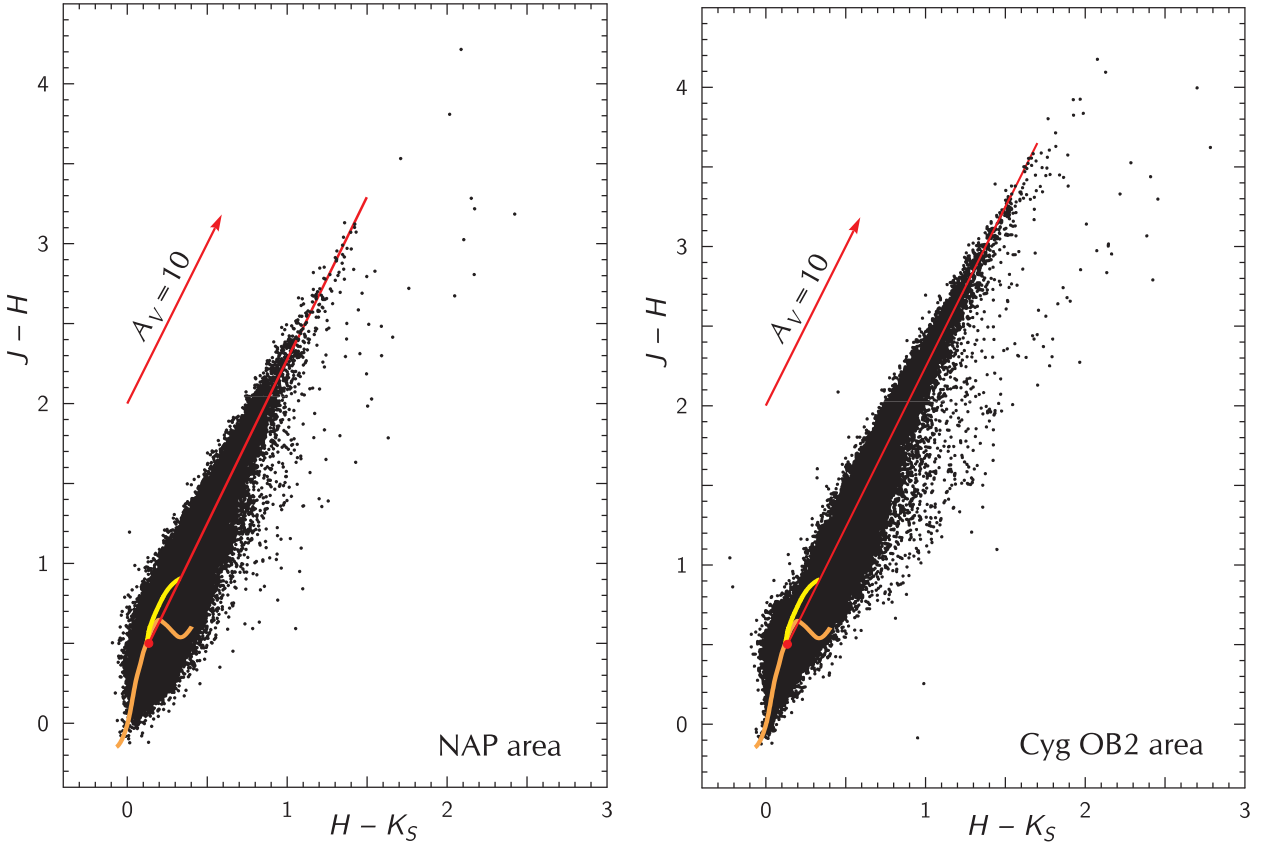


**Fig. 3.1.12.** (left) Two-color diagram for the NAP nebulae area of  $3^\circ \times 3^\circ$  size. The orange and yellow curves are intrinsic sequences of luminosity V and III stars. The red dot is the intrinsic position of the red clump giants, whose interstellar reddening is shown by the straight red line. The red line with an arrow is the reddening vector, its slope is  $E_{J-H} / E_{H-K_s} = 2.0$  and its length corresponds to the extinction  $A_V = 10$  mag.

**Fig. 3.1.13.** (right) The same as in Figure 3.1.12 but for the Cyg OB2 association area of  $3^\circ \times 3^\circ$  size and the center  $20^h 33^m, +41^\circ 20'$  (J2000).

area shows an increased value of  $R$ . For A-type stars we have accepted  $R = 3.50$ . This corresponds to  $R_{YY} = A_V/E_{Y-V} = 4.62$  in the Vilnius system. There are no evident reasons why this ratio should be increased: the cluster does not contain O-B stars, which could push out small dust particles, and the dust density around the cluster does not seem to be high enough to facilitate the coalescence of dust particles.

The ratios  $E_{J-H}/E_{H-K_s}$  determined so far in the 2MASS system in various Milky Way areas exhibit quite a wide range of values, between 1.6 and 2.1, the average value being close to 1.8. Our slopes of reddening lines in the NAP area and the Cyg OB2 association area both for O-B stars and K giants are near the upper limit of this range. Only for Globule 2 in the Coalsack Racca et al. (2002) in the CIT system obtained  $E_{J-H}/E_{H-K} = 2.08$ . If the ratio of colors in both systems given by Carpenter (2001) is valid also for color excesses, the ratio  $E_{J-H}/E_{H-K_s}$  in the 2MASS system should be 1.05 times larger, i.e., in the Coalsack it can be close to 2.2.

It is obvious that the variations of color-excess ratios in the infrared are related to sizes and compositions of dust grains. Most authors agree that between  $\sim 0.9 \mu\text{m}$  and  $\sim 5 \mu\text{m}$  the extinction curve can be approximated by a power law,  $A_\lambda \propto \lambda^{-\beta}$ . The most widely used is the value  $\beta = 1.8$ , representing the so-called ‘universal’ extinction curve in the infrared (Martin & Whittet 1990). However, in the last decade it was realized that  $\beta$  is not universal but has different values between 1.6 and 1.8 (see Draine 2003; Indebetouw et al. 2005; Flaherty et al. 2005; Froebrich & Burgo 2006; Froebrich et al. 2007). Since

$$\ln(A_1/A_2) = \beta \ln(\lambda_2/\lambda_1), \quad (3.1.17)$$

for the effective wavelengths of the passbands  $J$ ,  $H$  and  $K_s$  we can calculate the approximate

relation between  $\beta$  and the ratio of color excesses. Convolving the response functions given by Cutri et al. (2006) and Skrutskie et al. (2006) with spectral energy distributions of Kurucz models we obtain that  $\lambda_{\text{eff}}$  values for different temperatures are not very different, thus we took the values of 1.24, 1.64 and 2.14  $\mu\text{m}$  corresponding to solar-type stars. In this case

$$\beta = 2.045(E_{J-H}/E_{H-K_s}) - 1.722. \quad (3.1.18)$$

For the NAP area, where  $E_{J-H}/E_{H-K_s} = 2.0$ , we obtain  $\beta = 2.37$ . This value of  $\beta$  gives a relatively steep interstellar extinction curve in the 1–2  $\mu\text{m}$  range of wavelengths. A similar value of  $\beta$  was recently obtained by Larson & Whittet (2005) for high Galactic latitude clouds. Whittet (2008) estimates that such a value of  $\beta$  suggests smaller than average grain sizes, compared with the ‘typical’ value of  $\beta = 1.8$ . The curvature of the near IR segment of the extinction curve is a reflection of the fact that even the larger grains have sizes which are smaller than  $\lambda$ . In the small particle limit one would expect  $\beta = 4.0$  (Rayleigh scattering). On the other hand, for larger grains (e.g., with dimensions  $\sim 2 \mu\text{m}$ ) one would expect  $\beta \approx 1.0$ . It is not really possible to estimate average grain sizes from  $\beta$  but it should certainly follow the trend: larger  $\beta$ , smaller grains.

On the other hand, according to our earlier investigations, the dust in L 935 and the surrounding NAP area exhibits other peculiarities. Earlier we have obtained that the extinction law in the vicinity of NAP exhibits a smaller ‘knee’ in the blue part of the spectrum (Straizys et al. 1999) which is also consistent with smaller grains responsible for the extinction in the range of wavelengths covered by the  $B$  and  $V$  passbands.

To summarize, the following results of the present investigation may be listed:

1. A list of 95 O- and B-type stars with MK classifications, supplemented by the 2MASS  $J-H$  and  $H-K_s$  color indices, is compiled in the  $3^\circ \times 3^\circ$  area covering the North America and Pelican nebulae and including the L 935 dust cloud. For 37 stars spectroscopic MK types and for 40 stars photometric types are determined by the authors. The list is supplemented by 98 O–B1 type stars from the Cyg OB2 association.
2. Intrinsic color indices  $(J-H)_0$  and  $(H-K_s)_0$  are determined for spectral classes O8, B5.5 and B8.5 by dereddening bright stars with small interstellar extinction.
3. Interstellar reddening lines are calculated for stars of the three spectral groups: O–B1, B2–B6 and B7–B9.5. The slopes of the reddening lines, 2.00, 1.88 and 2.10, are obtained for the three groups.
4. The mean intrinsic colors  $J-H$  and  $H-K_s$  of seven red clump giants of spectral types G8–K2 III in the open cluster M 67 are determined. For areas of both the NAP nebulae and the Cyg OB2 association, joining the positions of the unreddened clump giants and the most heavily reddened stars in the  $J-H$  vs.  $H-K_s$  diagram, we obtain the reddening line slope of 2.06 and 2.02, respectively, which are in a good agreement with the slopes for O–B stars.
5. The mean ratio of color excesses  $E_{J-H}/E_{H-K_s} = 2.0$  may be recommended for the North America and Pelican nebulae region, as well as for the Cyg OB2 association. This value is somewhat larger than the ratios which are usually in use in the Cygnus direction.

### 3.2. Interstellar Extinction

#### 3.2.1. Introduction

This work continues the investigation of the area containing the North America and Pelican nebulae complex, using photometry of stars in the *Vilnius* seven-color photometric system and their two-dimensional classification. In the first paper (Straižys et. al 1989a, Paper I) the results of photoelectric photometry of 249 stars down to 11 mag, their two-dimensional classification, color excesses, interstellar extinctions and distances have been given. In the second paper (Straižys et. al 1989b, Paper II) interstellar extinction in the area was investigated. The dark cloud L 935, separating the North America and Pelican nebulae, was found to be at a distance of 550 pc. In the third paper (Straižys et. al 1993, Paper III) the cloud distance was revised to 580 pc, using photometry and classification of additional 564 stars down to 12.5 mag. In the above papers, the scale of absolute magnitudes of stars was based on the Hyades distance modulus  $V - M_V = 3.2$ . If we accept the new distance modulus of 3.3 (Perryman et al. 1998), the cloud distance determined in the last paper changes to 610 pc.

The present work starts a new series of investigations of the North America and Pelican nebulae complex, using CCD photometry in the *Vilnius* system obtained with the 35/51 cm Maksutov telescope of the Molėtai Observatory in Lithuania and with the 1 meter Ritchey telescope at the US Naval Observatory at Flagstaff, Arizona. The next section describes results from the Molėtai observations only.

#### 3.2.2. Relatively Transparent NAP Areas

We have divided the investigated area into two parts: one part is relatively transparent and includes a part of the North America Nebula, another one embraces the dark cloud L 935. For both areas the diagrams  $A_V$  versus  $r$  are shown in Figures 3.2.1, 3.2.2 and 3.2.3. Figures 3.2.1 and 3.2.2 are for the same area, but for different limiting distances. The stars with lower classification accuracy and the late F – early G stars classified without the ultraviolet color indices are shown as crosses. On all figures they are scattered in the same area, as the stars with all color indices available or with only  $U - V$  missing. Additionally, in the diagrams we plotted 105 brighter stars of the same area investigated in Papers I and III on the ground of their photoelectric photometry. Their distances determined in Papers I and III are multiplied by 1.05 to place them on the same scale. As a result, total number of stars plotted in Figures 3.2.1/3.2.2 and 3.2.3 are 354 and 242, respectively.

The dotted curves on the figures show the limiting magnitude effect for the stars of spectral classes B0 V, B2 V, B5 V, A0 V, A5 V, F0 V and F5 V. The stars of these spectral types above the corresponding curves are outside accessibility in the present program.

Let us discuss the distribution of stars in the  $A_V$  vs.  $r$  for the North America Nebula region shown in Figures 3.2.1 and 3.2.2. The following features can be noticed:

- (1) The stars with zero reddening are met from 100 to 600–700 pc. The same is true for the stars with small reddening, up to  $A_V = 0.5$  mag.
- (2) The upper limit of reddened stars gradually increases with increasing distance, reaching  $A_V \sim 0.8$  mag at 400 pc.
- (3) Approximately at this distance stars with higher extinction start to appear. The upper limit of  $A_V$  is  $\sim 4$  mag.
- (4) The area contains 20 OB-type stars and supergiants at distances between 2.0 and 6.5 kpc, their  $A_V$  values are between 1 and 4 mag. Most of these stars, if not all, should be inside the Orion spiral arm. Our line of view in this direction leaves this arm at about 4 kpc distance.

Such distribution of stars is consistent with the following model of distribution of interstellar dust. Up to a distance of  $\sim 600$  pc we see a general Galactic dust layer with an extinction gradient of  $\sim 1.0$  mag/kpc. Approximately at this distance a sharp increase of dust density takes place. If we accept a distance error of stars  $\pm 25\%$ , at 600 pc it corresponds to  $\pm 150$  pc. Due to this error, the expected scatter of stars reddened by the cloud should be observed between 450 and 750 pc. This is not far from reality, since we find the nearest stars with  $A_V > 1.0$  mag at  $\sim 400$  pc.

A more accurate distance of the dust cloud may be estimated by taking the average of

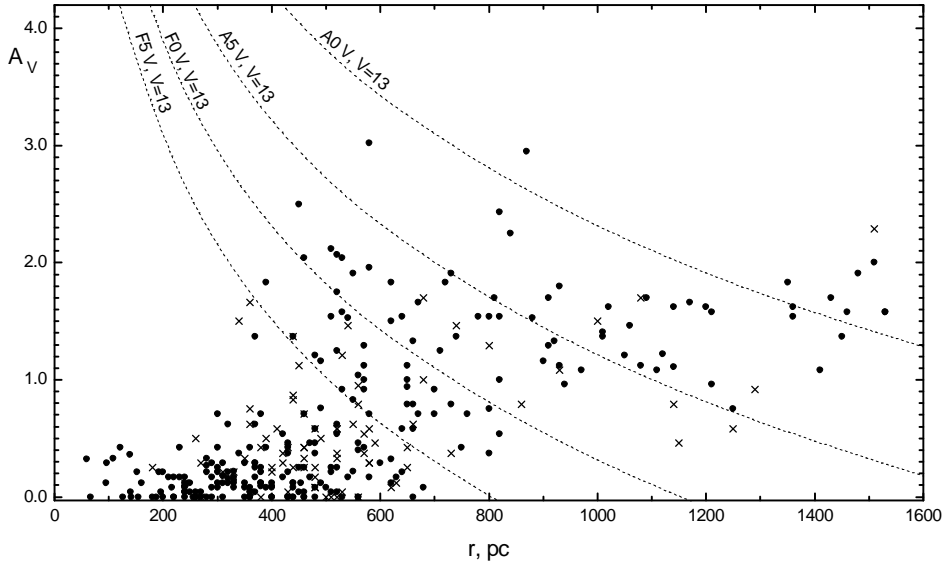


**Fig. 3.2.1.** The dependence of interstellar extinction  $A_V$  on distance up to 1.6 kpc for the North America Nebula area.

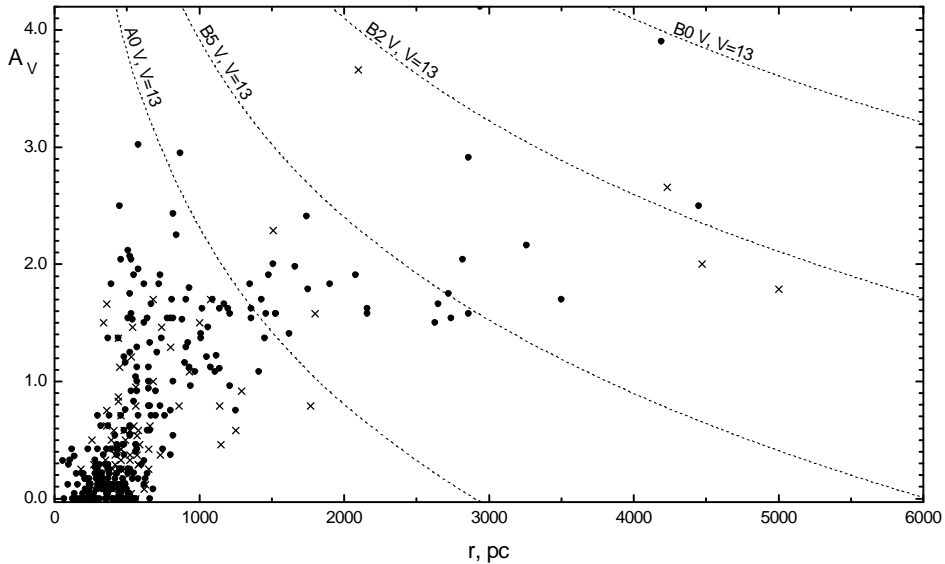


**Fig. 3.2.2.** The dependence of interstellar extinction  $A_V$  on distance up to 6 kpc for the North America Nebula area.

limiting distances to the nearest reddened stars and to the most distant unreddened stars. We suppose, both these limiting distances are caused by the same source – a dust cloud and the distance errors of stars inside the cloud and just behind it. The nearest stars with  $A_V > 1.0$  mag are at 400 pc and the farthest stars with  $A_V < 0.5$  mag are at 800 pc. The average of these distances is 600 pc. Thus, our results are consistent with the distance of the absorbing dust cloud at 600 pc, in good accordance with the cloud distance determined in Paper III.

Maximum extinction in the direction of the North America Nebula is not high: a lot of faint stars are seen on deep photos. Among the stars with the extinction  $A_V > 1.5$  mag, 31 are closer than 1 kpc, 22 are between 1 and 2 kpc and 20 are farther than 2 kpc. Stars which are closer than 1 kpc exhibit the maximum extinction values at  $\sim 3$  mag.

Now lets turn to the  $A_V$  vs.  $r$  graph for stars in the dark cloud area, shown in Figure 3.2.3. Although both transparent and dark areas are of comparable apparent size, the last one shows much smaller surface density of stars, and most of them are the foreground objects. Actually both areas are very similar with respect to the number of foreground stars and their distribution on the  $A_V$  vs.  $r$  diagrams. However, the dark area is very poor of stars with extinctions larger than 1.0 mag at distances farther than 800 pc. In the dark area, the nearest reddened stars with  $A_V > 1.0$  mag and the farthest stars with  $A_V < 0.4$  mag are

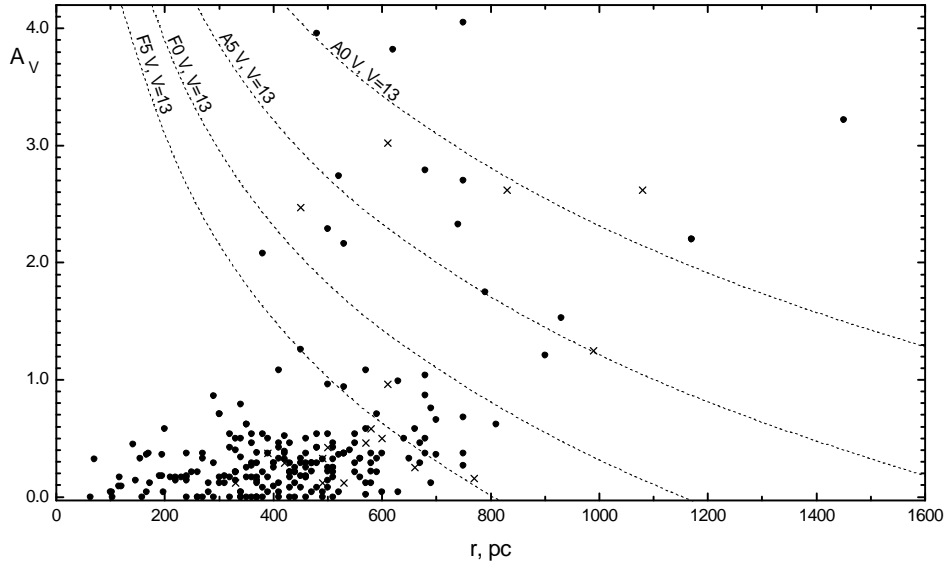


**Fig. 3.2.3.** The dependence of interstellar extinction  $A_V$  on distance for the area of the dark cloud L 935.

almost at same distances as in the transparent area discussed above: at 400 and 800 pc. Their average distance is 600 pc. It is difficult to estimate the error of the cloud distance since we do not know which stars reside in the cloud and which are behind it. Probably the distance is accurate within  $\pm 50$  pc.

Thus, we are safe to accept that the absorbing clouds in both areas are at the same distance. However, in the dark area the extinction is much larger, and here down to 13 mag we see only a few background stars. The majority of reddened stars with  $A_V > 1.5$  mag are situated within 400 and 800 pc, the limiting distances for stars residing within the dust cloud. The scarce background stars probably are seen through semitransparent cloud windows. In other directions the cloud in the optical wavelengths is almost black. According to Cambrésy et al. (2002), in some directions of our area the visual extinction may be considerably larger than 5 mag.

We have no idea how deep is the L 935 dust cloud, i.e., is there a single comparatively thin dust sheet or the cloud has extensions along the line of sight. If the cloud is approximately round, its thickness should not exceed 20–30 pc.

## RESULTS AND CONCLUSIONS:

(1) CCD photometry in the *Vilnius* seven-color system has been done for 690 stars down to 13.2 mag in the  $2 \times 2$  sq. degree area including the North America Nebula and the dust cloud L 935, separating the North America and Pelican nebulae. About 150 of these stars have been observed photoelectrically.

(2) Majority of the stars have been classified in spectral and luminosity classes. Their color excesses, interstellar extinctions and distances have been determined.

(3) The extinction vs. distance graphs have been plotted separately for the area of the North America Nebula and for the dust cloud L 935 area. It is shown that the interstellar extinction in both areas up to 600 pc distance is consistent with the general Galactic dust layer with a gradient of  $\sim 1.0$  mag/kpc.

(4) A steep increase of extinction is observed in both areas at  $\sim 400$  pc, which may be explained by the presence of a dust cloud at about 600 pc distance. In the area of the North America Nebula this cloud is relatively thin, its extinction does not exceed  $A_V = 3$  mag. In the area of the dark cloud L 935 the extinction is much larger. Due to the limiting magnitude effect, the stars with extinctions greater than 4 mag are not observable in both areas.

(5) This work shows that the Maksutov telescope of the Molėtai Observatory is an excellent instrument for a precise CCD photometry since in one exposure it gives a  $1.2 \times 1.2$  sq. degree field with a  $25 \times 25$  sq. mm CCD chip. However, the meniscus lens of the telescope should be replaced to one, more transparent in the ultraviolet. Also, a CCD chip with enhanced ultraviolet sensitivity is to be used.

### 3.2.3. The Region of NGC 6997

This work continues the investigation of the area containing the North America and Pelican nebulae complex, using photometry of stars in the *Vilnius* seven-color photometric system and their two-dimensional classification (Straizys et al. 1989a,b, 1993; Laugalys & Straizys 2002). In these papers the investigation was concentrated within the Local (Orion) spiral arm, trying to determine the distance of the dust cloud L 935, separating the North America and Pelican nebulae. It was found that this cloud, located at a distance of about 600 pc, extends also to the nearby areas giving an obscuration in the direction of the North America Nebula of about 3 mag in  $V$ .

In the present we are trying to investigate both the vicinity of the North America Nebula and more distant regions of the Galaxy behind it. We chose to investigate a region in the direction of the open cluster NGC 6997 which for a long time was confused with NGC 6996, a clump of stars  $1^\circ$  north (see Corwin 2004). NGC 6997 was studied in one of our previous papers (Zdanavičius & Straizys 1990, hereafter ZS90). In the present study a larger telescope and deeper exposures allow obtaining a two-dimensional classification of stars as faint as  $V = 17$  mag. Our intention is to obtain a better value of the cluster distance to check its relation to the L 935 dust cloud and the North America Nebula.

In this direction our line of sight crosses the outskirts of the dust cloud L 935 and runs along the Local spiral arm up to 3 kpc distance. Then it crosses the Perseus arm at 5–7 kpc and the Outer (Cygnus) arm at 9–11 kpc (see Vallée 2005). However, we have no hope of finding the tracers of the last arm in this investigation since most of them should be located above the Galactic plane due to the disk warp (see Russeil 2003, Fig. 6).

The North America and Pelican nebulae region has been investigated many times by radioastronomical techniques in the CO molecular lines (Bally & Scoville 1980; Dame et al. 1987, 2001; Leung & Thaddeus 1992; Odenwald & Schwartz 1993; Feldt & Wendker 1993; Dobashi et al. 1994). An analysis of radio line radial velocity profiles allows the possibility of identifying to which spiral arm a particular molecular cloud belongs. However, within the Local arm this method is not effective, and for the distance determination of molecular clouds usually the associated objects are used. The North America Nebula is situated at the edge of a giant complex of molecular and dust clouds known as the Great Cygnus Rift. Dame et al. (1987) place the Rift at a distance of 700 pc and give a 200 pc diameter to it. The next complex of molecular clouds in the same direction, belonging to the Local arm, is called Cyg X. It is located near the Galactic plane at a distance of about 1.7 kpc and covers the longitude range from  $73^\circ$  to  $87^\circ$ . The area of NGC 6997 is at the edge of the Cyg X complex, coinciding with one of its transparent windows (see Leung & Thaddeus 1992, Fig. 3).

In Figures 3.2.4 and 3.2.5 interstellar extinctions  $A_V$  are plotted against  $d$ , distances from the Sun. Figure 3.2.4 gives a large-scale extinction distribution up to 7 kpc, while Figure 3.2.5 is limited to 2 kpc. Here we show the situation for the enlarged value of  $R_{YV} = 4.62$ . The case of using the normal value of  $R_{YV} = 4.16$  will be also discussed.

The most prominent feature of both figures is the rise of extinction between 500 and 1500 pc from zero to  $\sim 3$  mag. The two dotted curves shown in Figure 3.2.4 correspond to the limiting magnitudes  $V = 16$  and 17 for A0 V stars. Between these two curves our two-dimensional classification of stars almost vanishes due to the limiting magnitude effect. Above and to the right of the A0 V,  $V = 17$  curve only some B-type stars and G–K giants of luminosities II and II–III are present. We suspect more O- and B-type stars to be present among the stars of magnitudes 16–17.5, but due to the absence of ultraviolet colors there is no possibility of reliably estimating their spectral and luminosity classes.

The present investigation gives better accuracy for the dust cloud distance in comparison to our earlier studies: a deeper limiting magnitude makes it possible to measure and classify K dwarfs as distant as the dust cloud. In Figure 3.2.5 the majority of stars with  $A_V < 1.4$  and closer than  $d = 800$  pc are G–K–M dwarfs. They give a distance to the front edge of the dust cloud with a rather good accuracy. Accepting a distance error of 20 %, we may estimate the distance of the dust cloud by looking for apparent distances of the reddened stars closest to the Sun. The closest reddened stars appear at about 400 pc if  $R_{YV} = 4.62$  and at about 440 pc if  $R_{YV} = 4.16$ . Thus the real distance of these stars should be either at  $400/0.8 = 500$  pc (if the ratio  $R_{YV}$  is 4.62) or  $440/0.8 = 550$  pc (if the ratio is 4.16).

These distances may be compared with the distances of the L 935 cloud and its surroundings found in our earlier papers. The results are summarized in the following table, after

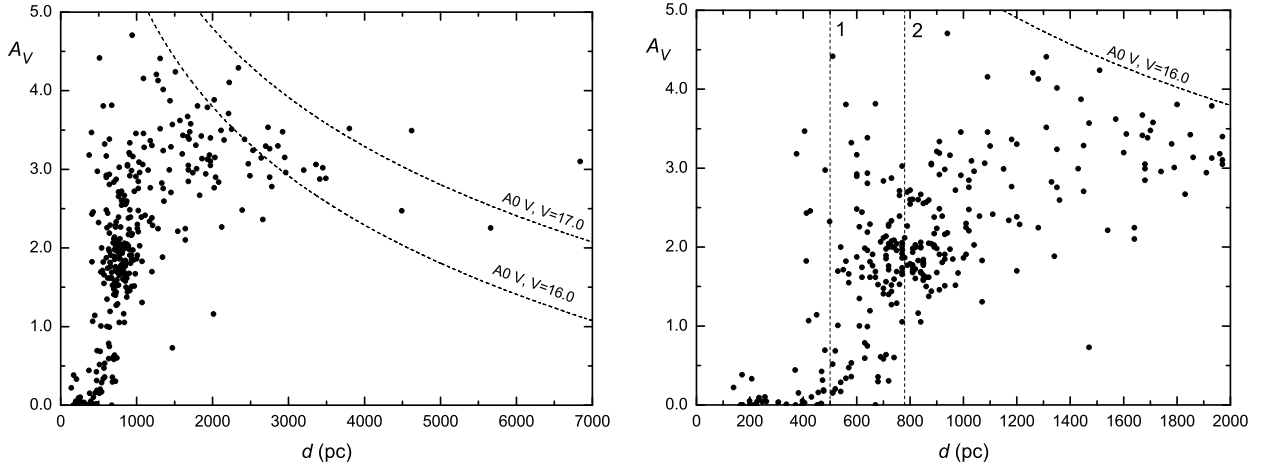


**Fig. 3.2.4.** (left) Interstellar extinction as a function of the distance up to 7 kpc. The two curves show the limiting magnitude effect for A0 V stars.

**Fig. 3.2.5.** (right) Interstellar extinction as a function of the distance up to 2 kpc. The two vertical lines show: 1 – the front edge of the dust cloud, 2 – the average distance of NGC 6997. The curve in the right corner shows the limiting magnitude effect for A0 V stars.

transformation of the original distances to the new Hyades distance modulus:

Straižys et al. (1989b) (with  $R_{BV} = 3.4$ ) – 578 pc,  
 Straižys et al. (1993) (with  $R_{BV} = 3.4$ ) – 609 pc,  
 Laugalys & Straižys (2002) (with  $R_{BV} = 3.1$ ) – 600 pc,  
 Present work (with  $R_{BV} = 3.5$ ) – 500 pc,  
 Present work (with  $R_{BV} = 3.1$ ) – 550 pc.

The agreement of the distance determinations is reasonable, taking into account possible errors. Our method is based on the distance of reddened stars which apparently are closest to the Sun on the “extinction vs. distance” plot. This method works well if we have a statistically significant number of reddened stars on the rising part of the plot. If their number is small, the result is not sufficiently reliable: some stars may seem to be closer to us not due to the dispersion of their absolute magnitudes but to their peculiarity, duplicity and other reasons. In our previous papers the number of reddened stars was not sufficient to get reliable results. Only in the present investigation we have more stars on the rising part of the dependence due to fainter limiting magnitude and use of reddened G-K dwarfs which are quite numerous in the general Galactic field. On the other hand, the distance differences of dark clouds, found in various papers, may be real since we are not sure that in all investigated areas dust clouds begin at the same distance.

Figure 3.2.4 shows that the extinction continues to grow behind the dark cloud. At the 1 kpc distance the average  $A_V$  is about 2.5 mag, at 2 kpc it is about 3.0 mag. The farther run of the mean extinction cannot be followed due to the limiting magnitude effect. Some tendency of its growth continues up to 3 kpc, where our line of sight leaves the Local arm. However, we do not observe in it any other cloud of the density comparable to the cloud at 500 pc. For example, there is no trace of Cyg X at 1.7 kpc. The reason is that the main mass of this cloud complex is concentrated at lower Galactic longitudes.

At about 5–7 kpc our line of sight should cross the Perseus spiral arm. At this distance with  $A_V = 4$  mag B0 V stars will be of  $V = 13.4$ – $14.1$  mag and B5 V stars – of 16.6–17.3 mag. Consequently, O and early B stars of the Perseus arm may be present in our catalog. Indeed, we find about 35 stars of magnitudes 16.0–17.5 which by photometric classification are similar to stars of spectral classes O–B5 with interstellar extinction between 3 to 5 mag. The extinction values of these stars are of reasonable accuracy but without reliable  $U$  and  $P$  magnitudes we cannot determine luminosity classes and distances of these stars. Some of them could also belong to the Outer (Cygnus) spiral arm but they should be scarce in the Galactic plane due to warp of the disk. CCD photometry with a larger telescope or with longer exposures could give an answer.

### 3.2.4. L 935 Dark Cloud Area

The North America and Pelican nebulae in Cygnus usually are considered as one large H II region, W 80, separated by the dark cloud L 935 (Lynds 1962) situated in front of it. This is confirmed by radio continuum observations of the ionized gas which seems to form one large structure with nearly circular symmetry and a diameter of about  $3^\circ$  (Wendker 1968; Goudis 1976a,b). Most probably, both the dust cloud and the emission nebulae are almost at the same distance. According to the recent investigation by Cambrésy et al. (2002), based on the 2MASS survey, the visual extinction of the cloud in the densest regions is as large as 35 mag, and its mass is about  $45\,000 M_\odot$  at a distance of 580 pc determined by Straizys et al. (1993).

The L 935 cloud is at the northern end of a large system of molecular and dust clouds, known as the Great Cygnus Rift. Radio observations of the area in CO molecular lines are listed in our previous work (Laugalys et al. 2006). A high resolution CO map of Leung & Thaddeus (1992) shows that the North America/Pelican molecular cloud is separated from the main body of the Great Cygnus Rift by a lane of lower density.

Since the cloud is in the same spiral arm as the Sun, its radial velocity with respect to the LSR is close to zero. Consequently, the radial velocity of the cloud gives no information about its distance. For a distance determination the associated objects should be used, for example, the stars located at the beginning of the cloud or inside it. We just should determine the distance at which the stars exhibit a sharp rise of the interstellar reddening caused by the cloud dust.

With this aim in mind we have started investigations of the interstellar extinction distribution with distance in various parts of the North America and Pelican nebulae complex using interstellar reddening-free two-dimensional classification of stars observed in the seven-color *Vilnius* photometric system. The first three papers (Straizys et al. 1989a,b, 1993) were based on photoelectric photometry of stars down to  $V \sim 12.5$  mag. This limiting magnitude was too bright to detect heavily reddened stars immersed in the dust cloud or located behind it. Also, at a distance of the cloud, which is found to be  $\sim 550$  pc, K0 and M0 stars of the main sequence are expected to be of 14.6 and 17.5 magnitudes (with zero interstellar extinction). Due to the luminosity function, these stars are much more frequent in space than F–G stars, and we may expect that many of them will be found at the cloud edge. Consequently, the appearance of reddened stars at some distance will indicate the front edge of the cloud.

This was the reason why we tried to apply CCD photometry to reach apparently fainter stars in the North America and Pelican nebulae complex. The first paper of the CCD series by Laugalys & Straizys (2002, hereafter Paper I) was only a test of the method, and we reached  $\sim 13.2$  mag stars with a relatively small 35/51 cm Maksutov-type telescope. At this limiting magnitude the number of foreground stars was still low. Joining the results of photoelectric and CCD photometry we came to the conclusion that the front edge of the dust cloud L 935 is at about  $600 \pm 50$  pc distance. In the next paper (Laugalys et al. 2006, hereafter Paper II) we investigated the interstellar extinction run with distance in the direction of the open cluster NGC 6997, which is located behind the North America Nebula, and found the cloud distance between 500 and 550 pc. The interstellar reddening law in the direction of North America and Pelican was investigated in Paper II and in one of our earlier papers (Straizys et al. 1999).

In the present work we present the results of the extinction investigation in four areas of the dust cloud L 935. Three contiguous areas are located south west of “Florida” and in the “Mexican Gulf”. The fourth area is about  $45'$  above them, at the edge of the dark cloud and the “North America”. Positions of the areas with respect to the emission nebulae are shown in Figure 3.2.1. A limiting magnitude of 17–18 mag makes it possible to observe numerous K and M dwarfs at the cloud distance.

Figures 3.2.7, 3.2.8, 3.2.9 and 3.2.10 exhibit the interstellar extinction  $A_V$  for the four areas plotted as a function of the distance in the same scale. In some respects all of them are quite similar. At first glance we clearly see a steep rise of extinction beyond the  $\sim 400$  pc distance signifying beginning of the dust cloud. In front of the cloud the extinction increases from zero to about 0.5–0.7 at 400 pc, but zero-extinction stars are found up to a distance of 600–650 pc. In Area I (Fig. 3.2.7) no reddened stars are seen at  $d > 850$  pc. For some reason we do not find any reddened star with  $A_V > 3.5$  mag. In Areas II, III and IV a few

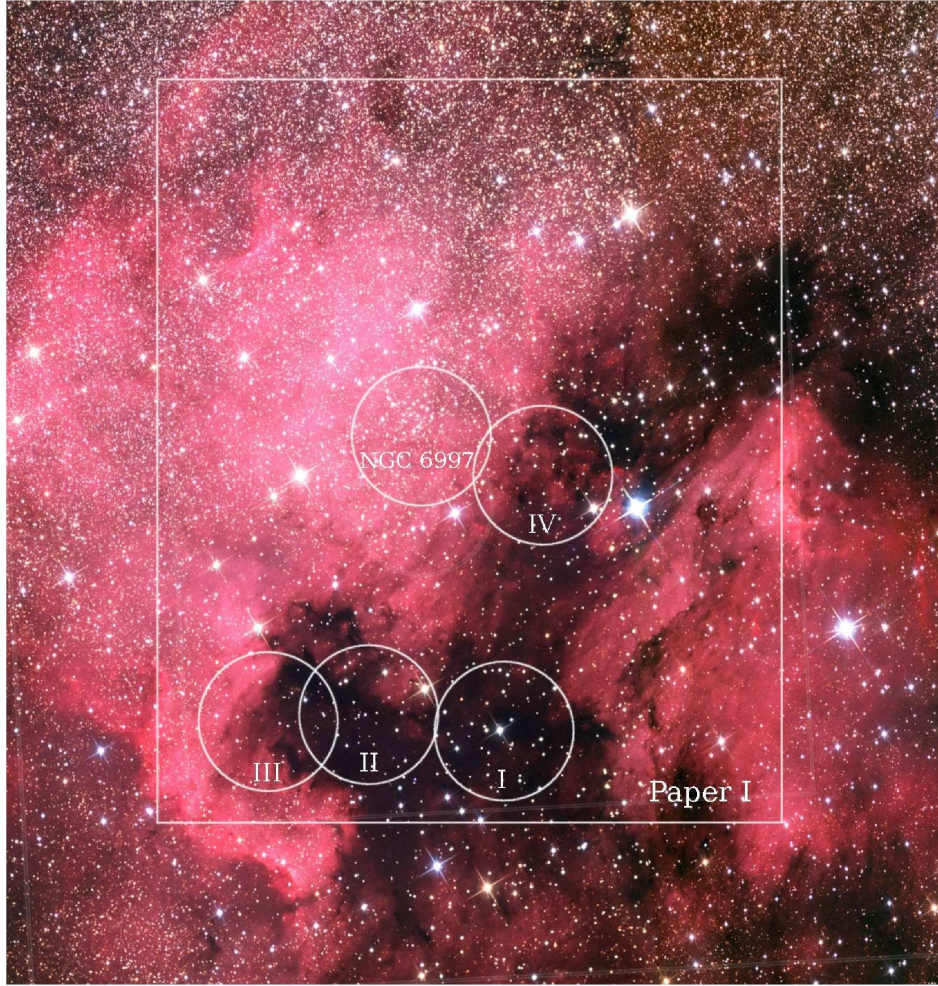


**Fig. 3.2.6.** The investigated areas. The rectangular area was investigated in Paper I, the open cluster NGC 6997 area – in Paper II and the Areas I, II, III and IV – in the present work.

heavily reddened stars ( $A_V$  between 3 and 6 mag) have been identified, some of them are located up to distances of  $\sim 3.5$  kpc. Much more heavily reddened stars are present among the classified B and A stars, however, their ultraviolet colors are either absent or are of low accuracy. Thus, we could not determine their luminosity classes and distances. Most of them should be distant objects located far behind the dust cloud.

Four stars, mostly K and M dwarfs, were found to exhibit excessively large extinctions at relatively small distances (200–300 pc). These stars were suspected being binaries and were not plotted in Figures 3.2.7–10. Their spectral types in Tables 3.2.1–4 (see in Appendix) are given in brackets with the notes at the end of Tables. In Areas III and IV two distant stars (between 1 and 3 kpc) exhibit too small interstellar extinction values. These stars are either seen through transparent windows or their spectra are peculiar. These stars should be investigated by spectroscopy.

The similarity of the extinction run with distance in the four areas offers an idea to join all four figures into one shown in Figure 3.2.11. It contains 289 stars measured and classified in the present investigation by CCD photometry and 6 stars projected on the same dark cloud and measured photoelectrically in the earlier investigations (Straižys et al. 1989a, 1993). Figure 3.2.11 is quite similar to Figure 6 from Paper I which corresponds to a brighter limiting magnitude of 13 mag but over a much larger area. In that figure the majority of stars at the beginning of the dark cloud are main-sequence stars of spectral classes F and G, while in Figure 3.2.11 almost all stars at this distance are K and M dwarfs. They are quite numerous even in the small CCD areas in front of the darkest regions of the cloud, and the appearance of reddened red dwarfs signifies the beginning of a dark cloud, as it was explained in Paper II.

The real distance of the dark cloud may be estimated from the apparent distances of the nearest reddened stars. Figure 3.2.11 shows that such stars are seen at a distance of 400 pc where they might appear due to absolute magnitude errors. If we accept the absolute

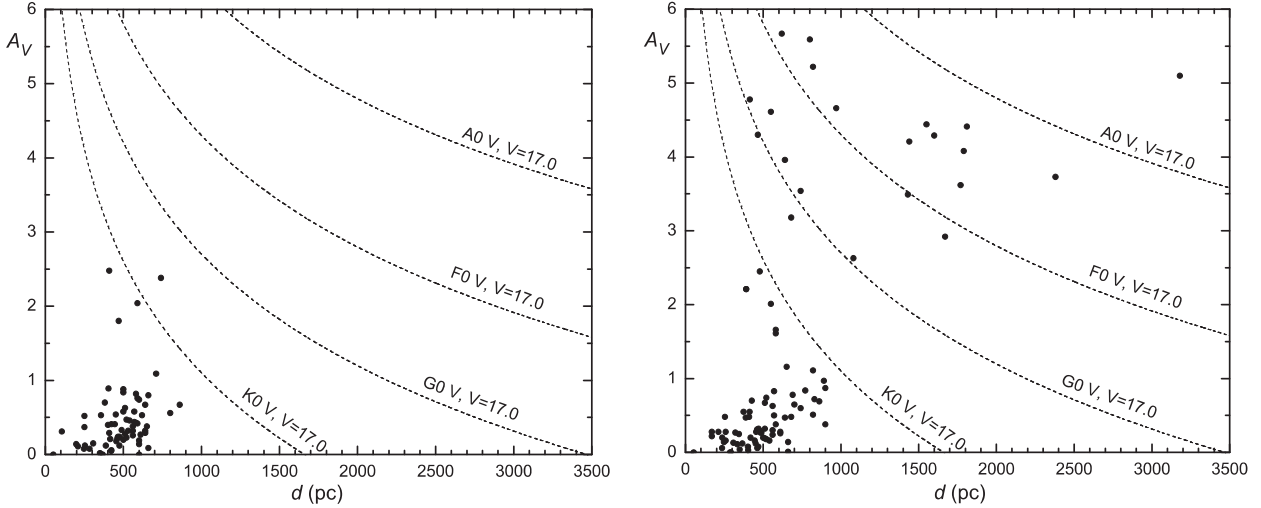


**Fig. 3.2.7.** (left) Interstellar extinction as a function of the distance up to 3.5 kpc in Area I. The four curves show the limiting magnitude effect for stars of spectral classes A0 V, F0 V, G0 V and K0 V.

**Fig. 3.2.8.** (right) The same as in Figure 3.2.7, but for Area II.

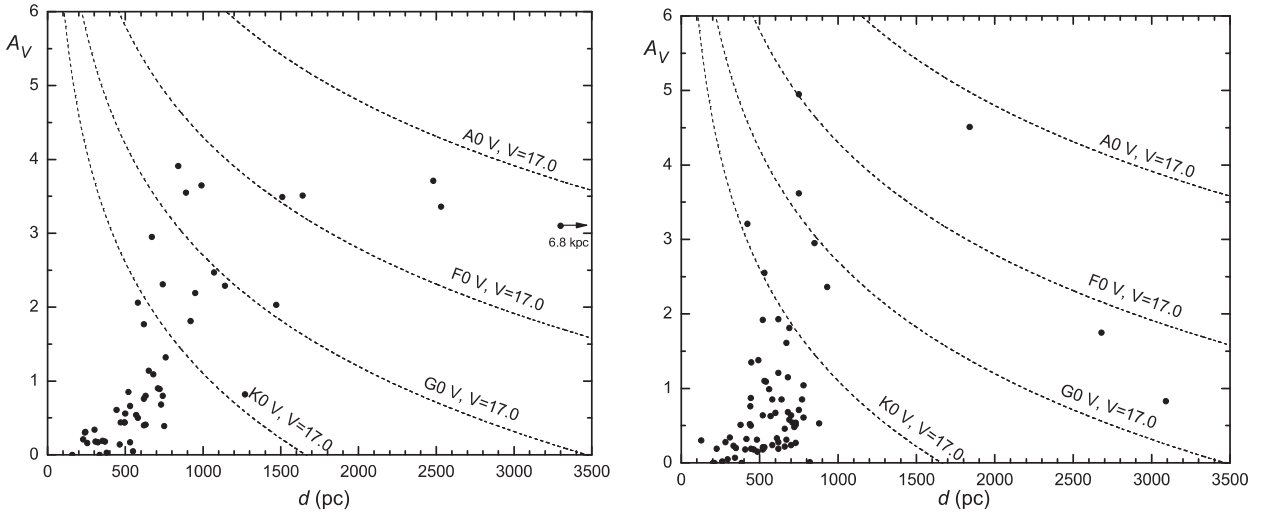


**Fig. 3.2.9.** (left) The same as in Figure 3.2.7, but for Area III.

**Fig. 3.2.10.** (right) The same as in Figure 3.2.7, but for Area IV.

error of  $M_V$  to be +0.5 mag, this gives an absolute distance error of -20 %. Then we should expect the cloud distance to be at  $d = 400 + 0.2d$  or  $d = 400/0.8 = 500$  pc. However, some reddened stars at a distance of 400 pc may be binaries consisting of two red dwarfs. In this case their real distance should be larger. If both components are of the same spectral type, the distance of the binary star system should be increased by a factor of 1.41. This introduces additional uncertainty in the distance determinations. On this basis we have rejected four stars at small distances (less than 300 pc) with outstanding extinction values, as was explained at the beginning of this section. It is important to check these rejected stars and other considerably reddened stars near the 400 pc distance for possible periodic changes of their radial velocities.

The other possibility of estimating cloud distance is by the use of stars with small reddening apparently seen at the largest distances. We may consider that these stars are reddened up to  $A_V \approx 0.5$  mag by the general dust layer of the Galaxy. The largest distances of such stars in Areas I, II, III and IV are the following: 650, 900, 750 and 800 pc, the average value being 775 pc. If the distance error of these stars is  $+0.26d$  (corresponding to an  $M_V$  error of 0.5), then  $d = 775/1.26 = 615$  pc. Consequently, the real distance of the cloud is somewhere between 500 and 615 pc, the average value being  $\sim 560$  pc.

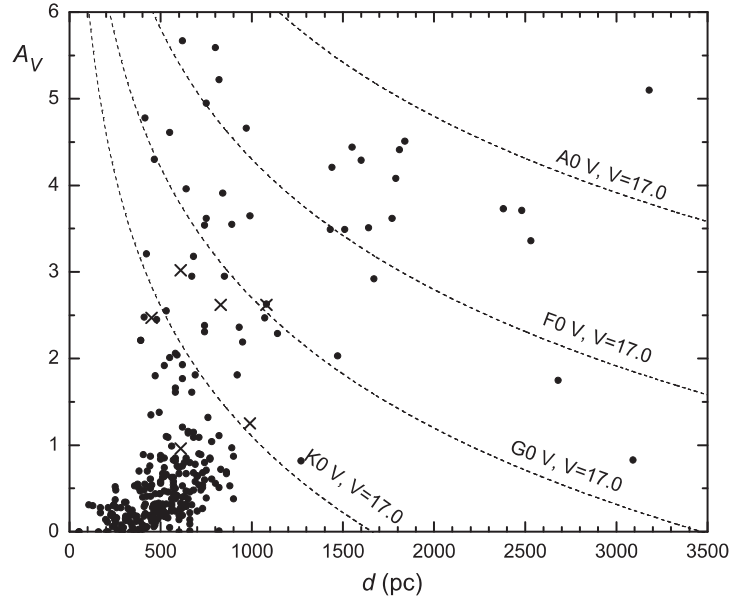


**Fig. 3.2.11.** Interstellar extinction as a function of the distance up to 3.5 kpc in all four areas together. The symbols  $\times$  denote six bright stars from the same areas measured photoelectrically in our earlier papers.

Both estimates may not coincide due to several reasons. One possibility is the underestimation of the errors of  $M_V$ . An increase of the  $M_V$  error only by 0.1 mag is more than sufficient to avoid the mentioned ambiguity of the distance. If the accuracy of  $M_V$  is  $\pm 0.6$ , then the distance errors are  $-24\%$  and  $+32\%$ , and the cloud distance determined for stars with large and small reddening is  $400/0.76 = 526$  pc and  $675/1.32 = 511$  pc, respectively. Both these values almost coincide, and we may assume that the cloud is located at a distance of 520 pc. However, in any case the absolute error of the cloud distance probably is not smaller than  $\pm 50$  pc.

### 3.2.5. The Region of Collinder 428

In Figure 3.2.12 interstellar extinctions  $A_V$  are plotted against  $d$ , distances from the Sun. The extinction run in the present area is quite similar to that found in Paper II for the NGC 6997 area, except that in Figure 3.2.12 we have a smaller number of stars due to lower accuracy of photometry and classification. As earlier, the most prominent feature is a steep rise of the extinction beyond  $\sim 400$  pc. The two dotted curves shown in the Figure correspond to the limiting magnitudes  $V = 16$  and  $17$  for A0V stars. Between these two curves our two-dimensional classification of stars almost vanishes due to the limiting magnitude effect.

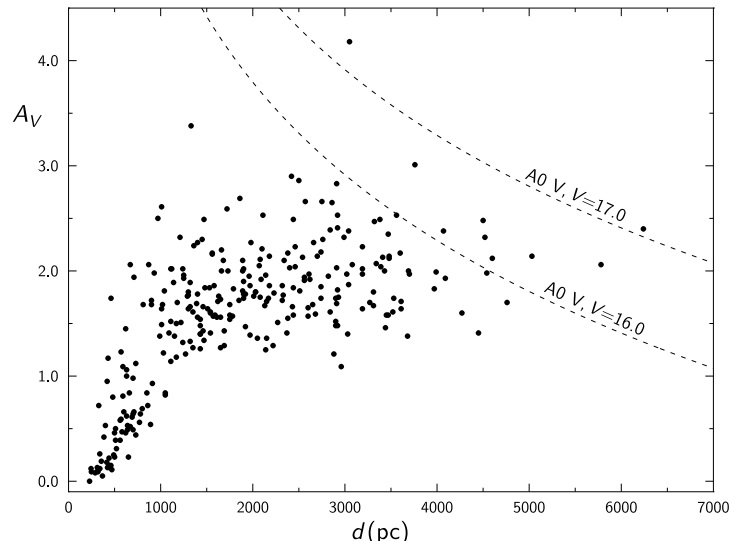


**Fig. 3.2.12.** Interstellar extinction as a function of the distance up to 7 kpc. The two curves in the right upper corner show the limiting magnitude effect for A0V stars.

Accepting a distance error of  $+26\%$ , we may estimate the distance of the dust cloud by looking for apparent distances of the reddened stars closest to the Sun. The closest reddened stars appear at about 400 pc. Their real distance should be at  $400/(1-0.26) = 540$  pc. This distance is comparable with the distances of the L 935 cloud and its surroundings found in our earlier papers.

### 3.2.6. Extinction from 2MASS star counts

The most detailed and deep investigation of interstellar extinction in the direction of the NAP complex was published by Cambrésy et al. (2002) who applied the method based on star counts in  $K_s$  magnitude and on statistical color excesses  $E_{H-K_s}$ . The angular resolution of the extinction map is  $4\text{--}7'$  in the high extinction areas with  $A_V$  between 20–30 mag. This means that smaller areas with high extinction cannot be resolved.

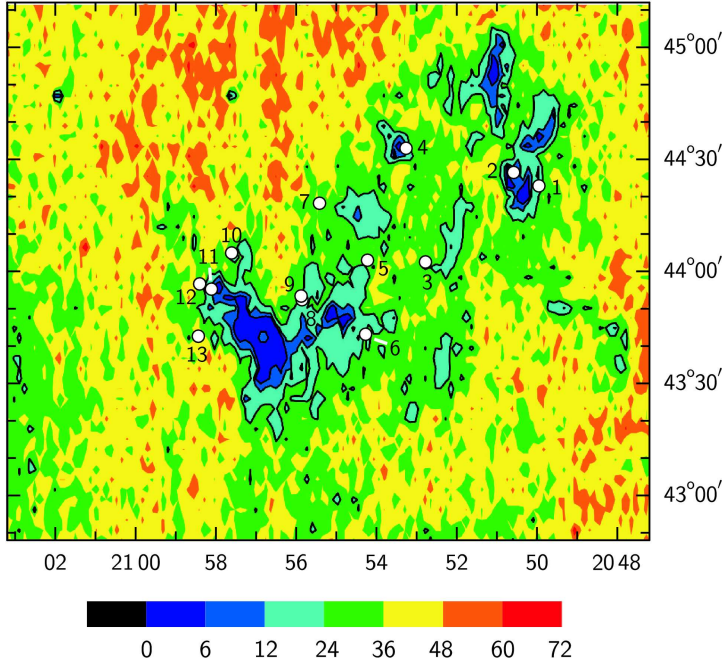


**Fig. 3.2.13.** The map of star counts in the  $K_s$  magnitude in  $2' \times 2'$  cells. The scale below the map indicates numbers of stars. The numbered white circles show the locations of the O-like stars from Table 4.2.1

To examine the extinction distribution in greater detail we have applied star counts in  $K_s$  within  $2' \times 2'$  cells. 500 000 stars with the indication of photometric uncertainty  $\sigma < 0.25$  were used. The number of stars falling in each cell varied from zero to  $\sim 70$ . The resulting star density map for RA  $20^{\text{h}}48^{\text{m}} - 21^{\text{h}}02^{\text{m}}$  and DEC  $43^{\circ} - 45^{\circ}$  is shown in Figure 3.2.13. It exhibits more details and broader boundaries of large extinction than the Cambrésy et al. (2002) map. Since we have no calibration of star counts in extinctions, the map can be used only for a qualitative estimate of the extinction in the NAP complex in the direction of O-like stars listed in Table 4.2.1.

We also applied another method to estimate the maximum extinctions in the vicinities of O-like stars, based on the reddenings of the background red-clump giants. From the  $J-H$  vs.  $H-K_s$  diagrams, plotted for the areas of  $20'$  diameters around these stars, the maximum values of  $J-H$  were read out taking into account only stars close to the reddening line with the slope  $E_{J-H}/E_{H-K_s} = 2.0$ , originating from the intrinsic position of red clump giants, i.e.,  $J-H = 0.50$ ,  $H-K_s = 0.14$  (see Straižys et al. 2008). Possible pre-main-sequence stars, identified by the criterion  $Q_{JHK_s} < 0.0$ , were excluded from consideration. Distances to 10 stars with maximum extinctions in each direction were calculated, accepting their  $M_K = -1.7$  and the extinctions determined from  $E_{J-H}$ . Most of these stars are located between 0.6 and 2 kpc, i.e., belong to the Local arm. We accept that their extinction originates mainly in the NAP complex, since no more distant dense clouds are known in this direction. The maximum values of  $A_V$  calculated by the equation:

$$A_V(\max) = E_{J-H} / 0.12 = (J - H - 0.50) / 0.12, \quad (3.2.1)$$

are given in Table 4.2.1.

## 4. YOUNG STARS AND IONIZING SOURCES

### 4.1. Suspected Emission-Line and T Tauri Type Stars

The investigated areas coincide with a star-forming region known as the Cyg T1 association (Khlopov 1959, 1970). Here tens of H $\alpha$  emission-line stars and T Tauri type stars were discovered and listed by Herbig (1958), Herbig & Rao (1972), Welin (1973), Gieseking (1973), Tsvetkov (1975), Gieseking & Schumann (1976), Marcy (1980) and Herbig & Bell (1988). Some of the discovered emission-line stars are Be-stars and have no relation to star-forming regions. However, late-type stars with H $\alpha$  emission should be either classical T Tauri type stars with the equivalent width of emission  $> 10 \text{ \AA}$  (CTTS) or weak-line T Tauri stars with fainter emission (WTTS, sometimes called post-T Tauri stars). Six of the Herbig stars fall into our Area II, for four of them CCD magnitudes and colors were measured, the remaining two are fainter than our limiting magnitude. Spectral types and spectral energy distributions between 430–670 nm for the four mentioned Herbig stars were determined by Cohen & Kuhi (1979).

As was shown by Meištas (1982), Paupers et al. (1989) and Straizys et al. (1998), the *Vilnius* system is very effective for identification of stars with H $\alpha$  emission. This is mainly based on photometric effect of H $\alpha$  emission in the *S* passband which has its mean wavelength at 656 nm and the half-width 20 nm. The emission makes the radiation intensity in *S* stronger, color index *V*–*S* larger and the reddening-free parameter

$$Q_{XZS} = (X - Z) - E_{X-Z}/E_{Z-S}(Z - S), \quad (4.1.1)$$

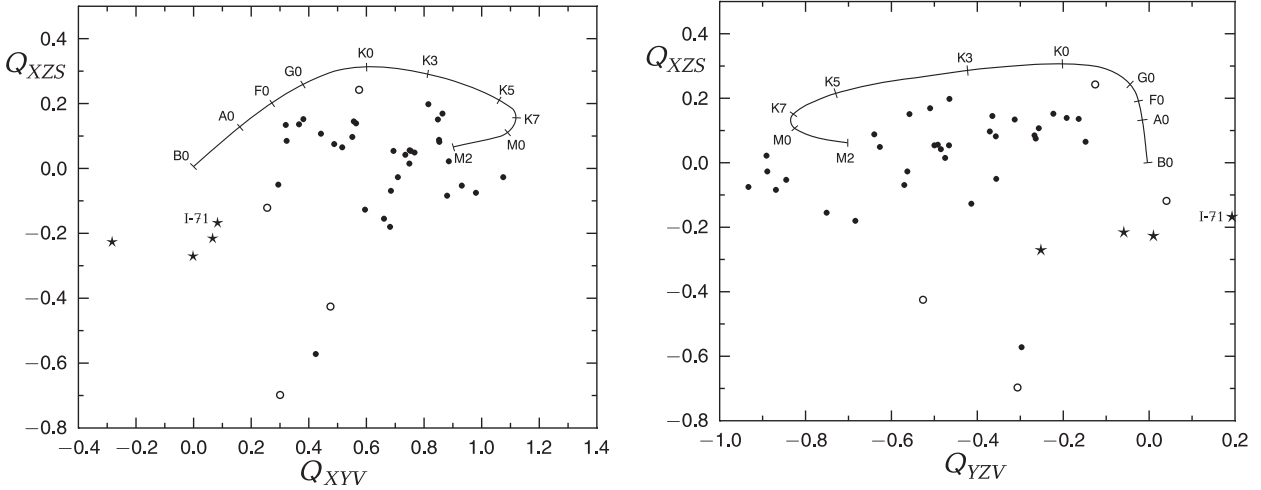
smaller than in the stars without emission. The mean wavelengths of the passbands *X* and *Z* are 405 and 516 nm. In some other color indices of the *Vilnius* system, the photometric effect is caused by other strong emission lines and by continuum emission in the ultraviolet. The most important reddening-free diagrams for the identification of T Tauri stars and other stars with strong H $\alpha$  emission are  $Q_{XZS}$  vs.  $Q_{XYV}$  and  $Q_{XZS}$  vs.  $Q_{YZV}$ . Here *Y* and *V* are the passbands at 466 and 544 nm. Both these diagrams do not contain ultraviolet passbands, and this makes observations more exact for the faintest stars near the limiting magnitude.

Figures 4.1.1 and 4.1.2 show these two reddening-free diagrams with 40 stars from our areas falling in the H $\alpha$  emission region. Four stars shown by open circles are V1539 Cyg, V521 Cyg, LkH $\alpha$  189 and LkH $\alpha$  191 (Herbig & Bell 1988). Most of other stars should be also either classical T Tauri stars (CTTSs) or post-T Tauri pre-main-sequence stars with weaker emission lines (WTTSs). Probably, they are not K or M dwarfs with chromospheric activity, since H $\alpha$  emission in these stars usually is too faint to be detected by medium-band photometry (Straizys et al. 1998). In Figures 4.1.1 and 4.1.2 the three LkH $\alpha$  stars deviate downward, as is expected for the stars with H $\alpha$  emission. However, LkH $\alpha$  191 shows no significant deviation from the main sequence. Probably, this star lost its envelope during the last 50 years.

For the majority of suspected H $\alpha$  emission K dwarfs, spectral classes and extinctions have been estimated photometrically, with somewhat lower accuracy. Almost all of them exhibit  $A_V$  values from 0.5 to 3.0 mag, and their distances are consistent with the distance of the dark cloud. This additionally confirms their dependence to the young dark cloud population.

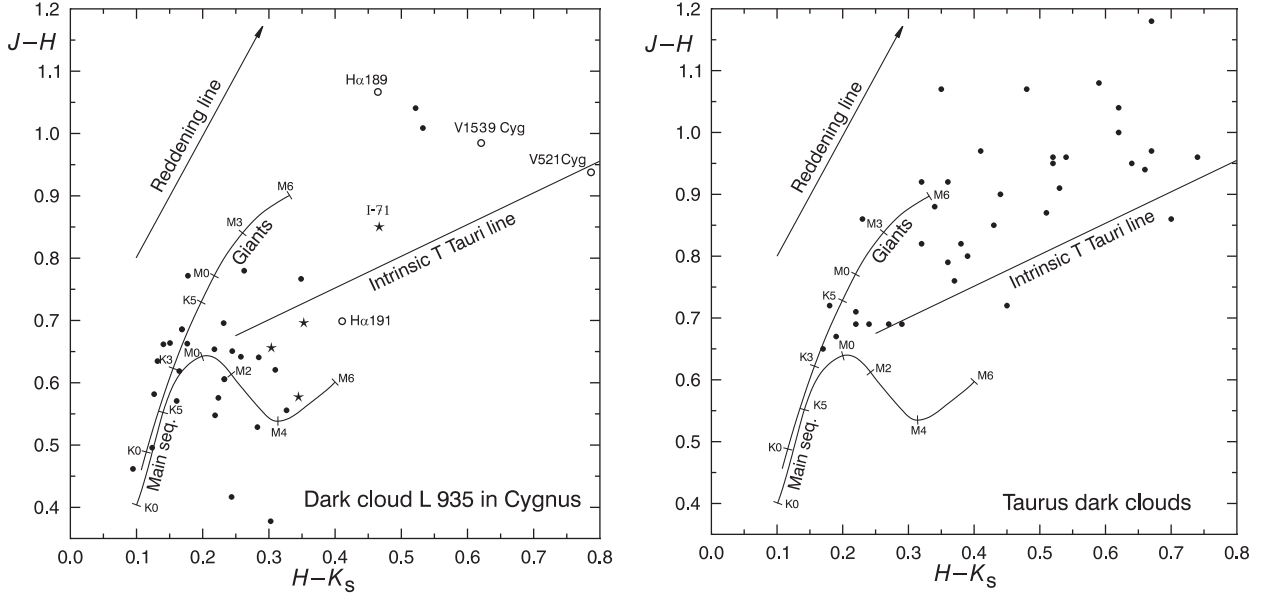
Young emission-line stars usually exhibit intrinsic infrared excesses caused by the thermal radiation of the hot dust disk. The *J*–*H* vs. *H*–*K* diagram is considered as one of the most informative diagrams of infrared photometry in which pre-main-sequence stars are well separated from the normal star sequences even in the presence of strong interstellar reddening. Moreover, Rydgren & Vrba (1981) and Rydgren et al. (1982) have shown that after interstellar dereddening most T Tauri and related young stars form a quite well defined sequence. The most recent analysis and modeling of this intrinsic sequence of T Tauri stars was analyzed by Meyer et al. (1997). The increase of the disk thickness (due to its accidental orientation) moves the star along this sequence to larger color indices. The increase of interstellar reddening moves the star upwards from this sequence.

Figure 4.1.3 shows the *J*–*H* vs. *H*–*K*<sub>s</sub> diagram with suspected emission-line stars in the L 935 cloud plotting the 2MASS survey data (Cutri et al. 2003a). The intrinsic lines of normal K–M dwarfs and giants are taken from Bessell & Brett (1988) after their transformation



**Fig. 4.1.1.** (left) Interstellar reddening-free diagram  $Q_{XZS}$  vs.  $Q_{XYV}$ . The solid line with ticks of spectral classes is the main sequence of solar composition stars. Dots are the stars suspected to have  $H\alpha$  line in emission. The four open circles are two T Tauri stars and two emission-line stars confirmed spectroscopically. The four star-like symbols denote suspected Be stars.

**Fig. 4.1.2.** (right) Interstellar reddening-free diagram  $Q_{XZS}$  vs.  $Q_{YZV}$ . Symbols are the same as in Figure 4.1.1.



**Fig. 4.1.3.** (left) Two-color diagram  $J-H$  vs.  $H-K_s$  in the 2MASS system for the investigated L 935 cloud. The main sequence and the giant sequence for K and M stars, the interstellar reddening line and the intrinsic line of T Tauri stars are shown. Dots are the stars with suspected  $H\alpha$  emission (the same as in Figures 4.1.1 and 4.1.2). Four open circles denote the known T Tauri and emission-line stars. The star-like symbols denote the suspected Be stars. One of them, labeled as I-71, is the star suspected being the O-type star ionizing the emission nebulae, see the text.

**Fig. 4.1.4.** (right) The same as in Figure 4.1.3 but for the Taurus dark clouds, see the text.

to the 2MASS system by the equations from Carpenter (2001, p. 2869). The slope of the interstellar reddening-line,  $E_{J-H}/E_{H-K} = 1.9$ , is taken from Bessell & Brett (1988). The intrinsic sequence of T Tauri stars from Meyer et al. (1997) is also plotted. It is evident that most of our stars suspected in emission are situated above the intrinsic K–M V sequence, except a few stars of spectral classes F and G. This location can be explained both by the thermal infrared emission in circumstellar dust disks and by interstellar reddening. The stars with the strongest dust emission are in the right upper corner of the diagram. The stars with low dust emission (most of them also exhibit a weak  $H\alpha$  emission) are clustering near

the main-sequence line, but exhibit some excess in  $J-H$ . Star LkH $\alpha$  191 is not far from the main sequence, exhibiting only a small dust emission. This is in agreement with the absence of a strong H $\alpha$  emission noted above.

Figure 4.1.4 shows the  $J-H$  vs.  $H-K_s$  diagram plotted for young Taurus cloud stars taking their 2MASS color indices from Briceño et al. (2002). To facilitate a comparison, we plotted only the stars falling in the same ranges of color indices as in Figure 4.1.3 and only the stars of spectral classes earlier than M4. It is evident that the color distribution of emission-line objects in the Cygnus and Taurus clouds is quite similar, however, in Taurus many more stars are located in the right upper part of the diagram (with larger dust emission).

Spectroscopic confirmation of the suspected emission-line stars for the presence of H $\alpha$  emission and monitoring of their variability are desirable, since this would increase considerably the number of known young stars in the Cyg T1 association. So far the majority of T Tauri stars in this association have escaped detection due to a large distance to it and a strong interstellar and circumstellar reddening.

## 4.2. Ionizing Sources

### 4.2.1. Introduction

In the past there were numerous attempts to identify the star (or stars) responsible for the ionization of the North America and Pelican nebulae (the H II region W80). The history of the search has been described recently by Comerón & Pasquali (2005).

The first true candidate for the ionizing star was HD 199579 ( $V = 6.0$ ), a single-line spectroscopic binary of spectral class O6 Ve, proposed by Sharpless & Osterbrock (1952). The star is located in the upper part of the North America Nebula and there are some signs of its interaction with the nearby gas – within about 0.5 degree from the star the thermal radio flux in decimeter waves has somewhat larger intensity (see, e.g., Matthews & Goss 1980). However HD 199579 alone cannot be responsible for the ionization of all the H II region since it is located too far from the center of the complex. Therefore a search for other ionizing stars has been continued. Herbig (1958) suggested that the true ionizing star can be located behind the dust cloud L 935 which separates the North America and Pelican nebulae.

Additional important information about the ionizing star was presented by Bally & Scoville (1980) who investigated the complex in  $^{12}\text{CO}$  radio line at 2.60 mm. From the analysis of line profiles they concluded that the molecular complex expands with a velocity of 5 km/s from the point near the peak of the thermal radio emission. This expansion was interpreted as the remnant of the ionization shock front system from the H II region which was once formed by a young O-type star (or stars) born off-center in the original molecular cloud about 3–8 million years ago. When the shock reached the back edge of the molecular cloud, an asymmetric flow of ionized gas was established, depressurizing the inner H II region. This outflow has formed a huge outer H II region on the opposite side of the L 935 dust and molecular cloud, the present NAP nebulae. In the direction of the Sun the front edge of dust/molecular cloud was much thicker and remained almost unaffected. In an attempt to find the ionizing O-B stars behind the L 935 cloud Bally & Scoville (1980) identified 11 infrared sources which might be the candidates.

This model was extended by Wendker et al. (1983) using the thermal radio continuum observations at 11 cm. The decimeter continuum reveals a complicated picture of the flux distribution with a number of local maxima, ridges, bright rims and other structural details. To explain these features, Wendker et al. proposed a model of the complex containing a group of eight O-stars, ionizing so-called cavities in the parent dust/molecular cloud. They supposed that the resulting small H II regions form the local radio flux maxima in the three ridges of increased radio emission crossing the L 935 cloud. No candidates for the ionizing stars were proposed.

One more feature which has played a significant role in the search for the ionizing stars were the bright rim structures. In the NAP nebulae Pottasch (1956) described seven rims seen in the optical. The bright rims are usually located at the edges of dark clouds where they meet the ionized region. The rims are sharply defined, especially from the dark side. The brightest portion of each rim is usually directed to the exciting star. In space they have a form of flat or curved sheets of ionized gas, and are best seen when viewed edge-on.

Matthews & Goss (1980) identified some of the Pottasch optical rims in the thermal radio map at 49 cm and nine additional rims which are seen only in radio – optically they are completely obscured by the dark cloud. Four new radio rims were added by Wendker et al. (1983). The orientation of the rims was an important factor in searching for places of the ionizing stars.

#### 4.2.2. The Comerón & Pasquali Star

Comerón & Pasquali (2005) in their search for the ionizing star have used the  $J-H$  vs.  $H-K_s$  and  $K_s$  vs.  $H-K_s$  diagrams in a circle of  $0.5^\circ$  radius centered on the coordinates RA (2000) =  $20^{\text{h}}55^{\text{m}}17^{\text{s}}$ , DEC (2000) =  $+43^\circ 47' 30''$ , near the geometric center of the complex. They identified 19 infrared objects lying near the interstellar reddening line of O-type stars in the  $J-H$  vs.  $H-K_s$  and  $K_s$  vs.  $H-K_s$  diagrams. For these objects the infrared spectra between 1.5 and  $2.4\ \mu\text{m}$  were obtained, and two early-type stars were found. Finally, optical spectra of these two stars were used for the identification of the star 2MASS J205551.25+435224.6 (hereafter CP05-4) as the best candidate. This star was classified as O5 V and recognized as the ionizing star for the entire H II complex. This star is present in the list of Bally & Scoville (1980) of the potential ionizing objects.

The four star-like symbols in Figures 4.1.1, 4.1.2 and 4.1.3 denote OB-type stars with suspected  $\text{H}\alpha$  emission. One of them, star No. 71 from Area I (hereafter I-71), was classified by Comerón & Pasquali (2005) as O5 V, and it was suspected of being the star responsible for the ionization of the North America and Pelican nebulae (it is designated as J205551.25+435224.6). The other three stars are from Area IV (Nos. 98, 105 and 124), and they have no relation to the cloud, being distant background objects ( $A_V$  between 5.5 and 7 mag,  $d$  between 3 and 4 kpc).

Our classification of star I-71 by reddening-free  $Q$ -parameters places it at early B spectral class, but with low accuracy. For it we find a negative  $Q_{XZS} = -0.17$  value which indicates a possible presence of  $\text{H}\alpha$  emission, since for a normal O5 V type star both  $Q$ s should be close to zero. Probably, either the star is peculiar or the absorbing dust properties in front of the star are modified by its radiation leading to non-standard color-excess ratios and, consequently, to wrong values of  $Q$ -parameters. Also, the reduction errors of color indices from the instrumental CCD system to the standard *Vilnius* system of such a heavily reddened star cannot be excluded.

If I-71 is indeed of spectral type O5 V, then our data give its reddening  $E_{Y-V} = 2.20$  and  $A_V = 9.2$  mag for the normal interstellar extinction law. In this case, adopting  $M_V = -4.5$ , we get  $d = 520$  pc, which is the cloud distance. However, the ratios  $E_{V-J}/E_{Y-V}$ ,  $E_{V-H}/E_{Y-V}$  and  $E_{V-K}/E_{Y-V}$  of this star are consistent with a larger ratio  $R$ , thus the value of  $A_V$  may be as large as 10 mag or even more. Also, the absolute magnitude of the star can be estimated from its spectral type only approximately. As a result, the distance to the star cannot be calculated with good accuracy. In any case, the star seems to be a reliable candidate as a source ionizing the North America and Pelican nebulae. To avoid the shielding by the L 935 dust cloud, the star must be located well behind it.

If the star is more luminous, its distance should be larger. Since we have no accurate estimation of its luminosity, the relation of this star to the ionization of the entire NAP complex is not secure. If the star is responsible for ionizing the complex, then, to avoid shielding of the ultraviolet photons, it must be located well behind the L 935 dust cloud, in a relatively transparent space where the parent dust/molecular cloud has been already destroyed.

Looking for young stellar objects (YSOs) in the NAP area, we have analyzed stars measured in different photometric systems covering a spectral range between 0.35 and  $8.3\ \mu\text{m}$ . We have found some stars behind the L 935 (Lynds 1962), or Tokyo 497 (Dobashi et al. 2005), dust/molecular cloud which are similar to heavily reddened O-type stars located at a distance of the nebulae. This stimulated the present search for stars which can be contributors to the ionization of the surrounding nebulae. For the investigation a  $3^\circ \times 3^\circ$  area centered at J2000:  $20^{\text{h}}56^{\text{m}}, +44^\circ$  was taken.

#### 4.2.3. More O-Like Stars Behind The L 935 Cloud

For the identification of potential ionizing stars behind the L 935 cloud in the 2MASS catalog we applied a method similar to that used by Comerón and Pasquali but with the

following alterations: (1) the search area was extended along all the length of the L935 cloud; (2) the magnitude  $K_s$  limit was changed to  $K_s < 5.6 + 1.8(H - K_s)$ ; this limit includes all main-sequence O-type stars up to 550 pc and more luminous stars at larger distances; (3) according to Straizys et al. (2008), the ratio of color excesses  $E_{J-H}/E_{H-K_s}$  in the  $Q$ -parameter was taken 2.0, i.e.,  $Q_{JHK_s} = (J - H) - 2.0(H - K_s)$ . The limits set to  $Q_{JHK_s}$  were the values between 0.05 and -0.15, obtained from the intrinsic  $Q_{JHK_s}$ -value of O-type stars, -0.05, taking into account the scatter of points in Figure 3.1.8. One more restriction was put on the accuracy of 2MASS photometry: all objects with the errors in  $J$ ,  $H$  and  $K_s$  magnitudes (given in the catalog) larger than 0.1 mag were not considered. According to Straizys & Lazauskaitė (2008), the ratio  $E_{J-H}/E_{H-K_s}$  depends slightly on the temperatures of stars: with decreasing  $T_{\text{eff}}$  the ratio also decreases. The expected difference in slopes between O- and K-type stars is only about 3%, and this effect was neglected in the present study.

The objects, satisfying the above conditions, were checked in the Simbad database, and all known stars of spectral class B and cooler were rejected. Among them quite numerous were N-type carbon stars. A few infrared objects, classified spectroscopically by Comerón & Pasquali (2005, Table 1) as carbon or AGB stars, were also excluded. We also excluded stars outside the L935 dust cloud and the Pelican Nebula where the  $A_V$  extinction lower than 10 mag is expected (Cambrésy et al. 2002). Most probably, these objects are not heavily reddened O-stars.

The remaining 13 objects are listed in Table 4.2.1 which includes also CP05-4, the confirmed O5 V star. The star No. 12 was included in the list despite its  $Q_{JHK_s} = -0.22$ ; see discussion in Section 4.2.7. All these objects hereafter will be called as ‘O-like stars’. No information about them is given in the Simbad database. Their DSS2 magnitudes  $V$ ,  $F$  and  $N$  were taken from the GSC-2.3 catalog available at Simbad. The  $J$ ,  $H$  and  $K_s$  magnitudes were taken from the 2MASS Point Source Catalog; in Table 4.2.1 their values are rounded to two decimal places. For most of the objects the MSX fluxes at 8.3  $\mu\text{m}$  are available and are given in Table 4.2.1. The next columns give the values of  $Q_{JHK_s}$ , maximum  $A_V$  expected (see Section 4.2.7) and the classification of the objects (see Sections 4.2.4, 4.2.5 and 4.2.6).

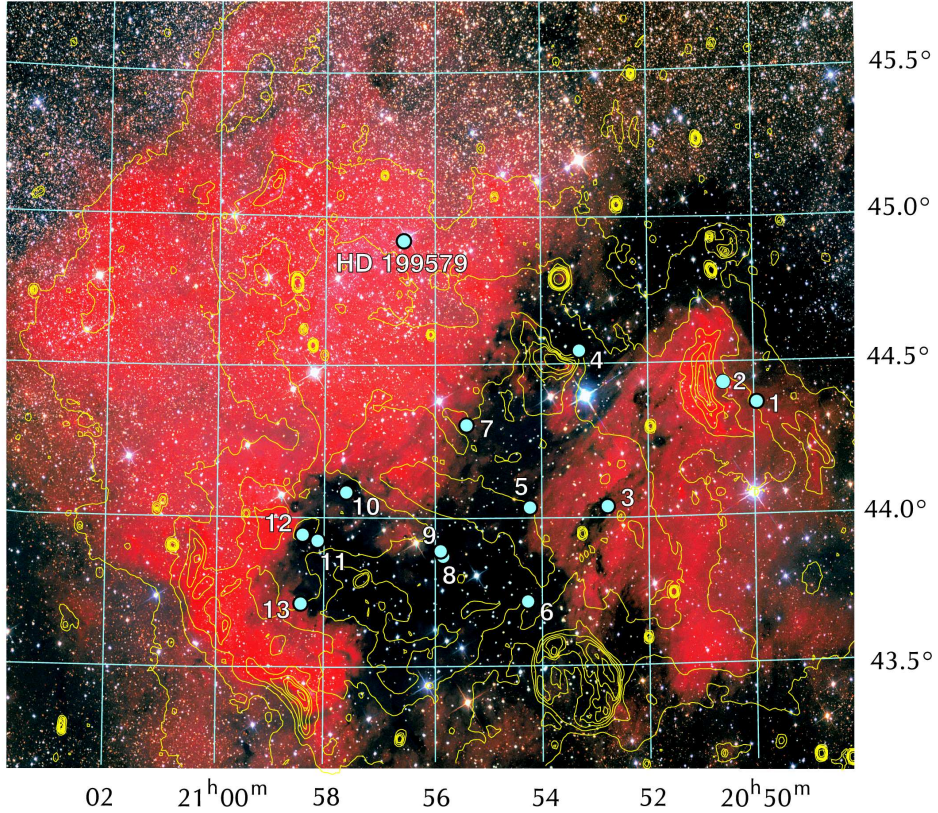
In Figure 4.2.1 the stars from Table 4.2.1 are plotted on a sky image, together with the nebulae and the radio continuum at 21 cm intensity isolines from the Canadian Galactic Plane Survey (Taylor et al. 2003). Figure 4.2.2 shows the positions of these stars in the  $K_s$  vs.  $H-K_s$  diagram.

**Table 4.2.1.** Stars in the North America and Pelican nebulae complex simulating heavily reddened O-type stars.

No.	RA (J2000)	DEC (J2000)	$V$	$F$	$N$ (or $I$ )	$J$	$H$	$K_s$	[8.3] Jy	$Q_{JHK_s}$	$A_V$ max.	Possible type
1	20 49 57.23	+44 22 53.8	—	—	—	12.01	9.31	7.98	—	0.04	23.4	O-B0?
2	20 50 35.05	+44 26 29.6	—	—	16.96	9.90	7.06	5.64	0.87	0.01	24.2	carbon?
3	20 52 46.79	+44 02 30.8	—	—	—	11.99	9.21	7.85	0.15	0.06	20.5	AGB?
4	20 53 15.82	+44 32 57.0	—	—	—	11.36	8.89	7.64	—	-0.03	18.7	O9-B0?
5	20 54 13.42	+44 02 58.9	—	18.40	13.21	8.37	6.48	5.58	0.78	0.08	21.1	AGB?
6	20 54 16.26	+43 43 09.1	—	18.77	15.85	8.24	6.36	5.46	1.06	0.08	22.0	AGB?
7	20 55 25.16	+44 18 14.4	19.06	17.43	13.32	7.96	6.20	5.29	0.86	-0.05	26.6	O5?
8*	20 55 51.25	+43 52 24.6	13.24*	10.69	8.86	6.36	5.51	5.04	0.84	-0.08	28.4	O5 V
9	20 55 52.70	+43 53 24.2	—	—	17.66	10.82	8.56	7.44	0.22	0.03	28.4	O9-B0?
10	20 57 36.47	+44 04 55.9	—	—	17.77	10.63	8.57	7.48	0.22	-0.12	19.3	AGB?
11	20 58 06.73	+43 55 14.1	—	—	—	12.88	8.66	6.57	0.80	0.04	26.6	O5, AGB?
12	20 58 24.24	+43 56 38.6	—	—	—	12.69	8.88	6.87	0.61	-0.22	26.6	AGB?
13	20 58 26.22	+43 42 38.5	17.56	15.04	12.53	8.33	6.42	5.49	0.66	0.05	24.7	carbon?

**Note:** No. 8 = CP05-4, its  $V$  magnitude is from Laugalys et al. (2006).

The ‘O-like stars’ can be either O-type stars or high-luminosity stars of other spectral classes located behind the L935 cloud, i.e. farther than 500–600 pc. All cooler main-sequence stars (including B-stars) behind the cloud are eliminated since in the  $K_s$  passband they are fainter than O-stars. Normal K and M red giants are excluded by the  $Q_{JHK_s} < 0.15$  criterion. However, B-stars of higher luminosities (from IV to I), supergiants of spectral classes A–F5 and AGB stars of the latest spectral classes (M6–M10 for oxygen-rich giants and N-stars for carbon-rich giants) can intervene the  $J-H$  vs.  $H-K_s$  and  $K_s$  vs.  $H-K_s$  diagram regions used to isolate possible O-type stars.



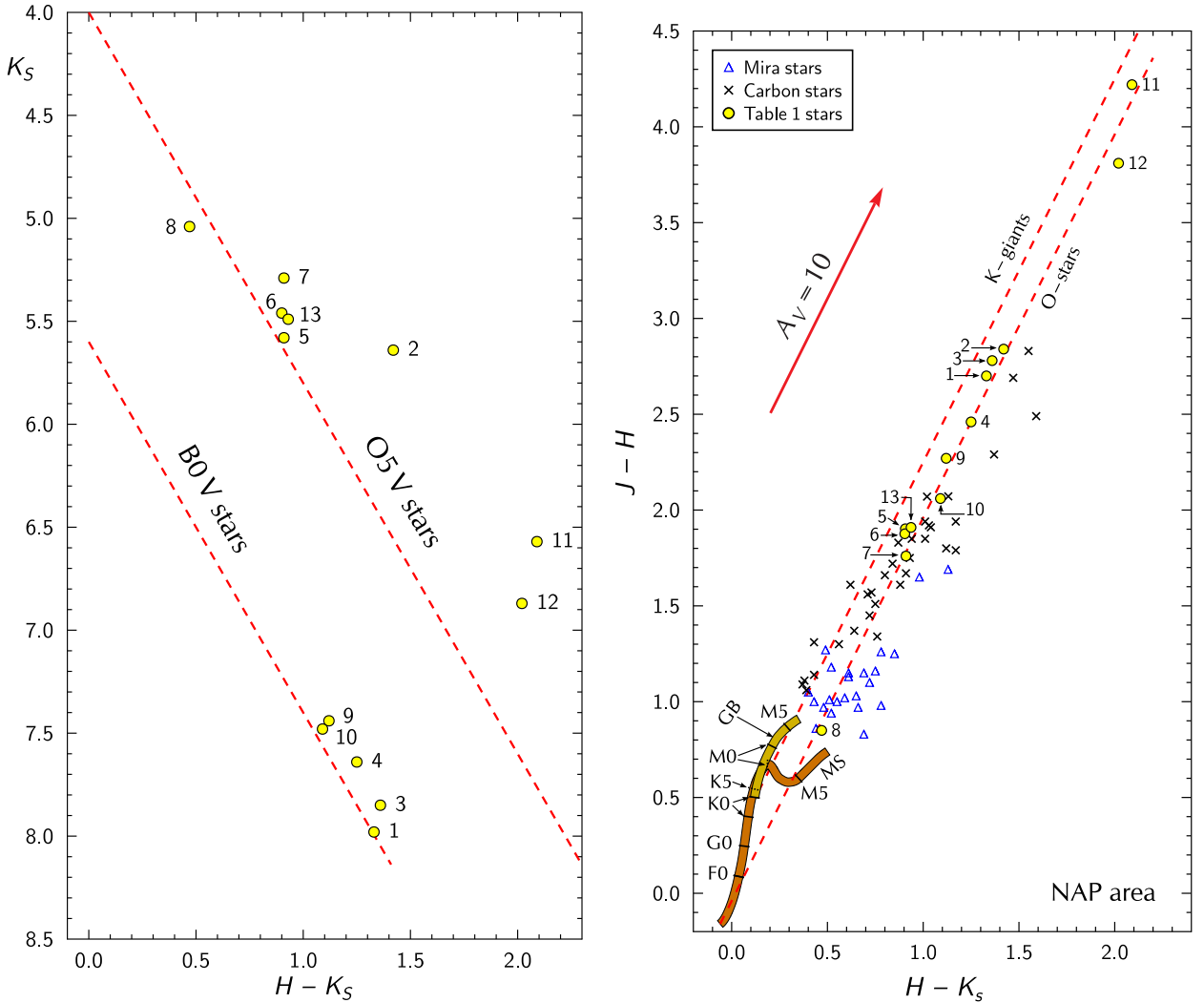
**Fig. 4.2.1.** The map of the NAP nebulae region with the radio continuum isolines from the Canadian Galactic Plane Survey and the stars from Table 4.2.1. The radio isolines correspond to the  $T_b$  values of 6, 8, 10, 12, 14, 16, 18, 20, 25 and 50 K. The oval feature of  $15' \times 20'$  size at  $20^{\text{h}}53.3^{\text{m}}$ ,  $+43^{\circ}27'$  is the supernova remnant SNR 084.2-00.8 located at a distance of 4.5 kpc (Matthews et al. 1977; Kaplan et al. 2004). Most of other small radio sources in the area are extragalactic objects (Matthews & Goss 1980).

Figure 4.2.3 shows the  $J-H$  vs.  $H-K_s$  diagram with the intrinsic lines of main sequence and late-type giants and the two reddening lines corresponding to red clump giants (G8–K2 III,  $Q_{JHK_s} = 0.22$ ) and O–B stars ( $Q_{JHK_s} = -0.05$ ). The crosses represent known N-type carbon stars (Table 4.2.2) selected in the NAP area of  $3^{\circ} \times 3^{\circ}$  size with the center given at the end of Section 4.2.2. The blue triangles are known Mira-type variables (Table 4.2.3) selected in a larger area around the NAP nebulae, with RA between  $20^{\text{h}}30^{\text{m}}$  and  $21^{\text{h}}30^{\text{m}}$  and DEC from  $+41^{\circ}$  to  $+46^{\circ}$ . Most (if not all) Mira variables are oxygen-rich (M-type) giants. It is evident that the reddened carbon stars and Miras completely cover the reddening line of O-type stars. Thus, the most important task is to identify these types of objects.

#### 4.2.4. The I-J vs. J-H Diagram

For the identification of carbon stars the  $I_C-J$  vs.  $J-H$  diagram, shown in Figure 4.2.4, can be used. Here  $I_C$  is the far-red magnitude close to the *Cousins* system. The intrinsic lines of normal main-sequence stars and cool giants were calculated in the following way. The intrinsic color indices  $I_C-J$  for main-sequence stars and K-giants were calculated from the tabulation of  $V-J$  by Koornneef (1983) and  $V-I_C$  by Straizys (1992). The same color indices for M0–M6 giants were calculated from  $V-J$  by Koornneef (1983) and  $V-I_C$  by The et al. (1990). The intrinsic color indices  $J-H$  for main-sequence stars and late-type giants were taken from Bessell & Brett (1988) after their transformation to the 2MASS system by the equations given in Carpenter (2001).

The intrinsic line of M giants was extended up to the spectral type M8 III taking its DENIS-based  $I-J = 3.8$  and  $J-H = 1.1$  from Glass & Schultheis (2002) and Groenewegen & Blommaert (2005). The difference between the 2MASS and DENIS systems was neglected. This value of  $J-H$  is confirmed by 2MASS results for the coolest Mira-type variables: R Cas



**Fig. 4.2.2.** (left) Color-magnitude diagram  $K_s$  vs.  $H-K_s$  for the stars from Table 4.2.1. The two parallel lines are the interstellar reddening lines for the stars of spectral types O5V and B0V at a distance of 550 pc.

**Fig. 4.2.3.** (right) The  $J-H$  vs.  $H-K_s$  diagram with the intrinsic main sequence (MS) and giant branch (GB). Two parallel broken lines (in red) are the interstellar reddening lines of O-type stars and red clump giants. Crosses designate known N-type carbon stars and blue triangles O-rich Mira variables located in the NAP area. The numbered yellow circles indicate the stars from Table 4.2.1.

(M6e–M10,  $P = 430$  d), W And (M7-Se, S6,1e–S9,2e,  $P = 397$  d) and RU Her (M6e–M9,  $P = 485$  d). Their  $J-H$  values from 2MASS are 1.01, 1.09 and 1.01, respectively. The intrinsic line of M-giants runs almost vertically due to increasing absorption in the TiO band at 850 nm.

To define the interstellar reddening line, in Figure 4.2.4 we plotted 58 O-type stars belonging to the Cyg OB2 association and listed in Table 3.1.5. Color indices  $I_C-J$  and  $J-H$  of these stars were calculated either from the  $I_C$  magnitudes given in Droege et al. (2006) or from the DSS2 photographic  $N$  magnitudes (given in the GSC-2.3 catalog, Simbad), and the  $J$  and  $H$  magnitudes from 2MASS.

<sup>1</sup> Additionally, we plotted two O-type stars with small interstellar reddening (S Mon and 10 Lac) and the O5-type star CP05-4 located in the background of the L935 dust

<sup>1</sup> We assumed that the far-red magnitude systems of  $I_C$  and  $N$  coincide. This assumption may not be strictly correct as the response curves of both magnitude systems and their mean wavelengths are slightly different (806 nm for  $I_C$  and 840 nm for  $N$ , see the *Asiago Database on Photometric Systems*, Fiorucci & Munari (2003)). However, the positions of reddened O-stars do not differ systematically when using either  $I_C$  from Droege et al. (2006) or  $N$  from GSC-2.3.

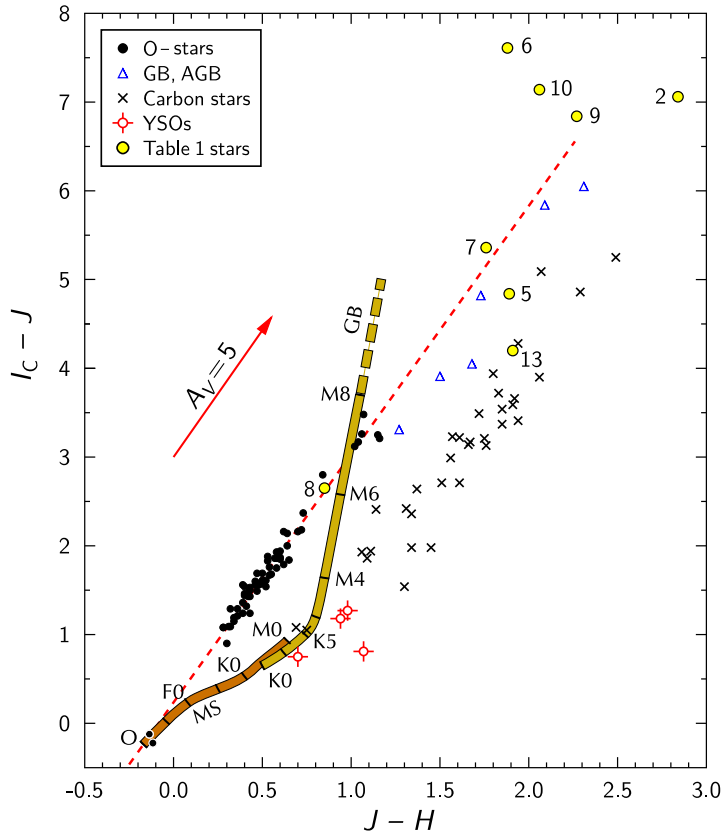


**Fig. 4.2.4.** The  $I_C - J$  vs.  $J - H$  diagram with the intrinsic main sequence (MS) and red giant branch (GB) (thick orange and yellow lines). Dots are O-B1 stars in the NAP and Cyg OB2 association areas, defining the interstellar reddening line. Crosses designate known N-type carbon stars in the NAP area and blue triangles designate GB and AGB stars classified by Comerón & Pasquali (2005). The numbered yellow circles indicate the stars from Table 4.2.1.

**Table 4.2.2.** Color indices of carbon stars in the  $3^\circ \times 3^\circ$  NAP area.

CGCS	$N - J$	$J - H$	$H - K_s$	CGCS	$N - J$	$J - H$	$H - K_s$
4982	4.28	1.94	1.01	5049	3.14	1.66	0.80
4986	1.93	1.06	0.39	5058	3.23	1.57	0.73
4992	1.05	0.75	0.17	5061	1.86	1.09	0.37
4993	5.09	2.07	1.02	5071	3.94	1.80	1.12
4996	3.59	1.91	1.04	5075	2.99	1.56	0.71
4998	3.49	1.72	0.84	5084	2.64	1.37	0.64
5002	3.90	2.06	1.11	5085	1.81	1.79	1.17
5003	3.13	1.76	0.91	5091	1.94	1.11	0.38
5007	3.66	1.92	1.03	5095	3.17	1.67	0.91
5010	3.54	1.85	0.94	5099	2.41	1.14	0.43
5014	3.41	1.94	1.17	5105	1.98	1.45	0.72
5017	2.71	1.61	0.88	5110	1.98	1.34	0.76
5020	3.72	1.83	0.87	5124	2.71	1.51	0.75
5021	3.37	1.85	1.01	5135	1.54	1.30	0.56
5027	1.08	0.69	0.22	CP05-10	4.86	2.29	1.37
6876*	3.21	1.75	0.93	CP05-16	—	2.69	1.47
5033	2.42	1.31	0.43	CP05-18	5.25	2.49	1.59
5035	3.22	1.61	0.62	CP05-19	—	2.83	1.55

Note: CGCS 6876 = CP05-6.

cloud (Comerón & Pasquali 2005). The slope of the reddening line is  $E_{I_C - J} / E_{J - H} = 2.84$  which is considerably larger than the value 1.78 calculated from the  $A_\lambda / E_{B-V}$  ratios given by Fitzpatrick (1999, Table 2). The reason for this disagreement probably is related to deviations of the Droege et al. (2006) and the DSS2 far-red systems from the standard  $I_C$  system, which itself has a poor definition and a number of versions.

**Table 4.2.3** Color indices of Mira variables in the NAP area.

Name	$J-H$	$H-K_s$	Name	$J-H$	$H-K_s$
BH Cyg	0.97	0.48	V603 Cyg	1.69	1.13
BL Cyg	0.83	0.69	V607 Cyg	0.94	0.52
DG Cyg	1.27	0.49	V780 Cyg	1.15	0.69
V506 Cyg	1.26	0.78	V1223 Cyg	1.16	0.75
V528 Cyg	1.25	0.85	V1225 Cyg	1.00	0.43
V580 Cyg	1.03	0.65	V1232 Cyg	1.00	0.55
V584 Cyg	1.02	0.59	V1234 Cyg	1.13	0.61
V593 Cyg	0.97	0.66	V1242 Cyg	1.18	0.52
V596 Cyg	0.86	0.44	V1243 Cyg	0.98	0.78
V597 Cyg	1.15	0.61	V1480 Cyg	1.05	0.40
V600 Cyg	1.10	0.72	V1660 Cyg	1.65	0.98
V601 Cyg	1.01	0.51			

Due to the band-width effect the ratio  $E_{I_C-J} / E_{J-H}$  depends slightly on the temperature of stars (Straižys & Lazauskaitė 2008): for K-type stars the ratio is by 3% *larger* than for O-type stars. However, taking into account a very poor knowledge of response functions of the far-red passbands ( $I$  or  $N$ ), this effect in Figure 4.2.4 is too small to be significant.

In Figure 4.2.4 we also plotted known N-type carbon stars selected in the NAP  $3^\circ \times 3^\circ$  area (Table 4.2.2). Their far-red  $I_C$  magnitudes were taken mostly from the GSC-2.3 (i.e., DSS2  $N$  magnitudes). For three stars we used the magnitudes from Droege et al. (2006) and for one star (CGCS 4996) from the *INT Photometric H $\alpha$  Survey of the Northern Galactic Plane*, IPHAS (Drew et al. 2005; González-Solares et al. 2008). The response curve of the IPHAS far-red magnitude  $i$  is shifted blueward from  $I_C$ , and has a mean wavelength of 774 nm. The  $i$  magnitude was transformed from the IPHAS system by the equation  $N = i - 1.10$  obtained from a comparison of six other carbon stars with both  $N$  and  $i$  magnitudes available.

It is evident that the reddening line of carbon stars is more or less parallel to the reddening line of O–B1 type stars but lies about 1.4 mag lower. This makes possible to identify carbon stars even at the level of relatively low accuracy of the photographic DSS  $N$  magnitudes. A considerable scatter of carbon stars around their mean line may be the result of low accuracy of their photographic far-red magnitudes, possible variability and the intrinsic peculiarities in their spectral energy distributions.

However, the  $I_C-J$  vs.  $J-H$  diagram is almost useless for the separation of O-type stars from oxygen-rich giants of spectral types M6 III and cooler. In Figure 4.2.4 we plot three GB and three AGB stars (triangles) classified by Comerón & Pasquali (2005), their  $N$  magnitudes being taken from GSC-2.3. All of them lie between the O-type reddening line and the carbon star sequence. Cooler AGB stars with the TiO-dominated spectra (Mira variables) in Figure 4.2.4 should cover both the reddening line of O-stars and the region above it.

To exhibit the location of YSOs, we plotted in Figure 4.2.4 two known T Tauri type stars and two H $\alpha$  emission stars which lie in the Gulf of Mexico (red crossed circles). With increasing reddening, these stars can overlap carbon-rich stars but will not be mixed with O-type stars.

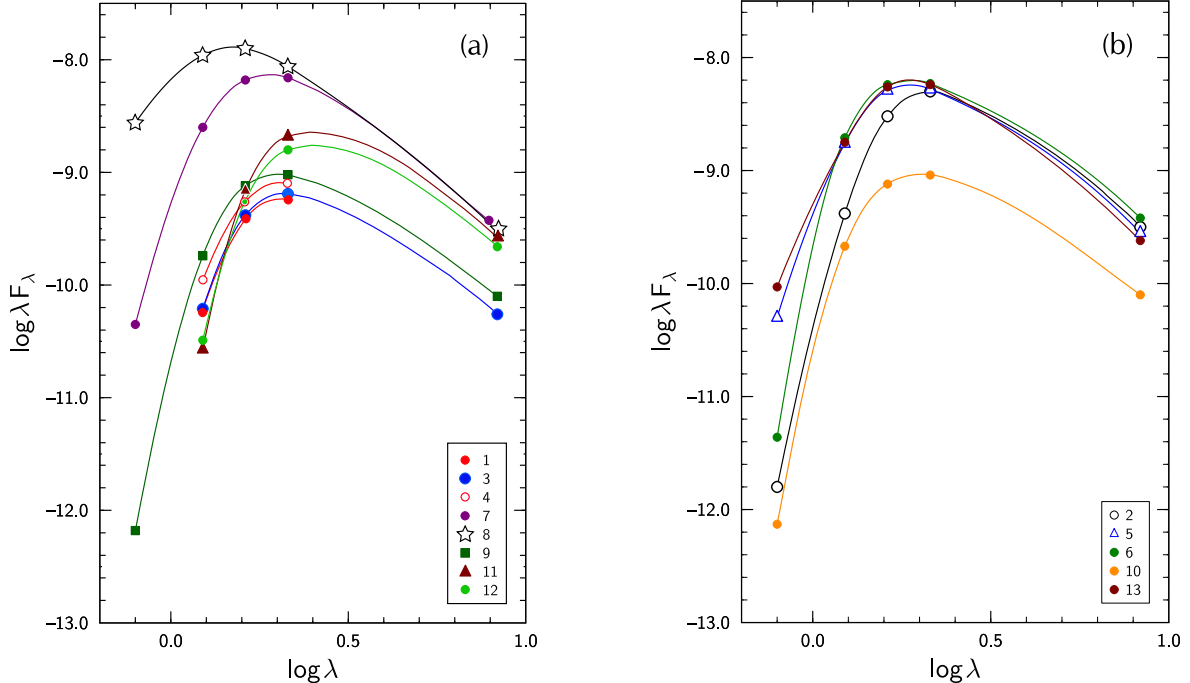
The O-like stars in Figure 4.2.4 are plotted as yellow circles, with their numbers from Table 4.2.1. Their far-red  $N$  magnitudes (when available) are taken from GSC-2.3. Of these stars only CP05-4 has another source of the far-red magnitude:  $I_C = 9.00$  in Droege et al. (2006). Other three stars (3, 7 and 13) were observed in the IPHAS project (González-Solares et al. 2008). For the sake of uniformity, we have opted to use the  $N$  magnitudes for these stars, too.

Figure 4.2.4 shows that only two stars from Table 4.2.1, Nos. 7 and 9, lie almost on the extension of the reddening line of O-stars. They are the best candidates for O-type stars. Probably, stars Nos. 2 and 13 are carbon stars, while Nos. 5, 6 and 10 are oxygen-rich AGB stars (M-type Miras or other M-type long-period variables). Although their belonging to O-type stars is doubtful, they should remain in the list for future verification of spectral types by spectroscopic means. Photometric classification of stars 1, 3, 4, 11 and 12 is impossible at this moment since they have no measured far-red magnitudes. They remain in the list of suspected O-type stars.

#### 4.2.5. Spectral Energy Distributions

With the aim to find further evidence that at least some of the selected stars belong to early-type stars, we calculated their spectral energy distributions (SEDs) between 0.8 and 8.3  $\mu\text{m}$  using the data given in Table 4.2.1. The values of  $\log \lambda F_\lambda$  for the  $N$  (or  $I_C$ ),  $J$ ,  $H$  and  $K_s$  magnitudes and the MSX 8.3  $\mu\text{m}$  flux were obtained as described in Straizys & Laugaly (2007, p. 341–342).

The SED curves obtained are shown in Figure 4.2.5. The star numbers in the inserts correspond to Table 4.2.1. All probable O-stars have their SED maxima at 2.2  $\mu\text{m}$  ( $K$  magnitude), except of the CP05-4 star which has maximum at  $H$  magnitude. The reddest is No. 4 but it has not been measured in the MSX band at 8.3  $\mu\text{m}$ . The form of the SED curves suggests that the ‘O-like’ stars have no infrared excesses at  $> 2.2 \mu\text{m}$ , i.e., they do not belong to YSOs or AGB stars with dust envelopes.



**Fig. 4.2.5.** Spectral energy distributions of the O-like stars between 0.8 and 8.3  $\mu\text{m}$ . Here  $\lambda$  is in  $\mu\text{m}$  and  $F_\lambda$  is in  $\text{erg} \times \text{cm}^{-2} \times \text{s}^{-1} \times \mu\text{m}^{-1}$ . Panel (a) shows the stars which are the candidates to O-type stars and panel (b) the candidates to AGB stars.

SEDS of the suspected AGB stars are not very different from O-like. At such high interstellar reddenings the intrinsic differences of SEDs between O-type stars and late M-type stars without circumstellar dust envelopes in the 1–3  $\mu\text{m}$  range become negligible if the photometric passbands do not contain strong TiO or H<sub>2</sub>O bands. The CO bands longward of 1.56 and 2.32  $\mu\text{m}$ , C<sub>2</sub> bands longward of 1.77  $\mu\text{m}$  and H<sub>2</sub>O at 1.3–1.5 and 1.7–2.0  $\mu\text{m}$ , present in the spectra of AGB stars, are too faint to create a measurable photometric effect in the broad-band  $J-H$  and  $H-K_s$  color indices. However, these spectral features are easily observable in infrared spectra at a resolution of  $\lambda/\Delta\lambda = 240$  (Comerón & Pasquali 2005).

#### 4.2.6. Comments on Individual Stars

##### 1 = 2MASS J20495723+4422538

The star is one of the reddest objects in Table 4.2.1. For it only 2MASS photometry is available. If the star is of O-type, its extinction  $A_V$  must be 22.7 mag. This is in agreement with the maximum extinction value of the background red giants given in Table 4.2.1. Its proximity within  $\sim 10'$  to the bright radio E-rim (Matthews & Goss 1980) and to the Pelican Nebula hot spot (Bally & Scoville 1980) makes it a good candidate for the ionizing source of the upper part of the Pelican head. Its position in the  $K_s$  vs.  $H-K_s$  diagram (Figure 4.2.2) is consistent with what we expect for a star of spectral class close to B0 V at a distance of 550 pc. If the star is more distant, its spectral type can be earlier.

##### 2 = 2MASS J20503505+4426296

Bally & Scoville (1980) suspected that this star (called as IRS4 in their paper) is re-

sponsible for the hot spot of the Pelican Nebula discovered in CO maps. However, the  $I_C - J$  vs.  $J - H$  diagram (Figure 4.2.3) suggests that the star is probably a carbon-rich object. In the color-magnitude diagram (Figure 4.2.2) it lies about 1 mag above the reddening line of O5 V stars. Presumably, the star can be matched with the IRAS 20487+4415 source. Consequently, this star probably is not related to the Pelican Nebula hot spot.

### **3 = 2MASS J20524679+4402308**

Both in the color-magnitude diagram (Figure 4.2.2) and in the  $J - H$  vs.  $H - K_s$  diagram (Figure 4.2.3) this star lies very close to star No. 1. Their spectral energy distributions are also very similar. On the sky the star is located in the emission opening below Pelican's beak. If the star is of spectral type near O9–B0, its extinction  $A_V$  must be about 23 magnitudes. This seems to be too high taking into account the maximum value of  $A_V = 20.5$  given in Table 4.2.1 and the absence of a dense dust condensation in this direction (Figure 3.2.13). Therefore, we cannot exclude that the star is a heavily reddened carbon- or oxygen-rich AGB object. For the verification the far-red magnitude  $I$  of the star would be important.

### **4 = 2MASS J20531582+4432570**

This star is located in a dense dust cloud within only a few arcminutes from the radio-bright J-rim discovered by Matthews & Goss (1980). A bright point-like radio source seen  $\sim 15'$  north of the rim, is not related to the NAP complex – it is a distant HII region in the Perseus arm (Wendker et al. 1983; Heske & Wendker 1985). If the star is of spectral class O, its  $A_V$  must be 21.3 mag, which is in contradiction to the expected maximum extinction (18.7 mag) given in Table 4.2.1. The latter value of extinction may mean that accidentally no background red giant is seen in the direction of a small dust condensation which covers star No. 4 and gives the extinction close to 21 mag. In the color-magnitude diagram (Figure 4.2.2) the star lies close to the reddening line of O9–B0 V type stars. Consequently, if the star belongs to the NAP complex at a distance of 500–600 pc, its ionizing possibility is not great. However, the star may be responsible for the creation of the dense ionized rim of the dust cloud. If the complex distance is 550 pc, the projected distance between the rim center and the star is 0.8 pc only. Its SED (Figure 4.2.5a) is not very informative, since the star has not been observed both in  $I$  and MSX passbands. However, the SED in the  $J$ ,  $H$  and  $K_s$  passbands seems to be quite similar to SEDs of stars Nos. 1 and 3.

### **5 = 2MASS J20541342+4402589**

The star is located in the dark cloud near the tip of Pelican's beak. In the color-magnitude diagram (Figure 4.2.2) the star lies almost on the interstellar reddening line of O5 V stars at a distance of 550 pc. As it was shown in Section 4.2.4, the star does not seem to be of spectral class O; probably it is an asymptotic giant branch object.

### **6 = 2MASS J20541626+4343091**

The star is located in the dark cloud below the tip of Pelican's beak. In the color-magnitude diagram (Figure 4.2.2) and the  $J - H$  vs.  $H - K_s$  diagram (Figure 4.2.3) the star lies very close to star No. 5. The diagram  $I_C - J$  vs.  $J - H$  (Figure 4.2.4) shows that both of them are AGB objects, but No. 6 is much cooler. This is confirmed also by their SEDs shown in Figure 4.2.5b.

### **7 = 2MASS J20552516+4418144**

As it was shown in Section 4.2.4, the star satisfies all our criteria for being an O-type star. In the color-magnitude diagram (Figure 4.2.2) it lies 0.5 mag above the interstellar reddening line of O5 V stars for a distance of 550 pc. This means that the star is either more luminous than the main-sequence stars or is located closer to the Sun than 550 pc. If the star is of spectral class O, its  $A_V$  should be about 16 mag. The star is located near the edge of the L935 dust cloud at the North America Nebula coast. In this direction the expected maximum extinction is more than sufficient to give  $A_V = 16$ . There is one more argument in favor of our suggestion that star No. 7 may be of spectral class O5: its SED looks like the additionally reddened SED of the known O5 V type star, CP05-4, described in Section 4.2.2. Luminosities of both stars coincide in the MSX passband at  $8.3 \mu\text{m}$  where the interstellar extinction is close to zero.

### **8 = 2MASS J20555125+4352246**

The Comerón and Pasquali star, CP05-4, described in Section 4.2.2.

### **9 = 2MASS J20555270+4353242**

This star is located very close to CP05-4, in projection they are separated only by  $62''$ . The star lies in the domains of reddened O-type stars in the three diagrams discussed above: the color-magnitude diagram  $K_s$  vs.  $H - K_s$  (Figure 4.2.2) and the two-color diagrams,  $J - H$

vs.  $H-K_s$  (Figure 4.2.3) and  $I_C-J$  vs.  $J-H$  (Figure 4.2.4). However, in the color-magnitude diagram it exhibits lower luminosity than its neighbor, CP05-4; if the star is at 550 pc, its spectral type must be around O9–B0 V, and the interstellar extinction  $A_V = 19.3$  mag. This value does not rise a problem with the expected extinction in this direction (Table 4.2.1).

### **10 = 2MASS J20573647+4404559**

The star is located at the northern coast of the Gulf of Mexico. Figure 4.2.4 shows that the star probably is an AGB star of late M spectral class.

### **11 = 2MASS J20580673+4355141**

The star is located at the left coast of the Gulf of Mexico. In the  $J-H$  vs.  $H-K_s$  diagram it lies almost exactly on the reddening line of O-type stars, at  $H-K_s = 2.09$ . Since the star is not seen in the DSS far red images, it has no  $N$  (or  $I$ ) magnitude available. Consequently, we had no possibility to verify whether it is a non-carbon star. In the color-magnitude diagram  $K_s$  vs.  $H-K_s$  (Figure 4.2.2) the star lies  $\sim 1$  mag above the reddening line of O5 V stars. The SED curve of the star in  $J$ ,  $H$  and  $K_s$  shows a heavy reddening but in the MSX passband at  $8.3 \mu\text{m}$  its intensity almost coincides with the O5 V star CP05-4. This means that the star could be of O5-type with the extinction  $A_V = 35.2$  mag. Such value of the extinction is considerably too large for this direction (see Table 4.2.1). However, the star can be heavily obscured by a small dust condensation which does not contain background red giants which would increase the value of  $A_V$  given in Table 4.2.1. Other alternative is to assume that we have here a very distant AGB star (of M or N type) which is so luminous that its apparent brightness at  $8.3 \mu\text{m}$  is equal to that of CP05-4 located at 550 pc.

### **12 = 2MASS J20582424+4356386**

The star is only  $3.5'$  from No. 11 and  $\sim 1'$  from the suspected cluster of infrared sources ([CBJ2002] 3a in Cambrésy et al. 2002). The SEDs of both stars are quite similar (Figure 4.2.5a), but No. 12 is either slightly warmer or has a lower extinction in its direction. Its  $H-K_s = 2.015$  and  $Q_{JHK_s} = -0.22$ , i.e. it is outside the range accepted for O-type stars. The star has no excess at  $8.3 \mu\text{m}$  (MSX), so it is not YSO. Probably, this star is a distant AGB object located far behind the NAP complex.

### **13 = 2MASS J20582622+4342385**

The star is located at the southern coast of the Gulf of Mexico. Although in the  $K_s$  vs.  $H-K_s$  diagram (Figure 4.2.2) the star is close to the reddening line of O5 V stars, in the  $I_C-J$  vs.  $J-H$  diagram (Figure 4.2.4) the star lies among carbon stars.

#### 4.2.7. Conclusions

1. In the area of the North America and Pelican nebulae we identified thirteen stars simulating heavily reddened O-type stars at a distance of the complex, 550 pc (Table 4.2.1). The stars were selected using the  $J-H$  vs.  $H-K_s$  and  $K_s$  vs.  $H-K_s$  diagrams based on 2MASS data. One of these stars is CP05-4 classified as O5 V by Comerón & Pasquali (2005). This set of stars may contain O-type stars, B-type stars of luminosities higher than V, A–F supergiants and cool AGB stars (both oxygen- and carbon-rich).

2. For eight stars of the set, far-red magnitudes  $I$  (including DSS2  $N$  magnitudes) were collected from the literature. Applying the  $I-J$  vs.  $J-H$  diagram, two carbon-rich and three oxygen-rich AGB stars were identified.

3. Spectral energy distributions, based on the  $I$ ,  $J$ ,  $H$ ,  $K_s$  and MSX photometry, give additional information about the selected stars.

4. To estimate the maximum interstellar extinction in the direction of the ‘O-like’ stars located behind the dark clouds of the NAP complex, we used the  $J-H$  vs.  $H-K_s$  diagrams for the supposed background K-type giants. The star count map in the  $K_s$  passband was also constructed and used to estimate the interstellar extinction in small areas of the complex.

5. Considering all the observational data together, we conclude that two stars in our set, Nos. 1 and 4, possibly are stars of late O subclasses responsible for the creation of the ionized radio rims E and J discovered by Matthews & Goss (1980).

6. Other two stars, Nos. 7 and 9, also have a considerable probability of being O-type stars. They both satisfy all photometric criteria for O-stars at a distance of the NAP with the  $A_V$  extinctions of 16 and 19 mag. Star No. 11 is also a probable O-star of early subclass.

7. The remaining stars in Table 4.2.1 can be heavily reddened cool AGB stars located at different distances in the background of the NAP. However, we cannot rule out the possibility that some of them still may be hot stars related to the complex. Only spectroscopy and photometry of these stars in the near and middle infrared can give the final answer.

## 5. OBSERVED OPEN CLUSTERS

### 5.1. NGC 6997

Some of the stars in the area should be members of the cluster NGC 6997. In the map of the area the cluster is seen as a round concentration of 7' radius. In Figure 3.2.5 these stars are seen as a swarm of dots on the rising part of the extinction, between 700 and 900 pc.

The investigation of the cluster by photoelectric photometry has been done by ZS90 in the *Vilnius* system and by Villanova et al. (2004) in the *UBVI<sub>C</sub>* system. The cluster distance obtained by ZS90 was 620 pc. After the reduction to the *Hipparcos* distance scale of the Hyades, the distance is 650 pc. However, this distance probably is too small since some non-member stars of the foreground and evolutionary deviated cluster stars were included in distance determination. The distance of the cluster found by Villanova et al., 760 pc, was determined by the best ZAMS fitting and should be more reliable.

It seems that nobody has investigated proper motions of the cluster. We did not find any radial velocity determinations. Only J. Sperauskas (Vilnius University Observatory, unpublished) has measured radial velocities of eight G–K stars in the cluster area. Therefore, for the selection of possible cluster members only photometric criteria can be applied.

The first criterion used by us for the selection of possible cluster members was their concentration in the circle of a radius of 7'. The second criterion was related to the distance of stars from the Sun. Considering that the errors of our absolute magnitudes of stars are of the order of  $\pm 0.5$  mag, we obtain that the distance errors should be between –20 % and +26 %. As a preliminary cluster distance we may take 800 pc, the middle point of the concentration of stars in Figure 3.2.5. For this distance we expect that the apparent distances of cluster members should be scattered between 640 pc and 1000 pc.

One more criterion of cluster membership could be the similarity of their interstellar extinctions. However, ZS90 found that the possible cluster stars exhibit quite different values of extinction  $A_V$  ranging between 1.2 and 2.5 mag. Consequently, we should not obey this criterion very strictly. However, we should not expect the extinctions of cluster members to exceed considerably the mentioned limits. We have accepted that the cluster stars should have the extinctions between 1.0 and 3.0 mag.

Combining these three criteria (concentration in the 7' circle, distance limits and extinction limits) we have isolated 47 probable cluster members among the main-sequence belt stars. Their spectral classes cover the range from A0 to K1. Three red giants – Nos. 243, 247 and 329, all of spectral class near G8 III, probably also belong to the cluster. Ten more stars near the main sequence satisfy the membership criteria described above but in the  $V_0$  vs.  $(Y-V)_0$  diagram they lie near the upper edge of the main sequence belt. These stars, in Figure 5.1.1 shown by crosses, can be either unresolved binaries with identical components (0.75 mag above ZAMS) or field stars.

The apparent distance of one more red giant of spectral class K1 III (No. 156) was found to be 990 pc, i.e., it is very near the expected upper limit of apparent distances of the cluster members due to absolute magnitude errors. However, this star has a much larger extinction than others ( $A_V = 3.46$  mag). Consequently, its membership in the cluster is doubtful.

Fifty probable and ten possible members of the cluster are plotted in the  $V_0$  vs.  $(Y-V)_0$  diagram (Figure 5.1.1) together with the ZAMS line fitted to the lower envelope of unevolved main-sequence stars. The ZAMS line for  $B-V < 0.5$  is the Victoria-Regina isochrone in the  $M_V$  vs.  $B-V$  diagram for solar chemical composition and the  $10^6$  yr age (VandenBerg et al. 2006). For cooler stars the ZAMS line corresponds to the lower envelope of the Hyades cluster stars (Perryman et al. 1998). This fit gives the distance modulus  $V - M_V = 9.50$ , which corresponds to a distance of 794 pc.

The average distance of 50 probable cluster members is  $781 \pm 61$  pc, and their mean interstellar extinction is  $1.92 \pm 0.40$  mag. This distance value is quite close to the distance obtained by fitting the ZAMS line of the cluster. Both these distances are determined using the extinctions calculated using the ratio  $R_{YY} = 4.62$ . In the case of normal extinction law with  $R_{YY} = 4.16$ , the average distance of 50 probable cluster members is  $854 \pm 69$  pc and  $A_V = 1.73 \pm 0.36$  mag.

The hottest cluster stars show an evolutionary deviation upward. The position of the turnoff point may be used for estimation of the cluster age. For this we have compared

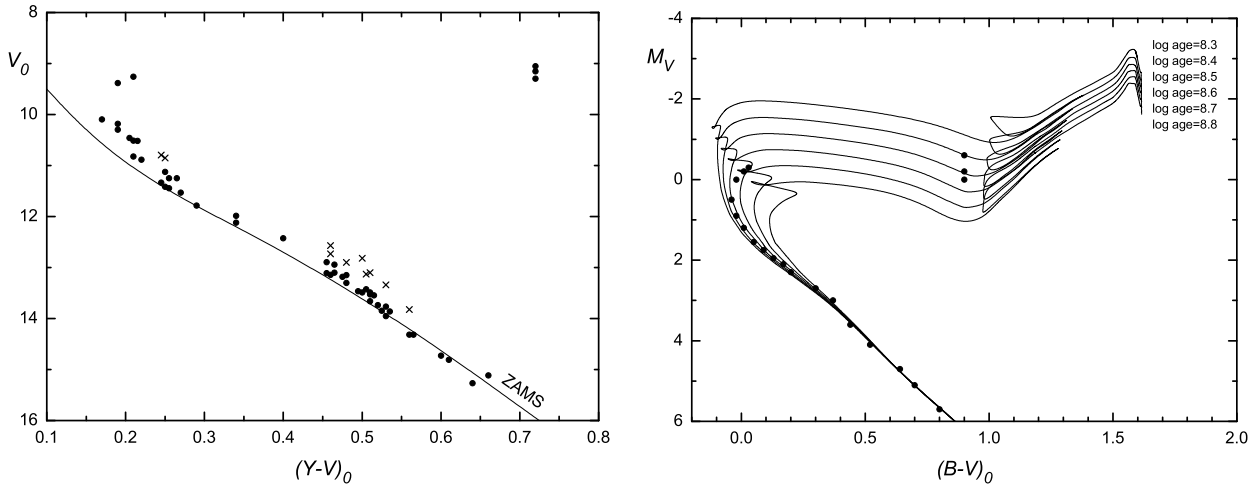


**Fig. 5.1.1.** (left) Interstellar extinction-free and reddening-free HR diagram for probable members of the cluster NGC 6997. Zero-age main sequence fitted to the lower envelope of the cluster stars is shown as a continuous line. The possible cluster binaries are shown as  $\times$  symbols.

**Fig. 5.1.2.** (right) Isochrones in the  $(B-V)_0$  vs.  $M_V$  diagram from Girardi et al. (2000) and the cluster NGC 6997 sequence.

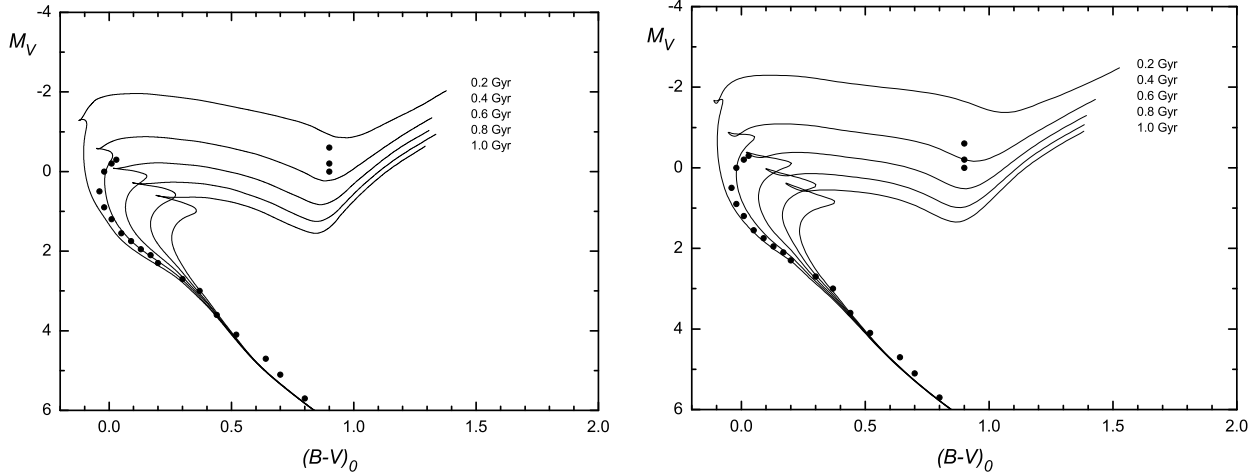


**Fig. 5.1.3.** (left) Isochrones in the  $(B-V)_0$  vs.  $M_V$  diagram from Demarque et al. (2004) and the cluster NGC 6997 sequence.

**Fig. 5.1.4.** (right) Isochrones in the  $(B-V)_0$  vs.  $M_V$  diagram from Vandenberg et al. (2006) and the cluster NGC 6997 sequence.

the main sequence of NGC 6997 with the isochrones in the  $M_V$  vs.  $B-V$  plane calculated by three different author groups (see below) for  $[Fe/H] = 0.0$ . The magnitudes  $V_0$  were transformed to  $M_V$  accepting the distance modulus of the cluster  $V - M_V = 9.50$ . Color indices  $(Y-V)_0$  were transformed to  $B-V$  using the relation determined by Sviderskienė & Straizys (1970).

Figures 5.1.2–4 show the lower envelope of the NGC 6997 main sequence plotted on the Girardi et al. (2000), Demarque et al. (2004) and Vandenberg et al. (2006) isochrones for  $[Fe/H] = 0.0$ . We considered that the cluster is of solar metallicity since in the process of classifying stars by the stellar box method in all cases the selected analogues for the cluster stars were of normal chemical composition. In all plots the isochrones more or less agree that the age of NGC 6997 is close to  $3.5 \times 10^8$  yr. The position of the three cluster G8 giants also confirms this conclusion. The age and the distance of the cluster show that it has no relation to the star-forming regions in the vicinity of the North America and Pelican nebulae (Herbig 1958; Herbig & Bell 1988; Shevchenko et al. 1988).

## RESULTS AND CONCLUSIONS:

(1) CCD photometry in the *Vilnius* seven-color system has been done for 620 stars down to 17.5 mag in a 20' diameter area including the open cluster NGC 6997.

(2) Majority of the stars have been classified in spectral and luminosity classes. Their color excesses, interstellar extinctions and distances have been determined.

(3) A comparison of color excesses  $E_{B-V}$  and the infrared color excesses from the 2MASS survey shows that in the area of the North America and Pelican nebulae the ratio  $R_{BV} = A_V/E_{B-V}$  is normal (about 3.15). A similar comparison of color excesses in the NGC 6997 area shows an increased value of  $R$ . For A-type stars we have accepted  $R = 3.50$ . This corresponds to  $R_{YV} = A_V/E_{Y-V} = 4.62$  in the *Vilnius* system. There are no evident reasons why this ratio should be increased: the cluster does not contain O–B stars, which could push out small dust particles, and the dust density around the cluster does not seem to be high enough to facilitate the coalescence of dust particles.

(4) In the direction of NGC 6997 a steep increase of extinction is observed at  $\sim 400$  pc, which may be explained by the beginning of a dust cloud at about 500 pc distance. This distance is slightly lower than distances of the L935 dust cloud and other clouds in the vicinity of the North America and Pelican nebulae found in our earlier papers.

(5) The extinction  $A_V$  reaches 2.5 mag at 1 kpc and 3.0 mag at 2 kpc. The stars with larger extinction values at larger distances are blocked out by the limiting magnitude effect. Some tendency of increase of  $A_V$  continues up to 3 kpc, where our line of sight leaves the Local (Orion) arm. Most stars between 2 and 3 kpc have  $A_V$  values between 2.5 and 4.2 mag.

(6) At about 5–7 kpc our line of sight crosses the Perseus spiral arm and at 9–11 kpc – the Outer (or Cygnus) arm. We find about 35 stars of magnitudes 16.0–17.5 suspected to be the stars of spectral classes O–B5 with interstellar extinctions between 3 and 5 mag. If their classification will be confirmed, most of them should belong to the Perseus arm and some – to the Outer arm.

(7) In the cluster NGC 6997, which was considered to have a 7' radius, we have identified 47 probable main-sequence members of spectral classes from A0 to K3 and 3 red giants. The  $V_0$  vs.  $(Y-V)_0$  diagram fitted with the ZAMS line gives a distance modulus of  $V - M_V = 9.50$ , which corresponds to the 794 pc distance if the ratio  $R_{BV} = 3.5$  is valid. The average distance of the individual distances of 50 probable cluster members is  $781 \pm 61$  pc and their interstellar extinction is  $1.92 \pm 0.40$  mag. In the case of normal extinction law, the average distance would be  $854 \pm 69$  pc and the extinction –  $1.73 \pm 0.36$  mag.

(8) The cluster age is estimated by comparing the position of its ZAMS and red giants with the isochrones of three groups of authors in the  $M_V$  vs.  $B-V$  plane. The age of the order of 350 million years was found.

(9) Both the cluster age and its distance indicate that it is not associated with the star-forming region in the North America and Pelican nebulae. Probably NGC 6997 is an ordinary Hyades-type cluster moving behind the complex of the dust and molecular cloud.

### 5.2. Collinder 428

Collinder (1931) gave the cluster size as  $18' \times 10'$ . This is the size of a group of stars of an irregular form which is surrounded by a  $\sim 5'$  wide belt with lower star density. This may be an indication that the cluster is not real but just a window in the dark cloud. Therefore it is important to verify if the clustering stars are at the same distance and if they form the main sequence in the color vs. magnitude diagram.

In Figure 5.2.1 we plot the diagram  $V_0$  vs.  $(Y-V)_0$  for all 290 stars which were classified in two dimensions (spectral class and luminosity class). Here  $V_0 = V - A_V$  and  $(Y-V)_0 = (Y-V)_{\text{obs}} - E_{Y-V}$ , i.e., the interstellar extinction and reddening are excluded for each star individually. The plot does not show any clear evidence of a cluster main sequence. The ‘cluster’ appearance is determined by a group of stars brighter than about 12th magnitude; Figure 5.2.1 shows that these stars have nothing in common.

Dias et al. (2006) for 130 stars from our catalog list UCAC2 proper motions and membership probability to the cluster. Figure 5.2.2 shows the plot of 34 stars for which spectral classes and luminosities are given in Table 2.2.9 and whose membership probability is  $\geq 70\%$ . Again, the evidence for the main sequence is very weak. The deviations of individual stars

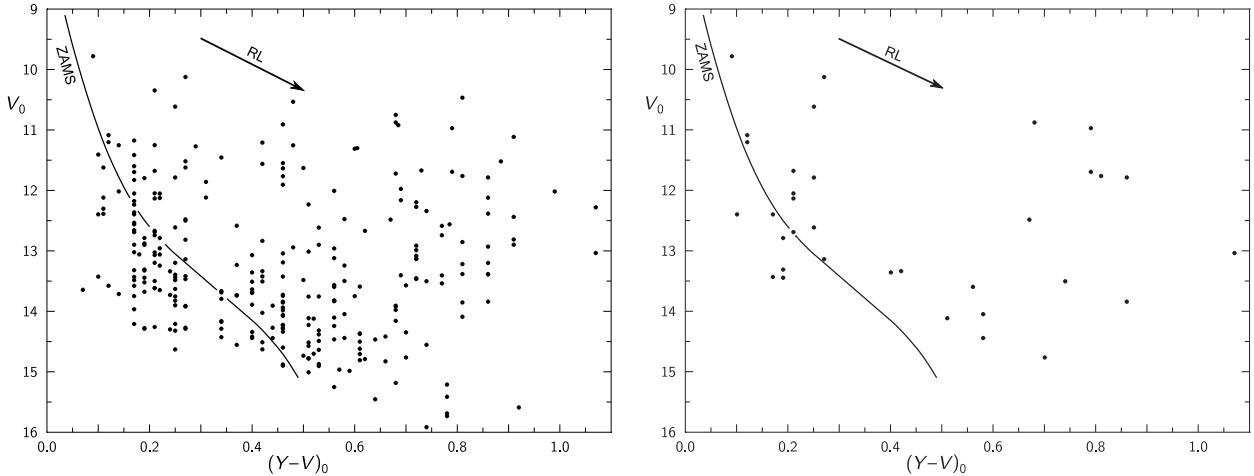


**Fig. 5.2.1.** (left) Interstellar reddening-free  $V_0$  vs.  $(Y-V)_0$  diagram for 290 stars for which two-dimensional spectral types are given in Table 2.2.9. The ZAMS line adjusted to  $V-M_V = 11.1$  mag is shown for reference, see the text. RL is the reddening line for  $E_{Y-V} = 0.2$  or  $E_{B-V} = 0.25$ .

**Fig. 5.2.2.** (right) Interstellar reddening-free  $V_0$  vs.  $(Y-V)_0$  diagram for 34 stars of high cluster membership probability estimated from proper motions by Dias et al. (2006). The ZAMS and reddening lines are the same as in Figure 5.2.1.

from the ZAMS line with  $V-M_V = 11.1$  mag shown in Figure 5.2.2 are too large to be explained by the classification errors. Among A-type stars near the main sequence the expected errors of spectral classes are  $\pm 1.0$  subclass and one luminosity class. This results in the errors of  $(Y-V)_0 = \pm 0.02$  mag. Adding the observational errors of similar size, we obtain  $\pm 0.03$  mag. The errors of  $V_0$  are larger by a factor of  $R=4.16$ , i.e., they are equal to  $\pm 0.125$  mag. Luminosity class error by  $\pm 1$  class leads to negligible errors of color excesses and extinctions; consequently, they have no effect on the errors of  $V_0$  and  $(Y-V)_0$ . The duplicity of stars, as well as the axial rotation and evolution effects shift the stars upward from the ZAMS, so the position of A-type stars below the main sequence in Figure 5.2.2 cannot be explained in any case. The positions of G-K stars in Figure 5.2.2 (with  $(Y-V)_0 > 0.55$ ) are also unexplainable in terms of their membership to the ‘cluster’. Probably Collinder 428 is not a real cluster.

In Figures 5.2.1 and 5.2.2 we plot the ZAMS line from Kazlauskas et al. (2006) adjusted to the distance modulus of 11.1 mag (1660 pc). This distance would be valid if a few of the brightest stars of spectral types B and A were members of the real cluster.

## RESULTS AND CONCLUSIONS:

(1) CCD photometry in the *Vilnius* seven-color system has been done for 860 stars down to  $V = 16.7$  mag in a  $20'$  diameter area centered on the supposed open cluster Collinder 428.

(2) 34% of the stars have been classified in spectral and luminosity classes. Their color excesses, interstellar extinctions and distances have been determined.

(3) In the direction of Collinder 428, a steep increase of extinction is observed at  $\sim 400$  pc, which may be explained by the beginning of a dust cloud at a distance of about 540 pc. This distance is in a good agreement with that of the L 935 dust cloud and other clouds in the vicinity of the North America and Pelican nebulae found in our earlier papers.

(4) The interstellar extinction-free color-magnitude diagrams for all 290 classified stars (Figure 5.2.1) gives no evidence of the presence of the main sequence of the cluster. The same result follows from the color-magnitude diagram for 34 stars with high membership probability ( $\geq 70\%$ ) selected from the Dias et al. (2006) proper motion study. Consequently, Collinder 428 seems to not be a real cluster.

## 6. THE MAIN RESULTS AND CONCLUSIONS

### 6.1. SUMMARY OF THE MAIN RESULTS

A Milky Way region in the direction of the North America and Pelican Nebulae is investigated using CCD photometry of 2600 stars in the *Vilnius* seven-color system. Its central part was covered with a CCD camera on the Maksutov wide-field telescope of the Moletai Observatory. Deeper CCD exposures for most interesting selected targets were taken with the 1 m telescope of the USNO Flagstaff Station. The author developed a new method for CCD data processing trying to reduce systematic errors and to increase photometric accuracy. This allowed us to measure M67 stars with high precision and use it as a CCD standard region in all our subsequent observations. To investigate interstellar extinction law in the area we obtained spectra for 33 B-type stars with the 2.3 m telescope of Steward Observatory at Kitt Peak. We also used near-infrared 2MASS data and other data sources when they were available. From photometric results in the *Vilnius* system we determined two-dimensional spectral types, color excesses, interstellar extinctions and distances of  $\approx 1300$  stars. For more accurate determination of open cluster ages we recalibrated the zero-age main sequence in absolute magnitude vs. color diagram of the *Vilnius* system. We also investigated the possible connection between two open clusters in the area and surrounding star-forming region. Young stellar objects and possible ionizing sources of the NAP gas clouds were identified.

The following main results are obtained:

1. We have obtained photometry of high accuracy for 412 stars of the M67 cluster down to  $V=16$  mag in the *Vilnius* photometric system. These standard stars were used for CCD large-scale field corrections and reductions to the *Vilnius* standard photometric system.

2. CCD photometry in the *Vilnius* system was also obtained for 2600 stars in the North America and Pelican region. It includes: (1) 690 stars down to  $\sim 13.2$  mag in the area of  $2^\circ \times 2^\circ$  degrees in the central part of NAP nebulae; (2) 430 stars down to  $V=16-17$  mag in four areas of the L935 cloud; (3) 620 stars in the area of open cluster NGC 6997 and (4) 860 stars in the area of a possible cluster Collinder 428.

3. The interstellar reddening law is derived for 15 heavily reddened stars in the area covering the North America and Pelican nebulae and the dark cloud between them. The method is based on photometry of these stars in the *Vilnius* seven-color system and on their MK spectral types.

4. For the majority of stars observed in *Vilnius* system, spectral and luminosity classes, color excesses, interstellar extinctions and distances were determined. After that these stars were used to investigate the interstellar extinction dependence on distance in different parts of the dust cloud and of the North America and Pelican nebulae.

5. The zero-age main sequence for solar metallicity stars in the absolute magnitude vs. color diagram of the *Vilnius* seven-color photometric system is determined. The calibration is based on the results of photoelectric photometry of stars in the Hyades, Pleiades and Praesepe open clusters and the Ori OB1 association. A theoretical Victoria-Regina isochrone, corresponding to an age of 10 million years, coincides well with the lower envelope of the unevolved main sequence.

6. A distance to the cluster NGC 6997 is found to be 790 pc by the ZAMS fitting method and 780 pc by averaging individual distances of 50 probable cluster members. The average value of interstellar extinction of the cluster,  $A_V$ , is 1.92 mag. Fitting the main sequence and red giants of the cluster to the isochrones in the  $M_V$  vs.  $(B-V)_0$  plane we obtain its age of  $3.5 \times 10^8$  yr.

7. Magnitudes and color indices of 860 stars down to  $V = 16.7$  mag in the *Vilnius* system were obtained in the area of the supposed open cluster Collinder 428 in the North America Nebula. Spectral types, color excesses, interstellar extinctions and distances of stars were determined for 290 stars from the photometric data. The plot of extinction vs. distance gives the front edge of the dust cloud at 540 pc, i.e., very close to the dust cloud L935. Our data show that Collinder 428 is not a real cluster but just a window among dust clouds.

8. In the area covering the complex of the North America and Pelican nebulae we identified 13 faint stars with  $J-H$  and  $H-K_s$  color indices which simulate heavily reddened O-type stars. Four or five stars are found to have a considerable probability of being O-type stars, contributing to the ionization of North America and Pelican. If they really are O-type stars, their interstellar extinction  $A_V$  should be from 16 to 35 mag.

9. From our observations about 40 stars in the L935 cloud, mostly K and M dwarfs, are suspected to have H $\alpha$  emission; most of these stars also exhibit infrared excesses, four

of them are known pre-main-sequence stars. Recently the presence of H $\alpha$  emission in 19 of these stars was confirmed by spectral observations (in press).

## 6.2. CONCLUSIONS

1. The application of the new method for determining of flatfielding corrections in the Flagstaff CCD exposures shows that large-scale errors in *Vilnius V* filter across the field of 20' do not exceed 1–2%. This proves that our method allows us to reduce CCD data with high accuracy.

2. High accuracy of M 67 HR diagrams in *Vilnius* system are plotted. They can be used for investigation of stellar evolution and binary stars in the cluster.

3. Interstellar extinction law in the North America and Pelican area is very similar to the law for a much wider area in Cygnus. It differs from the normal law by exhibiting somewhat stronger extinction in the violet and the near ultraviolet spectral regions.

4. The L 935 dark cloud, which separates North America and Pelican nebulae, begins at a distance of  $520 \pm 50$  pc.

5. The open cluster NGC 6997 has no genetic relation to the star-forming region in the North America and Pelican nebulae being located behind it.

## REFERENCES

- Anthony-Twarog B. J. 1982, AJ, 87, 1213  
 Ažusienis A., Straizys V. 1966, Bull. Vilnius Obs., No. 18, 3  
 Ažusienis A., Straizys V., Sūdžius J. 1966, Bull. Vilnius Obs., No. 18, 34  
 Bally J., Scoville N. Z. 1980, ApJ, 239, 121  
 Bally J. Reipurth B. 2003, AJ, 126, 893  
 Bessell M. S., Brett J. M. 1988, PASP, 100, 1134  
 Bochkarev N. G., Sitnik T. G. 1985, A&SS, 108, 237  
 Bogdanovich A., Straizys V. 1966, Bull. Vilnius Obs., No. 18, 25  
 Borgman J. 1961, BAN, 16, 99  
 Borgman J., Johnson H. L. 1962, ApJ, 135, 306  
 Boyle R. P., Kazlauskas A., Vansevičius V., Straizys V., Vrba F. J., Sūdžius J., Smriglio F. 1998, Baltic Astronomy, 7, 369, Paper I  
 Briceño C., Luhman K. L., Hartmann L., Stauffer J. R., Kirkpatrick J. D. 2002, ApJ, 580, 317  
 Brown A. G. A., de Geus E. J., de Zeeuw P. T. 1994, A&A, 289, 101  
 Carpenter J. M. 2001, AJ, 121, 2851  
 Cash W., Charles P., Bowyer S., Walter F., Garmire G., Riegler G. 1980, ApJ, 238, L71  
 Casu S., Scappini F., Cecchi-Pestellini C., Olberg M. 2005, MNRAS, 359, 73  
 Cambrésy L., Beichman C. A., Jarrett T. H., Cutri R. M. 2002, AJ, 123, 2559  
 Černiauskas A. 2004, *Zero-age Main Sequence in the Vilnius Photometric System*, Diploma Thesis, Vilnius Pedagogical University  
 Černis K. 1987, A&AS, 133, 355  
 Černis K., Bartašiūtė S., Straizys V., Janulis R. 1998, Baltic Astronomy, 7, 625  
 Cohen M., Kuhi L. V. 1979, ApJS, 41, 743  
 Collinder P. 1931, Lund Obs. Annals, No. 2  
 Comerón F., Pasquali A. 2005, A&A, 430, 541  
 Comerón F., Pasquali A., Rodighiero G., Stanishev V. et al. 2002, A&A, 389, 874  
 Corwin H. G. 2004, *History and Accurate Positions for the NGC/IC Objects*, CDS Catalog VII/239A; <http://www.ngcic.org/corwin/default.htm>  
 Cutri R. M., Skrutskie M. F., Van Dyk S., Beichman C. A. et al. 2003a, *2MASS All Sky Catalog of Point Sources*, NASA/IPAC Infrared Science Archive, <http://irsa.ipac.caltech.edu/applications/Gator/>  
 Cutri R. M., Skrutskie M. F., Van Dyk S., Beichman C. A. et al. 2003b, *Explanatory Supplement to the 2MASS All Sky Data Release, Section VI.4.2b*, <http://www.ipac.caltech.edu/2mass/releases/allsky/doc/>  
 Cutri R. M., Skrutskie M. F., Van Dyk S., Beichman C. A. et al. 2006, *Explanatory Supplement to the 2MASS All Sky Data Release and Extended Mission Products*, <http://www.ipac.caltech.edu/2mass/releases/allsky/doc/expsup.html>  
 Dame T. M., Hartmann D., Thaddeus P. 2001, ApJ, 547, 792  
 Dame T. M., Ungerechts H., Cohen R. S., de Geus E. J. et al. 1987, ApJ, 322, 706  
 Demarque P., Woo J.-H., Kim Y.-C., Yi S. K. 2004, ApJS, 155, 667  
 Dias W. S., Assafin M., Florio V., Alessi B. S., Libero V. 2006, A&A, 446, 949  
 Divan L. 1956, Ann. d'Astrophys., 19, 255  
 Djupvik A. A., André Ph., Bontemps S., Motte F. et al. 2006, A&A, 458, 789  
 Dobashi K., Bernard J.-P., Yonekura Y., Fukui Y. 1994, ApJS, 95, 419  
 Downes D., Rinehart R. 1966, ApJ, 144, 937  
 Draine B. T. 2003, *Interstellar Dust Grains*, ARA&A, 41, 241  
 Drew J. E., Greimel R., Irwin M. J. et al. 2005, MNRAS, 362, 753  
 Droege T. F., Richmond M. W., Sallman M. P., Creager R. P. 2006, PASP, 118, 1666; CDS catalog II/271  
 Dzervitis U., Paupers O. 1994, Baltic Astronomy, 3, 335

- Eiroa C., Hefele H., Zhong-yu Q. 1983, A&A, 54, 309
- Eglitis I. 2002, personal communication
- Fan X. H., Burstein D., Chen J.-S. et al. 1996, AJ, 112, 628
- Fehrenbach Ch., Petit M., Cruvellier G., Peyrin Y. 1961, J. des Observateurs, 44, 233
- Feldt C., Wendker H. J. 1993, A&AS, 100, 287
- Fernie J. D., Marlborough J. M. 1963, ApJ, 137, 700
- Fiorucci M., Munari U. 2003, A&A, 401, 781
- Fitzpatrick E. L. 1999, PASP, 111, 63
- Fitzpatrick E. L., Massa D. 2005, AJ, 130, 1127
- Fitzpatrick E. L., Massa D. 2007, ApJ, 663, 320
- Flaherty K. M., Pipher J. L., Megeath S. T., Winston E. M. 2007, ApJ, 663, 1069
- Froebrich D., del Burgo C. 2006, MNRAS, 369, 1901
- Froebrich D., Murphy G. C., Smith M. D., Walsh J., del Burgo C. 2007, MNRAS, 378, 1447
- Hanson M. M. 2003, ApJ, 597, 957
- He L., Whittet D. C. B., Kilkenny D., Spencer Jones J. H. 1995, ApJS, 101, 335
- Herbig G. H. 1958, ApJ, 128, 259
- Herbig G. H., Bell K. R. 1988, *Third Catalog of Emission-Line Stars of the Orion Population*, Bull. Lick Obs., No. 1111
- Herbig G. H., Rao N. K. 1972, ApJ, 174, 401
- Herbst W. 1975, AJ, 80, 498
- Heske A., Wendker H. J. 1985, A&A, 148, 439
- Hiltner W. A., Johnson H. L. 1956, ApJ, 124, 367
- Giesecking F. 1973, Veröff. Astron. Inst. Bonn, No. 87
- Giesecking F., Schumann J. D. 1976, A&AS, 26, 367
- Giesecking F. Schumann J.D. 1976, A&AS, 26, 367
- Gilliland R. L., Brown T. M., Duncan D. K. et al. 1991, AJ, 101, 541
- Girardi L., Bressan A., Bertelli G., Chiosi C. 2000, A&AS, 141, 371
- Glass I. S., Schultheis M. 2002, MNRAS, 337, 519
- González-Solares E. A., Walton N. A., Greimel R., Drew J. E. 2008, MNRAS, 388, 89
- Goudis C. 1976a, Ap&SS, 39, 173
- Goudis C. 1976b, Ap&SS, 44, 281
- Goudis C. Johnson P.G. 1978, A&A, 63, 259
- Goy G. 1972, A&A, 21, 11
- Greenberg J. M., Chlewicksi G. 1987, QJRAS, 28, 312
- Greenberg J. M., Meltzer A. S. 1960, ApJ, 132, 667
- Groenewegen M. A. T., Blommaert J. A. D. L. 2005, A&A, 443, 143
- Grubissich C. 1968, Z.f.Astroph., 68, 309
- Gurklytė A., Straižys V., Bartkevičius A. 1974, unpublished
- Indebetouw R., Mathis J. S., Babler B. L., Meade M. R. et al. 2005, ApJ, 619, 931
- Jaschek M. 1978, *Catalogue of Selected Spectral Types in the MK System*, CDS, Strasbourg
- Johnson H. L. 1965, ApJ, 141, 923
- Johnson H. L. 1968, in *Nebulae and Interstellar Matter*, eds. B. M. Middlehurst & L. H. Aller, Univ. of Chicago Press, p. 167
- Johnson H. L. 1977, Rev. Mexicana AA, 2, 175
- Johnson H. L., Borgman J. 1963, BAN, 17, 115
- Johnson H. L., Morgan W. W. 1954, ApJ, 119, 344
- Johnson H. L., Morgan W. W. 1955, ApJ, 122, 142
- Joner M. D., Taylor B. J. 1990, PASP, 102, 1004
- Kaplan D. L., Frail D. A., Gaensler B. M., Gotthelf E. V. et al. 2004, ApJS, 153, 269
- Kazlauskas A., Boyle R. P., Philip A. G. D., Straižys V., Laugalys V., Černis K., Bartašiūtė S., Sperauskas J. 2005, Baltic Astronomy, 14, 465
- Kazlauskas A., Straižys V., Bartašiūtė S., Laugalys V., Černis K., Boyle R. P., Philip A. G. D.

- 2006, Baltic Astronomy, 15, 511
- Kharadse E. K., Apriamashvili S. P., Kochlashvili T. A. 1964, Bull. Abastumani Obs., No. 31, 3
- Kholopov P. N. 1959, AZh, 36, 295
- Kholopov P. N. 1970, in *Eruptive Stars*, Nauka Publishing House, Moscow, p. 241
- Köhler U. 1967, Veröff. Remeis-Sternwarte Bamberg, Vol. 6, No. 47
- Koornneef J. 1983, A&A, 128, 84
- Koornneef J. 1983, A&A, 128, 84
- Kurilienė G. 1983, Bull. Vilnius Obs., No. 62, 26
- Laugalys V., Boyle R. P., Kazlauskas A., Vrba F. J., Philip A. G. D., Straižys V. 2003, Baltic Astronomy, 12, 497
- Larson K. A., Whittet D. C. B. 2005, ApJ, 623, 857
- Laugalys V., Kazlauskas A., Boyle R. P., Vrba F. J., Philip A. G. D. Straižys V. 2004, Baltic Astronomy, 13, 1
- Laugalys V., Straižys V. 2002, Baltic Astronomy, 11, 205
- Laugalys V., Straižys V., Vrba F. J., Boyle R. P., Philip A. G. D. Kazlauskas A. 2006a, Baltic Astronomy, 15, 327
- Laugalys V., Straižys V., Vrba F. J., Boyle R. P., Philip A. G. D. Kazlauskas A. 2006b, Baltic Astronomy, 15, 483
- Laugalys V., Straižys V., Vrba F. J., Černis K., Kazlauskas A., Boyle R. P., Philip A. G. D. 2007, Baltic Astronomy, 16, 349
- Leung H. O., Thaddeus P. 1992, ApJS, 81, 267
- Lombardi M., Alves J., Lada C. J. 2006, A&A, 454, 781
- López-Corredoira M., Cabrera-Lavers A., Garzón F., Hammersley P. L. 2002, A&A, 394, 883
- Lucke P. B. 1980, A&A, 90, 350
- Lynds B. T. 1962, ApJS, 7, 1
- Marcy G. W. 1980, AJ, 85, 230
- Martin P. G., Whittet D. C. B. 1990, ApJ, 357, 113
- Massey P., Thompson A. B. 1991, AJ, 101, 1408
- Matthews H. E., Baars J. W. M., Wendker H. J., Goss W. M. 1977, A&A, 55, 1
- Matthews H. E., Goss W. M. 1980, A&A, 88, 267
- McMillan R. S., Tapia S. 1977, ApJ, 212, 714
- Meištas E. 1982, Bull. Vilnius Obs., No. 61, 32
- Metik L. P. 1960, Izvestia Crimean Obs., 23, 60
- Meyer D. M., Savage B. D. 1981, ApJ, 248, 545
- Meyer M. R., Calvert N., Hillenbrand L. A. 1997, AJ, 114, 288
- Momany Y., Vandame B., Zaggia S. et al. 2001, A&A, 379, 436
- Montgomery K. A., Marschall L. A., Janes K. A. 1993, AJ, 106, 181
- Morgan W. W., Johnson H. L., Roman N. G. 1954, PASP, 66, 85
- Nandy K. 1964, Publ. Edinburgh Obs., 3, No. 6, 137
- Naoi T., Tamura M., Nakajima Y., Nagata T. et al. 2006, ApJ, 640, 373
- Neckel T., Harris A. W., Eiroa C. 1980, A&A, 92, L9
- Negueruela I., Marco A., Herrero A., Clark J. S. 2008, A&A, 487, 575
- Nishiyama S., Nagata T., Kusakabe N., Matsunaga N. et al. 2006, ApJ, 638, 839
- Odenwald S. F., Schwartz P. R. 1993, ApJ, 405, 706
- Osterbrock D. E. 1957, ApJ, 125, 622
- Paupers O., Dzervitis U., Straižys V., Černis K. 1989, Bull. Vilnius Obs., No. 84, 21
- Perryman M. A. C., Brown A. G. A., Lebreton Y. et al. 1998, A&A, 331, 81
- Pinsonneault M. H., Stauffer J., Soderblom D. R., King J. R., Hanson R. B. 1998, ApJ, 504, 170
- Pottasch S. 1956, BAN, 13, 77
- Racca G., Gómez M., Kenyon S. J. 2002, AJ, 124, 2178

- Reed B. C. 1998, ApJS, 115, 271
- Reed B. C. 2003, AJ, 125, 2531
- Reed B. C. 2005, *Photometry and Spectroscopy for Luminous Stars*, CDS catalogue V/125 <http://othello.alma.edu/reed/OBfiles.doc>
- Rieke G. H. 1974, ApJ, 193, L81
- Rieke G. H., Lebofsky M. J. 1985, ApJ, 288, 618
- Román-Zúñiga C. G., Lada C. J., Muñch A., Alves J. F. 2007, ApJ, 664, 357
- Rozis-Saulgeot A. M. 1956, Ann. d'Astrophys., 19, 274
- Russeil D. 2003, A&A, 397, 133
- Rydgren A. E., Schmelz J. T., Vrba F. J. 1982, ApJ, 256, 168
- Rydgren A. E., Vrba F. J. 1981, AJ, 86, 1069
- Sandquist E. L. 2004, MNRAS, 347, 101
- Scappini F., Casu S., Cecchi-Pestellini C., Olberg M. 2002, MNRAS, 337, 495
- Schalen C. 1959, Arkiv f. Astron., 2, 359
- Schild R. E. 1977, AJ, 82, 337
- Schwassmann A., van Rhijn P. J. 1938, Bergedorfer Spektral-Durchmusterung der 115 Nördlichen Kapteynschen Eichfelder, Vol. 2, Hamburger Sternwarte in Bergedorf, p. 293 (SA 40)
- Sharpless S., Osterbrock D. 1952, ApJ, 115, 89
- Shevchenko V. S., Grankin K. N., Melnikov S. J. 1988, Astron. Zh., 65, 1230 = Soviet Astron., 32, 641
- Skrutskie M. F., Cutri R. M., Stiening R., Weinberg M. D. et al. 2006, AJ, 131, 1163
- Serkowski K. 1963, ApJ, 138, 1035
- Serkowski K. 1968, ApJ, 154, 115
- Serkowski K., Mathewson D. S., Ford V. L. 1975, ApJ, 196, 261
- Soderblom D. R., Nelan E., Benedict G. F., McArthur B., Ramirez I., Spiesman W., Jones B. F. 2005, AJ, 129, 1616
- Stassun K. G., van den Berg M., Mathieu R. D., Verbunt F. 2002, A&A, 382, 899
- Straizys V. 1970, in *Multicolor Stellar Photometry*, Doctoral Dissertation, Institute of Physics, Vilnius
- Straizys V. 1977, *Multicolor Stellar Photometry*, Moksas Publishers, Vilnius
- Straizys V. 1983, Bull. Vilnius Obs., No. 62, 11
- Straizys V. 1992, *Multicolor Stellar Photometry*, Pachart Publ. House, Tucson, Arizona
- Straizys V. 1999, Baltic Astronomy, 8, 109
- Straizys V. 2005, personal communication
- Straizys V., Černis K., Meištas E. 1992, unpublished
- Straizys V., Corbally C. J., Laugalys V. 1999, Baltic Astronomy, 8, 355
- Straizys V., Corbally C. J., Laugalys V. 2008, Baltic Astronomy, 17, 125
- Straizys V., Drazdys R., Gurklytė A. 1970, Bull. Vilnius Obs., No. 29, 10
- Straizys V., Eimontas A., Sūdžius J., Bartašiūtė S., Černis K. 1998, Baltic Astronomy, 7, 589
- Straizys V., Goldberg E. P., Meištas E., Vansevičius V. 1989b, A&A, 222, 82
- Straizys V., Kalytis R., Sūdžius J. 1979, Bull. Vilnius Obs., 52, 3
- Straizys V., Kazlauskas A. 1993, Baltic Astronomy, 2, 1
- Straizys V., Kazlauskas A., Vansevičius V., Černis K. 1993, Baltic Astronomy, 2, 171
- Straizys V., Kazlauskas A., Boyle R. P., Vrba F. J., Smriglio F. 1996, Baltic Astronomy, 5, 165
- Straizys V., Laugalys V. 2007, Baltic Astronomy, 16, 327
- Straizys V., Laugalys V. 2008a, Baltic Astronomy, 17, 143
- Straizys V., Laugalys V. 2008b, Baltic Astronomy, 17, 253
- Straizys V., Lazauskaitė R. 2008, Baltic Astronomy, submitted
- Straizys V., Meištas E., Vansevičius V., Goldberg E. P. 1989a, Bull. Vilnius Obs., No. 83, 3
- Straizys V., Sviderskiene Z. 1972, Bull. Vilnius Obs., No. 35, 3

- Sūdžius J. 1974, Bull. Vilnius Obs., No. 39, 18
- Sviderskienė Z., Straižys V. 1970, Bull. Vilnius Obs., No. 28, 55
- Tapia M. 1981, MNRAS, 197, 949
- Taylor A. R., Gibson S. J., Peracaula M., Martin P. G. et al. 2003, AJ, 125, 3145
- The P. S., Thomas D., Christensen C. G., Westerlund B. E. 1990, PASP, 102, 565
- Torres-Dodgen A. V., Tapia M., Carroll M. 1991, MNRAS, 249, 1
- Tsvetkov M. K. 1975, Astrofizika, 11, 579
- Turner D. G. 1976, AJ, 81, 1125
- Vallée J. P. 2005, AJ, 130, 569
- VandenBerg D. A., Bergbusch P. A., Dowler P. D. 2006, ApJS, 162, 375
- Villanova S., Baume G., Carraro G., Geminale A. 2004, A&A, 419, 149
- Voelcker K., Elsässer H. 1973, in *Interstellar Dust and Related Topics* (IAU Symp. No. 52), eds. J. M. Greenberg & H. C. van de Hulst, Reidel Publ. Company, p. 529
- Voshchinnikov N. V., Ilyin A. E., Ilyin V. B. 1986, Astrofizika (Erevan), 24, 307
- Wampler E. J. 1961, ApJ, 134, 861
- Wampler E. J. 1962, ApJ, 136, 100
- Wampler E. J. 1964, ApJ, 140, 1615
- Warren W. H., Hesser J. E. 1977a, ApJS, 34, 115
- Warren W. H., Hesser J. E. 1977b, ApJS, 34, 207
- Warren W. H., Hesser J. E. 1978, ApJS, 36, 497
- Welin G. 1973, A&AS, 9, 183
- Wendker H. J. 1968, Z. Astrophys., 68, 368
- Wendker H. J., Benz D., Baars J. W. M. 1983, A&A, 124, 116
- Westerhout G. 1958, Bull. Astron. Inst. Netherlands, 14, 215
- Whiteoak J. B. 1966, ApJ, 144, 305
- Whittet D. C. B. 1977, MNRAS, 180, 29
- Whittet D. C. B. 1979, A&A, 72, 370
- Whittet D. C. B. 2008, personal communication
- Wilson R. 1960, MNRAS, 120, 51
- Wolf M. 1925, Astron. Nachr., 223, 89
- Zdanavičius K., Straižys V. 1990, Ap&SS, 173, 309 (ZS90)
- Zdanavičius J., Zdanavičius K., Straižys V., Kazlauskas A., Černis K., Chen C. W., Chen W. P., Boyle R. P., Tautvaišienė G. 2004, Baltic Astronomy, 13, 555
- Zdanavičius J., Straižys V., Chen C. W., Chen W. P., Zdanavičius K., Kazlauskas A., Černis K., Philip A. G. D., Boyle R. P., Tautvaišienė G. 2005, Baltic Astronomy, 14, 179

## ACKNOWLEDGMENTS

The author is grateful to the scientific adviser V. Straižys for his permanent interest, valuable suggestions and for the editorial aid, to R. P. Boyle (Vatican Observatory) and F. J. Vrba (US Naval Observatory) for their assistance observing at Flagstaff, Arizona, C. J. Corbally (Vatican Observatory) for his work on spectra of our most interesting stars, to A. G. Davis Philip (Institute for Space Observations, New York) and to S. Bartasiūtė for the editorial aid. Author is also thankful to K. Zdanavičius and K. Černis for their help in observations with the Maksutov telescope of the Molėtai Observatory and to J.-E. Solheim (Tromsø University, Norway) for the opportunity to use the Tromsø CCD camera. Author is also thankful to J. Zdanavičius, A. Kazlauskas and R. Janusz (Cracow, Poland) for their assistance in observations and data reductions, and to E. Meištas for his help in preparing publications.

The author acknowledges the stable support by all staff of the Molėtai Observatory. Thanks go to the Steward Observatory of the Arizona University and the US Naval Observatory Flagstaff Station for allocation of the observing time on their telescopes. I am also thankful to the Vatican Observatory community at Tucson for help and hospitality during the observing runs.

I am grateful for partial support to the Ministry of Education and Science of Lithuania, the American Astronomical Society Chretien Grant of 2000, the grant of the National Science Council of Taiwan and the BalticGrid and LitGrid projects.

The use of the 2MASS, MSX, IPHAS, CADC, SkyView, Gator, Simbad and Webda databases is acknowledged.

The author acknowledges the stable support by the authorities of the Institute of Theoretical Physics and Astronomy and the Astronomical Observatory.

## APPENDIX

**Table 2.2.4.** Results of photometry, interstellar extinctions, distances and cluster membership for stars in the NGC 6997 area.

No	RA(2000) h m s	DEC(2000) ° ' "	V mag	U-V mag	P-V mag	X-V mag	Y-V mag	Z-V mag	V-S mag	V-I mag	Photom. sp. type	A <sub>V</sub> mag	d pc and ZS No.
1	20 55 36.30	44 39 36.7	17.228			2.106	1.063:	0.405	0.852	1.59			
2	20 55 37.05	44 33 42.3	16.442	3.788:	3.148:	2.360	1.209	0.458	1.036	1.83	a		
3	20 55 37.09	44 36 23.7	14.153	3.914	2.912	2.006	1.040	0.391	0.954	1.63			
4	20 55 37.26	44 38 20.8	16.264	4.104:	3.139:	2.427	1.147	0.446	1.074	1.85	f-g		
5	20 55 37.85	44 33 26.8	16.044	3.491	2.839	2.182	0.995	0.386	0.961	1.58	g2 V	2.010	770
6	20 55 37.86	44 35 33.7	16.089	3.913:	3.010	2.236	1.048	0.394	1.009	1.75	g0 V	2.393	760
7	20 55 38.51	44 30 11.1	16.038			3.856	1.756	0.724	1.599	2.89	k2 IV	4.417	510
8	20 55 38.57	44 33 16.0	13.684	3.486	2.609	1.591	0.758	0.298	0.672	1.16	a3 V	2.486	910
9	20 55 40.44	44 39 24.1	16.232			3.457	1.543	0.575	1.399	2.44	g9 III:	3.710	2210
10	20 55 41.07	44 31 12.8	15.700	4.491:	3.296	2.191	1.125	0.415	0.994	1.81	a0 V	4.412	1310
11	20 55 41.53	44 37 22.2	11.833	2.579	1.932	1.129	0.488	0.192	0.429	0.60	a7 V	1.007	530
12*	20 55 41.78	44 39 14.8	15.778	3.566	2.975	2.133	0.891	0.347	0.865	1.35	g7 IV:	1.160	2010
13	20 55 41.80	44 39 25.1	13.944	2.740	2.249	1.583	0.662	0.264	0.616	0.89	g3 V:	0.471	570
14	20 55 43.25	44 33 52.6	16.664		3.071:	1.910	0.980	0.403	0.769	1.49			
15	20 55 43.47	44 38 03.2	16.231	3.945:	2.924	2.098	1.051	0.401	0.927	1.62	a-f		
16	20 55 43.55	44 40 42.9	16.055	3.884:	2.928	2.066	0.982	0.372	0.905	1.56	f8 V	2.181	940
17	20 55 43.59	44 34 14.3	16.997		3.225:	2.289	1.276:	0.465	1.030	1.84	b		
18	20 55 43.83	44 38 05.0	15.876		4.268:	3.060	1.362	0.556	1.259	2.13	k0 IV	3.058	880
19	20 55 43.83	44 28 25.8	17.159			2.475	1.146:	0.555	1.077	2.04			
20	20 55 44.95	44 41 52.8	16.525	3.818:	2.765	1.790	0.871	0.372	0.725	1.31	a-f		
21	20 55 44.95	44 28 43.9	16.336	4.000:	2.975:	1.948	1.007	0.389	0.850	1.58	a0		
22	20 55 44.99	44 38 39.9	17.028		2.958:	2.431	1.143:	0.447	1.028	1.78			
23	20 55 45.20	44 41 04.2	17.000		2.867:	1.877	1.027:	0.359	0.782	1.47			
24	20 55 45.36	44 38 30.4	16.102			3.627	1.535	0.684	1.417	2.43	k3 III	2.887	3490
25	20 55 45.42	44 35 54.7	14.856	3.308	2.582	1.864	0.892	0.337	0.824	1.35	f5 V	1.996	740
26	20 55 45.97	44 41 39.7	17.360		2.749:	1.739	0.966:	0.346	0.727	1.36			
27	20 55 46.05	44 36 52.2	16.555		3.021:	2.032	1.015	0.368	0.875	1.56	a-f		
28	20 55 46.17	44 35 58.6	15.427	3.868	2.892	2.051	1.019	0.373	0.930	1.59	f3 IV:	2.767	1180
29	20 55 46.24	44 35 54.4	16.867	3.730:	2.748:	1.744	0.941:	0.361	0.760	1.37	b9:		
30	20 55 46.37	44 37 11.0	15.897	3.908:	2.966	1.922	0.961	0.387	0.796	1.41	a5 V:	3.285	1450
31	20 55 46.52	44 39 38.9	17.176		3.076:	2.227	0.987:	0.369	0.928	1.66			
32	20 55 46.56	44 32 25.6	15.786	3.380	2.767	1.990	0.885	0.347	0.822	1.28	g2 V	1.501	860
33	20 55 46.88	44 42 19.0	15.803	3.733	2.855	1.999	0.997	0.396	0.839	1.46	f2 V	2.758	1020
34	20 55 47.07	44 36 27.9	16.793		3.023:	2.256	1.244:	0.477	0.980	1.64	g8:		
35	20 55 47.11	44 41 14.7	16.848			2.304	1.032:	0.438	1.005	1.69	b		
36	20 55 47.38	44 41 26.4	17.345			2.095	0.923:	0.440	0.871	1.50	k0 V:	1.307	1070
37	20 55 47.42	44 40 39.0	15.255	3.538	2.618	1.642	0.847	0.320	0.708	1.26	a0 V:	3.128	1930
38	20 55 47.51	44 34 09.0	17.080			2.476	0.928:	0.445	1.138	1.97	k3 V:	1.053	770
39	20 55 47.63	44 40 28.3	15.208			3.794	1.644	0.677	1.499	2.61	k2 III	3.622	1570
40	20 55 47.72	44 39 06.3	16.282	3.621:	3.001	2.230	1.010	0.436	0.955	1.57	g-k		
41	20 55 47.77	44 34 35.0	16.219	3.761:	3.122:	2.286	0.975	0.403	1.025	1.69	k0 V	1.548	570
42	20 55 48.74	44 42 38.0	17.169		2.971:	2.291	1.108:	0.453	0.978	1.63			
43	20 55 48.94	44 37 05.8	15.794	3.451	2.831	2.048	0.975	0.368	0.902	1.50	g0 V	2.056	770
44	20 55 48.98	44 36 52.5	16.577			2.842	0.961	0.657	1.130	1.75	k7 V	0.189	476
45	20 55 49.03	44 37 44.6	17.330			1.901	0.820:	0.337	0.902	1.64			
46	20 55 49.22	44 32 57.3	16.414		3.097:	2.210	1.114	0.411	0.108	1.86	a-f		
47	20 55 49.28	44 35 47.1	16.364	3.680:	2.878:	2.202	1.021	0.430	0.938	1.55			
48	20 55 49.42	44 36 20.4	16.965		3.028:	2.115	0.957:	0.385	0.959	1.69	g		
49	20 55 49.48	44 41 06.3	16.707	3.884:	2.830:	2.001	1.085	0.358	0.956	1.75	b5:		
50	20 55 49.53	44 38 30.6	16.303			2.694	0.930	0.623	1.009	1.49	k5 V	0.693	481
51	20 55 49.95	44 40 21.6	15.470	4.987:	4.296:	3.108	1.420	0.531	1.289	2.21	g		
52	20 55 50.17	44 37 41.4	15.598	3.591	2.933	2.142	0.990	0.391	0.950	1.53	g2 V	1.987	630
53	20 55 50.36	44 37 29.2	15.542	3.968	3.118	2.260	1.146	0.443	1.034	1.76	f5 V	3.169	600
54	20 55 51.52	44 34 47.0	16.495		3.471:	2.692	1.095	0.505	1.171	1.93	k3 V:	1.825	411
55	20 55 51.59	44 42 43.2	16.299	3.641:	2.695	1.814	0.922	0.348	0.758	1.28	a1 V:	3.382	2420
56	20 55 52.05	44 40 18.7	16.431	4.214:	3.319:	2.498	1.286	0.470	1.107	1.89	f5 V:	3.816	670
57	20 55 52.16	44 39 21.0	15.407	3.917	2.997	2.093	0.991	0.399	0.910	1.56	f		
58	20 55 52.30	44 37 20.8	16.068	4.027:	3.141:	2.342	1.135	0.447	1.033	1.73	f6 V	3.026	770
59	20 55 52.34	44 41 45.3	13.939	3.374:	2.554:	1.697	0.782	0.301	0.709	1.15	f3 IV	1.672	980
60	20 55 52.75	44 38 53.4	16.999	3.527:	3.092:	2.181	1.059:	0.355	0.977	1.59	f		
61	20 55 53.58	44 28 14.9	16.334		3.126:	2.193	1.191	0.449	1.140	2.15	o-b		
62	20 55 53.75	44 35 21.3	16.586			2.423	1.207	0.455	1.132	1.93	f3:		
63	20 55 54.13	44 38 20.6	15.983	4.173:	4.043:	2.755	0.914	0.627	1.048	1.55	k7 V	0.000	395
64	20 55 54.43	44 35 51.5	14.025	3.260	2.467	1.597	0.753	0.282	0.711	1.15	f0 IV	1.908	1010
65	20 55 54.68	44 43 35.5	16.530	3.667:	2.884:	2.091	1.023	0.422	0.913	1.52	f5:		
66	20 55 54.70	44 32 13.9	14.377			4.660	2.088	0.863	1.924	3.48	k-m		
67	20 55 54.93	44 33 52.8	15.471	3.246:	2.829:	2.014	0.753	0.424	0.818	1.26	k2 V:	0.337	560
68	20 55 55.51	44 41 32.6	16.519	4.079:	3.165:	2.259	1.114	0.406	1.047	1.77	f3:		
69	20 55 55.65	44 42 08.7	15.617	3.272	2.734	1.968	0.837	0.372	0.836	1.29	g9 V	1.003	610
70	20 55 55.77	44 33 43.7	16.743		3.284:	2.273	1.137:	0.427	1.039	1.74			
71	20 55 55.84	44 33 51.6	16.982		3.074:	2.002	0.949:	0.377	0.914	1.65	f		
72	20 55 56.06	44 29 50.6	14.552	3.688	2.829	1.924	0.948	0.343	0.945	1.62	f0 V	2.809	640
73	20 55 56.85	44 35 59.9	16.573	3.901:	2.977:	2.142	1.020	0.395	1.032	1.75	f-g		
74	20 55 57.99	44 40 17.3	15.144	3.276	2.747:	1.883	0.874	0.336	0.818	1.31	g2:		
75	20 55 58.00	44 26 16.2	14.547	3.028	2.558	1.781	0.722	0.343	0.628	0.97	g8 V	0.517	510
76	20 55 58.27	44 40 36.9	17.081		2.738:	1.734	0.992:	0.340	0.746	1.38			
77	20 55 58.29	44 40 09.8	11.667	2.196									

**Table 2.2.4.** Continued

No	RA(2000) h m s	DEC(2000) ° ′ ″	V mag	U-V mag	P-V mag	X-V mag	Y-V mag	Z-V mag	V-S mag	V-I mag	Photom. sp. type	$A_V$ mag	d pc	Memb. and ZS90 No.
94	20 56 01.74	44 41 16.2	17.278		1.950	1.023:	0.456	0.963	1.61					
95	20 56 01.77	44 27 16.4	14.597	3.220	2.533	1.978	1.168	0.398	1.035	1.80	b0-b2			
96	20 56 01.94	44 26 24.3	16.783		3.090:	2.108	1.151:	0.398	0.991	1.77	b			
97	20 56 02.13	44 44 12.4	16.264	3.510:	2.793	2.156	0.956	0.391	0.942	1.52	g6 V	1.691	750	
98	20 56 02.17	44 38 19.0	16.313	3.382:	2.755	1.975	1.153	0.410	0.949	1.67	o-b			
99	20 56 02.62	44 36 32.4	16.904			2.809	1.089:	0.591	1.256	1.99	m2 V	0.042	247	
100	20 56 02.70	44 35 59.6	16.331			3.120:	1.268:	0.560	1.372	2.24	m3 V:	0.222	139	
101	20 56 03.02	44 41 13.3	17.372			1.896	0.840:	0.384	0.810	1.43				
102	20 56 03.07	44 26 39.2	14.465	3.308:	2.901	1.952	0.713	0.367	0.733	1.01	k2 V	0.152	382	
103	20 56 03.11	44 41 56.4	16.493	3.733:	3.101:	2.207	1.004	0.382	0.973	1.56	g5:			
104	20 56 03.15	44 34 15.7	16.886		2.932:	2.181	1.094:	0.433	1.024	1.75				
105	20 56 03.39	44 33 52.6	17.107			2.426	1.169:	0.393	1.127	1.89				
106	20 56 03.41	44 27 01.0	17.194	3.242:	2.657:	1.938	1.086:	0.324	0.965	1.65				
107	20 56 03.83	44 29 50.2	16.984		3.009:	1.995	1.105:	0.352	0.902	1.66	o-b			
108	20 56 03.95	44 41 11.4	16.951			2.327	1.069:	0.413	1.042	1.64	g			
109	20 56 04.04	44 42 30.3	16.259	3.814:	2.896	1.772	0.892	0.338	0.767	1.36	a1 V	3.243	2530	
110	20 56 04.25	44 34 46.6	16.911		2.968:	1.891	0.877	0.345	0.832	1.47	f8:			
111	20 56 04.46	44 36 01.4	16.353	3.972:	3.179:	1.942	1.044	0.361	0.893	1.55	b			
112	20 56 04.46	44 38 28.6	15.099	3.884	2.923	1.883	0.951	0.342	0.854	1.47	a1 V	3.516	1310	
113	20 56 04.47	44 31 59.3	16.178	3.908:	3.280:	2.260	0.828	0.446	0.886	1.30	k3 V	0.591	630	
114	20 56 04.89	44 34 22.3	16.854		3.189:	2.401	1.164:	0.442	1.084	1.82	f8:			
115	20 56 04.94	44 28 04.8	16.700	3.270:	2.789:	2.082	1.195	0.394	1.071	1.84	o-b			
116	20 56 05.11	44 34 26.6	16.011	4.102:	3.132	2.073	0.939	0.362	0.919	1.57				
117	20 56 05.33	44 40 43.3	16.540	3.815:	3.062:	2.136	1.033:	0.392	0.969	1.54	f5:			
118	20 56 05.45	44 39 00.2	16.246	4.080:	3.160	2.296	1.099:	0.435	1.059	1.80	f8 V	2.721	800 m	
119	20 56 05.65	44 42 22.0	15.257	4.400:	3.422	2.357	1.164	0.442	1.114	1.91	f0 V	3.807	560	
120	20 56 05.67	44 31 56.3	16.016	4.022:	3.829:	2.547	0.817	0.538	0.952	1.43	k5 V	0.171	540	
121	20 56 05.79	44 42 06.1	17.167		2.936:	1.752	0.852:	0.307	0.802	1.36				
122	20 56 05.95	44 31 51.9	16.109	4.152:	3.079	1.950	1.011	0.360	0.898	1.64	a0 V	3.885	2020	
123	20 56 06.08	44 26 33.3	16.630		3.137:	2.459	1.157:	0.423	1.122	1.85	f-g			
124	20 56 06.30	44 38 48.0	14.867	3.294	2.640	1.906	0.903	0.323	0.863	1.37	f8 V	1.816	650	
125	20 56 06.49	44 29 29.3	17.098			1.989	1.217:	0.377	0.967	1.75				
126	20 56 06.61	44 38 35.0	16.619	3.870:	2.931:	1.951	1.033	0.377	0.916	1.58	b9:			
127	20 56 06.63	44 37 16.4	16.571	3.850:	2.964:	1.922	0.952	0.361	0.836	1.42	a-f			
128	20 56 06.79	44 44 55.0	16.881		3.233:	2.387	1.191:	0.549	0.990	1.76	f-g			
129	20 56 06.87	44 28 32.5	17.064			2.303:	1.167:	0.420	1.086	1.92				
130	20 56 06.88	44 29 11.1	16.846		2.965:	2.309	1.179:	0.421	1.065	1.72	a			
131	20 56 06.97	44 34 45.2	16.328	3.702:	2.878	1.998	0.996	0.366	0.956	1.62	f2:			
132	20 56 07.09	44 41 46.5	15.887	3.442	2.801	2.038	0.969	0.375	0.907	1.49	g0 V	2.028	820 m	
133	20 56 07.11	44 42 23.1	12.814	2.545	1.957	1.312	0.728	0.266	0.628	1.00	b4 V	2.994	1680	
134	20 56 07.15	44 42 44.1	12.052	2.304	1.805	1.208	0.514	0.202	0.479	0.63	f6 V	0.157	456	
135	20 56 07.73	44 42 01.9	17.137		2.782:	1.770	0.927:	0.360	0.723	1.36				
136	20 56 07.93	44 30 31.3	15.934			3.561	1.768	0.603	1.581	2.77	g			
137	20 56 08.15	44 41 25.8	16.892			2.261	1.125:	0.424	1.068	1.69	a-f			
138	20 56 08.42	44 40 24.2	15.783	3.925	2.977	1.899	0.994	0.375	0.855	1.48	a0 V	3.807	1800	
139	20 56 08.89	44 42 57.8	14.470	2.979	2.557	1.764	0.678	0.304	0.673	0.93	k0 V	0.176	477	
140	20 56 09.05	44 35 38.8	16.975			2.659	0.950:	0.561	1.020	1.53	k5 V	0.785	630	
141	20 56 09.23	44 39 47.2	16.943		3.015:	2.235	1.147:	0.457	1.004	1.73				
142	20 56 09.24	44 38 28.7	16.057	3.442	2.930	2.035	0.943	0.367	0.882	1.43	g0 V:	1.908	930	
143	20 56 09.51	44 39 27.2	15.130	3.289	2.634	1.888	0.909	0.336	0.818	1.30	f6 V	1.982	810 m	
144	20 56 09.58	44 25 37.6	13.427	3.349	2.944	1.992	0.710	0.379	0.742	1.03	k3 V	0.046	227	
145	20 56 09.70	44 41 14.3	15.048	4.013	2.912	1.801	0.945	0.339	0.821	1.44	a0 IV	3.580	1710	
146	20 56 09.92	44 36 04.3	17.236			1.956	0.947:	0.320	0.961	1.67				
147	20 56 10.06	44 28 13.8	16.840			2.466	1.362:	0.454	1.122	1.97	b			
148	20 56 10.22	44 31 05.0	16.626		3.073:	1.969	0.956	0.335	0.881	1.59	a-f			
149	20 56 10.42	44 36 49.2	15.367	3.099	2.561	1.813	0.788	0.299	0.783	1.19	g3 V	1.053	840 m	
150	20 56 10.48	44 35 09.9	16.407			3.252	1.387	0.480	1.435	2.42	g-k			
151	20 56 10.75	44 35 48.5	15.940	4.414:	3.185	2.095	1.099:	0.386	0.965	1.71	a0 III	4.292	2340	
152	20 56 10.91	44 29 25.6	16.422		3.029:	1.924	1.052:	0.349	0.873	1.58	b			
153	20 56 10.92	44 35 33.5	14.201	3.504	2.528	1.596	0.886	0.304	0.810	1.37	b8-b9			
154	20 56 10.97	44 39 13.1	11.388	3.200	2.275	1.278	0.624	0.230	0.549	0.89	a1 III	2.005	720 m	
155*	20 56 11.22	44 38 17.7	12.441	5.996	5.087	3.624	1.558	0.610	1.416	2.40	k1 III	3.456	990	
157	20 56 11.22	44 29 21.9	16.834			2.730	1.100:	0.590	1.275	2.06	m2 V	0.092	234	
158	20 56 11.42	44 27 56.0	15.322	3.222	2.406	1.595	0.872	0.299	0.794	1.33	b7 III	3.520	3800	
159	20 56 11.42	44 26 17.4	16.843		2.984:	1.882	0.980	0.354	0.856	1.54	a0:			
160	20 56 11.54	44 30 59.5	13.493	3.745	2.742	1.702	0.834	0.296	0.780	1.35	a5 IV	2.698	790 m:	
161	20 56 11.69	44 45 09.5	14.984	3.501	2.582	1.527	0.768	0.304	0.611	1.11	a1 V	2.670	1830	
162	20 56 11.69	44 36 45.3	14.748	3.308	2.635	1.849	0.860	0.324	0.849	1.38	f8 V	1.617	670 m:	
163	20 56 11.70	44 29 51.6	16.516			2.532	1.123:	0.471	1.169	1.91	g9 V:	2.324	499	
164	20 56 11.71	44 38 33.2	16.894		3.020:	1.242:	0.648	1.340	2.29	k-m				
165	20 56 12.14	44 43 26.9	15.490	4.015	3.583	2.594	0.919	0.578	1.009	1.53	m1 V	0.000	173	
166	20 56 12.23	44 28 10.8	16.844		3.248:	2.143	1.035:	0.366	0.967	1.75	a-f			
167	20 56 12.24	44 36 25.8	14.273	2.954	2.488	1.725	0.728	0.284	0.740	1.13	g5 V	0.684	520	
168	20 56 12.39	44 39 49.1	16.581			2.521	1.180	0.452	1.117	1.86	g4:			
169	20 56 12.81	44 28 58.2	16.707		3.138:	2.022								

**Table 2.2.4.** Continued

No	RA(2000)	DEC(2000)	V	U-V	P-V	X-V	Y-V	Z-V	V-S	V-I	Photom.	$A_V$	d	Memb. and
	h m s	° ' "	mag	mag	mag	mag	mag	mag	mag	mag	sp. type	mag	pc	ZS90 No.
191	20 56 17.09	44 31 45.3	16.616		2.441	1.226:	0.412	1.132	1.85	a-f				
192	20 56 17.27	44 43 21.7	14.955	2.838	2.215	1.682	0.950	0.350	0.839	1.40	b1-b5			
193	20 56 17.34	44 44 27.5	17.208			1.856	1.015:	0.365	0.888	1.48				
194	20 56 17.35	44 26 50.0	16.856			2.525	1.251:	0.473	1.162	2.01	f5:			
195	20 56 17.53	44 34 02.4	12.753	3.459	2.521	1.470	0.745	0.266	0.678	1.18	a0 V	2.656	760	m
196	20 56 17.82	44 43 47.3	16.092	3.437	2.478	1.508	0.801	0.271	0.641	1.13	a0:			
197	20 56 17.95	44 32 59.1	15.438	4.419:	3.198	2.082	1.088	0.389	0.983	1.76	a0 IV	4.241	1510	
198	20 56 18.14	44 34 59.7	16.646		3.375:	2.507	1.054	0.420	1.121	1.82	k1 V:	1.820	560	
199	20 56 18.40	44 44 43.7	14.351	4.776	3.956	2.877	1.292	0.491	1.168	1.96	g6 III	2.827	1330	
200	20 56 18.67	44 44 32.3	15.832	3.643	2.744	1.852	0.936	0.363	0.788	1.37	a-f			
201	20 56 18.71	44 41 48.8	13.829	3.300	2.490	1.582	0.732	0.277	0.673	1.11	a8 V	2.042	750	m
202	20 56 19.15	44 38 39.4	13.862	3.380	2.561	1.633	0.775	0.292	0.724	1.20	a7 V	2.333	730	m
203	20 56 19.27	44 40 34.5	14.921	3.626	2.673	1.666	0.873	0.311	0.759	1.33	b9 V	3.386	1690	
204	20 56 19.48	44 36 24.2	16.820		3.114:	2.097	1.127:	0.386	0.957	1.70	b			
205	20 56 19.48	44 39 39.7	16.354		3.118:	2.039	1.070	0.550	0.929	1.63				
206	20 56 19.84	44 39 59.9	17.115		2.902:	2.143	1.075:	0.390	1.050	1.74				
207	20 56 19.88	44 39 27.2	16.765		3.315:	2.042	0.948	0.391	0.881	1.62				
208	20 56 19.94	44 28 54.9	13.275	2.531	2.109	1.453	0.576	0.233	0.602	0.80	g5 V	0.000	452	
209	20 56 20.13	44 37 51.2	11.758	3.487	2.478	1.497	0.732	0.270	0.686	1.16	a		4	
210	20 56 20.65	44 38 11.9	12.245	3.183	2.314	1.323	0.637	0.232	0.567	0.94	a1 V	2.065	690	m, 5
211	20 56 20.75	44 45 10.9	16.152	3.677:	2.731	1.931	0.968	0.379	0.858	1.46	a-f			
212	20 56 20.88	44 36 28.7	16.910			2.214	1.158:	0.415	1.046	1.81	a0:			
213	20 56 21.53	44 32 30.7	14.270	3.619	2.736	1.753	0.821	0.290	0.785	1.31	a7 V	2.546	800	
214	20 56 21.59	44 33 23.6	15.846	3.670	2.895	2.097	0.989	0.366	0.982	1.62	f8 IV	2.213	1540	
215	20 56 21.75	44 27 18.7	13.253	2.553	2.034	1.402	0.592	0.214	0.578	0.80	g0 V	0.286	540	
216	20 56 21.94	44 40 23.6	13.474	2.987	2.601	1.747	0.658	0.316	0.665	0.91	k0.5 V	0.037	307	
217	20 56 21.95	44 42 09.7	15.796	3.607	3.146	2.172	0.778	0.419	0.840	1.24	k3 V	0.360	580	
218	20 56 22.01	44 35 37.4	12.530	3.259	2.377	1.349	0.646	0.232	0.593	1.00	a2 V	2.014	730	m
219	20 56 22.10	44 24 46.3	16.170	3.807:	2.821	1.860	0.944	0.386	0.828	1.52	b-a			
220	20 56 22.19	44 37 20.4	12.597	3.254	2.391	1.407	0.673	0.250	0.625	1.05	a2 V	2.139	710	m, 6
221	20 56 22.43	44 26 29.4	16.236	4.104:	3.037:	2.213	1.066	0.393	1.040	1.79	f8 V:	2.569	860	
222	20 56 22.77	44 36 03.2	15.343	3.362	2.663	1.906	0.913	0.319	0.888	1.46	f6 V	2.000	890	
223	20 56 22.84	44 43 15.5	15.381	3.210	2.585	1.881	0.876	0.330	0.831	1.32	f9 V	1.645	850	m
224	20 56 22.90	44 45 04.5	14.657	3.730	2.763	1.822	0.902	0.343	0.792	1.37	f0 III	2.596	1360	
225	20 56 23.55	44 36 48.5	16.304	3.588:	2.925	2.162	1.038	0.382	0.913	1.62	f9 V	2.393	920	
226	20 56 23.58	44 35 57.7	17.109			2.421	1.243:	0.431	1.231	2.06				
227	20 56 23.93	44 39 02.8	16.868		2.885:	2.220	1.324:	0.460	0.990	1.72	b			
228	20 56 23.96	44 35 53.9	17.145		2.004:	1.059	0.359	0.961	0.025	1.71				
229	20 56 23.96	44 32 17.6	16.877			2.333	1.212:	0.465	1.093	1.91	b-a			
230	20 56 24.06	44 40 26.4	15.971	3.676:	2.840	2.132	1.038	0.381	0.993	1.67	f-g			
231	20 56 24.53	44 34 04.9	13.573	3.487	2.597	1.567	0.737	0.261	0.670	1.13	a5 IV	2.250	1010	
232	20 56 24.61	44 39 21.4	11.067	1.963	1.541	0.955	0.486	0.187	0.448	0.65	b5 Vp:	1.830	1070	9
233	20 56 24.65	44 25 43.9	16.819	3.763:	3.244:	2.281	0.994	0.399	0.970	1.54	g8 V:	1.774	810	
234	20 56 24.77	44 27 05.4	15.379	5.077:	4.210:	3.214	1.537	0.544	1.416	2.45				
235	20 56 24.81	44 34 31.8	16.379	3.752:	3.077:	2.227	0.958	0.371	1.014	1.67	g7 V:	1.654	770	m
236	20 56 24.83	44 34 25.0	14.402	3.675	2.816	1.929	0.915	0.336	0.897	1.51	f3 III	2.287	1210	
237	20 56 25.00	44 44 12.3	14.783	3.150	2.463	1.762	0.827	0.300	0.776	1.26	f6 V	1.603	820	m
238	20 56 25.06	44 43 18.4	15.303	3.328	2.478	1.486	0.711	0.282	0.605	1.05	a3 V	2.268	2120	
239	20 56 25.33	44 33 14.1	16.365			3.312	1.534	0.609	1.514	2.60	k0:			
240	20 56 25.56	44 36 42.5	15.174			4.224	1.804	0.754	1.699	2.95	k3 III	4.130	1280	
241	20 56 25.57	44 26 19.3	15.020	3.221	2.540	1.824	0.863	0.324	0.811	1.31	f6 V	1.769	850	
242	20 56 25.66	44 38 55.8	15.715	3.211	2.390	1.573	0.866	0.316	0.747	1.26	b7 III	3.493	4620	
243*	20 56 25.72	44 43 45.5	10.893	4.529	3.757	2.658	1.119	0.420	0.917	1.62	g8 III	1.843	850	m
244	20 56 26.02	44 30 46.4	16.820		3.196:	2.064	1.040:	0.405	0.897	1.63	a-f			
245	20 56 26.07	44 41 24.8	15.644	4.934:	4.145:	2.925	1.386	0.494	1.319	2.22	g	2.846	1020	
246	20 56 26.13	44 45 33.9	15.987			2.787	1.266	0.494	1.228	2.12	g8 IV			
247*	20 56 26.58	44 41 35.3	11.057	4.478	3.693	2.624	1.099	0.419	1.017	1.64	g8 III	1.760	720	m, 11
248	20 56 26.61	44 42 51.4	15.497	3.646	2.611	1.611	0.833	0.312	0.713	1.23	a0 III	3.063	3360	
249	20 56 26.79	44 35 33.7	16.127	3.597:	2.857	2.103	0.998	0.362	0.978	1.59	f7 V	2.301	1010	
250	20 56 26.87	44 35 24.8	15.350	3.465	2.718	1.970	0.923	0.346	0.917	1.54	f6 V	2.047	870	m
251	20 56 27.07	44 24 46.0	17.019			2.054	1.034:	0.407	0.947	1.66				
252	20 56 27.12	44 37 14.2	15.315	3.624	2.802	2.069	1.025	0.351	0.914	1.71	g-k			
253	20 56 27.14	44 37 53.9	13.856	2.667	2.244	1.567	0.613	0.255	0.615	0.84	g8 V	0.014	466	12
254	20 56 27.35	44 41 30.2	14.590	3.486	2.504	2.054	0.876	0.323	0.772	1.30	b8-b9			
255	20 56 27.46	44 39 59.1	16.234	4.335:	3.249:	2.491	1.211	0.472	1.096	1.87	f7:			
256	20 56 27.53	44 29 05.9	16.917			2.625	1.158:	0.391	1.207	2.05	g5 III	2.255	5660	
257	20 56 27.60	44 39 51.3	15.760	3.334	2.724	1.993	0.952	0.363	0.871	1.43	f8 V	2.042	880	
258	20 56 27.72	44 44 07.2	15.151	3.769	2.628	1.683	0.906	0.330	0.770	1.34	b9-a0			
259	20 56 27.72	44 37 37.6	16.539	3.668:	3.113:	2.300	1.050	0.442	1.065	1.77	g5:			
260	20 56 28.02	44 25 47.1	16.519	3.551:	2.666:	1.768	1.022	0.354	0.896	1.52	o-b			
261	20 56 28.10	44 35 01.1	13.155	3.401	2.529	1.492	0.711	0.259	0.649	1.10	a3 V	2.268	790	m
262	20 56 28.11	44 36 23.5	15.420	3.430	2.644	1.905	0.930	0.334	0.891	1.47	f5 V	2.171	890	
263</														

**Table 2.2.4.** Continued

No	RA(2000) h m s	DEC(2000) ° ′ ″	V mag	U-V mag	P-V mag	X-V mag	Y-V mag	Z-V mag	V-S mag	V-I mag	Photom. sp. type	A <sub>V</sub> mag	d pc	Memb. and ZS90 No.	
288	20 56 31.69	44 36 36.0	13.786	3.349	2.492	1.592	0.756	0.280	0.713	1.19	a7 III:	2.245	1280		
289	20 56 32.17	44 35 36.3	13.934	3.408	2.591	1.746	0.811	0.295	0.788	1.29	f3 IV:	1.806	920		
290	20 56 32.26	44 28 06.7	14.599	3.195	2.453	1.717	0.828	0.297	0.773	1.25	f5 IV:	1.700	1200		
291	20 56 32.35	44 33 18.0	15.532	3.590	2.953	2.155	1.004	0.357	1.002	1.59	g0 V:	2.190	640	m:	
292	20 56 32.41	44 43 09.1	16.383			3.122	1.434	0.537	1.294	2.19	g8 III:	3.299	2860		
293	20 56 32.42	44 37 30.8	16.017	3.639	2.911	2.124	0.994	0.379	0.959	1.56	f8 V:	2.236	900		
294	20 56 32.51	44 43 39.9	15.625	3.636	2.842	2.121	1.088	0.415	0.996	1.65	b or sdf				
295	20 56 32.52	44 45 27.4	16.206	3.738	2.763	1.740	0.893	0.373	0.737	1.32	b9 V:	3.479	2920		
296	20 56 32.87	44 33 59.7	13.942	3.670	2.766	1.747	0.814	0.283	0.752	1.28	a5 V:	2.606	810	m	
297	20 56 32.88	44 34 52.4	15.549	3.470	2.713	2.012	0.948	0.342	0.913	1.50	f-g				
298	20 56 32.92	44 40 43.3	12.947	3.253	2.821	1.874	0.691	0.338	0.686	0.93	k2 V:	0.051	199	22	
299	20 56 33.03	44 31 53.5	15.437	3.678	2.691	1.764	0.914	0.307	0.887	1.50	b5-a0				
300	20 56 33.05	44 43 56.1	16.985			2.060	1.115	0.406	0.907	1.56	b				
301	20 56 33.10	44 38 10.5	11.604	3.127	2.240	1.246	0.581	0.219	0.524	0.86	a2 V:	1.714	550	21	
302	20 56 33.21	44 35 40.2	15.103	3.365	2.611	1.874	0.891	0.328	0.862	1.40	f5 V:	1.991	840	m	
303	20 56 33.29	44 36 22.6	11.984	4.599	3.779	2.720	1.191	0.443	1.125	1.84	g5 II:	2.361	2660	20	
304	20 56 33.62	44 28 17.9	14.701	2.992	2.605	1.794	0.684	0.311	0.685	0.96	k0 V:	0.203	520		
305	20 56 33.73	44 40 37.4	14.803	3.287	2.574	1.830	0.863	0.332	0.838	1.36	f5 V:	1.862	770	m	
306	20 56 33.87	44 44 45.6	14.162	3.101	2.379	1.609	0.776	0.288	0.696	1.13	f2 V:	1.737	770	m	
307	20 56 34.15	44 36 35.8	16.861		3.077	2.180	1.039	0.392	1.012	1.66	f8:				
308	20 56 34.51	44 34 19.0	16.356	4.087	3.095	1.993	0.966	0.348	0.885	1.58	a5 V:	3.308	1780		
309	20 56 34.52	44 39 31.9	16.091	3.973:	2.946	2.211	1.105	0.416	1.006	1.71	f-g				
310	20 56 34.67	44 43 17.3	14.466	5.995:	5.148:	3.658	1.526	0.658	1.387	2.33	k3 III:	2.846	1680		
311	20 56 34.70	44 35 13.3	17.011			2.216	1.069	0.379	1.015	1.75					
312	20 56 34.74	44 32 03.6	16.440	3.514:	2.712	1.806	0.904	0.315	0.913	1.51					
313	20 56 34.81	44 37 29.3	13.792	2.530	2.015	1.411	0.636	0.238	0.587	0.85	f8 V:	0.582	700		
314	20 56 34.99	44 32 20.6	16.109	3.952:	2.873	1.832	0.939	0.307	0.880	1.50					
315	20 56 35.04	44 41 26.5	15.981		3.133	2.181	1.095	0.381	1.010	1.76	f2 V:	3.211	900		
316	20 56 35.08	44 34 41.7	16.509	3.904:	3.015:	2.289	1.036	0.414	1.043	1.72	g5-g8				
317	20 56 35.32	44 32 44.6	16.213		3.848:	2.893	1.488	0.523	1.322	2.27	a-f				
318	20 56 35.54	44 30 52.7	16.534	4.001:	3.027:	1.934	0.991	0.358	0.821	1.52	a0				
319	20 56 35.60	44 36 12.6	14.871	3.413	2.600	1.795	0.855	0.314	0.822	1.39	f2 III:	2.102	1640		
320	20 56 35.65	44 34 23.9	16.190	3.891:	3.268	2.334	1.069	0.385	1.047	1.70	g5 V:	2.259	610		
321	20 56 35.83	44 43 56.1	14.871	3.583:	2.753	2.033	0.997	0.376	0.910	1.51	f5 V:	2.481	600		
322	20 56 36.06	44 31 56.3	16.070	3.619:	3.255	2.205	0.764	0.404	0.854	1.25	k3 V:	0.296	680		
323	20 56 36.13	44 28 15.3	13.493	3.093	2.315	1.414	0.643	0.295	0.600	0.98	a7 V:	1.723	820		
324	20 56 36.14	44 40 07.4	15.621	3.589	2.672	1.821	0.886	0.339	0.791	1.32	f2 IV:	2.245	1640		
325	20 56 36.40	44 38 44.4	13.601	3.242	2.482	1.688	0.787	0.289	0.748	1.22	f2 IV:	1.788	800	24	
326	20 56 36.52	44 42 39.3	15.331	3.937	2.980	2.015	1.003	0.364	0.962	1.70	f0 IV:	3.063	1080		
327	20 56 36.77	44 35 38.9	10.267	2.215	1.693	0.892	0.334	0.136	0.309	0.38	a-f		26		
328	20 56 36.85	44 35 11.8	15.079	3.283	2.579	1.849	0.850	0.306	0.836	1.35	f7 V:	1.617	860	m	
329*	20 56 37.14	44 40 09.2	11.243	4.729	3.930	2.785	1.172	0.447	1.102	1.76	g8 III:	2.088	740	m,25	
330	20 56 37.50	44 43 31.5	17.014		2.854:	1.915	1.023:	0.418	0.815	1.43					
331	20 56 37.53	44 34 22.2	15.266	4.302	2.958	1.897	1.017	0.352	0.921	1.59	a-f				
332	20 56 37.63	44 28 40.8	14.874	3.511	3.031	2.069	0.722	0.372	0.763	1.06	k3 V:	0.102	431		
333	20 56 38.06	44 35 41.3	15.759	3.897:	2.895	1.822	0.931	0.325	0.775	1.40	a1 V:	3.423	1850		
334	20 56 38.46	44 40 09.8	16.911		3.330:	2.403	1.164:	0.481	1.065	1.87	f-g				
335	20 56 38.76	44 28 27.3	15.302		3.095:	2.259	1.396	1.771	0.698	1.609	2.79	k2 III:	4.209	1260	
336	20 56 38.76	44 25 36.5	16.113	4.061:	2.991	2.102	1.099	0.409	0.961	1.66	b9				
337	20 56 38.77	44 32 42.2	13.699	6.416:	5.450	3.940	1.696	0.634	1.525	2.63	k				
338	20 56 39.30	44 38 27.3	12.675	5.088	4.192	3.039	1.361	0.499	1.277	2.17	g2 Ib:	3.100	6840		
339	20 56 39.50	44 38 21.7	11.703	3.583	2.552	1.508	0.739	0.262	0.678	1.17	a2 III:	2.444	620	m	
340	20 56 39.78	44 37 44.1	16.114	4.068:	2.999	1.876	1.035	0.368	0.850	1.52	b2-b5				
341	20 56 39.82	44 29 49.8	15.404	2.995	2.539	1.817	0.717	0.298	0.747	1.09	k0 V:	0.356	680		
342	20 56 40.01	44 30 28.3	16.651		3.500:	2.782	1.296	0.482	1.254	2.08	g				
343	20 56 40.20	44 41 49.9	15.633	3.428	2.681	1.962	0.975	0.362	0.918	1.48	f5 V:	2.379	890		
344	20 56 40.25	44 39 26.4	13.491	3.636	2.680	1.607	0.787	0.287	0.722	1.26	a2 V:	2.666	840	m,28	
345	20 56 40.92	44 31 25.8	17.186		2.395		1.118:	0.426	1.054	1.85					
346	20 56 40.93	44 42 16.1	16.419		3.095:	2.259	1.250	0.401	1.107	1.89	o-b				
347	20 56 40.97	44 28 26.1	17.036		2.917:	2.249	1.252:	0.411	1.108	1.87					
348	20 56 41.24	44 33 01.0	16.110	3.667:	3.235	2.183	0.875	0.381	0.870	1.29	k1 V:	0.993	640	m	
349	20 56 41.32	44 26 09.1	15.297	4.871:	4.072:	2.972	1.322	0.531	1.270	2.13	k0 IV:	2.874	730		
350	20 56 41.74	44 27 55.5	16.921		2.971:	2.004	1.119:	0.344	0.915	1.61	b				
351	20 56 41.88	44 38 06.1	15.230	3.239	2.569	1.873	0.875	0.334	0.839	1.32	f8 V:	1.686	810	m	
352	20 56 41.88	44 41 13.8	12.585	3.197	2.372	1.401	0.659	0.253	0.619	1.03	a2 V:	2.074	730	m,30	
353	20 56 42.02	44 44 07.3	17.229		2.443		1.064:	0.500	1.044	1.69	k0 V:	1.959	750	m	
354	20 56 42.07	44 26 38.4	17.047		2.400		1.005:	0.452	0.971	1.55	k1 V:	1.594	740		
355	20 56 42.09	44 43 42.2	16.496	4.078:	3.032:	2.222	1.094	0.419	1.031	1.72	f3:				
356	20 56 42.28	44 39 16.8	13.989	3.398	2.389	1.507	0.819	0.302	0.740	1.22	b9 III:	3.137	1860	29	
357	20 56 42.69	44 26 37.7	16.862		3.184:	2.253	0.912	0.398	1.022	1.56	k1 V:	1.164	830		
358	20 56 42.77	44 38 36.7	14.866	3.105	2.453	1.740	0.798	0.306	0.766	1.21	f7 V:	1.377	870	m	
359	20 56 42.80	44 26 57.2	17.344		2.267	0.968:	0.448	0.106	1.73	1.00	k0 V:	1.515			









































**Table 3.1.5** Continued

Name*	BD, HD	RA (2000)	DEC (2000)	<i>V</i>	Sp	<i>J-H</i>	<i>H-K<sub>s</sub></i>
LSV07-827		21 03 58.01	44 35 32.8	14.40	b9 III-IV	0.179	0.070
LSV07-479		21 03 15.67	44 41 21.2	15.79	b6 IV	0.161	0.154
LSV07-665		21 03 34.33	44 45 24.0	15.83	b9 Vp?	0.171	0.157
LSV07-447		21 03 12.27	44 37 37.7	15.98	b8 IV	0.157	0.176
LSV07-438		21 03 11.06	44 46 43.0	16.17	b3 V	0.200	0.137
LSV07-690		21 03 36.08	44 26 40.4	16.30	b7 V	0.408	0.173
ALS 17987	BD+45 3387	21 04 18.21	46 31 52.8	8.61	B8 III	-0.008	0.003
ALS 11718	BD+45 3406	21 06 32.43	45 51 31.0	9.52	B1 Iab	0.134	0.112
ALS 17980	BD+44 3710	21 07 14.94	44 40 26.7	7.38	B8 III	-	-
Cyg OB2 association: brightest stars							
VI Cyg 1		20 31 10.55	41 31 53.5	11.06	O9 V	0.412	0.191
VI Cyg 2		20 31 22.04	41 31 28.4	10.61	B1 Ib:	0.325	0.122
VI Cyg 3	BD+40 4212	20 31 37.50	41 13 21.0	10.35	O9:	0.497	0.253
VI Cyg 4	BD+40 4219	20 32 13.83	41 27 12.0	10.07	O7 III	0.334	0.143
VI Cyg 5*	BD+40 4220	20 32 22.43	41 18 19.1	9.21	O7e	0.442	0.406
VI Cyg 12		20 32 40.96	41 14 29.2	10.40	B5 Iab:	1.155	0.808
VI Cyg 6		20 32 45.46	41 25 37.4	10.65	O8 V:	0.336	0.196
VI Cyg 9		20 33 10.75	41 15 08.2	10.78	O5 Ie	0.571	0.327
VI Cyg 7		20 33 14.11	41 20 21.8	10.50	O3 I	0.430	0.207
VI Cyg 8B		20 33 14.76	41 18 41.6	10.31	O8	0.447	0.192
VI Cyg 8A	BD+40 4227	20 33 15.08	41 18 50.5	8.99	O5.5 I	0.402	0.218
VI Cyg 8D		20 33 16.34	41 19 01.8	12.02	O8 V	0.418	0.185
VI Cyg 8C		20 33 17.99	41 18 31.1	10.08	O5 III	0.373	0.213
VI Cyg 10	BD+41 3804	20 33 46.10	41 33 01.1	9.89	O9.5 Ia	0.455	0.257
VI Cyg 11	BD+41 3807	20 34 08.50	41 36 59.2	10.08	O5 If	0.424	0.236
Cyg OB2 association: Massey & Thompson (1991) stars							
MT91-299		20 32 38.57	41 25 13.7	10.84	O7.5 V	0.276	0.202
MT91-556		20 33 30.78	41 15 22.6	11.01	B1 Ib	0.602	0.349
MT91-601		20 33 39.10	41 19 25.8	11.07	O9.5 III	0.485	0.263
MT91-258		20 32 27.66	41 26 22.0	11.10	O8 V	0.342	0.172
MT91-259		20 32 27.74	41 28 52.2	11.42	B0.5 V	0.296	0.129
MT91-227		20 32 16.56	41 25 35.7	11.47	O9 V	0.325	0.204
MT91-145		20 31 49.63	41 28 26.5	11.52	O9.5 V	0.306	0.134
MT91-417		20 33 08.79	41 13 18.2	11.55	O4 III(f)	0.570	0.314
MT91-531		20 33 25.56	41 33 26.9	11.58	O8.5 V	0.420	0.225
MT91-339		20 32 50.02	41 23 44.6	11.60	O8.5 V	0.391	0.206
MT91-605		20 33 39.79	41 22 52.3	11.78	B0.5 V	0.333	0.264
MT91-642		20 33 47.83	41 20 41.5	11.78	B1 III-Ib	0.499	0.278
MT91-516		20 33 23.46	41 09 13.0	11.84	O5.5 V(f)	0.645	0.330
MT91-480		20 33 17.48	41 17 09.3	11.88	O7.5 V	0.465	0.240
MT91-745		20 34 13.50	41 35 02.7	11.91	O7 V	0.402	0.227
MT91-376		20 32 59.19	41 24 25.4	11.91	O8 V	0.362	0.210
MT91-473		20 33 16.34	41 19 01.7	12.02	O8.5 V	0.418	0.185
MT91-771		20 34 29.59	41 31 45.5	12.06	O7 V	0.530	0.321
MT91-485		20 33 18.03	41 21 36.6	12.06	O8 V	0.429	0.202
MT91-138		20 31 45.40	41 18 26.7	12.26	O8.5 I	0.513	0.293
MT91-793		20 34 43.58	41 29 04.6	12.29	B1.5 III:	0.498	0.415
MT91-696		20 33 59.52	41 17 35.4	12.32	O9.5 V	0.394	0.251
MT91-588		20 33 37.00	41 16 11.3	12.40	B0 V	0.515	0.239
MT91-470		20 33 15.71	41 20 17.2	12.50	O9.5 V	0.398	0.210
MT91-555		20 33 30.30	41 35 57.8	12.51	O8 V	0.546	0.271
MT91-174		20 31 56.94	41 31 47.8	12.55	B1.5 V	0.388	0.182
MT91-507		20 33 21.01	41 17 40.1	12.70	O8.5 V	0.402	0.227
MT91-611		20 33 40.86	41 30 18.9	12.77	O7 Vp	0.397	0.252
MT91-736		20 34 09.51	41 34 13.6	12.79	O9 V	0.412	0.246
MT91-455		20 33 13.69	41 13 05.7	12.92	O8 V	0.475	0.279
MT91-5		20 30 39.81	41 36 50.7	12.93	O6 V(f)	0.524	0.261
MT91-403		20 33 05.26	41 43 36.7	12.94	B1.5 V	0.432	0.230
MT91-390		20 33 02.92	41 17 43.1	12.95	O8 V	0.553	0.292
MT91-429		20 33 10.50	41 22 22.4	12.98	B0 V	0.424	0.216
MT91-70		20 31 18.33	41 21 21.6	12.99	O9 V	0.561	0.300
MT91-534		20 33 26.74	41 20 59.5	13.00	O7.5 V	0.537	0.269
MT91-292		20 32 37.02	41 23 05.2	13.08	B1 V	0.465	0.221
MT91-187		20 32 03.77	41 25 10.4	13.24	B0.5: V	0.405	0.235
MT91-248		20 32 25.49	41 24 52.0	13.36	O5.5 V	0.344	0.203
MT91-575		20 33 34.33	41 18 11.3	13.41	B1.5 V	0.679	0.572
MT91-467		20 33 15.31	41 29 56.7	13.43	B1 V	0.456	0.230
MT91-378		20 32 59.64	41 15 14.6	13.49	B0 V	0.596	0.307
MT91-716		20 34 04.86	41 05 12.9	13.50	O9 V	0.466	0.259
MT91-692		20 33 59.25	41 05 38.0	13.61	B0: V	0.421	0.266
MT91-448		20 33 13.26	41 13 28.7	13.61	O6 V(f)	0.636	0.337
Cyg OB2 association: Comerón et al. (2002) stars							
CPR02-A4		20 31 36.25	41 22 03.2	15.0	-	1.149	0.655
CPR02-A5		20 35 09.75	41 35 29.7	16.2	-	1.040	0.611
CPR02-A6		20 32 08.33	40 25 06.9	17.5	-	1.055	0.548
CPR02-A7		20 34 42.96	40 29 30.2	17.7	-	1.072	0.541
CPR02-A8		20 33 41.61	41 47 57.0	15.5	-	1.165	0.564
CPR02-A9		20 35 32.71	41 20 55.0	17.2	-	1.019	0.498
CPR02-A10		20 34 55.11	40 34 44.3	15.6	-	0.840	0.451
CPR02-A11		20 32 31.54	41 14 08.2	12.5	O7.5 Ib-II	0.723	0.430
CPR02-A12		20 33 38.21	40 41 06.4	12.1	B0 Ia	0.734	0.425
CPR02-A13		20 33 01.24	40 32 33.7	15.1	-	0.745	0.398
CPR02-A14		20 31 18.99	42 02 55.9	14.3	-	0.768	0.402
CPR02-A15		20 31 36.90	40 59 09.2	13.0	O7 Ib(f)	0.705	0.397
CPR02-A16		20 34 36.94	40 41 01.9	15.0	-	0.737	0.386
CPR02-A17		20 32 35.34	41 14 45.4	14.5	-	0.644	0.388
CPR02-A18		20 30 07.88	41 23 50.4	14.0	~O8 V	0.658	0.374
CPR02-A19		20 31 25.91	41 16 02.7	14.1	-	0.659	0.341
CPR02-A20		20 33 02.92	40 47 25.4	12.0	O8 IIIf	0.619	0.358
CPR02-A21		20 29 34.80	41 20 08.9	13.7	-	0.635	0.331
CPR02-A22		20 33 11.29	40 42 33.8	13.4	-	0.649	0.330
CPR02-A23		20 30 39.70	41 08 48.9	11.3	B0.7 Ib	0.600	0.348

**Table 3.1.5** Continued

Name*	BD, HD	RA (2000)	DEC (2000)	V	Sp	J-H	H-K <sub>s</sub>
CPR02-A24		20 34 44.10	40 51 58.4	12.7	O6.5 III(f)	0.609	0.348
CPR02-A25		20 32 38.43	40 40 44.5	13.0	~O8 III	0.642	0.322
CPR02-A26		20 30 57.72	41 09 57.5	13.1	O9.5 V	0.579	0.316
CPR02-A27		20 34 44.71	40 51 46.5	11.4	B0 Ia	0.621	0.331
CPR02-A28		20 34 16.04	41 02 19.6	13.4	—	0.579	0.313
CPR02-A29		20 34 56.05	40 38 18.0	11.7	O9.7 Iab	0.581	0.314
CPR02-A30		20 31 22.10	41 12 02.9	13.1	~B2 V	0.469	0.299
CPR02-A31		20 32 39.49	40 52 47.5	13.1	~B0.5 V	0.595	0.285
CPR02-A32		20 32 30.33	40 34 33.2	12.1	O9.5 IV	0.527	0.295
CPR02-A33		20 32 34.98	40 52 39.0	13.0	B2.5 V	0.541	0.289
CPR02-A34		20 31 36.93	42 01 21.8	11.3	B0.7 Ib	0.399	0.299
CPR02-A35		20 30 55.52	40 54 54.1	12.8	~B0 V	0.488	0.285
CPR02-A36		20 34 58.78	41 36 17.4	11.5	B0 Ibn	0.538	0.299
CPR02-A37		20 36 04.51	40 56 12.9	12.3	O5 Vf	0.600	0.283
CPR02-A38		20 32 34.86	40 56 17.4	13.1	O8 V	0.524	0.294
CPR02-A39		20 32 27.34	40 55 18.4	11.9	B2 V	0.466	0.277
CPR02-A40		20 35 13.66	40 55 25.0	12.5	—	0.608	0.257
CPR02-A41		20 31 08.38	42 02 42.2	12.4	O9.7 II	0.536	0.269
CPR02-A42		20 29 57.01	41 09 53.8	12.3	B0 V	0.417	0.250
CPR02-A44		20 31 46.05	40 43 24.6	—	B0.5 IV	0.426	0.227
CPR02-A45		20 29 46.66	41 05 08.3	11.9	B0.5 Vn	0.397	0.179
CPR02-A46		20 31 00.19	40 49 49.7	11.3	O7 Vf	0.362	0.190

**Notes:**

ALS = Reed (1998, 2005);

CP05 = Camerón &amp; Pasquali (2005);

CPR02 = Camerón et al. (2002);

MT91 = Massey &amp; Thompson (1991);

SMV89 = Straizys et al. (1989a);

SKV93 = Straizys et al. (1993);

LS02 = Laugalys &amp; Straizys (2002);

LSV06-1 = Laugalys et al. (2006a);

LSV06-22 = Laugalys et al. (2006b, Table 2);

LSV07 = Laugalys et al. (2007);

VI Cyg = numbers of the Cyg OB2 association stars from Johnson & Morgan (1954) and Morgan et al. (1954). VI Cyg is the former name of the Cyg OB2 association.

SMV89-248 = V2200 Cyg (B9p,  $\alpha^2$  CVn type);

VI Cyg 5 = V729 Cyg, EB;

ALS 11633, SMV89-159 and SMV89-188 – spectral binaries;

ALS 17620, ALS 17622 and SMV89-185 – visual binaries.

The stars with spectral types marked by asterisks are classified in MK system by C. J. Corbally: one asterisk – published in Straizys et al. (1999), two asterisks – published in the present table. Here are notes on the spectra of individual stars (IS means the interstellar band at 443 nm). Interstellar extinction values  $A_V$  are from Laugalys & Straizys (2002).

LS02-40: IS band slight;

LS02-209: IS band moderate,  $A_V = 2.9$ ;LS02-217: IS band slight, He slightly strong,  $A_V = 2.3$ ;LS02-222: very strong IS band, quite strong IS Ca K,  $A_V = 4.2$ ;

LS02-229: sharp hydrogen line cores, moderate IS band, Hg-Mn, Cr-Sr;

LS02-230: emission in H and He, with normal decrement, spectral class is an estimate from H wings and He I D-series, IS band moderate,  $A_V = 2.5$ ;

LS02-267: IS band strong,  $A_V = 2.2$ ;LS02-401: IS band slight, IS Ca K quite strong,  $A_V = 1.9$ ;LS02-463: all He lines are filled in by emission,  $A_V = 1.9$ ;LS02-476: IS band moderate;  $A_V = 2.7$ ;LS02-537: IS band moderate,  $A_V = 2.2$ ;LS02-584: IS band moderate, IS Ca K line strong,  $A_V = 3.9$ ;LS02-608: Balmer line decrement weak, IS band slight, IS Ca K line moderate,  $A_V = 1.8$ ;LS02-691: noisy spectrum, IS band strong,  $A_V = 5.2$ .**Table 3.2.1.** Results of photometry, photometric spectral types, interstellar extinctions and distances for stars in Area I.

No.	RA(2000) h m s	DEC(2000) ° ' "	V mag	U-V mag	P-V mag	X-V mag	Y-V mag	Z-V mag	V-S mag	Photom. sp. type	$A_V$ mag	d pc
1	20 54 22.57	43 51 34.2	17.377			2.804	0.982	0.685	1.001	k7 V:		
2	20 54 27.07	43 49 16.0	17.685			2.724:	0.985	0.612	1.109	k6 V:	0.56	800
3	20 54 27.69	43 54 12.0	10.525	2.524	1.838	1.140	0.488	0.229	0.396	f3 III	0.28	510
4	20 54 29.54	43 49 22.4	16.298	4.208:	3.699	2.618	0.920	0.582	0.971	k5 V	0.58	500
5	20 54 31.32	43 44 40.7	15.781	3.987	3.378	2.304	0.852	0.476	0.846	k3 V	0.63	510
6*	20 54 31.90	43 51 37.8	15.433	4.439	3.857	2.787	0.980	0.625	1.074	(k7 V)		
7	20 54 37.28	43 43 33.9	12.510	3.148	2.681	1.746	0.673	0.277	0.673	k0 V	0.14	197
8	20 54 37.55	43 53 17.6	12.890	2.353	1.847	1.260	0.545	0.209	0.502	f7 V	0.19	600
9	20 54 38.10	43 47 35.8	15.540	3.555	2.984	2.081	0.838	0.360	0.819	k0 V	0.82	580
10	20 54 39.61	43 46 00.6	11.107	2.479	2.037	1.393	0.576	0.222	0.574	g1 V	0.11	209
11	20 54 39.83	43 55 59.4	17.452			2.851	1.012	0.622	1.139	k7 V	0.38	650
12*	20 54 40.64	43 52 47.2	17.146			3.025	1.297	0.627	1.318	k3 V,e?	2.48	410:
13*	20 54 42.08	43 45 57.3	17.505			2.867	1.190:	0.618	1.234	k3 V,e?	2.04	590:



**Table 3.2.2.** Continued

No.	RA(2000)	DEC(2000)	V	U-V	P-V	X-V	Y-V	Z-V	V-S	Photom.	A <sub>V</sub>	d
	h m s	° ′ ″	mag	mag	mag	mag	mag	mag	mag	sp. type	mag	pc
16	20 56 32.74	43 56 02.6	17.037			2.799	1.332	0.512	1.198	g6 IV	2.92	1670
17	20 56 32.82	43 56 53.4	17.580			2.509	1.286	0.433	1.085	a-f		
18	20 56 33.25	43 43 51.7	17.266			2.897	1.175	0.653	1.255	k5:sd?		
19	20 56 33.87	43 57 22.1	17.559			2.451	1.251	0.460	1.043	a7 V	4.08	1790
20	20 56 35.88	43 57 14.7	16.081	4.767:	3.409	2.307	1.181	0.411	1.012	a		
21	20 56 36.12	43 57 43.4	17.326			2.177	1.144	0.482	0.961	b or f		
22	20 56 36.44	43 57 41.6	14.965	6.115:	4.947	3.626	1.629	0.635	1.488	k0.5 III	3.49	1430
23	20 56 37.14	43 55 05.5	14.267	3.857	2.990	2.407	1.372	0.467	1.220	b1		
24	20 56 37.22	43 57 20.3	15.310	3.302	2.800	1.957	0.752	0.356	0.766	k1 V	0.38	580
25	20 56 37.28	43 52 11.5	17.172			2.810	1.380	0.505	1.303	g0 V	3.54	740
26	20 56 37.80	43 54 24.9	16.810	4.405:	3.228	2.120	1.106	0.385	0.920	a2 V	3.73	2380
27	20 56 38.98	43 50 46.0	16.263	4.584	3.759	2.850	1.132	0.627	1.256	m2 V	0.22	170
28	20 56 41.03	43 43 00.7	17.711			3.015	1.178:	0.668	1.171	k5 V	1.66	580
29	20 56 41.10	43 42 26.9	11.826	2.399	1.971	1.417	0.599	0.224	0.607	g2 V	0.16	259
30	20 56 41.29	43 53 22.9	16.979	4.229:	3.135	2.227	1.291	0.442	1.164	a0		
31	20 56 42.04	43 53 40.8	14.624	3.373	2.802	1.949	0.803	0.333	0.783	g8 IV-V	0.72	830
32	20 56 42.08	43 54 26.4	17.616			2.722	1.529:	0.590	1.208	b		
33	20 56 42.25	43 59 30.0	17.333			3.166	1.619:	0.620	1.505	f8 V:	4.61	550
34	20 56 43.60	44 00 02.1	17.371			3.181	1.593:	0.613	1.417	g3 V:	4.30	465
35	20 56 43.74	43 53 25.3	17.622			2.448	1.347:	0.484	1.086	b8 V:	5.10	3180
36	20 56 43.80	43 51 49.7	13.253	2.266	1.790	1.247	0.544	0.202	0.534	f8 V:	0.14	660
37	20 56 44.03	43 41 17.3	17.944			3.098:	1.328:	0.680	1.219	k4 V:	2.45	478
38*	20 56 44.15	43 57 12.1	16.998			3.739	1.694	0.691	1.519	k2 III-IV		
39	20 56 44.63	43 57 34.8	13.957	2.902	2.451	1.690	0.647	0.290	0.670	k0 V	0.03	403
40	20 56 44.87	43 50 11.7	12.203	2.338	1.877	1.304	0.540	0.207	0.546	f9 V	0.08	402
41	20 56 45.74	43 53 12.1	17.605			3.041	1.511:	0.526	1.414	g2 V:	3.96	640
42	20 56 46.01	43 58 29.5	13.060	2.503	1.982	1.389	0.572	0.226	0.574	g0 V	0.18	520
43	20 56 47.35	43 41 27.6	13.700	3.838	2.802	1.716	0.853	0.294	0.747	a3 IV	2.63	1080
44	20 56 47.91	44 00 25.7	14.808	6.100:	5.004	3.700	1.783	0.703	1.563	g5 III-IV	4.78	414
45	20 56 48.98	43 47 21.5	11.333	2.793	2.290	1.575	0.637	0.254	0.633	g4 V	0.28	170
46	20 56 49.25	43 56 22.3	16.581			2.867	1.504	0.532	1.280	a5 V	5.22	820
47	20 56 50.09	43 56 23.8	15.455	4.401	3.254	2.208	1.186	0.396	0.994	b9.5 IV	4.29	1600
48	20 56 50.98	43 58 01.8	17.300			2.828	1.461	0.543	1.266	f0 V	4.66	970
49	20 56 51.10	43 56 23.1	15.705			3.972	1.823	0.701	1.610	k1 III	4.21	1440
50*	20 56 51.69	43 42 52.0	15.310	3.912	3.365	2.334:	0.873	0.519	0.996	k4 V,e?	0.55	373:
51	20 56 51.91	44 00 08.7	17.059			4.135:	2.028	0.751	1.765	g8 III-IV	5.59	800
52	20 56 52.88	43 54 39.1	16.299	4.404	3.828	2.736	0.967	0.628	1.047	k7 V	0.20	418
53	20 56 53.22	43 42 32.9	17.546			2.888	0.981	0.584	1.146	k5 V	0.84	770
54	20 56 54.39	43 59 20.0	13.618	2.597	2.085	1.468	0.618	0.247	0.599	g1 V	0.28	610
55	20 56 56.07	43 52 30.0	16.029			2.999	1.582	0.516	1.417	a3 V	5.67	620
56	20 56 56.53	43 52 36.2	13.165	3.195	2.762	1.836	0.708	0.340	0.694	k1 V	0.20	236
57	20 56 58.82	43 40 16.0	14.805	3.125	2.674	1.837	0.705	0.359	0.752	k1 V	0.19	510
58	20 57 00.32	43 56 39.8	9.129	3.644	3.039	2.088	0.789	0.327	0.738	k0 III	0.08	468
59	20 57 01.35	43 51 58.0	16.235	4.378	3.741	2.721	0.983	0.611	1.072	k6 V	0.55	413
60	20 57 02.64	43 57 51.3	16.715	4.041	3.498	2.520	0.852	0.569	0.968	k6 V	0.01	660
61	20 57 03.52	43 59 54.8	13.708	2.681	2.243	1.566	0.628	0.266	0.622	g5 V	0.20	500
62	20 57 07.24	43 50 06.8	13.521	4.506	3.833	2.797	1.052	0.611	1.220	m2 V	0.00	53
63	20 57 07.26	43 55 11.7	15.534	5.403:	3.829	2.633	1.417	0.480	1.239	a		
64*	20 57 07.57	43 41 59.7	17.641			3.076:	1.410:	0.718	1.508	k-m V,T?		
65	20 57 07.67	43 48 28.1	14.771	2.773	2.286	1.620	0.683	0.264	0.697	g3 V	0.51	820
66	20 57 07.86	43 41 55.4	16.309			3.185	1.327	0.680	1.398	k5:sd?		
67*	20 57 09.06	43 44 44.5	17.297			2.765	1.183	0.590	1.320	k3 V,e?	2.01	550:
68	20 57 09.24	44 01 10.2	17.265			2.785	1.364	0.529	1.268	g1:sd?		
69	20 57 09.64	43 45 04.2	14.116	3.938	3.446	2.387	0.795	0.519	0.878	k5 V	0.06	235
70	20 57 10.61	43 41 28.0	12.703	2.479	2.001	1.373	0.569	0.225	0.580	g0 V	0.16	445
71	20 57 12.55	43 54 40.5	17.682			2.845	1.090:	0.619	1.221	m2 V:	0.04	348
72	20 57 13.37	43 59 50.5	18.088			2.614:	1.437:	0.508	1.282	b		
73	20 57 13.70	43 46 19.7	15.340	4.504	3.859	2.834	0.987	0.628	1.134	k7 V	0.28	258
74	20 57 15.37	44 01 22.9	15.941	4.767:	3.673	2.677	1.558	0.570	1.299	b5-a0		
75	20 57 17.48	43 49 48.5	12.223	2.272	1.763	1.187	0.554	0.201	0.518	f6 V	0.31	460
76	20 57 21.98	43 50 14.3	16.313	4.246	3.719	2.612	0.914	0.573	1.026	k6 V	0.27	489
77*	20 57 22.25	43 57 53.4	15.111	3.337	2.790	1.930	0.801	0.420	0.824	k0 V,e?	0.67	510:
78	20 57 22.33	43 46 16.9	15.555	3.003	2.484	1.789	0.755	0.321	0.733	g6 V	0.69	860
79	20 57 22.94	43 47 37.3	16.393	3.931	3.424	2.382	0.853	0.533	0.901	k4 V	0.47	640
80	20 57 23.10	43 45 15.2	14.544	3.263	2.712	1.847	0.741	0.319	0.721	g9 IV-V	0.38	900
81	20 57 23.35	43 49 44.0	13.558	2.549	2.007	1.388	0.625	0.240	0.577	f6 V	0.60	740
82	20 57 23.36	43 49 21.9	14.951	2.824	2.306	1.639	0.740	0.295	0.713	g0 V	0.87	900
83	20 57 23.40	43 50 40.4	17.437			2.828	1.221	0.701	1.125	k-m V		
84	20 57 23.80	43 59 33.6	13.140	2.781	2.252	1.581	0.675	0.277	0.662	g2 V	0.48	410
85	20 57 26.27	43 49 09.9	14.041	2.703	2.255	1.564	0.651	0.275	0.634	g5 V	0.30	560
86	20 57 27.45	43 50 35.8	17.745			2.768	1.206:	0.568	1.362	m3 V:	0.00	286
87	20 57 27.71	43 56 24.7	14.399	3.932	3.469	2.433	0.855	0.551	0.953	k4 V	0.48	254
88	20 57 28.11	43 51 46.0	12.785	2.455	1.979	1.355	0.584	0.223	0.542	f9 V	0.27	483
89*	20 57 28.64	43 58 31.6	16.332	4.602:	3.759	2.785	1.192	0.602	1.280	k3 V,e?	2.21	390:
90	20 57 32.14	43 58 09.6	12.446	2.705	2.104	1.461	0.647	0.250	0.615	f6 V	0.70	427
91	20 57 32.53	43 46 16.2	17.099			2.781	1.044	0.620	1.182	m1 V	0.27	321
92	20 57 33.78	43 44 47.1	11.883	2.195	1.661	1.076	0.474	0.177	0.440	f5 V	0.06	462
93	20 57 34.54	43 59 54.7	16.333			2.597	1.274	0.443	1.177	f8 V	3.18	680
94	20 57 35.43	43 55 12.8	10.430	3.521	2.990	2.006	0.747	0.344	0.730	k1 IV	0.00	292
95	20 57 35.80	43 49 09.9	15.971	3.421	2.942	2.036	0.816	0.412	0.841	k1 V	0.65	700
96	20 57 36.23	43 57 27.9										

**Table 3.2.2.** Continued

No.	RA(2000)	DEC(2000)	V	U-V	P-V	X-V	Y-V	Z-V	V-S	Photom.	A <sub>V</sub>	d
	h m s	° ' "	mag	mag	mag	mag	mag	mag	mag	sp. type	mag	pc
113*	20 57 56.51	43 52 36.3	16.297	4.052	3.495	2.491	0.919	0.605	1.096	k6 V,e?	0.29	481:
114*	20 57 57.50	43 50 09.0	17.010	4.324:	3.697:	2.772	1.114	0.680	1.229	m2 V,e?	0.14	248:
115	20 57 58.44	43 54 43.2	14.331	3.358	2.908	1.992	0.740	0.369	0.754	k2 V	0.25	344
116	20 57 58.48	43 55 43.3	16.804	4.508:	3.961:	2.878	1.147	0.621	1.313	m2 V	0.28	211
117*	20 57 59.87	43 53 26.0	15.470	3.134	2.803	2.439	1.149	0.515	1.622	T <sub>2</sub>		
118*	20 57 59.93	43 51 21.2	16.769	4.712:	3.926:	2.848	1.231	0.613	1.314	k3 V,e?	2.21	391:
119	20 58 00.07	43 47 34.9	14.971	3.417	2.965	2.058	0.748	0.384	0.795	k2 V	0.28	455
120	20 58 02.10	43 47 52.1	15.989	4.271	3.714	2.705	0.878	0.585	1.039	k6 V	0.12	451
121	20 58 04.26	43 46 49.0	15.913	3.634	3.169	2.311	0.829	0.586	0.861	k-m V		
122*	20 58 06.05	43 49 33.0	17.664			3.128:	1.216:	0.730	1.399	k-m V,e?		
123	20 58 06.11	43 53 01.2	17.427			3.338:	1.366	0.751	1.449	k-m V		

**Notes to Table 3.2.2:** 64, 102, 107, 108 and 117 – probable T Tauri type stars; 50, 67, 77, 89, 109, 113, 114, 118 and 122 – probable emission in H $\alpha$ ; 38 – spectral type outside the calibration range.

**Table 3.2.3.** Results of photometry, photometric spectral types, interstellar extinctions and distances for stars in Area III.

No.	RA(2000)	DEC(2000)	V	U-V	P-V	X-V	Y-V	Z-V	V-S	Photom.	A <sub>V</sub>	d
	h m s	° ' "	mag	mag	mag	mag	mag	mag	mag	sp. type	mag	pc
1*	20 57 48.80	43 50 23.7	16.580		2.927:	1.306:	0.641	1.388	k-m V,e?			
2	20 57 54.63	43 49 34.8	12.723	2.625	2.198	1.523	0.621	0.266	0.562	g5 V	0.17	324
3	20 57 55.48	43 49 54.5	13.165	2.501	2.067	1.443	0.593	0.246	0.534	g3 V	0.14	463
4*	20 57 56.51	43 52 36.3	16.251	3.953:	3.192:	2.526	0.966	0.637	1.001	k-m V,e?		
5	20 57 58.44	43 54 43.3	14.328	3.360	2.958	1.963	0.726	0.368	0.705	k2 V	0.19	353
6*	20 57 59.86	43 53 26.1	15.489	3.113	2.672	2.283	1.130	0.512	1.603	K6,T		
7	20 57 59.93	43 51 21.2	16.775		2.863:	1.186:	0.610	1.286	m2 V:			
8	20 58 00.08	43 47 35.0	14.942	3.435	2.973	2.009	0.806	0.398	0.712	k1 V	0.61	444
9	20 58 02.10	43 47 52.1	15.920	4.191:	3.608:	2.677	0.927	0.638	0.930	k7 V	0.03	379
10	20 58 04.27	43 46 49.0	15.896	3.645	3.202	2.218	0.819	0.509	0.817	k3 V	0.50	580
11	20 58 11.60	43 52 04.9	10.587	2.220	1.638	0.789	0.290	0.113	0.219	a5 V	0.17	530
12	20 58 12.47	43 52 34.8	15.941	4.148:	3.596:	2.379	0.792	0.511	0.969	k5 V	0.05	550
13	20 58 16.05	43 43 44.7	13.909	2.977	2.564	1.747	0.682	0.318	0.668	k0 V	0.18	369
14	20 58 18.47	43 56 55.7	15.288	3.246	2.804	1.854	0.738	0.307	0.774	k0 V	0.41	630
15	20 58 20.11	43 48 34.0	16.110	4.065:	3.656:	2.588	0.885	0.564	1.034	k5 V	0.44	495
16	20 58 20.97	43 40 32.3	15.265	2.879	2.382	1.784	0.703	0.324	0.665	g8 V:	0.39	750
17*	20 58 23.78	43 53 11.5	13.666	3.476	2.748	2.015:	1.014	0.347	1.209	K5,T		
18*	20 58 23.98	43 53 54.7	16.690		2.781:	1.358:	0.646	1.600	K6,e			
19	20 58 26.26	43 52 23.7	15.892		2.744:	1.079	0.597	1.224	m2 V	0.00	158	
20	20 58 26.94	43 47 51.0	12.812	2.480	1.921:	1.291	0.590	0.213	0.557	f5 V	0.54	570
21	20 58 30.01	43 52 25.8	15.005	4.398	3.766	2.720	0.970	0.624	1.129	k7 V:	0.21	229
22	20 58 30.57	43 43 00.0	14.294	2.692	2.178	1.582	0.694	0.281	0.641	g0 V	0.68	730
23	20 58 30.63	43 41 59.7	13.432	2.834	2.257	1.623	0.714	0.277	0.632	f8 V	0.85	520
24	20 58 31.50	43 52 28.8	15.475	3.631	3.148	2.120	0.815	0.402	0.855	k2 V	0.56	500
25	20 58 34.23	43 48 16.1	12.846	2.655	1.981	1.198	0.531	0.197	0.484	f0 V	0.80	740
26	20 58 34.59	43 55 02.3	16.544		2.743:	0.906	0.524	1.171	k V			
27	20 58 35.77	43 49 43.7	16.258	4.023:	3.359:	2.333	0.836	0.470	0.936	k4 V	0.40	620
28*	20 58 36.77	43 58 10.3	16.767		2.450:	1.156:	0.336	1.201	–			
29	20 58 39.40	43 58 51.9	16.692		2.452:	1.340:	0.437	1.145	b:			
30	20 58 39.64	43 49 09.3	15.118	4.706:	3.940	2.955	1.119	0.611	1.115	k5 V:		
31*	20 58 43.53	43 39 00.3	14.936	4.812:	3.957:	2.964	1.310	0.555	1.168	k1 IV-V		
32	20 58 47.77	43 51 41.6	14.137	3.792	3.273	2.316	0.814	0.494	0.914	k4 V	0.31	243
33	20 58 52.15	43 45 29.9	14.329	2.935	2.386	1.753	0.744	0.293	0.742	g2 V	0.76	620
34	20 58 52.38	43 57 05.2	15.776	3.980:	3.030	2.193	1.055	0.360	1.043	g		
35	20 58 52.54	43 54 51.0	12.620	2.631	2.185	1.547	0.622	0.279	0.536	g5 V	0.18	308
36	20 58 53.26	43 59 07.1	16.914		2.645:	0.767:	0.657	1.028	k:			
37	20 58 54.31	43 55 09.6	16.554	3.628:	3.036:	2.242	0.896	0.464	0.884	k2 V	0.90	710
38	20 58 54.64	43 56 53.5	14.821	3.382	2.572	1.884	0.917	0.326	0.855	f-g, MDG?		
39*	20 58 58.16	43 49 30.2	16.784		2.497:	1.135:	0.536	1.068	k0 V,e?	2.06	580:	
40	20 58 58.65	43 57 15.4	11.219	2.479	1.839	1.151	0.507	0.175	0.465	f2 IV	0.44	495
41	20 58 58.82	43 54 46.2	16.161		2.729:	1.226	0.477	1.202	k0 IV-V	2.31	740	
42	20 59 03.32	43 50 25.4	15.681	3.426:	2.943	2.028	0.831	0.368	0.823	k0 V	0.80	630
43	20 59 03.95	43 45 51.3	15.758	3.472	2.919	2.076	0.873	0.359	0.868	g8 V	1.09	680
44	20 59 05.53	43 39 55.5	15.233	3.848	3.365	2.458	0.913	0.524	0.878	K3 V:		
45*	20 59 05.80	43 57 03.2	13.040	3.506	2.863	2.117	0.894	0.366	0.958	K6,e		
46	20 59 07.67	43 49 33.7	16.814		2.599:	0.974:	0.496	1.008	k3 V:	1.14	650	
47	20 59 09.15	43 44 09.0	14.821	3.184	2.526	1.834	0.836	0.334	0.756	f9 V	1.32	760
48	20 59 09.94	43 42 07.4	16.463		2.386:	1.193:	0.427	1.080	f:			
49	20 59 10.03	43 48 19.3	15.367	4.240:	3.491	2.472	1.150	0.457	1.039	g5 IV:	2.29	1140
50	20 59 10.35	43 55 12.4	16.845		2.399:	1.042:	0.318	1.138	–			
51	20 59 10.81	43 41 07.1	16.715		2.456:	1.208:	0.456	1.134	g			
52	20 59 12.01	43 45 20.0	11.932	2.853	2.098	1.290	0.555	0.204	0.500	f0 III-IV	0.89	720
53	20 59 12.17	43 49 12.1	12.450	3.521	2.601	1.761	0.846	0.300	0.766	f3 III	1.77	620
54	20 59 16.18	43 40 25.2	16.060	3.970:	2.932	2.316	1.362	0.447	1.176	b8		
55	20 59 16.19	43 56 03.3	16.005		2.434:	1.264	0.376	1.158	a-f			
56	20 59 19.72	43 43 26.5	16.084		2.330	1.242	0.390	1.019	a			
57	20 59 20.88	43 48 51.9	14.391	4.107	3.614	2.529	0.852	0.549	0.943	k5 V	0.30	239
58	20 59 22.44	43 57 10.9	15.368	3.846	2.776	1.776	0.932	0.268	0.796	b9-a0		
59	20 59 22.55	43 52 39.3	12.920	2.642	2.220	1.516	0.601	0.254	0.584	g7 V	0.00	334
60	20 59 22.56	43 54 31.6	15.315	4.720:	3.432	2.341	1.272	0.411	1.098	b9p:		
61	20 59 24.93	43 44 15.2	16.096		2.329:	1.227	0.413	0.997	a-f			
62	20 59 24.94	43 54 19.6	14.634		4.682:	2.067	0.821	1.873	k-m			
63	20 59 25.42	43 51 38.0	15.997	4.041:	3.694:	2.586	0.885	0.559	1.119	k5 V	0.44	470
64	20 59 25.70	43 50 04.1	15.736	4.523:	3.869:	2.846	1.001	0.640	1.107	k		

**Table 3.2.3.** Continued

No.	RA(2000) h m s	DEC(2000) ° ′ ″	V mag	U-V mag	P-V mag	X-V mag	Y-V mag	Z-V mag	V-S mag	Photom. sp. type	A <sub>V</sub> mag	d pc
71*	20 59 29.29	43 45 56.5	16.805			2.180	1.035:	0.451	0.920	f,g,e?		
72	20 59 29.39	43 52 28.6	16.752			2.293:	1.328:	0.478	1.093	o-b1		
73	20 59 30.22	43 55 31.8	14.325			3.767	1.688	0.633	1.537	k1 III	3.65	990
74	20 59 31.01	43 42 38.8	16.367	3.690:	3.290:	2.278	0.978	0.382	0.880	g		
75	20 59 31.23	43 49 19.2	10.800	2.299	1.795	1.202	0.519	0.202	0.479	f6 V	0.16	256
76	20 59 31.29	43 52 11.1	14.282	3.024	2.505	1.750	0.739	0.291	0.706	g5 V	0.66	530
77	20 59 31.46	43 47 54.3	16.408			2.400	1.269	0.481	0.994	a-f		
78	20 59 32.11	43 50 46.8	16.719			2.233:	1.214:	0.437	0.944	b6-a0		
79	20 59 32.26	43 53 10.6	15.367	4.165	3.212	2.409	1.174	0.409	1.054	f-g		
80*	20 59 32.79	43 46 31.7	14.567			4.317	1.796	0.739	1.605	k4 II	3.10	6800
81	20 59 33.62	43 44 51.9	14.691	3.878	2.870	1.856	1.009	0.342	0.790	a0 IV:	3.49	1510
82	20 59 33.70	43 52 43.0	16.287			2.504	1.147	0.446	1.044	g7 IV-V	2.19	950
83	20 59 33.88	43 54 03.8	15.630	3.436	2.744	2.047	0.946	0.368	0.930	f8 V:	1.81	920
84	20 59 34.00	43 51 05.8	17.175			2.014:	0.911:	0.276	0.895	g:		
85*	20 59 35.36	43 52 03.7	16.589			2.157:	1.057:	0.491	0.841	g:,e?		
86	20 59 36.82	43 49 19.2	16.997			2.363:	1.138:	0.344	1.104	f-g		
87	20 59 37.32	43 50 47.0	16.491			2.251	1.234:	0.416	0.994	b:		
88*	20 59 37.54	43 49 43.4	15.628	3.348	2.803	2.010	0.826	0.342	0.775	g8 IV-V	0.82	1270
89	20 59 37.72	43 53 43.1	14.757	3.952	2.888	1.884	0.962	0.306	0.824	a3p:		
90	20 59 38.01	43 53 46.2	14.383	4.173	2.958	1.880	1.013	0.341	0.814	a0 III	3.51	1640
91	20 59 38.10	43 46 24.4	15.542	3.876	2.909	1.851	0.906	0.366	0.747	a5		
92	20 59 38.38	43 49 48.8	16.290			3.393:	1.533:	0.660	1.396	k2 IV or V		
93	20 59 38.45	43 50 28.7	16.419			2.173	1.026	0.347	0.945	g		
94	20 59 38.54	43 47 39.2	16.171			3.380:	1.547:	0.568	1.387	g9 III	3.36	2530
95	20 59 38.93	43 49 11.7	15.702	4.551:	3.274	2.145	1.141	0.363	0.965	a2		
96	20 59 40.37	43 52 51.6	16.214	3.740:	2.991	2.188	1.073	0.390	0.954	f6 V:	2.47	1070
97	20 59 40.66	43 52 46.9	16.375			1.989	0.949	0.336	0.804	f5 V:	2.03	1470
98	20 59 41.30	43 50 58.1	16.262	3.939:	2.914	2.071	1.125	0.368	0.867	b8		
99	20 59 43.87	43 50 34.9	15.253	3.904	2.787	1.766	0.868	0.309	0.793	a7		

**Notes to Table 3.2.3:** stars from 2 to 10 are common with area II; 6 = LkH $\alpha$  185 = V 1539 Cyg (T Tauri type), Welin (1973) No. 89; 17 = LkH $\alpha$  188 = V 521 Cyg (T Tauri type), Welin (1973) No. 90; 18 = LkH $\alpha$  189; 45 = LkH $\alpha$  191; 1, 4, 39, 71 and 85 – probable emission in H $\alpha$ ; 28 – classification impossible; 31 – a nearby star with too high extinction; 80 – the most distant star in the four areas (6.8 kpc); 88 – a distant star with low extinction.

**Table 3.2.4.** Results of photometry, photometric spectral types, interstellar extinctions and distances for stars in Area IV.

No.	RA(2000) h m s	DEC(2000) ° ′ ″	V mag	U-V mag	P-V mag	X-V mag	Y-V mag	Z-V mag	V-S mag	Photom. sp. type	A <sub>V</sub> mag	d pc
1	20 53 42.29	44 27 03.8	14.428	3.817	3.371	2.287	0.806	0.532	0.819	k4 V	0.28	282
2	20 53 42.58	44 28 30.6	16.475	4.266:	3.599:	2.463	0.957	0.563	0.911	k3.5 V	0.99	560
3	20 53 46.96	44 23 01.4	11.990	3.360	2.574	1.896	1.035	0.346	0.886	b5		
4	20 53 48.04	44 29 16.1	16.993			2.634	1.121	0.452	1.072	k0 IV	1.75	2680
5*	20 53 51.88	44 24 10.1	16.703	4.313:	3.813:	2.172	1.094	0.519	0.983	T?		
6	20 53 53.89	44 26 47.0	15.714	4.556:	3.846	2.819	1.152	0.619	1.222	m2 V	0.30	127
7	20 53 54.54	44 32 28.5	16.708			3.097	1.593:	0.568	1.528	a-f		
8	20 53 56.11	44 23 42.0	15.451	3.248	2.774	1.918	0.751	0.335	0.780	k0 V	0.46	660
9	20 53 58.45	44 32 35.1	16.828			3.560:	1.804:	0.686	1.729	g3		
10	20 53 59.86	44 25 40.1	12.893	2.452	1.847	1.191	0.549	0.182	0.518	f3 V	0.54	710
11	20 54 00.20	44 35 01.4	11.111	2.258	1.752	1.141	0.553	0.260	0.406	f		
12	20 54 01.03	44 20 22.1	14.124	2.701	2.161	1.532	0.653	0.248	0.614	g0 V	0.51	730
13	20 54 02.62	44 24 39.3	15.360	4.046	3.093	2.284	1.164	0.378	1.040	g,MD?		
14	20 54 02.63	44 28 53.7	13.686	2.449	1.968	1.371	0.584	0.222	0.569	f9 V	0.27	730
15	20 54 04.28	44 21 36.7	15.041	4.138	3.637	2.554	0.835	0.554	0.960	k5 V	0.23	333
16*	20 54 04.77	44 35 07.5	10.577	3.177	2.635	1.828	0.783	0.340	0.643	g5 IV-V		
17	20 54 07.67	44 28 26.4	16.866			2.466	1.295:	0.420	1.195	a-f		
18	20 54 08.11	44 26 34.3	13.494	2.836	2.153	1.452	0.690	0.239	0.647	f		
19	20 54 10.18	44 36 30.2	13.802	3.186	2.800	1.922	0.765	0.472	0.630	k1 V		
20	20 54 11.02	44 27 31.2	17.535			3.022:	0.983:	0.726:	1.204	k-m		
21*	20 54 12.94	44 23 21.6	16.377	4.205:	3.557	2.447	0.959	0.437	0.940	k1 IV	0.83	3090
22	20 54 13.03	44 27 41.7	17.801			2.800:	1.127:	0.672:	1.205:	m2 V:	0.20	348
23	20 54 16.08	44 24 10.6	17.224			3.286:	1.701:	0.590	1.607	-		
24	20 54 16.65	44 25 06.3	16.601			2.727	1.564	0.505	1.290	b0-2		
25	20 54 16.88	44 32 51.6	14.321	2.788	2.372	1.643	0.660	0.287	0.651	g8 V	0.21	530
26	20 54 19.53	44 32 29.9	12.262	2.708	2.278	1.600	0.645	0.273	0.647	g7 V	0.19	226
27	20 54 20.21	44 20 13.4	15.335	3.826	3.353	2.282	0.820	0.456	0.864	k3 V	0.50	444
28	20 54 20.74	44 32 04.8	12.277	2.396	1.888	1.277	0.522	0.199	0.494	f9 IV	0.01	820
29	20 54 21.30	44 29 28.8	15.648	3.808	3.339	2.295	0.783	0.458	0.876	k4 V	0.18	520
30	20 54 21.34	44 26 46.2	16.225	4.458:	3.392:	2.468	1.383	0.482	1.214	b6-7		
31	20 54 22.20	44 33 54.3	14.108	2.767	2.335	1.637	0.651	0.284	0.650	g7 V	0.21	520
32	20 54 22.95	44 32 12.2	15.754	3.452	3.014	2.056	0.746	0.402	0.808	k3 V	0.19	620
33	20 54 23.02	44 19 15.4	15.957			3.163	1.628	0.536	1.473	f-g		
34	20 54 23.12	44 27 00.6	17.445			2.440	1.397:	0.461	1.197	o-b0		
35	20 54 23.66	44 33 42.6	13.452	2.461	1.957	1.360	0.584	0.218	0.564	f8 V	0.31	670
36	20 54 23.67	44 27 21.2	14.599	3.332	2.845	1.861	0.702	0.325	0.699	k1 V	0.18	462
37	20 54 24.16	44 32 50.4	17.307			2.738	1.411:	0.510	1.170	a-f		
38	20 54 24.56	44 21 31.7	13.008	2.576	1.987	1.382	0.597	0.201	0.561	f-g, RHB?		
39*	20 54 25.54	44 23 02.0	17.373			2.755:	1.116:	0.524	1.376	k-m,e?		
40*	20 54 25.80	44 19 07.2	17.503			2.720	1.165:	0.587	1.262	k3 V,e?	1.93	620:
41	20 54 26.12	44 19 07.9	15.402	4.303	3.788	2.740	0.931	0.609	1.062	k7 V	0.05	296
42	20 54 26.40	44 27 22.5	16.084	4.282:	3.257	2.420	1.274	0.388	1.128	-		
43	20 54 26.47	44 22 08.8	17.353			2.844:	1.111:	0.645	1.160	k6 V:	1.09	540
44	20 54 27.14	44 18 34.8	14.686	3.127	2.718	1.841	0.697	0.356	0.704	k1 V	0.15	486
45	20 54 28.40	44 27 32.3	16.496	4.503:	3.859:	2.810	1.064	0.577	1.210	k4 V	1.35	446
46	20 54 29.65	44 30 23.2	14.113	2.996	2.446	1.688	0.724	0.281	0.670	g4 V	0.64	520

**Table 3.2.4.** Continued

No.	RA(2000)	DEC(2000)	V	U-V	P-V	X-V	Y-V	Z-V	V-S	Photom.	A <sub>V</sub>	d
	h m s	° ' "	mag	sp. type	mag	pc						
47	20 54 30.20	44 29 58.0	14.950	5.142	3.663	2.461	1.328	0.433	1.148	a-f		
48	20 54 32.49	44 23 08.4	13.974	2.778	2.276	1.552	0.629	0.244	0.643	g4 V	0.24	580
49	20 54 34.47	44 23 14.5	16.856			2.640	0.917	0.589	1.001	k6 V	0.28	620
50	20 54 34.59	44 19 12.0	16.410	4.529:	3.764	2.758	1.056	0.636	1.141	k-m V		
51	20 54 34.68	44 22 30.9	16.235	4.504:	3.726	2.736	0.964	0.619	1.051	k7 V	0.18	408
52	20 54 35.21	44 21 16.1	17.264			2.886	1.274	0.540	1.337	k1 V	2.55	530
53	20 54 37.32	44 23 45.3	13.451	3.113	2.293	1.493	0.727	0.238	0.673	f0 V	1.61	670
54	20 54 38.57	44 25 40.5	12.600	2.665	2.246	1.546	0.615	0.256	0.633	g8 V	0.02	261
55	20 54 38.71	44 19 55.3	14.076	2.536	2.062	1.458	0.619	0.241	0.578	g2 V	0.24	700
56	20 54 40.27	44 37 01.7	16.286			3.960	1.900	0.717	1.739	g9 III-IV	4.95	750
57	20 54 40.28	44 27 06.3	17.616			2.783:	1.135:	0.527	1.255	k3 V:	1.81	690
58	20 54 43.09	44 29 49.3	17.211			2.465	1.148	0.461	0.988	g5 V:	2.36	930
59	20 54 43.93	44 18 48.1	16.566	3.785:	2.910	2.206	1.165	0.405	1.012	f-g		
60	20 54 44.53	44 33 26.2	15.625	3.856	3.406	2.331	0.815	0.500	0.874	k4 V		
61	20 54 44.66	44 31 44.3	15.049	4.698	3.732	2.806	1.408	0.499	1.290	g, RHB?	0.31	482
62*	20 54 45.36	44 33 02.8	17.236			2.923	1.411	0.600	1.372	k0 V,e?	3.21	422:
63	20 54 46.27	44 32 02.9	17.707			3.139:	1.185:	0.725	1.144	k7 V:	1.10	530
64	20 54 46.28	44 30 10.7	11.803	2.652	1.974	1.209	0.549	0.208	0.450	f0 V	0.87	443
65	20 54 47.19	44 17 02.4	15.526	3.426	2.892	2.019	0.811	0.412	0.813	k1 V	0.63	570
66	20 54 47.26	44 20 29.4	13.577	2.521	1.952	1.357	0.607	0.213	0.555	f5 V	0.61	780
67	20 54 47.48	44 32 00.1	13.840	3.155	2.717	1.823	0.676	0.322	0.706	k1 V	0.07	343
68*	20 54 49.64	44 34 12.6	12.354	3.293	2.770	1.884	0.742	0.338	0.737	(k0 V)		
69	20 54 51.10	44 24 07.9	12.965	2.430	1.866	1.236	0.551	0.200	0.510	f3 V	0.54	730
70	20 54 52.55	44 36 33.5	13.977	3.071	2.558	1.785	0.762	0.307	0.703	g5 V	0.76	441
71	20 54 54.95	44 25 50.4	15.824	3.584	3.019	2.072	0.887	0.362	0.835	g8 V	1.15	680
72	20 54 56.25	44 32 04.1	17.102			2.569	1.310	0.519	1.166	f5		
73	20 54 56.49	44 23 16.5	16.625	4.247:	3.566:	2.484	0.925	0.522	0.952	k3.5 V:	0.85	640
74	20 54 57.02	44 32 56.5	17.140			2.635	0.931	0.567	0.998	k4.5 V	0.71	750
75	20 54 58.81	44 19 19.9	16.479	4.364:	3.926:	2.694	1.035:	0.642	1.027	k-m V		
76	20 54 59.75	44 34 31.3	17.830			2.639:	1.061:	0.621:	1.201:	m2 V:	0.00	385
77	20 54 59.97	44 22 02.1	16.424	4.416:	3.592:	2.710	1.046	0.583	1.195	m2 V	0.00	202
78	20 55 00.58	44 34 53.8	17.278			2.574	1.425:	0.535	1.283	b		
79	20 55 01.07	44 17 43.8	13.293	3.038	2.566	1.705	0.691	0.344	0.632	g8 V:	0.34	310
80	20 55 01.30	44 29 15.6	15.310	3.946	3.432	2.302	0.816	0.491	0.830	k4 V	0.32	416
81	20 55 00.24	44 29 49.0	13.996	2.781	2.179	1.514	0.709	0.255	0.653	f5 V	1.04	780
82	20 55 02.48	44 26 34.9	15.297	3.990	3.538	2.451	0.862	0.540	0.905	k4 V	0.51	378
83	20 55 02.52	44 22 46.2	14.238	3.072	2.375	1.713	0.808	0.288	0.718	f,g,MD?		
84	20 55 03.68	44 34 24.4	10.633	2.185	1.734	1.169	0.493	0.177	0.489	f8 V	0.00	212
85	20 55 04.07	44 35 51.9	17.300			2.241	1.172:	0.398	0.997	a		
86	20 55 04.88	44 34 34.9	15.021			4.018	1.890	0.762	1.770	k2		
87	20 55 05.13	44 34 03.2	16.681	3.948:	3.431	2.438	0.880	0.501	0.916	k4 V	0.58	690
88*	20 55 05.18	44 36 31.1	17.930			2.297:	1.075:	0.477:	1.026:	g,e?		
89	20 55 05.83	44 34 30.4	17.301			2.862	1.474:	0.521	1.405	a-f		
90	20 55 05.83	44 28 59.1	17.454			2.796:	1.013	0.620	1.150	k6 V	0.68	680
91	20 55 06.90	44 22 33.7	16.699	4.197:	3.330	2.390	1.237	0.431	1.036	f3		
92	20 55 07.33	44 35 49.1	12.263	2.937	2.274	1.795	1.059	0.369	0.939	b1		
93	20 55 07.69	44 31 00.2	12.921	2.357	1.842	1.232	0.532	0.199	0.515	f6 V	0.22	660
94	20 55 08.31	44 25 57.9	17.375			2.940:	1.555:	0.576	1.334	a-f		
95	20 55 08.31	44 29 44.5	14.818	4.204	3.052	1.962	1.037	0.343	0.845	a1		
96	20 55 09.22	44 20 27.5	16.417	4.293:	3.660:	2.519	0.931	0.630	0.937	k-m V		
97	20 55 09.24	44 25 10.8	17.032			2.909	1.111	0.662	1.123	k5 V	1.38	491
98*	20 55 11.23	44 24 05.3	16.235			2.699	1.701	0.603	1.389	B,e?		
99	20 55 12.14	44 20 25.2	16.756			2.694	0.940	0.592	1.001	k5 V	0.67	600
100	20 55 12.44	44 31 36.4	14.559	2.664	2.178	1.517	0.658	0.258	0.640	g0 V	0.53	880
101	20 55 13.03	44 32 27.0	16.083	4.316:	3.414	2.477	1.290	0.455	1.184	f3 V	3.62	750
102	20 55 13.04	44 35 36.5	17.488			2.216	1.242:	0.467	0.968	b		
103	20 55 15.19	44 25 54.3	16.375	3.758:	3.134	2.158	0.865	0.411	0.841	k1 V	0.85	770
104	20 55 16.16	44 21 26.2	17.276			2.813:	1.055:	0.680	1.116	k6 V	0.85	580
105*	20 55 16.45	44 27 01.6	17.293			2.584	1.438:	0.533	1.413	B,e?		
106*	20 55 18.21	44 24 21.1	17.883			2.739:	1.260:	0.520:	1.305:	G,e?		
107	20 55 20.70	44 32 02.3	17.308			2.307	1.333:	0.506	1.127	o-b		
108	20 55 20.82	44 31 45.6	17.487			2.247	1.179:	0.439	1.118	a-f		
109	20 55 21.72	44 28 06.5	16.426	4.173:	3.219	2.456	1.216	0.424	1.124	f-g		
110	20 55 22.81	44 33 56.6	12.691	3.886	2.731	1.682	0.899	0.311	0.754	aI III	2.95	850
111	20 55 23.30	44 30 36.9	17.319			2.615	1.389:	0.522	1.258	a		
112	20 55 23.64	44 29 05.1	13.956	3.448	2.569	1.797	1.048	0.363	0.925	b8		
113	20 55 24.61	44 34 04.5	16.221	4.635:	3.494	2.617	1.379	0.512	1.216	a-f		
115	20 55 25.71	44 34 15.7	15.501	3.892	2.929	2.039	1.043	0.408	0.946	a-f		
116	20 55 26.12	44 31 16.7	17.469			2.180	1.135:	0.422	1.025	a		
117	20 55 26.17	44 25 09.0	10.920	2.135	1.615	0.917	0.394	0.149	0.389	a7 V	0.52	437
118	20 55 27.54	44 29 36.9	17.761			2.338	1.164:	0.372	1.205:	f		
119	20 55 27.62	44 31 12.1	17.303			2.560	1.260:	0.440	1.184	g		
120*	20 55 27.98	44 28 26.3	16.039	3.104	2.490	1.850	0.856	0.364	0.812	F,e?		
121	20 55 28.31	44 33 22.6	13.031	2.551	2.096	1.433	0.606	0.255	0.562	g2 V	0.19	445
122	20 55 29.34	44 29 32.3	12.752	2.381	1.883	1.244	0.540	0.184	0.544	f5 V	0.33	610
123	20 55 29.56	44 26 10.6	15.903	4.177	3.111	2.211	1.149	0.414	1.067	a-f		
124*	20 55 29.82	44 28 41.0	17.518			2.454	1.404:	0.590	1.243	B,e?		
125	20 55 32.02	44 31 12.5	17.640			2.687:	1.368:	0.483	1.227	f		
126	20 55 32.10	44 29 31.4	17.303			2.266	1.163:	0.385	0.995	a		
127	20 55 32.47	44 32 13.4	15.905	4.229	3.155	2.052	1.087	0.434	0.920	a0		
128	20 55 33.92	44 27 30.4	10.555	3.637	3.033	2.074	0.836	0.295	0.776	g8 III	0.48	720
129	20 55 34.26	44 29 27.6	16.993			2.468	1.297:	0.415	1.152	a3		
130	20 55 34.38	44 27 11.5	13.896	2.7								